

Solid-State Technology for Domestic Microwave Heating Applications

A thesis submitted in fulfilment of the requirements
for the degree of Doctor of Philosophy

By
Kauser A Chaudhry B.Eng.Hons, MSc., PGCE-FE
December - 2019

Department of Electrical and Electronic Engineering
Cardiff University
United Kingdom

Copyright © 2019 Kauser A. Chaudhry.

ABSTRACT

The use of solid-state power for microwave heating, first proposed in the late 1960's and early 1970's, is now an area of growing interest and research for a number of stakeholders; semiconductor device manufacturers, domestic and commercial microwave oven manufacturers, large-scale heating industry and consumers.

The traditional way of generating power for these applications has been through the use of a high power magnetron source, the power is then coupled into the cavity via a waveguide. Although cost effective, the magnetron source is limited in that it has a relatively small bandwidth (20MHz) which means that only a small number of modes are excited. The different ingredients in a meal often have different dielectric properties and require multi-mode excitations over the entire (2.4-2.5GHz) band to distribute heat evenly and prevent uneven heating of the load. Its other limitations include no direct means of quantifying forward and reflected powers, the transit time becoming an appreciable portion of the signal cycle which decreases efficiency has been well documented. The recent advances and developments in semiconductor device technology (LDMOS, HVLD MOS and GaN-on-Si) has alleviated some of the earlier obstacles relating to low-power and poor-efficiency. However, concerns remain about cost, device reliability and output power levels. For example the relatively recent, sufficiently high power levels from a single transistor (300W, CW), and the use of new power combining techniques are factors that are increasing the viability of solid-state power in microwave heating.

This thesis focuses on a proposed application that involves the use of RF generated power from a solid-state amplifier, at the heart of the SSPA is the "power transistor", which generates power to heat the loads (e.g. food) in resonant cavities. From an energy consumption perspective, the solid-state source is a key element that must be designed to satisfy stringent efficiency requirements. Device and circuit related efficiencies are required to maintain an efficient transfer of power into the cavity under variable loading conditions which poses an even greater challenge. The delivery of power into a cavity

under variable loading conditions usually leads to impedance mismatch, highly reflective states and associated heating inefficiency.

Addressing this set of unique challenges has led to continuous research to improve the efficiency and reliability of power transistors. For example, new power transistor technologies (GaN, SiC) offer increased performance compared to traditional silicon components. These transistors can operate at higher power levels, frequencies and temperatures with an improved energy efficiency with respect to that guaranteed by previous generation. From a solid-state heating perspective most of this research has focused on high power and high efficiency PA architectures and device reliability, there is little literature addressing the importance of a coupling structures and the potential performance enhancements they may offer in solid-state implementations. The coupling structure plays an important role in transferring available SSPA power into the cavity to heat the load.

The novel work presented in this thesis includes capturing cavity impedance behaviour of different cavity geometries under variable loading conditions and introduces a coupling architecture through which these changes are identified and optimally matched to maintain system and heating efficiency. Following extensive research into means of transferring SSPA power into the cavity efficiently, maintaining device reliability and realizing the goal of homogeneous heating, the study has led to the development of a novel coupling structure. This structure ensures an optimised match under variable loading conditions by incorporating harmonic tuning elements for improved efficiency. The novel research introduced in this work shows how device reliability and efficiency can be improved along with improving heating uniformity.

ACKNOWLEDGEMENTS

First and foremost, I would like to thank my supervisor, Dr. Jonathan Lees, for invaluable discussions and advice throughout the course of this research, and for many helpful comments on the draft of this thesis. I also want to thank him for giving me the opportunity to experiment with my own ideas and for all the brain storming sessions and discussions around the challenges of this research.

I would also like to thank Dr Roberto Quaglia and Professor Steve C Cripps for giving me the opportunity to carry out research work on load modulated PA's this past year, whilst allowing me the time and space to write my thesis. I am grateful to Professor Adrian Porch for sharing his knowledge and expertise in the field of electromagnetism and cavity design. I appreciate all their contributions of support, time, feedback and constructive comments that were inspiring and helpful. Thank you to all my colleagues in both the RF and EM group(s) with whom I have shared the past few years.

DEDICATED TO

With deepest gratitude to my parents and wife for her support and patience.

Saif, Kasim, Alina and Essa – love you always.

LIST OF PUBLICATIONS

- 1 Kauser Chaudhry and Dr J Lees (2016) ‘Power Amplifier, Microwave Cavity and Waveguide design considerations for Domestic Microwave Cooking Applications’ – A presentation to RF Energy Alliance members – European microwave conference 2016
- 2 Kauser Chaudhry and J Lees (2018) ‘Two Port Cylindrical Cavity Enables Efficient Power Delivery’ - Through Power Combining & Scaling in a Solid State System. In: ARMMS Conference Digest. ARMMS RF & Microwave Society Conference, 23-24 Apr 2018, The Oxford Belfry, Nr Thame
- 3 Kauser Chaudhry and Dr J Lees (2018) ‘Solid State Sources for Domestic Microwave Cooking Applications’. Conference: IET Active and Passive RF Devices Seminar, 30 Apr 2018, Savoy Place, London.
- 4 Kauser Chaudhry and Dr J Lees (2018) ‘Cylindrical Cavity Characterization and Coupling Structure Optimization for Solid-State Heating Applications’ In: ARMMS Conference Digest. ARMMS RF & Microwave Society Conference, 19-20 Nov 2018, Wyboston, Bedfordshire. ARMMS.
- 5 Kauser Chaudhry, Roberto Quaglia, Steve Cripps “A load Modulated Balanced Amplifier with Linear Gain Response and Wide High-Efficiency Output Power Back-Off Region – INMMc, 16-17 July 2020, Cardiff
- 6 Kauser Chaudhry & J Lees ”A Broadband, Harmonically Tuned Coupling Technique to Simplify System Architecture and Enable Efficient Power Delivery in Solid-State Microwave Ovens” Journal of Microwave Power and Electromagnetic Energy – submitted 2019

-
- 7 Kauser Chaudhry and Dr J Lees “Design and Reliability Considerations of Single and Multi-Channel Microwave Heating Apparatus in the absence of a circulator” - THE INTERNATIONAL MICROWAVE POWER INSTITUTE (IMPI) – in progress
 - 8 Kauser Chaudhry & J Lees “A Novel, Direct Energy Coupling Technique Enables Efficient Power Delivery in a Solid State Microwave Oven, Simplifies System Architecture and Reduces Cost.” Journal of Microwave Power and Electromagnetic Energy – in progress

PAPER REVIEWS

1. Journal of Microwave Power and Electromagnetic Energy – “Anode Shaping for rejection of π -mode in relativistic A6 magnetron”.
2. Journal of Microwave Power and Electromagnetic Energy - "Comparison of the microwave drying kinetics of culture and natural asparagus"
3. Journal of Microwave Power and Electromagnetic Energy - "Determination and Modelling of Dielectric Properties of the Cherry Leaves Depending on the Moisture Content and the Frequency

PATENT APPLICATIONS

- 1 Wideband Coupling Structure - The invention relates to architecture(s) that are capable of coupling RF generated power into the cavity under variable loading conditions over a wide bandwidth – without any physical or electromechanical re- alignment.
- 2 Intelligent Frequency Hopping with a wideband coupling Structure - ensures that the source is always operating into an optimally matched load. This increases cavity efficiency of greater than 99 percent. It enables multi-channel (port) applications by continuing to ensure that each of the sources is optimally matched to an impedance point (null) in its allocated bandwidth determined through the use of the wideband coupling structure. This ensures multi-mode excitation without experiencing interference (or reflected power) from the neighbouring source.
- 3 Harmonic Tuning with a Wideband Coupling Structure - Single or multichannel (Port) operation with a return loss of -10dB or better at the fundamental frequency (2.4-2.5GHz) and a short at the second harmonic frequencies (4.8-5.0GHz) under variable loading conditions. Tuning of second harmonic frequency optimises system efficiency by up to 5 percent and enhances device reliability by preventing hostile harmonic loading conditions.

LIST OF TERMS

RF	Radio Frequency
LDMOS	Laterally diffused metal-oxide semiconductor
GaN	Gallium Nitride
SSPA	Solid State Power Amplifier
E-Field	Electric Field
H-Field	Magnetic Field
ISM	Industrial Scientific and Medical
IEC	International Electrotechnical Commission
HEECS	High Efficiency Electronic Cooking Systems
TE	Transverse Electric
TM	Transverse Magnetic
u_E	The energy density in a region of free space occupied by an electric field
PWM	Pulse Width Modulation
P_{out}	Output Power (CW unless stated otherwise)
PAPR	Peak to average power ratio
Z_L	Load Impedance
Z_0	Characteristic Impedance
Γ	Reflection Coefficient
S	Power per unit at a distance, d
P_t	Transmit Power
ITU	International Telecommunications Union
EM	Electromagnetic
CAD	Computer Aided Design
Q-Factor	Quality Factor
RLC	Resistor-Inductor-Capacitor
PAE	Power Added Efficiency
MAG	Maximum Available Gain
OMN	Output Matching Network
VDS	Drain-Source Voltage
VGS	Gate-Source Voltage
CW	Continuous Wave
DUT	Device Under Test
VNA	Vector Network Analyzer
PWM	Pulse Width Modulation
VSWR	Voltage Standing Wave Ratio
P_F	Forward Power
P_R	Reverse Power

CONTENTS

CHAPTER 1 - INTRODUCTION	1
1.1 Microwave Heating.....	1
1.2 Research Motivation.....	4
1.3 Thesis Outline	11
1.4 References	20
CHAPTER 2 THEORY	23
2.0 Introduction.....	23
2.1 Electromagnetic Radiation	24
2.2 Electromagnetic Waves:.....	25
2.3 Wave Propagation	26
2.4 Maxwell's Equations	28
2.5 Electric Field:	30
2.6 Magnetic Field	31
2.7 Lambert's Law vs Maxwell's Equations	33
2.8 Waveguides	34
2.9 Modes of Propagation	36
2.10 Rectangular Cavity.....	38
2.11 Cylindrical Cavity	40
2.12 Coupling Structures	43
2.12.1 Coupling Slots	44
2.12.2 Electric Coupling Probes	45
2.12.3 Magnetic Coupling Loop.....	46
2.12.4 Patch Antenna Coupling	47
2.12.5 Horn Antenna.....	49
2.13 References	51
CHAPTER 3 – LITERATURE REVIEW	53
3.1 Fundamentals of Microwave Heating	53
3.2 Magnetron Based Microwave Heating	54
3.3 The Magnetron.....	57
3.4 Magnetron Power.....	58
3.5 Magnetron Frequency	59
3.6 Microwave Heating in Domestic Ovens	60
3.7 Solid-State Based Microwave Heating	62
3.7.1 Solid State Microwave Oven.....	63
3.7.2 Microwave Heating with Control.....	67
3.7.3 Microwave Heating with Distributed Semiconductor Sources	70
3.7.4 Microwave Heating with Predefined Modes.....	71
3.7.5 Microwave Heating with SSPA and Antenna Array(s).....	73
3.7.6 Microwave Heating Versatility.	74
3.7.7 The future of Microwave Heating	75
3.7.8 The constraints for practical implementation of solid-state technology	77
3.8 Factors Influencing Microwave Heating	79
3.8.1 Dielectric Properties	79

3.8.2	Physical Properties	82
3.8.3	Chemical Composition	84
3.8.4	Placement inside the cavity.....	84
3.9	Summary.....	85
3.10	References	86
CHAPTER 4 – POWER AMPLIFIER DESIGN CONSIDERATIONS		97
4.1	Power Amplifier Key Parameters.....	97
4.2	Power Amplifier modes of operation.....	98
4.3	SSPA Architectures	105
4.3.1	Envelope Tracking	105
4.3.2	Doherty Amplifier	107
4.3.3	Chireix’s Outphasing Amplifier	109
4.4	RF Matching Network Design Considerations	111
4.5	PA Design Considerations for Microwave Heating Applications	114
4.5.1	Overview.....	114
4.5.2	Single Port Cavity Excitation.....	117
4.6	Two port cavity excitation	126
4.6.1	Load variations in a two port cavity.....	127
4.6.2	Phase variations in a two-port cavity	128
4.6.3	Coupling coefficient	131
4.7	Summary.....	132
4.8	References	134
CHAPTER 5 - COUPLING ENERGY INTO THE CAVITY		139
5.0	Power Coupling:	139
5.1	Coupling Structures	142
5.1.1	Magnetic Coupling.....	142
5.1.2	Electric Coupling	142
5.1.3	Electric probes and Current loops	143
5.2	Loop coupling structure	143
5.2.1	Loop coupling structure - matching considerations	146
5.3	Single loop coupling structure.....	149
5.3.1	Single loop lumped element model:	149
5.3.2	Single loop lumped element model with harmonic tuning - cylindrical cavity	152
5.3.3	Single loop coupling structure construction and integration into a cylindrical Cavity.	155
5.4	Single loop coupling structure characterisation using a cylindrical cavity. ..	157
5.4.1	Limitations of a single loop under variable loading conditions.....	159
5.5	The optimised coupling structure with a wider bandwidth and tolerance to load variations.....	160
5.6	Single loop coupling structure characterisation for using a rectangular cavity	163
5.6.1	Limitations of single loop coupling structure in a rectangular cavity	165
5.6.2	Load variations in a rectangular cavity	166

5.6.3	Single loop lumped element model with harmonic tuning-rectangular cavity	169
5.7	The optimised coupling structure - rectangular cavity	170
5.8	Summary	174
5.9	References	176
CHAPTER 6–MEASUREMENT AND CHARACTERISATION OF SOLID STATE HEATING USING A CYLINDRICAL CAVITY		181
6.1	Overview	181
6.1.0	Single mode cylindrical cavity	181
6.1.1	Characterisation of cylindrical cavity operating environment under variable loading conditions.	182
6.1.2	Characterisation of cylindrical cavity operating environment due to a changes in load temperature.	185
6.1.3	Limitations of using a single loop coupling structure.....	187
6.1.4	Optimising the loop coupling structure for variable loading conditions. ..	188
6.2	Two port system overview	191
6.2.1	Two port cylindrical cavity	191
6.2.2	Single loop coupling structure limitations in a 2 port network	192
6.2.3	Measurements using single loop coupling structure in a two port cylindrical cavity	194
6.2.4	Measurements using optimized loop coupling structure	197
6.3	Summary	199
6.4	References	200
CHAPTER 7- MEASUREMENT AND CHARACTERISATION OF SOLID STATE HEATING USING A LARGE RECTANGULAR CAVITY		203
7.1	Overview	203
7.1.1	Load variation in large rectangular cavities:	204
7.1.2	Verification of the coupling structure	206
7.1.3	Single-point vs swept frequency heating	214
7.1.4	Microwave Oven Efficiency Comparisons	215
7.1.5	Cavity heating uniformity relative to load placement.....	217
7.1.6	Cavity heating uniformity – surface temperature	220
7.1.7	The impact of temperature variation	222
7.2	Summary	225
7.3	References	227
CHAPTER 8 CONCLUSIONS AND FUTURE WORK		231
Appendix A - Rectangular Waveguide		237
Appendix B - Rectangular Cavity		238
Appendix C - Eigen Values – Unloaded Rectangular Cavity		239
Appendix D - Eigen Values – Unloaded Rectangular Cavity		240
Appendix E – Single Mode Cylindrical Cavity.....		241
Appendix F - RF Transistor Device Technology Comparisons		241

LIST OF TABLES

Table 1.1	Currently Available Solid-State Generators
Table 2.1	Checking of modes in rectangular waveguides
Table 2.2	Different types of horn antennas, common types are listed below:
Table 2.3	Horn antenna design equations
Table 3.1	Penetration depths of microwave energy for various materials at 2450MHz
Table 5.1	S_{11} as a function of variable load – Static Single loop
Table 6.2	Single loop coupling measurements
Table 7.2	Time to heat a 0.325litre load – measured values using a frequency sweep (2400_2500MHz) with 1MHz steps
Table 7.3	Solid State heating temperature measurement comparison

LIST OF FIGURES

- Fig.1.1 Solid-State Power Microwave Heating System
- Fig 2.1 The placement of various elements within the electromagnetic spectrum.
- Fig 2.2 (a)Electric field of a positive & negative charge (b) magnetic field induced by current flow in a wire (c) Electric and Magnetic fields propagating through space
- Fig 2.3 Wave Propagation from low-density medium to a high-density medium
- Fig 2.4 Electric field distribution between two parallel plates.
- Fig 2.5 Magnetic field distribution in a cylindrical cavity.
- Fig 2.6 A solenoid inductor of length l , area A and n number of turns
- Fig 2.7 EM Wave propagation in a rectangular waveguide
- Fig 2.8 An integral number of $\frac{1}{2}$ wavelengths in a waveguide
- Fig 2.9 Examples of TE_{mn} – voltage and TM_{mn} – current modes in rectangular waveguides;
- Fig.2.10 Rectangular Cavity
- Fig 2.11 Cylindrical Cavity Resonator, Electric and magnetic field components inside a cylindrical cavity.
- Fig 2.12 Slot coupling and current flow in a waveguide walls for a dominant mode
- Fig 2.13 Coupling of an electric field through an aperture – Normal to plane of aperture
- Fig 2.14 Coaxial Feed Coupling Probe – coupled to a cavity resonator
- Fig 2.15 Loop Coupling Structure – coupled to a cavity resonator
- Fig 2.16 Patch Antenna
- Fig 2.17 Horn Antenna
- Fig 3.1 (a) Water-Electric dipole moment (b) Variation of microwave propagation in time.

-
- Fig 3.2 Production figures and user unit costs of magnetrons – past and projected (H. K. Jenny, “Electron tubes—A technology forecast,” Technology Trend (75CH1005-8 TFA), IEEE, NY (1975)).
- Fig 3.3 Magnetron based microwave oven.
- Fig 3.4 Schematic of a typical microwave oven.
- Fig 3.5 Solid-state powered microwave oven
- Fig 3.6 Microwave oven with a plurality of solid-state oscillators
- Fig 3.7 A Combination Microwave Oven
- Fig 3.8 Microwave Oven – multiple couplers & solid state sources
- Fig 3.9 Solid-State Microwave Oven – multiple solid state sources
- Fig 3.10 Controlled Heating Microwave Oven
- Fig 3.11 Microwave Heating System comprising of multiple sources
- Fig 3.12 Microwave heating comprising of distributed sources
- Fig 3.13 Compartmented Microwave Heating
- Fig 3.14 Microwave heating system with antenna arrays
- Fig 3.15 Versatile Microwave Heating
- Fig 3.16 Standing Waves – lead to hot and cold spots
- Fig 3.16 Standing Waves – lead to hot and cold spots
- Fig 3.17 High Power RF transistors specifically designed for RF Energy applications
- Fig 4.1 The power capacity comparisons of Class A, Class B and Class C amplifiers [35].
- Fig 4.2 Typical Class F Amplifier
- Fig 4.3 Class-F Voltage and Current Waveforms [23]
- Fig 4.4 Class-J Amplifier Matching Network
- Fig 4.5 Fundamental and 2nd Harmonic Voltages (left) and Class-J Voltage & Current Waveform [20]
- Fig 4.6 Simplified Envelope tracking amplifier
- Fig 4.7 Envelope tracking concept [28]
- Fig 4.8 Symmetrical Doherty Amplifier with a 6dB PAR ($\alpha = \frac{1}{2}$)

-
- Fig 4.9 Asymmetrical Doherty Amplifier with a 9.5dB PAR ($\alpha = 1/3$)
- Fig 4.10 Drain Efficiency vs Normalised load voltage amplitude []
- Fig 4.11 Simplified block diagram of Outphasing system
- Fig 4.12 Theoretical efficiency of Chireix's Outphasing system at four different compensation angles [34]
- Fig 4.13 Low pass (left) and band pass (right) matching topologies
- Fig 4.14 Input return and circuit losses - Narrow Band (V-Shaped) vs Broadband (W-Shaped) response.
- Fig 4.15 Cavity equivalent lumped element model.
- Fig 4.16 Impedance mismatches between transmission line and the load.
- Fig 4.17 Simulation Test Bench used for characterising cavity loading conditions.
- Fig 4.18 The impedance, Z, return loss S11 and VSWR as a functions of load (as it is varied from 5 to 95 Ω in 20 Ω steps).
- Fig 4.19 ADS test bench for 1 port analysis.
- Fig 4.20 (a) Output Voltage as a function of load mismatch, (b) Output Current as a function of load mismatch (c) Output power as a function of load mismatch. (Phase = 0 deg. Coupling Coefficient C=1.0)
- Fig 4.21 (a,b) Current and Voltage spectrum in time domains as function of phase mismatch (c) average power spectrum as function of phase mismatch, load = 377 Ω Coupling Coefficient =1
- Fig 4.22 (a,b) Current and Voltage spectrum in time domain as function of phase mismatch (c) average power spectrum as a function of phase mismatch, load = 1 Ω Coupling Coefficient 1.0
- Fig 4.23 S11 as a function of coupling coefficient – (a) 50 Ohm load phase = 0 degrees (b) 50 Ohm load phase = 30 degrees
- Fig 4.24 A two-channel system feeding into a single cavity.
- Fig 4.25 S11 as a function of impedance mismatch in a 2 port system – constant phase. T=0.7
- Fig 4.26 Peak voltage and current as a function of phase mismatch in a 2 port system; load = 50 Ω

-
- Fig 4.27 Cavity load impedance as a function of coupling coefficient in a 2 port system; phase =0, $Z=50\Omega$
- Fig 4.28 Peak voltage and current as a function of load mismatch in a 2 port system; load = 377Ω .
- Fig 4.29 Peak voltage and current as a function of load mismatch in a 2 port system; load = 5Ω .
- Fig 5.1 Equivalent circuit for input Z of a small loop
- Fig 5.2 Thevenin equivalent circuit for the receiving loop
- Fig 5.3 Typical matching networks used with coupling loops. Match to a resistance R_o
- Fig 5.4 Means of adjusting coupling in loop.(a,b) Modifying the shape of the loop (c) modifying angular orientation of the loop (d) modifying loop distance inside the cavity
- Fig 5.5. a, b, c. General depiction of magnetically coupled resonant loop (a); its ideal circuit model (b) and its lumped element equivalent model (c)
- Fig 5.6 Simulated (using lumped element equivalent model fig.5.5b, c) impedance at the fundamental (900MHz-930MHz) and 2nd harmonic (1.8-1.86 GHz) freq's under fixed load (R_L) conditions is shown in both polar complex (a) and magnitude log-lin format (b, c).
- Fig 5.7 Simulated (using lumped element equivalent model fig.5.5c) impedance at the fundamental (900MHz-930MHz) and 2nd harmonic (1.8-1.86 GHz) freq's under variable load (R_L) conditions is shown in both polar complex (a) and magnitude log-lin format (b, c).
- Fig 5.8 Single Loop equivalent lumped element model with a harmonic tuning element (a) and its physical realisation (b) cylindrical cavity with the loop attached
- Fig 5.9 Simulated (using lumped element equivalent model fig.5.8) impedance at the fundamental (900MHz-930MHz) and 2nd harmonic (1.8-1.86 GHz) freq's under fixed load (R_L) conditions is shown in both polar complex (a) and magnitude log-lin format (b, c).

-
- Fig 5.10 Simulated (using lumped element equivalent model fig.5.8) impedance at the fundamental (900MHz-930MHz) and 2nd harmonic (1.8-1.86 GHz) freq's under variable loading (R_L) conditions is shown in both polar complex (a) and magnitude log-lin format (b, c).
- Fig 5.11 Measurement set-up used for characterising a coupling loop within a cylindrical cavity resonator.
- Fig 5.12 Measured impedance data is shown in polar complex form (a) and magnitude log-lin format along with the forward/reflected powers and the VSWR (b) at the Fundamental frequency (900MHz-960MHz) for a fixed load (0.085l of water) using a single loop coupling structure shown in fig.5.8.
- Fig 5.13 Measured impedance data is shown in polar complex form (a) and magnitude log-lin format (b) at the Fundamental frequency (900MHz-960MHz) under variable loading conditions (0.04l-to-0.12l of water) using a single loop coupling structure shown in fig.5.8.
- Fig 5.14 Equivalent lumped element of the 2-loop broadband coupling structure with harmonic tuning (a) and its physical realisation.
- Fig 5.15 Measured impedance data is shown in polar complex form (a) and magnitude log-lin format (b) at the Fundamental frequency (900MHz-960MHz) for a fixed load (0.085l of water) using a single and two loop coupling structures shown in fig.5.8 and fig.5.14.
- Fig 5.16 Equivalent lumped element model of a 3 loop broadband coupling structure (with harmonic tuning) optimized for variable loading conditions
- Fig 5.17 Simulated impedance data is shown in polar complex form (a) and magnitude log-lin format (b) at the Fundamental (900MHz-960MHz) and 2nd harmonic frequencies for a range load impedances (R_L , 10 Ω -to-100 Ω) using a three loop coupling structures lumped element equivalent model shown in fig.5.16.

-
- Fig 5.18 Single Loop equivalent lumped element model with a harmonic tuning element (a) and its physical realisation (b) rectangular cavity with the loop attached
- Fig 5.19 Measured impedance data is shown in polar complex form (a,c) and magnitude log-lin format (b,d) at the fundamental (2400MHz-2500MHz) and 2nd harmonic frequencies (4800-5000MHz) under variable loading conditions (0.1l-to-1.0l of water) using a single loop coupling structure shown in Fig.5.8.
- Fig 5.20 Equivalent lumped element model of a 3 loop broadband coupling structure (with harmonic tuning) optimized for variable loading conditions
- Fig 5.21 Measured impedance data is shown in polar complex form (a,c) and magnitude log-lin format (b,d) at the fundamental (2400MHz-2500MHz) and 2nd harmonic frequencies (4800-5000MHz) under variable loading conditions (0.1l-to-1.0l of water) using a three loop coupling structure shown in Fig.5.8.
- Fig.5.22 Simulated load impedance using a 3 loop coupling structure shown in polar complex and log-lin format at the fundamental) 2.4-.5) and 2nd harmonic frequencies (4.8-5.0GHz) as the load (R_L) is varied from 10 Ω -to-100 Ω .
- Fig.5.23 Rectangular cavity loop development for extended bandwidth
- Fig 5.24 Measured S_{11} using a four loop coupling structure for 0.325l of water, load showing 4 resonances (optimally matched frequency points) which combine to give a broader (200MHz) bandwidth with a return loss of better than -15dB
- Fig.5.25 Block diagram (a) Solid state system (Conventional Approach) (b) Solid – state system (Proposed Approach)
- Fig 5.26 Transforming Cavity load impedance (a): to 50 Ω (b): to 5 Ω using loop coupling structure lumped element model.

-
- Fig 6.1 VSWR measurements 0.04-0.12l of water load.
- Fig 6.2 Impedance variations due to changes in temperature (0.085l of water load).
- Fig 6.3 Reflection coefficient measurements with temperature variations ($^{\circ}\text{C}$) 0.085 l of water load.
- Fig 6.4 VSWR measurements 0.085-0.12 l of water load.
- Fig 6.5 (a) S_{11} and (b) delivery efficiency using a single loop for three different loads (0.04l, 0.08l and 0.12l of water load).
- Fig 6.6 (a) S_{11} and (b) delivery efficiency using three loop coupling structure for three different loads (0.04l, 0.08l and 0.12l of water load).
- Fig 6.7 S_{11} (single mode vs proposed) with temperature (22°C , 30°C and 52°C) - 0.085l of water load
- Fig 6.8 Measurement set-up used for monitoring the forward, reflected power and temperature rises inside a 2 port cylindrical cavity.
- Fig 6.9 Two port cylindrical cavity (a) E & H Field strength as a function of phase (b) Top and side views of field strength with phase at 0 degrees (c) Top and side views of field strength with phase at 180 degrees.
- Fig 6.10 Shows incident power measurements at port 2 - (i) in the presence of a coupling structure at port 1 (ii) In the presence of coupling structure at port 1 with low RF power.
- Fig 6.11 Shows P_{inc} measurements at port 1 - (i) in the presence of a coupling structure at port 2 (ii) In the presence of coupling structure at port 2 with low RF power.
- Fig 6.12 Shows P_{del} and P_{ref} measurements at port A & port B where the forward power at port A is set to 37dBm and the forward power at port B is varied between 37 and 26 dBm in 1 dB steps.
- Fig 7.1 Resonant modes that exist within an empty rectangular microwave oven cavity (size = 36litre), with associated mode distributions (Eigenvalues) for some of these.

-
- Fig 7.2 Mode Distribution (Eigenvalues) inside a loaded (1 l of water) Microwave Oven (size = 36litre)
- Fig 7.3 Concept Evaluation – measurement setup
- Fig 7.4 Forward and reflected power measurements across the 2400 – 2500 MHz frequency band, 0.325l water load.
- Fig 7.5 S_{11} at the fundamental (2.4-2.5GHz) and second harmonic (4.8–5.0GHz) for a 0.325l water load using coupling structure shown in Fig.7.3c, shown in (a) both polar complex (b) magnitude log-lin format.
- Fig 7.6 Forward and reflected power measurements across the 2.4–2.5 GHz frequency band for a 0.325l water load, measured using the optimised coupling structure shown in Fig.7.3c
- Fig 7.7 Single frequency vs continuous frequency sweep temperature measurements for a 0.325l water load, with a 150W SSPA.
- Fig 7.8 Microwave Oven Efficiency comparison between a Solid-State (160W) microwave oven and a Magnetron based (800W) microwave oven.
- Fig 7.8 Microwave Oven Efficiency comparison between a Solid-State (160W) microwave oven and a Magnetron based (800W) microwave oven.
- Fig 7.9 $P_{\text{delivered}}$ Efficiency comparison for different volumes of water over the operating frequency band
- Fig 7.10 Load placement locations within the oven (b)Magnetron based microwave oven, Δ ($^{\circ}\text{C}$) temperature variations from central location, 0.1l water load, heating time = 60 seconds
- Fig 7.11 SSPA based microwave oven. Optimally matched frequency points are shown (MHz) for different placement locations 0.1l water load (b) SSPA based microwave oven, Δ temperature ($^{\circ}\text{C}$) variations from central location, 0.1l of water heating time = 60 seconds
- Fig 7.12 SSPA based microwave oven, S_{11} (dB) at optimally matched frequency points, 0.1l of water

-
- Fig 7.13 Surface temperature measurements using a 800W magnetron based microwave oven, 0.325l water load in a container of diameter 17cm, heating time = 60 seconds
- Fig.7.14 Surface temperature measurements using a 200W solid-state microwave oven, 0.325l water load in a container of diameter 17cm, heating time = 240 seconds
- Fig 7.15 S_{11} at the Fundamental (2.4GHz-2.5GHz) and 2nd Harmonic (4.8 GHz-5.0 GHz) freq's measured using coupling structure shown in Fig.7.3b, shown in both polar complex (a) and magnitude log-lin format (b).

CHAPTER 1 - INTRODUCTION

1.1 Microwave Heating

Traditional magnetron based microwave heating systems (operating over the 2.4-2.5GHz for domestic and 896MHz (UK), 915MHz (USA, China) for industrial applications) are limited by inflexible, load-dependent heating transfer rates and “hot–cold” effects. The ITU (1947) designated these bands specifically for microwave heating due to the relatively low power required to heat the food and the fact that this power could easily be contained within the cavity. These non-uniform volumetric temperature effects are attributed to uneven distribution of dielectric and thermal properties of the load, microwave standing waves and finite penetration depth. The resulting formation of cold spots is then associated with changes in food texture, sensory and nutritional quality. A modern day healthy and environmentally conscious consumer wants control over power, efficient cooking cycles, nutrient retention, wireless connectivity and reduced energy consumption [1]. This is difficult to achieve with a magnetron-based microwave oven, which lacks control and responsiveness to uneven and unpredictable field distributions, resulting from variable loading conditions. These variations require an operating system where changes in the load impedance can be detected and optimally matched.

Such hot and cold effects are a significant contributor to energy loss. Higher than optimal temperature and longer time combinations are used to eliminate cold spots to ensure food safety. The presence of these non-uniformities is associated with inefficient energy distribution (per unit volume of the load). Microwave heating applications over the decades have been powered by vacuum electronic devices such as magnetrons, klystrons and gyrotrons. Of these, magnetrons are the cheapest and most efficient which has led to their dominance over other generators [6]. Magnetrons typically have a maximum power generation efficiency¹ of 70% (at 2450MHz), and 88% (at 915MHz) [2]

¹ The power generation efficiency (η) is expressed as the product of electronic efficiency, η_e and the circuit efficiency η_c where $\eta_e = \frac{\text{input power converted to rf power in anode block}}{\text{input power}}$;
and $\eta_c = \frac{\text{rf power transmitted to the load}}{\text{rf power generated}}$

whilst the absorption efficiency is determined by the degree of impedance match between the magnetron source and the load being heated. The load impedance varies over time with changes in (food) temperature and also in space due to inhomogeneity in load (thermal & dielectric properties), non-uniform spatial temperatures and volumes of food being heated. These variations in impedance result in mismatches which lead to reflected power and reduced absorption. This in turn causes microwave oven efficiencies² to drop to around 25-55% [8]. To ensure acceptable heating uniformity, more energy needs to be delivered to the “cold spots” (for example, to reach food safety temperatures), consequently more energy will also be delivered at “hot spots”, degrading food quality (over-cooking) and degrading energy efficiency. This phenomena is also undesirable in other industrial applications, such as in composite curing of mechanical parts where it can lead to weaknesses in the structure.

Moreover, microwave efficiency² is at its highest at the beginning of a heating cycle, where the load water content tends to be maximum, and the load is able to absorb most of the available power beyond which reflections dominate (unmatched condition), leading to reduced energy performance [4]. With increasing temperatures, there is a drop in water content whereby less and less of the incident power is absorbed and more is reflected (unmatched condition), leading to increased energy losses. In order to maintain high levels of efficiency, some degree of control of either source or load or the matching mechanism between them is needed. Generally, this is not possible with inflexible magnetron generators, which lack the required control and feedback mechanisms.

The energy performance of microwave heating systems is typically quantified either in terms of the specific energy consumption or the energy efficiency. The overall

² The efficiency of a microwave oven is determined by calculating the amount of electrical energy used by the microwave to heat the water. The electrical energy used $= P \cdot \frac{E}{t}$; where P = power rating of the microwave oven (Watts), E = electrical energy used by the microwave oven (joules), t = time the microwave oven is ON. The amount of energy converted to heat energy is calculated using $Q = m c_{\text{water}} (T_{\text{final}} - T_{\text{initial}})$ where Q = heat transferred to water, m = mass of water (kg), c_{water} = specific heat of water (4186) kg⁻¹C⁻¹) Microwave Oven efficiency(%) = $\frac{E-Q}{E} \cdot \frac{100}{1}$

energy efficiency (η) is defined as the product of microwave generation efficiency (η_{gen}) and the microwave absorption efficiency (η_{abs}) (eqn's 1.1-1.3) [5]. It is important to calculate the efficiency values with real time measurements as the magnetron output power drops over time, a 33% drop has been reported after 5–10 years of operation [6]. Further, during a continuous 30 minute operation, the microwave oven transient output drops by 15% [7] as operating into mismatched loads leads to high reflected power states and heating of the magnetron source. A combination of these factors contribute to lower microwave oven efficiencies [8]. The reasons for this drop in power and magnetron fail mechanisms are listed and discussed in various literatures [36-37].

$$\eta = \eta_{gen} \cdot \eta_{abs} \quad (1.1)$$

$$\eta_{gen} = \frac{P_{out}}{P_{in}} \quad (1.2)$$

$$\eta_{abs} = \frac{P_{heat}}{P_{out}} \quad (1.3)$$

Where:

P_{out} = Output power (generated power)

P_{in} = Electrical Input Power

P_{heat} = Thermal Power (power used to heat the load)

η_{gen} = Source Efficiency

η_{abs} = is dependent on the impedance match (Source to load) and load dielectric properties.

The efficiency calculation of domestic microwave ovens can be ambiguous as it typically involves heating 1000g \pm 5g of water, inside a cylindrical borosilicate glass container (external diameter 190mm, height 90mm), from 10°C \pm 1°C to 20°C \pm 2° [9]. The required output power to heat the load is then calculated using eqn.1.4. Whereas typical usage involves heating much smaller volumes of water; different foods and container types, all of which are likely to have a detrimental effect on the efficiency. Besides providing optimally matched loading conditions (maximum power to heat the load), the choice of operating conditions is based on minimising heat loss and container

heat capacity. An output power (P_{out}) approximation is used as an acceptable means by which the thermal energy delivery to the load is calculated and the electrical input power (P_{in}) compared to determine the absorption efficiency (1.3).

$$P_{out}(W) = \frac{(4.18 \cdot \text{Water}_{(g)}) \cdot (T_F - T_I) + (0.55 \cdot \text{Container}_{(g)}) \cdot (T_F - T_A)}{\text{Measured time}_{(s)}} \quad (1.4)$$

Where;

T_F = Final Temperature

T_I = Initial Temperature

T_A = Ambient Temperature

Water(g) = Mass of water in grams

Container(g) = Mass of Container in grams

4.18 = Specific heat of water (1 calorie/gram °C = 4.186 joule/gram °C)

0.55 = Specific heat capacity of container

The HEECS (2001) proposed a new standard [10], to better reflect true usage, that included different volumes of water, (1000 ±1g, 350g ±1 g, and 275g ±1g) as a test load in different shaped containers; [2000ml (diameter ϕ , 190±1mm, height 90±1mm, 900ml (diameter- ϕ , 140mm±1mm, height 76±mm) and 600ml (ϕ , 120mm±1mm, height 90±1mm)] to approximate true usage conditions. This was later adopted as a IEC standard (IEC60705, 2010). This standard was formulated by heating each of the loads from 10°C±0.5°C to between 60-65°C and then to between 55-60°C. The use of this technique gives a more accurate approximation of microwave oven energy efficiency, it is however far from perfect for applications where the load is continuously changing.

1.2 Research Motivation

Overcoming the limitations of magnetron based systems [11-13] requires an innovative technology. Both appliance manufacturers and consumers would like ovens that provide controlled and efficient volumetric heating processes and methodologies for

delivering optimally cooked food that retains high nutritional and sensory quality. This requirement is equally important in other emerging areas that are at the cusp of using solid-state technology. Therefore the main focus of this research is to study techniques and methodologies that help improve heating uniformity, cavity and heating efficiencies, whilst preserving device and system reliability at a reduced cost. Factors hampering the implementation of solid-state technology are identified and means of overcoming these obstacles are proposed.

In the work described in this thesis, the identification and capture of well-matched impedance nulls corresponding to mode excitations over a wide (100 MHz) bandwidth has been identified as one way of improving heating patterns and control. Conveniently, solid-state power amplifiers can be designed to operate over the 2.4-2.5GHz frequency band with output power and efficiencies remaining reasonably flat across the band (± 0.5 dB variation in power and ± 2 percent variation in efficiency). In order to capitalise on the extended bandwidth of SSPA's and improve heating uniformity a novel means of coupling power into the cavity is presented.

An increased use of modern electrical appliances, the scarcity of energy resources and the need to reduce carbon emissions has led regulatory authorities to place stringent efficiency requirements on household appliances[4-5]. It has been reported [14] that 92% of UK households use microwave ovens for heating food whilst the market penetration rate is of the order of 101% due to some households having multiple microwave ovens [12]. It is further reported that over 70 million microwave ovens are sold annually (worldwide) whilst the global number of microwave ovens in operation is of the order of 1 billion [15].

European domestic microwave ovens alone consume about 12.4 TWh of energy per year, with a rather poor conversion efficiency (electricity-to-heat) of 50% or less [16] which is unacceptable by today's standards. This in itself is a significant motivation for enhancing efficiency, and with relatively small improvements will translate into

significant reductions in domestic carbon footprint. The development, implementation and commercialization of solid-state microwave ovens is the subject of on-going research, with companies like Gogi, Whirlpool and Miele leading the way.

A life cycle analysis [17] concluded that the energy consumption of microwave ovens during the use-phase has the highest environmental impact, and outweighs cost of raw material extraction, production, distribution and recycling. Besides the domestic microwave oven applications, the use of microwave energy in other applications is also on the rise, this includes heating/drying (sterilization/pasteurization) in the food industry to control pathogenic and spoilage micro-organisms, industrial heating applications such as sintering of ceramic/metal powders and melting of glass/rubber; medical applications (hyperthermia treatments, diagnostic imaging, cancer treatments); material characterisation (graphene, fibres, gases etc.); image scanning systems to detect images of buried objects and rock crushing; tar road comminuting in the civil engineering applications.

Solid-state microwave heating is a promising technology for many of the above applications and the use of solid state power generators as an alternative to the magnetron has been considered for some time. Its widespread use however, is limited by discrete device power capability, cost and reliability. Due to the limited power capability of earlier solid-state microwave transistors (typically tens of watts) power combining to reach 1kW power levels was generally not feasible due to the large number of transistors required. Added cost, complexity and combining losses made such systems unattractive and inefficient. Whilst power limitations have been overcome to some extent with recent advances in semi-conductor device technology (it is now possible to attain power levels of up to 500 Watts (CW) from a single power transistor operating in the ISM band – Ampleon BLC2425M10LS500P), questions still remain over cost and reliability. This level of available power from a single device makes the use of solid-state technology more feasible and worthy of further exploration.

The cost of solid-state technology is significantly high compared to the magnetrons generators. A study of earlier magnetron based systems [18] show that a growth in volume drove the cost down, whilst further refinement and ease of manufacture over the years has ensured the costs remain low. Whilst concerns relating to device reliability are well founded and need addressing, the solid-state technology offers significant benefits over the magnetron, including power scalability, reduced energy consumption (carbon footprint) to lessen impact on the environment and low voltage operation which helps create portability.

Besides the limited power capability and acquisition costs, energy-inefficiency issues have also hindered the adoption of solid-state technology in microwave heating in the past. As of March 2019, the maximum power output (Pout) of the cheapest solid-state devices (Laterally Diffused Metal Oxide Silicon LDMOS technology) was about 300W in a single ended package and 500W in a push-pull package, with typical drain efficiencies of 69% at 2450MHz. The power capability of a single RF transistor is limited in comparison to the magnetron which means that a four transistor SSPA combination will be required to generate comparable (1kW) power levels. Whilst the drain efficiency of a SSPA is approaching that of a magnetron, the power added efficiency of a two stage PA line is expected to be around 55-60 percent..

In recent years the output power capability and device efficiencies have increased tremendously. Table 1 shows a representative summary of currently available solid-state power transistors, with achievable power output and drain efficiencies, capable of operating within the frequency ranges relevant for microwave heating. As shown in Table 1, power levels of up to 750W (896/915MHz), and 500W (2450MHz) are available in push-pull (dual lead) packages with drain efficiencies of 69%. This performance is comparable to typical magnetrons efficiency (70%) at 2450MHz, and approaching the 88% attainable with magnetrons at 896/915MHz.

Further benefits of solid-state heating systems include feedback capability on the dynamic states of the load, with precise and immediate control over power delivery (relative phase for multi-feed systems, frequency and amplitude) to improve the heating profile of the load [19-24]. Control can be further enhanced at a system level through the intelligent combination of multiple, phase coherent generators, which can potentially, significantly improve the heating uniformity. Control over the frequency and magnitude of the signal, in combination with multiple feeds can for example excite multiple cavity modes and their associated field distributions in the ISM frequency range. This opens up the possibility of resolving the non-uniform heating issues associated with traditional magnetron based systems and making the process energy efficient [25]. Moreover, the use of optimisation algorithms to adapt excitation frequency can help minimise reflected energy, and increase absorption efficiencies, close to 100% [26].

Table 1 – Currently Available Solid-State Generators

Part No	Manu	Process	Freq.	Pout	Gain	Drain Efficiency
BLC2425M10LS500P	Ampleon	LDMOS-32V	2.4-2.5GHz	500W – push-pull	15.0	67.0
BLC2425M10LS250	Ampleon	LDMOS-32V	2.4-2.5GHz	250W – single ended	15.2	68.8
BLF0910H9LS750P	Ampleon	LDMOS-50V	0.9-0.928GHz	750W – push-pull	21.	69.0
BLF0910HLS600	Ampleon	LDMOS-50V	0.915GHz	600W – single ended	19.8	68.5
MHT1003GN	NXP	LDMOS-32V	2.4-2.5GHz	300W – Single Ended	15.2	57.9
MHT1002GN	NXP	LDMOS-50V	0.915GHz	350W – Single Ended	20.7	66.9

A solid-state microwave heating system (Fig.1.1) consists of a small-signal generator and a solid state power amplifier (magnetron replacement), mounted on a suitable heat sink, and includes a power supply unit. The small-signal generator is essentially an oscillator that generates a low-power microwave signal, which is used as the input to the power amplifier. When supplied with DC power, the SSPA converts the low power signal to a higher power microwave signal at the same frequency, which is then coupled into the resonant cavity to heat the load. Through careful design of both device technology and supporting circuits, solid-state power generation efficiencies have risen steadily over the past decade and while still currently lower than that of the magnetron, a break-even point is expected in 2024 [27].

Based on the current rate of efficiency improvement (3% every 2–3 years) [28], this rise in energy efficiency at the required power level is expected to continue to improve over the coming years until it surpasses magnetron-efficiency. Having said this, existing inefficiencies of SSPA's can be countered by targetting significantly higher absorption efficiencies possible with solid-state technology. The cheapest solid-state technology (LDMOS) is currently of the order of, \$0.25/W, whilst magnetrons costs are around \$0.01/W to \$0.1/W [29]. Even in the face of a significant cost differential, industry and research groups are actively persuing solid-state heating [30-35], as it is believed that if accepted as a viable technology, the increased volumes and economies of scale would substantially reduce the cost of solid-state power generation, allowing the microwave power transistor to compete with the magnetron.

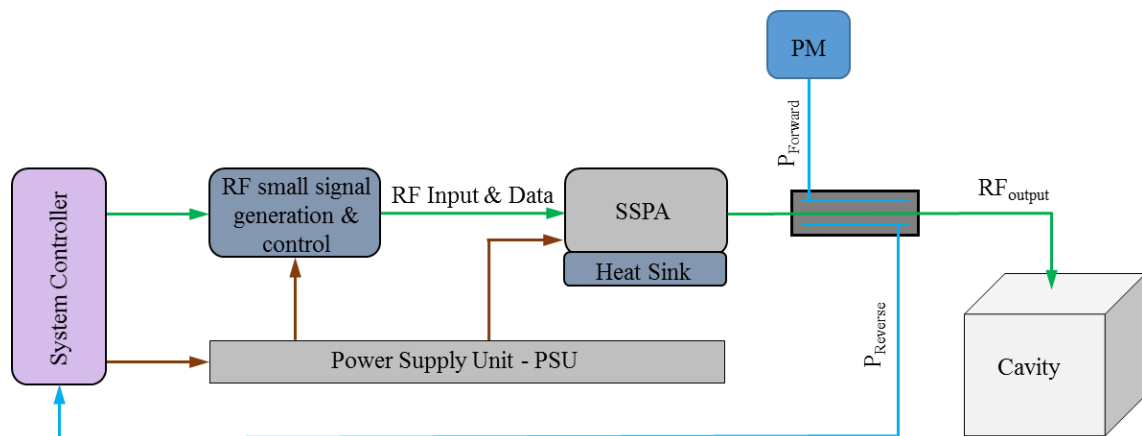


Fig.1.1 Simple Solid-State Power Microwave Heating System

The relatively high cost of RF power transistors is partly due to the expensive, low-loss, high reliability, air cavity ceramic packages that are typically used. Plastic over-moulded alternatives have been under development for some time with a good degree of success, especially at the lower power levels. Work on higher power solid-state plastic packages continues [38] and it is anticipated that the availability of these alternatives will enable semiconductor device manufacturers in the future to offer lower cost devices for volume solid-state power amplifier development.

In traditional magnetron based systems, power is delivered to the resonant cavity via an open ended rectangular waveguide. The magnetron interfaces with the waveguide feed structure via a ‘launcher’ which couples the energy produced by the magnetron into the cavity E- field exciting the dominant TE_{10} mode at the boundary edge of the cavity. This simple approach has been used successfully in domestic microwave heating applications where a magnetron-based source generating typically 1kW of power is deemed sufficient. However, the inability to capture and adapt to load variations, results in high levels of reflected powers in unmatched regions, which, although easily tolerated by the magnetron, can be catastrophic for solid-state transistors. As a result, the degradation and possible catastrophic destruction of solid state sources in microwave heating applications has been long recognised.

K. K. Chang, 1972 [39] cited the use of a micro-strip circulator and high power resistive load as a solution. A circulator is a directional element that protects a power transistor from the voltage and current maxima associated with reflected states by directing the energy to a resistive load where it can be absorbed and dissipated as heat. This heat must then be safely removed to preserve system reliability which in turn decreases system efficiency. Isolators and associated dissipative loads also tend to be relatively expensive.

Another aspect of the research presented in this thesis centers on developing a broadband coupling structure capable of delivering power into both cylindrical and rectangular cavities at the SSPA operating frequencies. This needs to be achieved without physical or mechanical re-alignment of the coupling structure, and under variable loading conditions. The study is expanded to consider approaches that can improve oven efficiency as well as reducing overall system development costs without comprising device reliability. The idea of ‘isolator-less’ power amplifier operation is considered as a major driving factor in reducing the overall system cost.

Practical microwave heating systems, to be efficient, must accommodate

impedance variations that arise within the heating cavity. The experimental work during the course of this study considers this by characterising the natural impedance environment of both cylindrical and rectangular cavities, using volumes of water at different temperatures and at different locations within the cavity. For solid-state heating systems, access to matched points (regions of low reflection) over a bandwidth much wider than that which is achievable in magnetron based systems, raises the possibility of exciting multiple modes within a cavity, and thus improving heating uniformity together with system efficiency. With magnetron generators, owing to their limited bandwidth, this has not been possible.

In conclusion, commercially available, ‘intelligent’, solid-state heating systems with the means of identifying optimally matched conditions, and with the required control to excitations at the required operating frequencies, which are available at a low cost are most likely to appeal to the manufacturers and consumers.

1.3 Thesis Outline

Chapter 1 – Gives a brief overview of microwave heating systems by discussing the limitations of existing system architectures. Due to the limitations of these existing systems, an alternative form of heating (solid-state) is introduced. Research motivation considers factors hindering practical implementation of solid-state technology under variable loading conditions, that leads to high reflective states which compromise device reliability and system-heating efficiency. Whilst a circulator and a high power load are readily used in communication systems to protect the device against load mismatch conditions, their use in solid-state mass-market heating systems is not advocated due to cost and associated power losses which leads to heating inefficiency.

Chapter 2 – A brief introduction to electromagnetic wave theory along with the fundamentals of microwave heating and waveguide structures is presented. The knowledge of these basic concepts forms an important part in bringing different

technological concepts together for this research. The wave equation and the concept of wave propagation in enclosed metal structures is introduced. The wave equation is derived from Maxwell's equations and the homogeneous form of these equations with their definition is listed. Lambert's law is also included as it is used to approximate microwave power dissipation in dielectric materials. The concept of E & H field is introduced through the use of a parallel plate capacitor and a solenoid which leads to wave propagation through waveguides. The means of mode identification and excitation of modes in rectangular waveguides is also discussed.

This leads to the introduction of rectangular cavity structure which in essence is a rectangular waveguides with its ends closed. It is a multi-mode device used extensively in microwave cooking applications where the incoming waves reflect off boundary walls creating standing waves. Similarly cylindrical cavities are a form of short-circuited circular waveguides, which resonate energy in either TM or TE modes at the frequency of resonance. TE modes have no electric field in the direction of propagation and the TM mode has no magnetic field in the direction of propagation.

The energy is coupled into the waveguide through different means from where it is transferred into the cavity to heat the load. The coupling devices used are a means of transferring energy from the source to the resonator. Those considered suitable for microwave heating applications are discussed in this chapter.

Chapter 3 – A brief introduction to the fundamentals of microwave heating along with an historical overview of magnetron based microwave heating systems is presented. The need to control the heating source and the importance of a “coupling circuit” in practical implementations was recognised in these earlier systems. The ISM bands were specified and limits placed on out of band radiation leakage. The earlier struggles and success of the technology are listed together with the benefits (i.e. high power generator) and limitations (i.e. lack of control and non-uniform heating) of the magnetron source.

A historical overview of solid state heating is also presented. There are significant performance benefits of solid-state technology over the magnetron based systems as well as challenges relating to successful implementation and reliability. Solid-state architectures (through power, phase and frequency control) enable microwave heating appliances to have complex heating combinations and resolution control which helps improve cooking consistency whilst reducing cooking time. A potential use of multiple channels (antenna feeds) can help create a steady input of microwave energy into the cavity, which allow creation of various cooking profiles by directing energy into defined areas through phase shifting (steering of energy). This offers a more convenient way of combining power as well as a potential means of further control through relative phase adjustments, an area that needs further investigation.

The means of linear energy delivery into the cavity through power control (through PWM) are explored and realisation of an intelligent heating apparatus through forward and reverse power measurements is discussed. A measure of return-loss profile shows optimally matched energy absorption regions (across the frequency band). The feedback loop can be used to ensure energy is directed at the right frequencies and couples efficiently into the load.

Other potential advantages of solid-state technology (such as an accurate and stable frequency source with precise amplitude and phase control and digital signal processing which can help spread energy across the operating bandwidth) are highlighted. The availability of multi-output and phase locking synthesisers facilitates multi-source operation, with each emitting energy at the same frequency to achieve higher power levels within the cavity. Uneven heating (hot and cold spots) can be minimised by changing the relative phase (from one source to another) to alter the energy distribution such that it is continuously changing.

Solid-state sources like to operate into a matched load, and deviations from this result in a loss in performance which may also compromise device reliability. The

challenges in the form of variable loading conditions arise from changes in material dielectric properties which may stem from changes in physical properties, chemical composition and placement inside the cavity. These challenges are listed and discussed in this chapter whilst the means to overcome these limitations are presented in the proceeding chapters

Chapter 4 - A brief outline of power amplifier design concepts (modes of operation) is presented along with a discussion on their suitability for solid-state heating applications. At the heart of any amplifier design is a RF power transistor which is designed to operate over a single or a range of frequencies. Due to its internal structure and physical properties the impedance at the device plane is non-50 Ω and usually very low. In practical applications there is a requirement to match this low impedance to the system impedance (50 Ω). High power transistors designed to meet power requirements of solid-state applications have lower impedances which leads to complex and physically larger matching networks. RF matching networks design consideration (narrow band vs broadband) and concerns relating to device reliability are identified and addressed.

A typical SSPA is designed to operate under matched (50 Ω) conditions, which usually ensures a smooth transition of power from the source to the load. However the load environment in microwave heating applications is non-constant. This variable impedance environment causes a mismatch between the source and the load which gives rise to high reflective states.

Cavities and waveguides used extensively in microwave heating applications have similarities with RLC circuits. This includes energy storage in the electric & magnetic fields, energy exchange between electric & magnetic fields. When an external source is excited at the same frequency as the resonance frequency (of the RLC circuit or cavity) an EM field is generated. Owing to these similarities an equivalent circuit lumped element model is used to demonstrate approximate cavity behaviours. This model is used to study single, and two channel systems to ascertain forward and reverse power behaviours under

variable load and phase conditions. The method has limitations in that single-mode cavities are distributed resonant structures and as such cannot be represented accurately by lumped element equivalent models over a wide range of parameters.

Chapter 5 - This chapter presents a novel approach for designing high efficiency; broadband coupling structures for delivering RF generated power into a cavity. These structures are compact and can easily be integrated into solid-state microwave ovens used for heating and cooking applications. A domestic microwave oven (multi-mode rectangular cavity) has been adapted and used in the measurement set-up. The load and frequency dependent variations in the fundamental and resonant harmonic impedance environments inside the cavity have been captured and characterised to formulate and help define the requirements of a wideband coupling structure. As well as launching energy into the cavity, this structure transforms the cavity impedance to a 50-ohms load environment, which will be presented to a solid-state amplifier. Control over second harmonics is also demonstrated using this structure by successfully transforming the second harmonic impedance to short circuit.

The broadband nature of the coupling structure lends its use for an intelligent frequency hopping technique where power is delivered into the cavity at optimally matched frequency points or regions. This approach results in a highly efficient power delivery into the cavity under variable loading conditions. Compact size and simple construction makes this structure suitable for cooking and heating applications.

Transformation of cavity load impedance to 50Ω load environment without the use of complicated and physically large matching networks is demonstrated. It has been further shown that besides being broadband, the coupling structure is tolerant to variable loading conditions (0.1l-to-1.0l of water) where the return loss (S_{11}) is below -14dBs across the operating bandwidth. Importantly, the structure has the potential to match cavity load impedance points directly to the device optimal impedance identified during the device design cycle using load and source pull techniques, which can remove the need

for physically large and lossy matching elements in the PA itself. This supports the idea of completely integrating the PA and the coupling structure, which will help reduce physical size requirements.

Selecting a set of cavity reflection coefficients from within the cavity load impedance environment can start the fundamental and harmonic load transformation process. The identified cavity reflection coefficients for first and second harmonics can be transformed to transistor's optimal points. This simplifies the matching networks, improves system performance by reducing path losses and makes implementation in multi-mode systems a reality. The concept is a significant development for microwave heating and in particular isolator-less microwave heating applications where the transistor may be subjected to high VSWR conditions.

Chapter 6 - The the challenges of using SSPAs for microwave heating applications where the loading conditions are non-constant are presented. To investigate this, a cylindrical cavity has been measured and its impedance behavior characterised under variable loading conditions (different volumes of water) and temperature variations. It is demonstrated that such variations in load present different impedances at the transistor's current generator plane leading to high reflective states, typically requiring a realignment (re-positioning) of the single loop coupling structure.

An alternative coupling structure is presented that demonstrates how it is possible to accommodate these changes over a wider bandwidth (70MHz) and adapt the SSPA frequency of operation to ensure a power delivery efficiency of greater than 97%. This is explained by reflection coefficient measurements of better than -15dB across the operational bandwidth. Using this technique and methodology, a power amplifier can continue to operate into a suitably matched load. The ability to constrain the match to within a vswr of 2.:1 ensures device reliability is not compromised, and raises the possibility of reducing the cost of SSPA modules by removing the need for circulators and other associated hardware.

An approach to free-space power combining for attaining high power and efficient power delivery into a single mode cylindrical cavity is also presented. It is shown (experimentally) that for a two-port system, power combining has been successfully attained. The results for the two-port system (using a novel broadband coupling structure) show that it is possible to sweep the entire frequency band of interest in order to determine the optimum matching condition for each of the sources ensuring power efficiency (delivery into the cavity) of greater than 98 percent. This is explained by reflection coefficient measurements of better than -20dB. Using this technique and methodology both the power amplifiers continue to operate into a safe operating load. The ability to constrain the match to within 2.3:1 VSWR contours ensures that device reliability is not compromised.

Chapter 7 - The concepts and key elements used in microwave heating systems have been introduced in previous chapters, where the magnetron is identified as a high power, robust device that can tolerate reflections introduced by variable loading conditions at the expense of a shorter lifecycle, however it has a limited bandwidth (emitting microwaves at $2.45\text{GHz} \pm 10\text{ MHz}$) which means that it can only excite a limited number of modes. Measurements have shown that the modes for a loaded microwave oven are shown to be scattered over a wider than the magnetron operating bandwidth. The magnetron based technology lacks intelligence and there is no direct means of identifying and exciting frequency regions or points over which the load is matched. Direct excitation of modes outside of this bandwidth is un-realizable leading to imprecise and uncontrolled heating.

Owing to these limitations of the magnetron, solid state heating has been introduced as it promises large performance benefits. Whilst the performance benefits are clear several hurdles needed overcoming. For example, the power capability of a single RF transistor is limited in comparison to a magnetron and a multiple transistor (SSPA) combination is required to generate comparable power levels. Mounting multiple, traditional waveguide feed structures to the outer walls of a resonant cavity will increase the overall oven volume significantly, resulting in a much larger microwave oven than

those currently available. For this reason the waveguide feed structure whilst simple and realizable for single channel applications, was considered impractical for two, four or multi-channel microwave heating applications.

Besides the high-power, high-efficiency and low-cost requirements of the SSPA, a need for transferring the available power into the cavity under variable loading conditions was identified as a key performance criteria along with an ability to excite multiple modes (scattered) over the operational bandwidth. For this to happen the coupling structure needed to have an operating bandwidth that is equal to or larger than the SSPA bandwidth. This led to the development of a novel, wide-band coupling architecture (chapter 5) which has made it possible to capture optimally matched frequency points under variable loading conditions.

In order to improve SSPA efficiency, the harmonic load impedance can be precisely controlled. Presenting a near short-circuit to the device current generator plane at second harmonic frequencies can help shape the voltage and current waveforms for maximum SSPA efficiency, whilst limiting the excursions of the voltage, thus protecting it from voltage breakdown problems. Harmonic terminations are typically synthesised alongside the fundamental matching networks on a PA PCB, however circuit complexity and size constraints can make its implementation challenging. In order to simplify matching network design at PCB level, there is a potential to incorporate second harmonic tuning in the coupling structure. Whilst control over second harmonic impedance (via lumped element and small signal measurements) has been demonstrated in chapter 5, its effectiveness under large signal conditions is explored and presented by the measurement data.

Further, from a device reliability and heating perspective, SSPA's must operate into a matched load (ideally $S_{11} < -10\text{dB}$). With $S_{11} < -18\text{dB}$ over the 100MHz operating bandwidth, frequency sweep operation (to excite multiple modes) is shown not to compromise heating efficiency and device reliability. This has been demonstrated through

single point vs swept frequency measurements for a 0.325l water load. During single frequency operation greater than ninety-nine percent of available power was delivered to the cavity. Under frequency sweep operating conditions (1MHz step size) this dropped to between 96-99% due to variations in the matching conditions. In both instances the SSPA continues to operate into a match load.

Non-uniform heating in magnetron based microwave oven is attributed to travelling wave behavior and lack of control over mode selection (excitation) inside the cavity. This is demonstrated by placing the load at different locations inside the cavity. Measurements have shown that a change in the load position results in the optimally matched points to vary in frequency from their original state to a new state. These changes, whilst unrecognisable and undersirable in magnetron based systems, have been clearly identified using the proposed coupling structure. This means that an intelligent frequency hopping technique can be used to change the SSPA frequency of operation and thereby ensuring maximum power transfer into the cavity.

Heating uniformity was also characterized by monitoring surface heating pattern. A temperature profile of the exposed surface (0.325l water load) over 60 seconds' shows a uniform heating pattern with the solid-state system ($\pm 0.2^{\circ}\text{C}$). Similar measurements with a magnetron based system show a greater, 13°C temperature variation.

Chapter 8 – This chapter summarizes the important outcome from this research work and suggests further ideas and modifications for the future work.

1.4 References

- [1] Lorinczi K. (2008) The effect of health conscious trends on food consumption. University of Debrecen, Centre for Agricultural Sciences and Engineering, Debrecen, Hungary.
- [2] Albert J Forman, Magnetron Testing, The Michigan Technic
- [3] William R. Hendee Physics of Thermal Therapy, Fundamental and Clinical Applications
- [4] Z. Lukasiki, A. Kusminska-fijalkowskai, W.Nowakowski “Europe's energy efficiency requirements for household appliances”, Uniwersytet Technologiczno-Humanistyczny w Radomiu, Wydział Transportu i Elektrotechniki
- [5] Commision Delegated Regulation (EU) No 65/2014 of 1 Oct. 2013 supplementing Directive 2010/30/EU of the European Parliament and of the Council with regard to the energy labelling of domestic ovens and range hoods
- [6] Edgar RH, Osepchuk J (2001) Consumer, commercial, and industrial microwave ovens and heating systems. In: Datta AK, Anantheswaran RC (eds) Handbook of Microwave Technology for Food Applications, pp 215–277
- [7] Swain et al. 2006 Effect of continuous (intermittent) use on the power output of domestic microwave ovens, International Journal of Food Science & Technology 41(6):652 – 656
- [8] Wang et al. 2016 Dielectric properties of peanut kernels associated with microwave and radio frequency drying, Biosystems Engineering, Vol.145).
- [9] (IEC 60705, 1999),
- [10] HEECS. 2010. High efficiency electronic cooking systems. Accessed 12/09/ 2017 from http://www.eniac.eu/web/downloads/projectprofiles/call3_heecs.pdf
- [11] Vadivambal, R., and D. S. Jayas 2010. Non-uniform temperature distribution during microwave heating of foods a review. Food and Bioprocess Technology 3:161–171.
- [12] Euromonitor International. 2017. Microwaves in the United Kingdom. Accessed 12/09/2017 (<http://www.euromonitor.com/microwavesin-the-UK-report>)

- [13] Gaukel, V., T. Siebert, U. Erle 2017. Microwave-assisted drying, In: M., Regier, K., Knoerzer, H., Schubert (Eds.), *The Microwave Processing of Foods*, 2nd edition, pp. 152–178. Cambridge: Woodhead Publishing.
- [14] ONSUK. 2017. Percentage of households with microwave ovens in the United Kingdom (UK) from 1994 to 2014. Office for National Statistics, UK. Accessed 14/09/2017 from <https://www.statista.com/statistics/289155/household-microwave-penetration-in-the-uk/>
- [15] Osepchuk, J. 2013. Microwave ovens: an overview (Revised edition). Accessed 18/11/2017 from <http://impi.org/microwave-ovens-an-overview-2013/>
- [16] HEECS. 2010. High efficiency electronic cooking systems. Accessed 12/09/2017 from http://www.eniac.eu/web/downloads/projectprofiles/call3_heecs.pdf
- [17] Kim, S., E. Eriksson, and K. Lee 1996. Screening LCA of a microwave oven. Proceedings of SETAC Case Study Symposium, December, Brussels, Belgium,
- [18] H. K. Jenny, “Electron tubes—A technology forecast,” *Technology Trend (75CH1005-8 TFA)*, IEEE, NY (1975)
- [19] Bows, J. R. 1999. Variable frequency microwave heating of food. *The Journal of Microwave Power and Electromagnetic Energy: A Publication of the International Microwave Power Institute* 34(4): 227-238. ;
- [20] Antonio and Dean 2005: Comparison of linear and non-linear sweep rate regimes in variable frequency microwae technique for uniform heating in material processing, *Jounal of Materials Preprocessing Technology*, Vol.168
- [21] Yang, H. W. and S. Gunasekaran. 2004. Comparison of temperature distribution in modelfood cylinders based on Maxwell's equations and Lambert's law during pulsedmicrowave heating. *Journal of Food Engineering* 64(4): 445-453
Gunasekaran and Yang 2007;
- [22] Dominguez-Tortajada et al. 2007 ‘Optimisation of electric field uniformity in microwave heating systems by means of multi-feeding and genetic algorithms;
- [23] Liao et al. 2016; A phase-shifting method for improving the heating uniformity of microwave processing materials. *Journal of Hazardous Materials*, Vol.322,

- [24] Bae et al. 2017. A continuous Power-Controlled Microwave Belt Drier Improving Heating Uniformity, *IEEE Microwave and Wireless Components Letters*, Vol 27.
- [25] Yakovlev, V. 2016. Computer modelling in the development of mechanisms of control over microwave heating in solid-state energy systems. *AMPERE Newsletter* 89:18–21.
- [26] Korpas, P., A. Wieckowski, M. Kryszicki, and M. Celuch 2013. Application study of new solid-state high-power microwave sources for efficiency improvement of commercial domestic ovens. *Proceedings, 47th Microwave Power Symposium, Rhode Island. (Korpas et al. 2013).*
- [27] J. C. Atuonwu & S. A. Tassou (2018): Energy issues in microwave food processing: A review of developments and the enabling potentials of solid-state power delivery, *Critical Reviews in Food Science and Nutrition*, DOI: 10.1080/10408398.2017.1408564
- [28] Wesson, R. 2016. Solid-state-microwave cooking. *AMPERE-Newsletter* 89:27–32.
- [29] J. C. Atuonwu & S. A. Tassou (2018): Energy issues in microwave food processing: A review of developments and the enabling potentials of solid-state power delivery, *Critical Reviews in Food Science and Nutrition*, DOI: 10.1080/10408398.2017.1408564
- [30] <https://rfenergy.org>.
- [31] <https://www.electronicshobby.com/news/design/the-future-of-microwave-cooking-is-solid-state-2016-01/>
- [32] <https://www.digikey.co.uk/en/product-highlight/i/infineon/microwave-oven>
- [33] <https://www.nxp.com › products › rf-power › rf-cooking:RF-COOKING>
- [34] <https://www.macom.com › applications › rf-energy › industrial-cooking>
- [35] <https://www.ampleon.com › applications › rf-energy › solid-state-cooking>
- [36] <http://www.thehomantra.com/kitchen/appliances>
- [37] https://www.thermex-thermatron.com/2015/11/FailureOfMagnetron_v3.pdf
- [38] <https://www.nxp.com/docs/en/white-paper/RFPLASTICWP.pdf>
- [39] K.K. Chang, Solid-state microwave heating apparatus, US patent 3,691,338.

CHAPTER 2 THEORY

2.0 Introduction

In this chapter a brief introduction to electromagnetic wave theory, along with the fundamentals of microwave heating and wave guide structures that are relevant to the project, are presented. The knowledge of these basic concepts forms an important part in bringing different technological aspects together for this research, so have been included here in some detail. The wave equation and the concept of wave propagation in enclosed metal structures is introduced. The wave equation is derived from Maxwell's equations and the homogeneous form of these equations with their definitions is listed. Lamberts law is also included as it is used to approximate microwave power dissipation in dielectric materials. The concept of E & H field is introduced through the use of a parallel plate capacitor and a solenoid which leads to wave propagation through waveguides. The means of mode identification and excitation of these modes in rectangular waveguides is briefly introduced.

This leads to the introduction a of rectangular cavity structure which in essence is a rectangular waveguide with its ends closed. It is a multi-mode device used extensively in microwave cooking and heating related applications where the incoming waves reflect off boundary walls creating standing wave patterns. Similarly cylindrical cavities are a form of short-circuited circular waveguides, which radiate energy in either TM or TE modes at the frequency of resonance. The fundamental concept of rectangular waveguides and circular cavities are similar.

The energy is coupled into the waveguide through different means, from where it is transferred into the cavity to heat the load. The coupling devices are a means of transferring energy from the source to the resonator. Those considered suitable for microwave heating applications are discussed in this chapter.

2.1 Electromagnetic Radiation

Electromagnetic radiation is a form of radiation in which the electric and magnetic fields vary simultaneously. This includes elements of the electromagnetic spectrum which contains radio waves, microwaves, infrared, visible light, ultraviolet, x rays and gamma rays. The placement of these elements inside the electromagnetic spectrum, according to their wavelengths, types of radiation and the sources responsible for producing the radiations, are shown in Fig.2.1. The domestic microwave oven is listed at a frequency of 2.45 GHz within this spectrum.

Electromagnetic radiation travels in waves and the measurement of wavelength helps identify the type of radiation being emitted. A wave is described as a disturbance or an oscillation accompanied by a transfer of energy that travels through space or dielectric mediums. The wave motion therefore being responsible for transferring energy from one place to another. A wave can be *transverse* or *longitudinal* and the speed of the wave is determined by the medium it travels through.

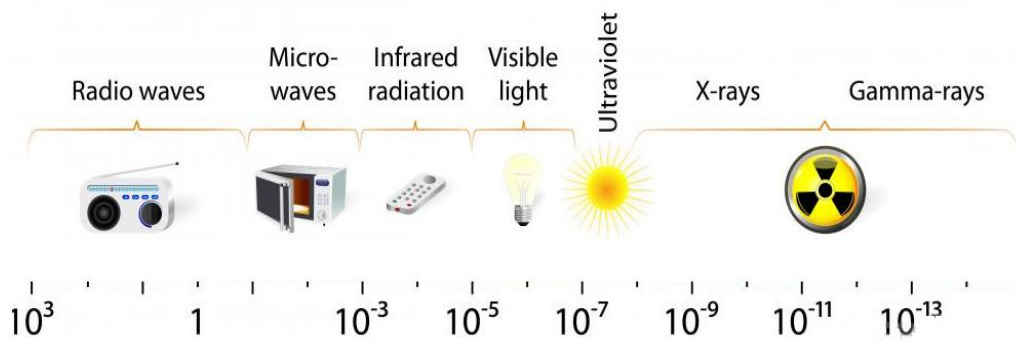


Fig. 2.1: The placement of various elements within the electromagnetic spectrum [14].

2.2 Electromagnetic Waves:

An electromagnetic wave is as an electric and magnetic disturbance that propagates through space (or vacuum) at the speed of light. The electric charges produce the electric fields \vec{E} (Coulomb's law) and the electric currents produce the magnetic fields \vec{B} (Ampere's law) as shown in Fig.2.2 (a & b) & c. An electromagnetic wave therefore is a combination of electric and magnetic fields that vibrate together in space and time in a synchronous fashion as shown in Fig. 2.2c. Furthermore the electric field \vec{E} and the magnetic field \vec{B} are always perpendicular to one another and to the motion of the wave. A poynting vector represents the directional energy flux (the energy transfer per unit per unit time) area of an electromagnetic field.

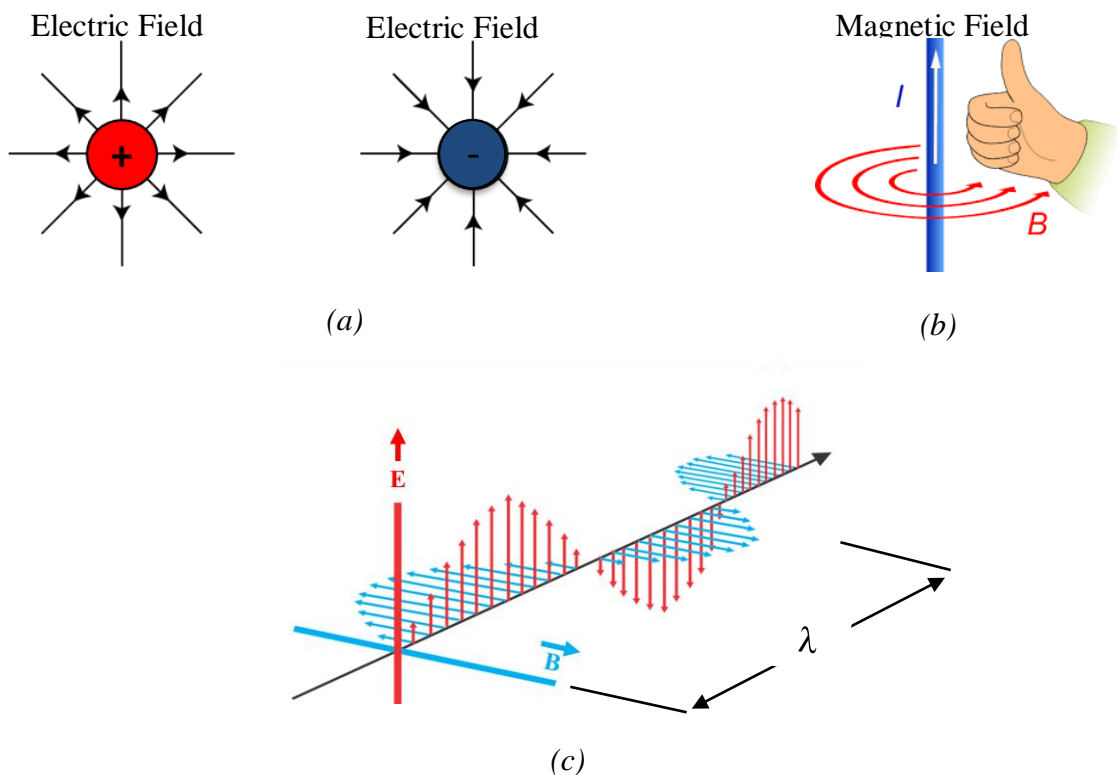


Fig. 2.2 (a): Electric field of a positive & negative charge (b) magnetic field induced by current flow in a wire (c) Electric and Magnetic fields propagating through space [15-17]

2.3 Wave Propagation

As discussed in earlier sections, microwave radiation is a form of energy which is transported via electromagnetic waves. These electromagnetic waves can propagate through a vacuum (are not reliant on any medium for transfer of energy) and have their electric \vec{E} and magnetic \vec{B} field components characterised by frequency, velocity and field strength. The fundamental components of an oscillatory wave are frequency and the wavelength. The relationship between frequency and the wavelength is presented by eqn.2-1.

$$\lambda = \frac{c}{f} \quad (2.1)$$

Where:

c = Speed of light in the medium (m/s),

f = Frequency of the wave (Hz),

λ = Wavelength (m).

The electric and magnetic field components vary in time and space when they propagate through a medium as shown in Fig.2.3. The propagation of an electromagnetic wave can be described by considering a point source that emits radiation spherically in space. As the wave propagates through space its intensity weakens. This is due to losses, absorption in the dielectric medium and variations in frequency. The energy spreads with increasing distance away from the point source and the intensity reduces at a rate that is an inverse square of the distance. The power per unit area at a distance, $d = S = \frac{P_t}{4\pi} \left(\frac{1}{d^2}\right)$ and the total free space path loss, $FSPL = \frac{P_t}{P_r} = \left[\frac{4\pi df}{c}\right]^2$.

When a wave travels from one medium to another, e.g., cavity into a food source, its speed and wavelengths reduce whilst the frequency remains constant. Typical wavelengths at centre frequencies for ISM bands (886-906 MHz & 2400-2500 MHz) dedicated for microwave cooking and heating applications are of the order of 0.33m (λ_{900} - MHz) and 0.122m (λ_{2450} MHz).

The absorption of microwave energy is determined by the material's attenuation factor (α'), and the penetration depth (z) below the surface (eqns 2.2-2.3). The electric field strength below the surface is inversely proportional to the attenuation factor. The microwave energy penetration depth is greater at 900 MHz than at 2450 MHz.

$$\alpha' = \frac{2\pi}{\lambda} \left[\frac{\varepsilon'}{2} (\sqrt{1 + \tan^2 \delta} - 1) \right]^{\frac{1}{2}} \quad (2.2)$$

$$z = \frac{2\pi}{\lambda} \left[\frac{2}{\varepsilon' (\sqrt{1 + \tan^2 \delta} - 1)} \right]^{\frac{1}{2}} \quad (2.3)$$

Where:

ε' = Relative dielectric constant

$\tan \delta$ = loss tangent

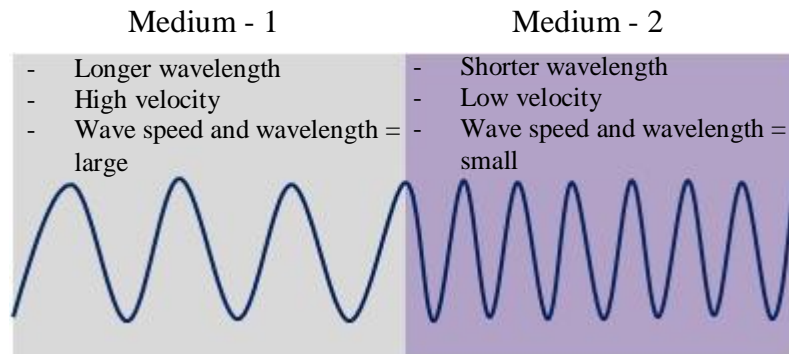


Fig. 2.3: Wave Propagation from low-density medium to a high-density medium [22]

The penetration depth for microwave power is defined in two ways:-

(1). Distance from the surface of a dielectric material to where the power has reduced to $(\frac{1}{e})$ of the incident power. Lamberts expressions for power absorption are readily used to express this relationship (eqn's.2.4–2.6).

$$\frac{P_d}{P_i} = \frac{1}{e} \quad (2.4)$$

$$2\alpha'd = 1 \quad (2.5)$$

$$d = \frac{1}{2\alpha'} \quad (2.6)$$

(2). The distance from the surface of a material where the power is one-half of the incident power. This is known as half-power depth (eqn's.2.7–2.9).

$$\frac{P_d}{P_i} = \frac{1}{2} \quad (2.7)$$

$$e^{-2\alpha'd} = \frac{1}{2} \quad (2.8)$$

$$d = \frac{0.347}{\alpha'} \quad (2.9)$$

Where:

- P_i = incident power
- P_d = power at penetration depth
- d = penetration depth
- α' = attenuation factor
- e = mathematical constant ($\frac{1}{e} \approx 0.37$)

2.4 Maxwell's Equations

Electromagnetic waves can also be described by the wave equation. Derived from Maxwell's first order differential equations (eqn's.2.10-2.13), the wave equation is an important partial differential equation describing the propagation of electromagnetic waves as they travel through a medium or in a vacuum. The homogeneous form of the equations written in terms of the electric field \vec{E} and magnetic field \vec{B} is given by eqn's-2.14 to eqn.2.17.

$$\nabla \cdot \mathbf{D} = \rho_v \quad (\text{Gauss's Law}) \quad (2.10)$$

$$\nabla \times \mathbf{E} = -\frac{\partial \mathbf{B}}{\partial t} \quad (\text{Faraday' Law}) \quad (2.11)$$

$$\nabla \cdot \mathbf{B} = 0 \quad (\text{Gauss's Law for magnetism}) \quad (2.12)$$

$$\nabla \times \mathbf{B} = \mu_0 \epsilon_0 \frac{\partial \mathbf{E}}{\partial t} \quad (\text{Ampere's Law}) \quad (2.13)$$

$$(v_{\text{ph}}^2 \nabla^2 - \frac{\partial^2}{\partial t^2}) \mathbf{E} = 0 \quad (2.14)$$

$$(v_{\text{ph}}^2 \nabla^2 - \frac{\partial^2}{\partial t^2}) \mathbf{B} = 0 \quad (2.15)$$

$$\frac{1}{c_0^2} \frac{\partial^2 \mathbf{E}}{\partial t^2} - \nabla^2 \mathbf{E} = 0 \quad (2.16)$$

$$\frac{1}{c_0^2} \frac{\partial^2 \mathbf{B}}{\partial t^2} - \nabla^2 \mathbf{B} = 0 \quad (2.17)$$

Where:

$$v_{\text{ph}} = \frac{1}{\sqrt{\mu\epsilon}} \mu = \text{Permeability}$$

$$\epsilon = \text{Permittivity}$$

$$c_0 = \frac{1}{\sqrt{\mu_0\epsilon_0}} \cong 3 \times 10^8 \text{ ms}^{-1}$$

The first of Maxwell's equation's (2.10) is referred to as Gauss's law. It describes the pattern and size of electric field around electric charges. The total amount of charge inside a given volume being proportional to the electric flux (D) exiting the surface. Gauss' law can be summarised by the observation that the D and E field lines diverge away from positive and towards negative charges. The divergence of the D field over a given region is equal to the total amount of charge in that region.

The second of Maxwell's equations (2.11) is referred to as Faraday's law. It states that the voltage induced in a closed loop is proportional to the rate of change of the magnetic flux around the loop. In the absence of current, no magnetic flux can be induced. Faraday's law has a symmetry where an electric current gives rise to a magnetic field and a changing magnetic field gives rise to an electric field circulating around it.

The third of Maxwell's equations (2.12) is referred to as Gauss' law of magnetism. It states that in the absence of magnetic monopoles (North and South Poles), the total magnetic flux through a closed surface is zero. The divergence of the magnetic flux density (B) is zero. In instances where the magnetic monopoles do not exist and the

divergence of B or H fields through a volume is zero, magnetic fields flow in a closed loop away from the magnetic dipoles. This is also true of plane waves.

The fourth of Maxwell's equations (2.13) is referred to as Ampere's law. It states that the magnetic field induced around a closed loop is proportional to the rate of change of electric field that the loop encompasses

2.5 Electric Field:

Electric field (created by electric charges and by time varying magnetic fields) is a region around an electrically charged object, where a force is exerted on other charged objects. The energy per unit volume in an electric field can be derived by considering a parallel plates capacitor. This has a cross sectional area A separated by a distance d as shown in Fig 2.4. The application of a potential difference results in an electric field being generated across the two plates.

The value of capacitance is determined by the surface area A of the plates, the separation distance d between them and the ability to store charge Q , (eqns.2.18-2.19). The electric field is proportional to the area of the plates divided by the separation distance. In free space this value is represented by equation eqn.2.19. The energy stored (Es) in the capacitor and the electric field (E) generated across the plates can be derived using eqn's.2.20 and eqn.2.21 respectively whereas the energy per unit volume can be calculated by using eqn.2.23.

$$C = \frac{Q}{V} \quad (2.18)$$

$$C = \epsilon_0 \frac{A}{d} \quad (2.19)$$

$$\text{Energy Stored, } E_s = \frac{CV^2}{2} \quad (2.20)$$

$$\text{Electric Field, } E = \frac{V}{d} \quad (2.21)$$

$$Es = \frac{\epsilon_0 A}{2 d} E^2 d^2 \qquad Es = \frac{\epsilon_0}{2} A. d. E^2 \qquad (2.22)$$

$$\text{Energy stored per unit volume} = u_E = \frac{\epsilon_0}{2} E^2 \qquad (2.23)$$

Where:

Q = Amount of charge per unit volt

V = Potential Difference

A = Cross-sectional area of the plates

d = Separation distance

ϵ_0 = Permittivity of free space

A. d = Volume

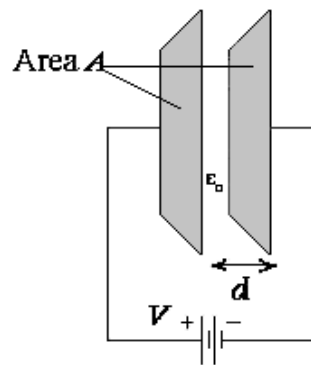


Fig. 2.4: Electric field distribution between two parallel plates.

2.6 Magnetic Field

Magnetic field is a pictorial representation of the magnetic force distribution in a given space. It can be described as a vector field where each vector has a magnitude, the size of which is dependent on the strength of the magnetic force. From the field lines shown in Fig.2.5, it can be ascertained that:

1. The field lines do not cross each other, (the direction of field is indicated by arrowheads).

2. The lines are in close proximity to each other where the magnetic field is strongest, (the density of the field lines is indicative of the strength of the field).
3. The lines form a closed loop by continuously rotating inside the cavity

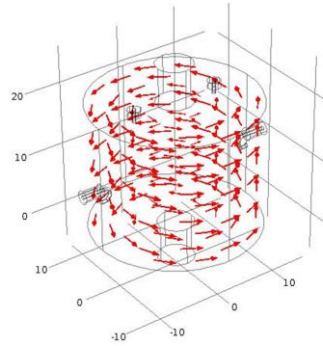


Fig. 2.5: Magnetic field distribution in a cylindrical cavity.

The energy per unit volume in a magnetic field can be derived by considering current flow in a hollow pipe of length L , and cross sectional area A , as shown in Fig.2.6. The inductance (L), magnetic field (B) and magnetic flux (Φ) of the solenoid inductor can be calculated using eqn.2-24 to 2-26. The energy stored per unit volume is given by eqn.2-27

$$\text{Inductance, } L = \mu_0 n^2 A l \quad (2.24)$$

$$\text{Magnetic Field, } B = \mu_0 n I \quad (2.25)$$

Where:

μ_0 = the permeability of free space

n = number of turn per unit length

l = Length of solenoid

$$\text{Potential energy, } U = \frac{1}{2} L I^2 = \frac{1}{2\mu_0} B^2 (A l) \quad (2.26)$$

$$\text{Energy density of a magnetic field} = u_B = \frac{U}{Al} = \frac{1}{2\mu_0} B^2 = \frac{\epsilon_0}{2} E^2 \quad (2.27)$$

In an EM wave, the energy per unit volume in a magnetic field is exactly the same as the energy per unit volume in an electric field. This is shown through derivation of simple energy relationships for a *parallel plate capacitor* and a *solenoid inductor*.

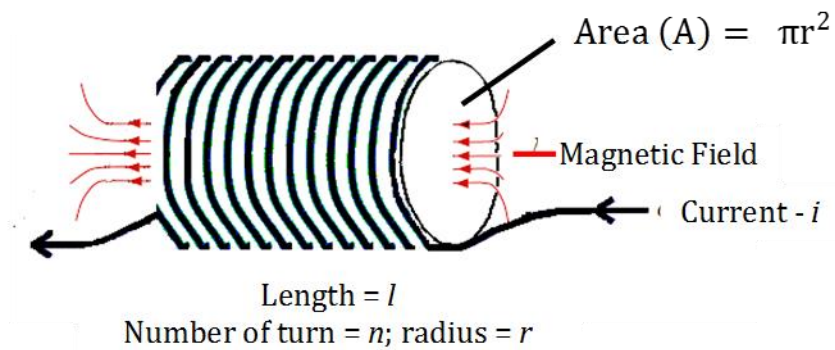


Fig. 2.6: A solenoid inductor of length l , area A and n number of turns

2.7 Lambert's Law vs Maxwell's Equations

Lambert's law is an approximation used to determine the microwave power dissipation in dielectric materials eqn.2.28. It assumes an exponential decay of microwave energy as it propagates through dielectric materials.

$$P(x) = P_0 e^{-2\beta x} \quad (2.28)$$

Where:

$P(x)$ = Power dissipation value at depth x

x = the depth from the surface (m),

P_0 = Incident power at the surface

β = Attenuation Constant (m^{-1})

Studies comparing the validity of Lambert's law with Maxwell's equations [21] have concluded that, whilst Lambert's law is valid for infinitely thick loads, it offers a poor approximation and is of limited use in practical applications. In Lambert's law, electric field distribution inside a food material is not required to calculate the power dissipation term. This is contrary to Maxwell's equations, where electric field distributions are required. The main limitations of Lambert's law is the assumption that microwave energy is one-dimensional, standing waves are not taken into account.

2.8 Waveguides

Waveguide structures are designed and fabricated using metal or dielectric substrates. They transfer power (electromagnetic radiation) from a source to the load. The energy of radiation is confined within the physical boundaries of the structure. This is in contrast to the broadcast world where the antennas radiate energy in all directions, some of which may be wasted as it spreads.

As a wave propagates along a rectangular waveguide it can be seen to be travelling in the direction of the z plane (Fig.2.7). The wave is always reflected off the metal boundary walls. It does not travel outside of the waveguide and its angle of incident is equal to the angle of reflection. An electromagnetic wave travelling in a waveguide experiences less attenuation losses compared to a transmission line. The total wave energy can be represented by eqn.2.29

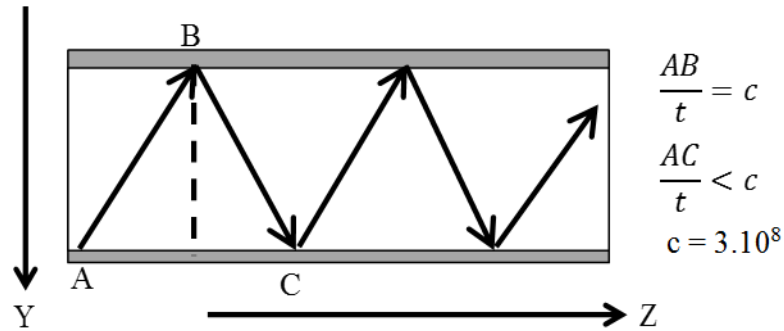
$$E_r = E_y \cdot \sin(kx - \omega t) \cdot \sin(k_x x) \quad (2.29)$$

Where:

$E_y \sin(kx - \omega t)$ = wave oscillating in y direction

$\sin(k_x x)$ = Standing wave

k = wavenumber = $2\pi/\lambda$



(a)

Fig. 2.7 EM Wave propagation in a rectangular waveguide

A standing wave of half a wavelength, $\lambda/2$ confined within a “boundary condition” of two metals walls, must have its E fields at both ends equals to zero. This suggests that an integral number of half wavelengths must fit inside the distance a (Fig.2.8).

In an enclosed metal structure, wave propagation can be characterized by reflections from the inner conducting walls. In TE mode there is no electric field flow in the direction of propagation. Similarly, in TM mode there is no magnetic field in the direction of propagation. The dimensions of the cross section are engineered such that the waveguide operates with a single mode of operation TE_{10} . In order to transmit multiple frequencies simultaneously, waveguides do not require filters to separate them, instead propagation in different modes is used.

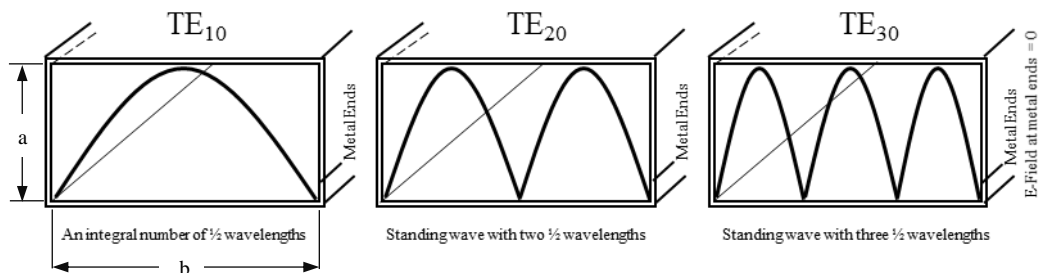


Fig. 2.8 An integral number of 1/2 wavelengths in a waveguide

The cut off frequency (eqn.2.30-2.32) of a waveguide is defined as “the frequency below which the signal cannot propagate”. At and below the cut-off frequency, energy is dissipated as heat in the walls of the waveguide. The resulting *evanescent wave* has its amplitude decaying exponentially along the waveguide. In order for the wave to propagate, the waveguides are operated at a frequency, which is above their respective TE or TM cut off frequency

$$f_c = \frac{c}{2b} \quad (2.30)$$

$$(f_c)_{mn} = \frac{1}{2\pi\sqrt{\mu\epsilon}} \sqrt{\left(\frac{m\pi}{a}\right)^2 + \left(\frac{n\pi}{b}\right)^2} \quad [\text{Hz}] \quad (2.31)$$

$$(\lambda_c)_{mn} = \frac{2}{\sqrt{\left(\frac{m}{a}\right)^2 + \left(\frac{n}{b}\right)^2}} = [\text{m}] \quad (2.32)$$

Where:

f_c = cut off frequency

$(f_c)_{mn}$ = cut off frequency

$(\lambda_c)_{mn}$ = minimum wavelength

c = speed of light

b = inner width of the waveguide

2.9 Modes of Propagation

When wave dimensions are short or irregular, the modes are not allowed to develop fully. If a TE wave has ‘ m ’ half wavelengths in ‘ a ’ direction and ‘ n ’ wavelengths in ‘ b ’ direction, than the wave is said to be in a TE_{mn} mode. Mode type(s) can be determined from the number of field variations (horizontal and vertical directions) as shown in Fig. 2.9. Definitions and conditions for mode propagation are listed in table 2.1.

Rectangular waveguides are one of the earliest types of transmission lines and have been used extensively in microwave cooking and heating applications. A rectangular waveguide supports both TE and TM modes but does not support TEM waves, due to the fact that there is only a single conductor in the waveguide. The energy generated from a

microwave source is transferred (via a waveguide) to a chamber generally referred to as the cavity; of which there are two standard types, rectangular and cylindrical.

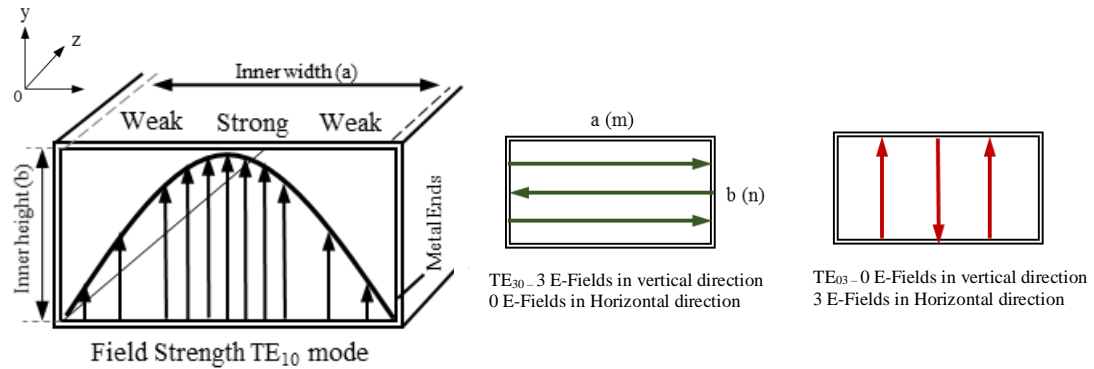


Fig. 2.9 Examples of TE_{mn} – voltage and TM_{mn} – current modes in rectangular waveguides;

Table 2.1 - Checking of modes in rectangular waveguides

TM_{10}	TM_{01}	TM_{11}	TM_{21}	TM_{12}	TM_{22}
TE_{10}	TE_{01}	TE_{11}	TE_{21}	TE_{12}	TE_{22}
- $TM_{10} - TM_{01}$ modes are not possible in rectangular waveguides – evanescent modes		<ul style="list-style-type: none"> - Only TE or TM modes can propagate in rectangular waveguides - Same cut off frequency and wavelength - Check for TE_{10}, TE_{01} and TE_{11} modes – if these are not present than other modes will not be possible 			
- Degenerate Mode		<ul style="list-style-type: none"> - Two modes are considered to be degenerate when they share the same resonant frequency – a rectangular cavity with dimensions a & b; where a=b; will have a TE_{43} mode that is equal to TE_{34} mode – same cut off frequency. 			
- Dominant Mode		<ul style="list-style-type: none"> - Mode with the lowest cut off frequency – TE_{10} where a = b; two dominant modes can exist 			
- Conditions for Propagation		<ul style="list-style-type: none"> - $\lambda_c > \lambda_0$ - λ_c = cut off wavelength - λ_0 = operating wavelength - $\lambda_c = \frac{2ab}{\sqrt{m^2b^2 + na^2}}$ - $\lambda_c_{TE_{10}} = 2a$ - $f_c = \frac{c}{2} \sqrt{\left(\frac{m}{a}\right)^2 + \left(\frac{n}{b}\right)^2}$ - $f_{c_{TE_{10}}} = \frac{c}{2a}$ 			

2.10 Rectangular Cavity

Domestic microwave oven consists of a generator (magnetron), an applicator (rectangular cavity where the field interacts with the load) and a transmission medium (waveguide for delivering microwave energy into the cavity). The temperature distributions within the food is related to the distribution of electric fields within the cavity. The cavity, therefore, is a critical part of microwave heating and the type of cavity used depends on the load type. Single mode cavities are used in applications where the field needs to be concentrated over a specific region, whereas multi-mode cavities are used for heating larger loads or a batch of loads.

A rectangular cavity (Fig.2.10 below), in essence, is a rectangular waveguide with its ends closed. It's ability to sustain multiple oscillations (modes) means it is extensively used in microwave cooking and heating related applications. This is where the incoming waves reflect of boundary walls creating standing waves.

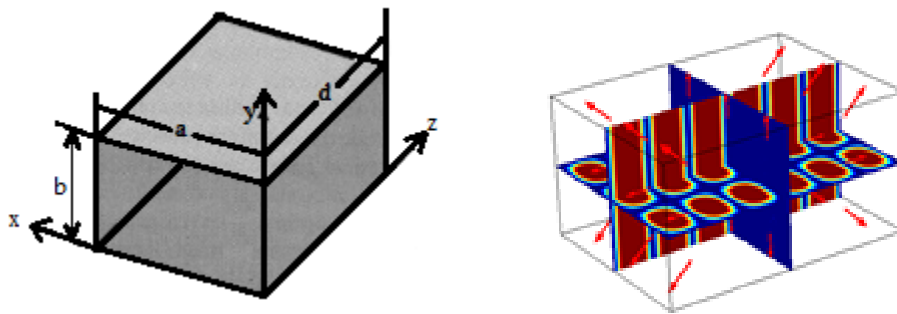


Fig.2.10. Rectangular Cavity – modes inside a rectangular

For transverse magnetic (TM) wave the wave equations are listed below:

$$E_z = E_0 \sin(\beta_x x) \sin(\beta_y y) (e^{-j\beta_z z} + \rho e^{j\beta_z z}) \quad (2.33)$$

$$E_x = \frac{-j\beta_x \beta_z}{\beta_x^2 + \beta_y^2} E_0 \cos(\beta_x x) \sin(\beta_y y) (e^{-j\beta_z z} + \rho e^{j\beta_z z}) \quad (2.34)$$

$$E_y = \frac{-j\beta_y \beta_z}{\beta_x^2 + \beta_y^2} E_0 \sin(\beta_x x) \cos(\beta_y y) (e^{-j\beta_z z} + \rho e^{j\beta_z z}) \quad (2.35)$$

Where:

sin - terms indicate direction of field is parallel to the direction of propagation

cos - terms indicate direction of field in perpendicular to the direction of propagation

In order to satisfy the boundary conditions, $E_x(z = 0) = E_y(z = 0)$, $\rho = 1$ the new expressions for E_z , E_x and E_y becomes:

$$E_z = 2E_0 \sin(\beta_x x) \cos(\beta_y y) \cos(\beta_z z) \quad (2.36)$$

$$E_x = \frac{-2\beta_x \beta_z}{\beta_x^2 + \beta_y^2} E_0 \cos(\beta_x x) \sin(\beta_y y) \sin(\beta_z z) \quad (2.37)$$

$$E_y = \frac{-2\beta_y \beta_z}{\beta_x^2 + \beta_y^2} E_0 \sin(\beta_x x) \cos(\beta_y y) \sin(\beta_z z) \quad (2.38)$$

Furthermore when $E_x(z = -d) = E_y(z = -d) = 0$, it implies that

$$\beta_x = \frac{p\pi}{d}, \text{ for } p = 0, 1, 2, 3, \dots \quad (2.39)$$

The TM mode in a cavity is classified as TM_{mnp} ; where p can be zero whilst $E_z \neq 0$.

$$\omega^2 \mu \epsilon = \beta_x^2 + \beta_y^2 + \beta_z^2 = \left(\frac{m\pi}{a}\right)^2 + \left(\frac{n\pi}{b}\right)^2 + \left(\frac{p\pi}{d}\right)^2 \quad (2.40)$$

For given values of m , n and p only a single frequency can satisfy the above equation. This frequency is referred to as the *cavity resonant* frequency as only at this frequency the cavity can sustain free oscillations. At all other frequencies the fields add destructively and it becomes difficult to sustain free oscillations. The resonant frequency for a TM_{mnp} is given by the equation below:

$$\omega_{mnp} = \frac{1}{\sqrt{\mu \epsilon}} \sqrt{\left(\frac{m\pi}{a}\right)^2 + \left(\frac{n\pi}{b}\right)^2 + \left(\frac{p\pi}{d}\right)^2} \quad (2.41)$$

Similar expressions can be derived for a transverse electric (TE) mode:

$$H_z = H_0 \cos(\beta_z x) \cos(\beta_y y) \sin(\beta_z z) \quad (2.42)$$

$$H_x = \frac{j\omega\mu\beta_y}{\beta_z^2 + \beta_y^2} H_0 \cos(\beta_z x) \sin(\beta_y y) \sin(\beta_z z) \quad (2.43)$$

$$H_y = \frac{-j\omega\mu\beta_z}{\beta_x^2 + \beta_y^2} H_0 \sin(\beta_z x) \cos(\beta_y y) \sin(\beta_z z) \quad (2.44)$$

Where:

cos - terms indicate direction of field is parallel to the direction of propagation

sin - terms indicate direction of field is perpendicular to the direction of propagation

When $p = 0$, $H_z = 0$, TE_{mn0} mode does not exist and the boundary conditions require that;

$$\beta_x = \frac{p\pi}{a}, \beta_y = \frac{p\pi}{b} \text{ and } \beta_z = \frac{p\pi}{d}$$

TE_{0np} or TE_{m0p} modes at resonant frequency can be calculated from the equation [2.33-2.45], however in instances where $a > b > d$, the lowest resonant mode occurs at TM_{110} and can be calculated using the equation below; where $E_z \neq 0$, $H_x \neq 0$, $H_y \neq 0$, and $E_x = E_y = 0$

$$\omega_{110} = \frac{1}{\sqrt{\mu\epsilon}} \sqrt{\left(\frac{\pi}{a}\right)^2 + \left(\frac{\pi}{b}\right)^2} \quad (2.45)$$

2.11 Cylindrical Cavity

Cylindrical cavities are a form of short-circuited circular waveguides, which radiate energy in either TM or TE modes at the frequency of resonance. The fundamental concept of cylindrical waveguides and circular cavities are similar. Fig. 2.11 below shows an illustration of a cylindrical cavity.

The electric and magnetic fields within the cavity resonator contribute to the total energy of the electric and magnetic fields stored within the cylindrical chamber. Available power is dissipated in metal walls of the cavity resonator as well as in the dielectric material, the load. The level of power absorption by the load is dependent on the material's dielectric properties. A change in the materials dielectric properties will affect the resonant frequency and the Q-value. The setting up of TE and TM modes has an influence on the dimensions, resonant frequencies and the Q-values.

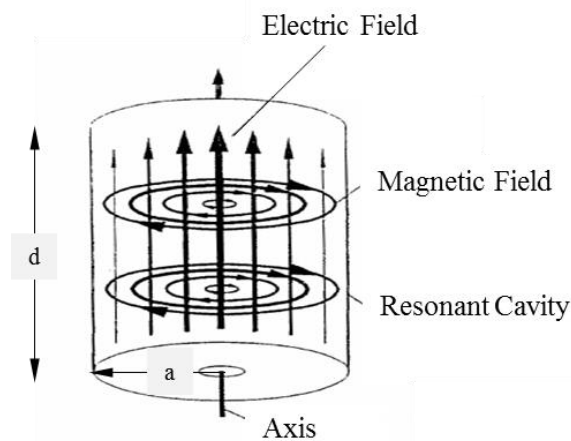


Fig. 2.11 Cylindrical Cavity Resonator, Electric and magnetic field components inside a cylindrical cavity.

In order to heat the load inside the resonant cavity, power needs to be coupled by means of a coupling device. The energy is transmitted from source to the cavity through the coupling structure. The form and implementation of the structure vary depending on which mode (TE or TM) is being excited. The propagation constant of a TM_{nm} mode can be calculated using the equation below:

$$\beta_{nm} = \sqrt{k^2 - \left(\frac{p_{nm}}{a}\right)^2} \quad (2.46)$$

Where:

k = wave number of the resonant wave

a = radius of the cylindrical cavity resonator

The resonance frequency of a cylindrical cavity can be determined from its physical dimensions and the material it is made from, as illustrated in the equation below:

$$f_{mnp} = \frac{c}{2\pi\sqrt{\mu_r \epsilon_r}} \sqrt{\left(\frac{P_{nm}}{a}\right)^2 + \left(\frac{p\pi}{d}\right)^2} \quad (2.47)$$

Where:

f_{mnl} = frequency of the cylindrical cavity resonator

c = the speed of light

μ_r = Permittivity of the filled material inside the cylindrical cavity resonator

ϵ_r = Permeability of the filled material inside the cylindrical cavity resonator

d = the height of the cylindrical cavity resonator

The dominant mode referred to as TM_{mnl} occur at TM_{010} (short cylinders) and TE_{111} (tall cylinders) [1]. This is the mode at which the magnetic field is perpendicular to the electric field whilst being parallel to the cavity cylindrical dimensions. The density of the magnetic field is concentrated at the centre, becoming less dense towards the boundary edges.

The quality factor (Q-factor) is an important parameter in determining the quality of cavity resonators. A high Q-value is indicative of accuracy and the narrow bandwidth of the cavity resonator. This is generally listed in two common forms, unloaded Q-value and loaded Q-value. An unloaded Q-value (Q_0) is the value measured in the absence of any loads (inside the cavity) and is related to the conductivity of the material from which the cavity has been constructed.

$$Q_0 = \left(\frac{1}{Q_c} + \frac{1}{Q_d}\right)^{-1} \quad (2.48)$$

Where:

Q_c = Q-value of conductive boundary all

Q_d = Q-value of the filled material

$$Q_0 = Q_c = \frac{2V}{s \sqrt{\frac{2}{\omega \mu \sigma}}} \quad (2.49)$$

Where:

V = volume of the cavity resonator

S = the surface area of the cavity resonator

σ = the conductivity of the metal wall

In practical applications, the cavity resonator is filled with a load, which dampens the Q-value. The unloaded and loaded Q values of a cavity resonator connected to an external circuit (represented by lumped elements R, L, C) can be calculated as shown:

$$\frac{1}{Q_L} = \frac{1}{Q_0} + \frac{1}{Q_e} \quad (2.50)$$

$$\text{The unloaded } Q = Q_0 = \frac{R}{\omega_0 L} \quad (2.51)$$

$$\text{The external } Q = Q_e = \frac{R_L}{\omega_0 L_L} \quad (2.52)$$

2.12 Coupling Structures

In domestic microwave ovens the energy is traditionally coupled from the magnetron into the waveguide through an aperture (iris), which can vary in size and shape to suit impedance match requirements. The energy is then transferred from the waveguide, via a coupling device, into the cavity where it heats the load. The coupling device [10-12] is therefore a means of transferring energy from the source to the resonant cavity. Those considered suitable for microwave heating applications are discussed briefly in this section.

2.12.1 Coupling Slots

The hole (slot) in the wall of a waveguide is a means through which energy can escape or enter a waveguide structure. Coupling through one or more slots is an accepted means of feeding energy from a waveguide to cavity resonators. The coupling slots used with waveguide structures are of two distinct types; *Electric and Magnetic*. The exact type can be determined from its orientation with respect to the field. The slots are fabricated such that the tangential magnetic or normal electric fields are able to penetrate the aperture and couple to the resonance mode of the waveguide. The electric and magnetic fields are continuously changing with time. The physical orientation of the coupling structure must be such that its modes have a coupled field component.

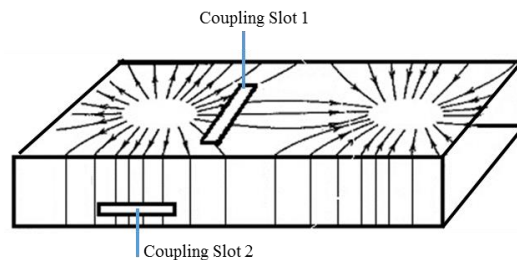


Fig. 2.12: Slot coupling and current flow in a waveguide walls for a dominant mode [21]

When coupling does take place, it is either because electric field lines (that would have been terminated by a wall) enter the cavity or a second waveguide. Alternatively the placement of a slot interrupts the flow of wall current and a magnetic field is set up which extends into the cavity or a second waveguide guide. In some instances (depending on the orientation of the slot), it is possible for both effects to take place at the same time. In Fig. 2.12 *slot 1* situated in the top wall allows electric coupling to take place, however some of the wall current is shown to be interrupted, which means that there will also be some magnetic coupling. The position of *slot 2* (at a point of zero electric field) means that it interrupts a sizable wall current flow; thus coupling here is primarily through the magnetic field.

E-Field coupling exists where the field is either normal or parallel to the surface of the aperture. A slot normal to the electric field ensures that there are no surface charge terminations, allowing the field lines to pass through it and induce charges on the external metal surfaces. Fig.2.13 below shows the fields propagating through and away from the slot.



Fig. 2.13: Coupling of an electric field through an aperture – Normal to plane of aperture

Magnetic Field coupling in contrast is more dominant when the aperture is designed such that its longest sides are normal to the surface current, or when the longest sides are parallel to the surface of the magnetic field lines.

2.12.2 Electric Coupling Probes

Coupling probe structures are made from co-axial feeding cables, which have been extended a small distance into the cavity resonator. This extension into the cavity resonator is relatively small compared to the wavelength and overall size. The extension length typically equating to a quarter wavelength with an input impedance that is equivalent to an open circuit is illustrated in Fig. 2.14. Although the magnitude of current in these instances is small, the presence of a voltage creates an electric field between the adjacent cavity wall and the probe. The resulting field is then able to radiate energy into the cavity in a manner which is similar to a monopole antenna. The operating principle of monopole is based on the fact that the current distribution is only a quarter wave in length and identical to that of a half-wave dipole.

The probe will automatically couple to an electric field that is perpendicular to it. The coupling is at its strongest where the field appears in close proximity to the probe. Coupling to unwanted modes can be avoided by strategically placing additional probes in places where the electric field is zero. This concept is further illustrated in [11].

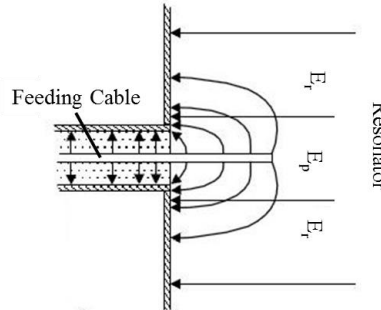


Fig. 2.14: Capacitive Coupled Probe (coaxial feed) a cavity resonator [20]

2.12.3 Magnetic Coupling Loop

Extending a metal conductor (coaxial cable) some distance into the cavity resonator, and then forming a bend such that one of the ends is grounded onto the cavity wall forms a coupling loop. An example of an inductive coupled loop is illustrated in Fig. 2.15. The physical dimensions of the coupled loop are small compared to the wavelength. The voltage is almost negligible, current is large and the resulting input impedance approaches a short circuit. The presence of a large current generates a magnetic field, and the emerging radiation pattern is similar to that of a magnetic dipole placed tangential to the wall. The resulting dipole moment is proportional to the size of the loop. The orientation of the loop therefore plays a significant role. The principle of coupling power into a cavity resonator via loop structures is well documented in literature [3], [10]. The generic expression for calculating the size of the loop is given by eqn.2.54.

$$R_c = \frac{(\omega\mu A)^2}{2\pi a(h+a)R_s} \quad (2.53)$$

Where:

R_c = cavity resonator – resistance

a = cavity resonator - radius

h = cavity resonator – height

R_s = cavity resonator – surface resistivity

μ = Permeability

A = captured area of the coupled loop

The radius of a coupling loop can be calculated by rearranging eqn.2.53.

$$r = \sqrt{\frac{2\sqrt{R_c 2\pi a(h+a)R_s}}{\omega\mu\pi}} \quad (2.54)$$

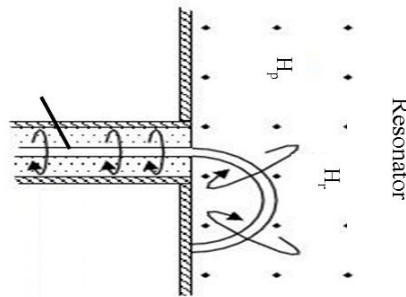


Fig. 2.15: Loop Coupling Structure – coupled to a cavity resonator [20]

2.12.4 Patch Antenna Coupling

The use of micro-strip or patch antennas has become more widespread owing to their low cost and ease of manufacturability. A typical patch antenna is printed directly on a dielectric substrate. It comprises of a length L , width W and is etched on top of a substrate of height h , having a permittivity ϵ_r as shown below in Fig. 2.16.

The frequency of operation is determined by the length, which is typically equal to one half of a wavelength within the chosen dielectric substrate medium. The width W controls the input impedance and the radiation pattern. A large width can increase the bandwidth and reduce the impedance.

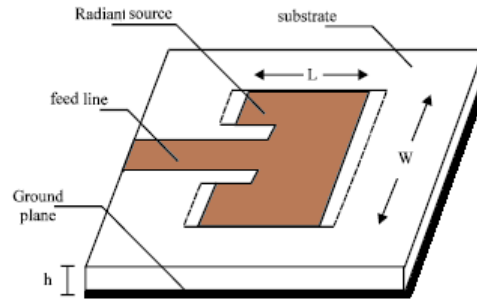


Fig. 2.16: Patch Antenna – with an insert feed [18]

$$\text{Resonance frequency of a patch antenna} = f_r \sim \frac{c}{2L\sqrt{\epsilon_r}} = \frac{1}{2L\sqrt{\epsilon_0\epsilon_r\mu_0}} \quad (2.55)$$

$$\text{Width of a patch} = (W) = \frac{c}{2f_r\sqrt{\epsilon_r+1}}; \epsilon_{\text{eff}} = \frac{\epsilon_r+1}{2} + \frac{\epsilon_r-1}{2} \left[\frac{1}{\sqrt{1+12\left(\frac{h}{W}\right)}} \right] \quad (2.56)$$

$$\text{Length of a patch} = (L) = \frac{c}{2f_r\sqrt{\epsilon_{\text{eff}}}} - 0.824h \left[\frac{(\epsilon_{\text{eff}}+0.3)\left(\frac{W}{h}+0.264\right)}{\epsilon_{\text{eff}}-0.258\left(\frac{W}{h}+0.8\right)} \right] \quad (2.57)$$

The length (L_g) and the width (W_g) of the ground plane can be calculated using the equations below and the radiation pattern is given by equation 2.60.

$$L_g = 6h + L \quad (2.58)$$

$$W_g = 6h + W \quad (2.59)$$

Radiation pattern:

$$E_\theta = \frac{\sin\left(\frac{kW\sin\theta\sin\phi}{2}\right)}{\frac{kW\sin\theta\sin\phi}{2}} \cos\left(\frac{kL}{2}\sin\theta\cos\phi\right) \cos\phi \quad (2.60)$$

Where:

k = free-space wave number

c = speed of light

h = height of substrate

Patch antennas are voltage radiators, with a high Q and narrowband characteristics, which exhibit high loss and a shift in resonance due to fringing effects. The fringing fields on the edges of the structure are responsible for the radiation patterns. Owing to the low power handling capability their use is limited to low power applications (~ 100watts.). The patch antenna feed techniques have been discussed in detail [23-24].

2.12.5 Horn Antenna

A pyramidal horn is a rectangular waveguide with a flare out at the end. The inclusion of flares enables the antenna to have a higher directivity than a normal waveguide. The general form of a pyramidal horn (Fig.2.17) has a wide bandwidth, and its input impedance is fairly constant over a wide frequency range. A long horn with smaller flare angles gives uniform aperture distribution, however for practical reasons the horn is kept as short as possible. The commonly used horn antenna along with their typical properties are listed in table 2.2

Table 2.2 Different types of horn antennas, common types are listed below:

Antenna Type	Properties
Sectoral Horn	<ul style="list-style-type: none"> - Energy flares out in one direction only - Flaring in the direction of E-vector produces sectorial E-plane horn - Flaring in the direction of H-plane produces sectorial H-plane horn
Pyramidal Horn	<ul style="list-style-type: none"> - Energy flares in both E & H planes
Conical Horn	<ul style="list-style-type: none"> - Energy flares in walls of a cylindrical waveguide.

The design parameters (flares and feed structure) and a set of design equations for a typical horn antennae are listed in table 2.3. An increase in aperture and flare angle increases the energy directivity whereas the bandwidth reduces such that in order for a horn to be realizable $R_E=R_H=R_P$.

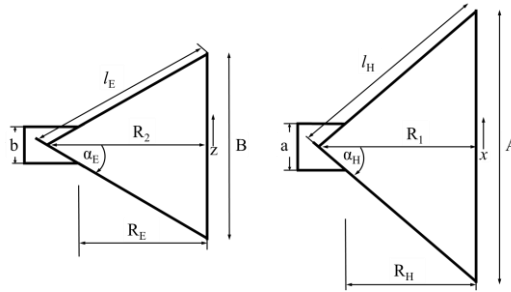


Fig. 2.17: Horn Antenna – image adopted from[19]

$$G = \epsilon_{ap} \cdot \frac{4\pi}{\lambda_0^2} \cdot A_{ap} \tag{2.61}$$

Where:

λ_0 is the wavelength

ϵ_{ap} is the effective aperture coefficient

A_{ap} is the area of aperture (AxB).

Table 2.3 Horn antenna design equations

Antenna Parameter	Design Equation
A	- $0.45\lambda\sqrt{G}$
B	- $\frac{1}{4\pi} \frac{G\lambda^2}{0.51A}$
R_1	- $\frac{A^2}{3\lambda}$
R_2	- $\frac{B^2}{2\lambda}$
R_E	- $R_2 \left(1 - \frac{a}{A}\right); \frac{R_2}{R_E} = \frac{A}{(A-a)}$
R_H	- $R_1 \left(1 - \frac{b}{B}\right); \frac{R_1}{R_H} = \frac{B}{(B-b)}$
l_E	- $\sqrt{R_2^2 + \left(\frac{A}{2}\right)^2}$
l_H	- $\sqrt{R_1^2 + \left(\frac{B}{2}\right)^2}$

2.13 References

- [1] David M. Pozar, *Microwave Engineering*, Third Edition, John Wiley & Sons, Inc. 2005.
- [2] *Electromagnetic Fields and Public Health: Mobile Phones – Fact Sheet No 193*
- [3] Peter Russer, *Electromagnetics, Microwave Circuit and Antenna Design for Communications Engineering*.
- [4] R. J. Cook, “Microwave cavity methods” in *High Frequency Dielectric Measurement (Conf. Proc., March 1972)*, J. Chamberlain and G. W. Chantry, Eds. Guildford, U.K.: IPC Science and Technology Press, 1973, pp. 12-27.
- [5] Ebbe G. Nyfors, “Cylindrical microwave resonator sensors for measuring materials under flow,” presented from Helsinki University of Technology, Finland.
- [6] G. Birnbaum and J. Franeau, “Measurement of the dielectric constant and loss of solids and liquids by a cavity perturbation method,” *J. Appl. Phys.*, vol. 20, pp. 817-818, 1949.
- [7] R. A. Waldron, “Perturbation theory of resonant cavities,” *Proc. IEEE*, vol. 170C, 272-274, 1960.
- [8] Mi Lin and Mohammed N. Afsar, “A new cavity perturbation technique for accurate measurement of dielectric parameters,” presented from High frequency materials measurement and information center, USA.
- [9] R. N. Clarke and C. B. Rosenberg, “Fabry-perot and open resonators at microwave and millimeter wave frequencies, 2 - 300 GHz.” *J. Phys. E: Sci. Instrum.*, vol. 15, pp. 9-24, Jan. 1982.
- [10] Robert E. Collin, *Foundations for Microwave Engineering*, Second Edition, IEEE, Inc., New York.
- [11] Ebbe G. Nyfors, “Cylindrical microwave resonator sensors for measuring materials under flow,” presented from Helsinki University of Technology, Finland.
- [12] Robert E. Collin, *Field Theory of Guided Waves*, McGraw-Hill, Inc., 1960. [28]

- Permeability (Electromagnetism), Wikipedia, Available:
[http://en.wikipedia.org/wiki/Permeability_\(electromagnetism\)](http://en.wikipedia.org/wiki/Permeability_(electromagnetism))
- [13] Ref: homepage.physics.ulowa.edu.
- [14] <https://www.shutterstock.com/image-vector/electromagnetic-spectrum-vector-diagram-different-types-154169990?src=-1-1>
- [15] <https://www.ck12.org/physics/electric-fields/lesson/Electric-Fields-MS-PS/>
- [16] <http://hyperphysics.phy-astr.gsu.edu/hbase/magnetic/magcur.html>
- [17] https://www.researchgate.net/profile/Katrin_Lindbaeck
- [18] <https://Antenna-Theory.com>
- [19] Aperture-Fed Waveguide Horn Antenna – microwavetools.com
- [20] Xiuping Li, Yan Jiang, ‘ Design of Cylindrical Cavity Resonator for Measurements of Electrical Properties of Dielectric Materials, Semantic Scholar.org 2010
- [21] <https://www.eeeguide.com/methods-of-exciting-waveguides/>
- [22] <https://empossible.net/wp-content/uploads/2018/03/Lecture-3a-Electromagnetic-Waves-and-Polarization.pdf>
- [23] Dalia M. Elsheikh, Esmat A. Abdallah “Different Feeding Techniques of Microstrip Patch Antenna with Spiral Defected Ground Structure for Size Reduction and Ultra-Wide Band Operation” Journal of Electromagnetic Analysis and Applications, 2012, 4, 410-418.
- [24] Kashyap Sreenath, Raithatha “Microstrip Patch Antenna Parameters, Feeding Techniques & Shapes of the Patch – A Survey”, International Journal of Scientific and Engineering Research, Vol.6 2015/04/10.

CHAPTER 3 – LITERATURE REVIEW

3.1 Fundamentals of Microwave Heating

Microwave heating takes place due to polarization of water molecules in dielectric materials at frequencies ranging from 300MHz to 300GHz. In domestic microwave ovens, the process involves microwave energy penetrating a dielectric substrate which comprises of polar water molecules. The electrical dipole moment, with a positive charge at one end and a negative charge at the other (shown in Fig.3.1a and represented by eqn.3.1) rotate around their axis at a rate of 2.45 billion times per second until they align themselves in the direction of an EM field. This results in volumetric heat distribution. A dipole moment occurs between two ions of an ionic bond or between two atoms of a covalent bond and is due to separation of charges and the differences in electronegativity. A large difference in electronegativity leads to a greater dipole moment whilst charge separation distance determines the overall size of the dipole moment.

A water based dipole moment arises due to oxygen being more electronegative than hydrogen. This has the effect of pulling electrons closer, which increases electron density and creates an electric dipole moment vector with partial negative charge on the oxygen atom as shown in Fig. 3.1b.

$$\text{Dipole moment} = \mu = q \cdot d \quad (3-1)$$

Where:

μ = Debye: (0 = non-polar; N = polar)

q = Charge

d = distance

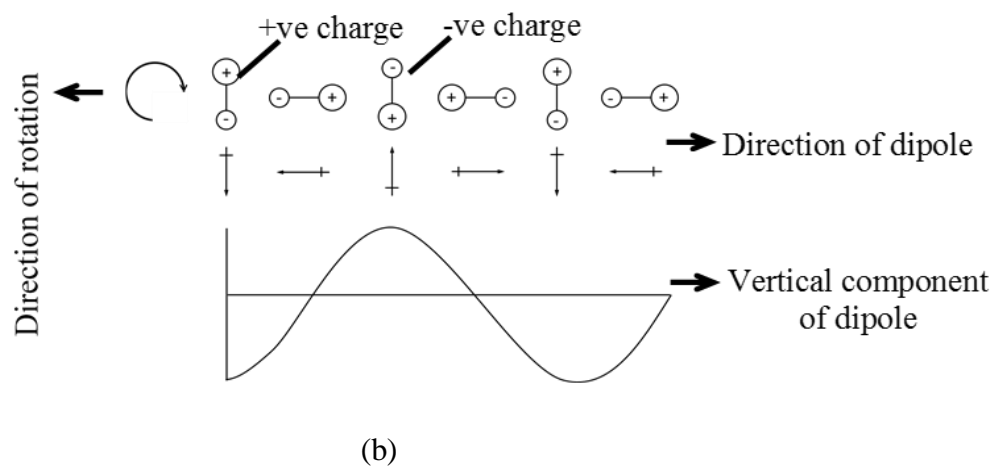
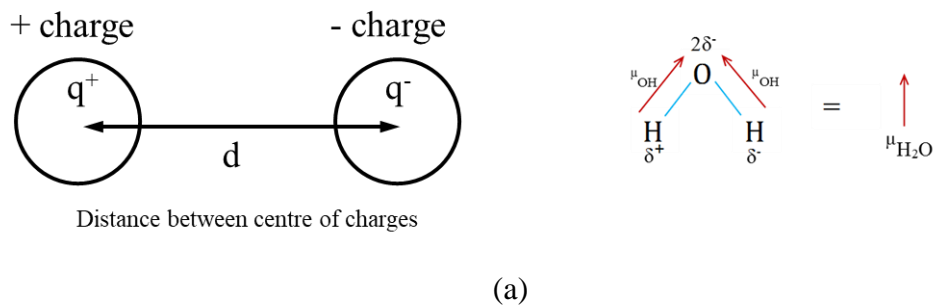


Fig.3.1:- (a) Water-Electric dipole moment (b) Variation of microwave propagation in time.[125-126]

3.2 Magnetron Based Microwave Heating

There is very little evidence of microwave heating prior to World War II as microwaves were still in their infancy, however patent literatures making loose reference to the use of microwave energy for industrial applications exists. Kasner 1937 alludes to these applications in his patents on spark-gap microwave generators [26]-[28]. Other evidence of pre-war interest is a patent describing the concept of matching a lossy dielectric load to a radiating dipole by W. M. Hahnemann 1939 [29]. Practical uses of microwave heating were not considered until after the war [30]-[31]. W. C. White (1962) [31], states that the industrial use of dielectric heating did not come into effect until 1940.

With the concepts of microwave heating well established by the mid 1940's; the need to control the heating source and the importance of a "coupling circuit" in practical implementations was recognised [32]-[33]. The ISM bands were specified with severe limits on out of band radiation leakage leading to adoption of FCC Part 18 ($25\mu\text{V/m}$ below 500Watts & $25\sqrt{\text{Power}/500}$ above 500Watts). Whilst the general usefulness of microwave heating for industrial applications remained unproven; T. M. Shaw et al, 1949, proposed its use for food processing [34].

Continued interest in industrial heating led to the development of a heating apparatus by Percy Spencer 1945. This comprised of two magnetrons in parallel, feeding a waveguide. The microwave power exits the waveguide and enters the cavity where it impinges upon the food source. P. W. Morse & H.E. Rivercomb 1947, reported a prototype oven operating at 915 MHz, which was used to thaw and heat pre-cooked frozen meals in restaurants [35]. The GE authors preferred 915MHz over 2450MHz claiming that thermal runaway was worse at higher frequencies and penetration depth too small. Their rivals Raytheon favoured microwave oven frequency of 2450MHz arguing that higher frequency operation permitted improved coupling to small loads, such as a frankfurter sausage, whilst the increased number of modes offered better randomisation and heating uniformity. This led to allocation of two frequency bands by the FCC, $915\pm 25\text{MHz}$ and $2450\pm 50\text{MHz}$. Little attention was paid to the theory of microwave heating at the time other than the recognition that "electronic heating of food" produced heat from within".

Whilst earlier magnetrons were pulsed tubes developed for radar applications, W, C. Brown and Palmer Derby 1943-44 established design rules [36] enabling choice of CW or pulsed operation to ensure mode stability. Naval interest in jamming application of CW mode of operation led to a greater activity and a step towards commercial heating applications. Soon, it was widely accepted [37] that a magnetron with high efficiency was ideal for industrial heating applications. Variations on waveguide-aperture feeds and mode stirrers also found their way into products in the search for uniform heating [38].

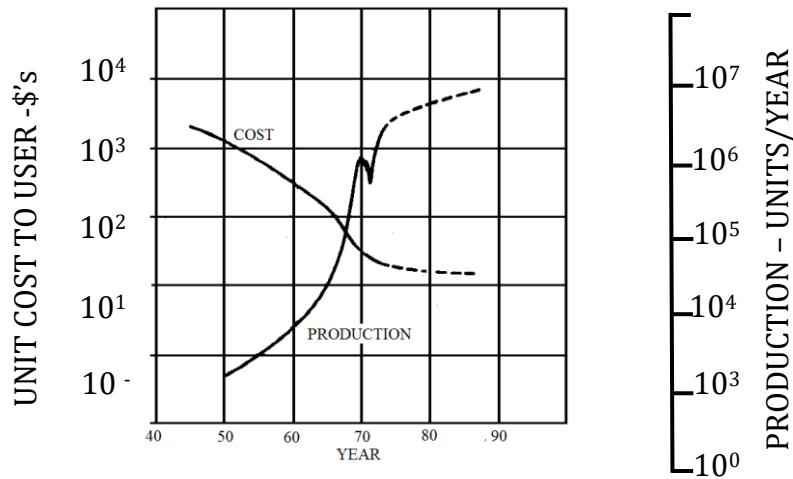


Fig. 3.2 Production figures and user unit costs of magnetrons – past and projected (H. K. Jenny, “Electron tubes—A technology forecast,” Technology Trend (75CH1005-8 TFA), IEEE, NY (1975)).

Tappan 1955 [39] introduced a 220V, 900W, 24 in-wide oven, with an electric heating element at the top of the cavity for “browning”, retailing at \$1200.00. Marketing and sales campaigns of the time stressed advantages of cooking speed, cool oven utensils, and unique reheating capability. Tappan 1965 also introduced the first “microwave cooker”, a microwave oven mounted above a conventional range, retailing for well over \$1000.

By the 1960’s Raytheon had forged a modest commercial market share and Tappan had an equally modest domestic market share. There was little evidence of growth, which lead R.V. Decareau to remark [40] that “it is extremely doubtful if the microwave oven business has come close to breaking even”. This may have been the case if it were not for the vision and faith of Charles Francis Adarns. He foresaw the potential and backed the microwave oven during its many profitless years while President of Raytheon Mfg. Co. This lack of growth in part was attributed to most microwave companies concentrating on military, radar, ECM, communications and space applications.

Magnetron development continued steadily but doubts remained over its performance compared to tubes (TWT) and solid-state devices until a paper by Twisleton (1964) demonstrated magnetrons efficiencies of 80–90-percent at 915MHz. This led Norman Moore (Litton) 1966 to anticipate a significant rise in countertop units [41]. Tappan's 230-V free-standing microwave had a price of \$1000 whereas Litton-Atherton magnetron ovens had a price of \$360-\$400. As Roper Co. and Amana entered the market, Amana had specific plans and an aggressive price strategy (~\$495) for a counter top oven, triggering a price war in the consumer oven market. The magnetron prices changed significantly with a growth in microwave oven market (Fig. 3.2).

Marketing of microwave ovens began soon after, in rest of the world. First in Japan and to a lesser extent in Western Europe and Scandinavia, whilst there was also evidence of microwave ovens being marketed in the USSR in 1971 [42]. Technical advances over the years have added performance enhancements, such as microprocessors [45] for timing, power control and potential use of solid-state sources for microwave ovens. The practical application of the latter seemingly a distant away at the time is now close to reality.

3.3 The Magnetron

The Magnetron (Fig.3.3) first invented in 1921 and refined over the years for continuous and pulsed modes of operation is capable of generating very high power levels (megawatts) over a wide range of frequencies 1-40GH and has a typical lifetime of about 4500hrs when operating into a matched load – this reduces to ~1000hrs under variable loading conditions (back-bombardment of the electrons results in filament wearing off). It comprises of a cylindrical cathode surrounded by a hollow anode with a few millimetres separation. The anode has a number of vanes designed to resonate at specific frequencies ($2.45\text{GHz}\pm 50\text{MHz}$). Application of voltage (kV) between the electrodes and a magnetic field aligns the electric and magnetic fields such that they are perpendicular to each other.

As electrons emitted by the cathode begin to accelerate; a sufficiently large magnetic field restricts their movement to circular paths (around the cathode) ensuring they do not escape to the anode. The interaction of vanes with the electrons (accelerating or decelerating them), leads to self-sustaining oscillations and power generation. A portion of the power is extracted via a coupling loop and transferred to a rectangular waveguide (Fig.3.4).

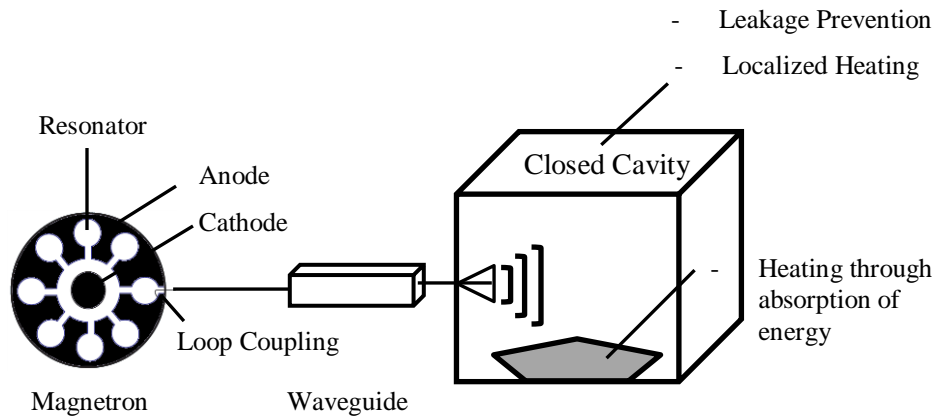


Fig. 3.3 Magnetron based microwave oven.

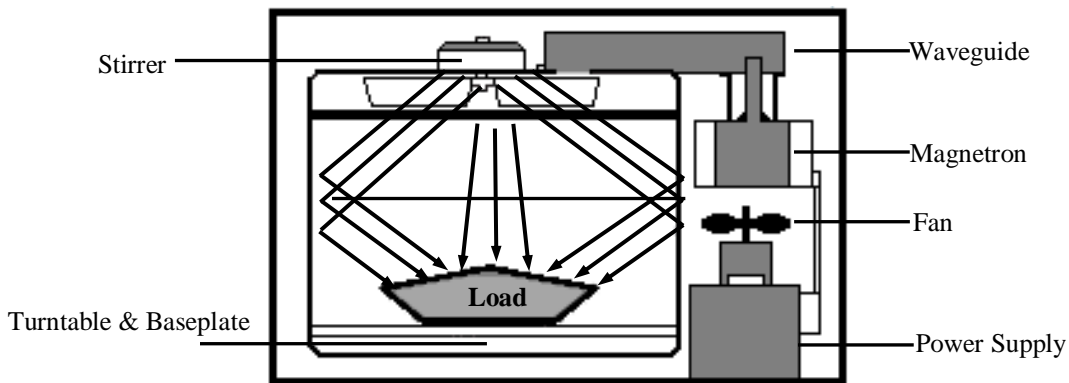


Fig. 3.4 Schematic of a typical microwave oven.

3.4 Magnetron Power

Magnetron based RF sources are widely used in microwave cooking and heating related applications due to their high energy conversion at a very low cost. Determining

the output power rating of a magnetron based microwave oven involves heating a 1000g of water for 60 seconds in a glass container (IEC 60705, 1999). As the water is lossy, the majority of power delivered is absorbed and there are little or no reflections. The power rating of a domestic microwave can thus be calculated using equation 3.2.

$$\text{Power rating} = \frac{(\text{volume of water}).(\text{Temperature rise}).(\text{Specific heat capacity of water})}{\text{ON time}} \quad (3.2)$$

3.5 Magnetron Frequency

The instantaneous frequency emitted by a magnetron in a microwave oven depends on two parameters, the cathode-anode voltage and the high frequency output impedance of the magnetron, which is set by the load (Ghammaz et al., 2003) [47]. Heating of the load changes the material dielectric properties, leading to variations in load impedance, which in turn shifts the frequency of the magnetron. The frequency shift not only changes the heating rate but also changes the field distribution (Celuch and Kopyt, 2009) [48]. Yakovlev (2006) [49] mentions that a typical magnetron operating frequency deviates about 50MHz. The simulated temperature profiles, Yakovlev obtained for these frequencies were compared with the experimental temperature profiles and the root mean square error (RMSE) was derived using equation 3.3

$$\text{RMSE} = \frac{1}{n} \sum_{t=1}^n (T_p - T_0)^2 \quad (3.3)$$

Where:

T_p is the predicted temperature,

T_0 is the observed temperature, and

n is the number of data points on the time-temperature profile.

The determination of exact magnetron power is important as this helps generate the desired electric field. The value of electric field E can be estimated using empirical techniques described by (Soltysiak et al., 2008) [57].

$$E = \frac{2 \times P_m}{(1 - |S_{11}|^2)} \quad (3.4)$$

Where:

- E - Electric field strength (V/cm),
- P_m - Power output of a magnetron (W),
- S_{11} - Reflection coefficient as a function of frequency.

3.6 Microwave Heating in Domestic Ovens

The domestic microwave oven is a common household appliance in the developed and emerging countries. It fits in with modern pace of life by offering speed and convenience. In order to ensure food safety, heating uniformity of the food source is essential for inactivating foodborne pathogens.

Non-uniform heating can pose a serious health hazard; it is therefore fundamental to ensure heating homogeneity and personal safety when consuming microwave heated food. K.Pitachai et al (2012) have described in some detail non-uniform heating due to irregular dielectric properties, shapes and consistency. Pitachai's team developed a finite-difference time domain EM heat transfer model using numerical methodology to study complex interaction of microwaves with food sources.

Microwave heating of food sources in domestic microwave oven takes place due to the polarization effect of electromagnetic radiation at 2.45 GHz. The microwave energy penetrates the surface of food products, generating localised heating due to molecular friction caused by dipolar rotation of polar solvents (water molecules present in the food). The resulting dipolar rotation is due to changes in electric and magnetic fields for the duration of the heating process. Despite numerous efforts, the issue of non-uniform heating still exists, and whilst the causes of non-uniform heating have been identified, the challenges in ascertaining homogeneity remain. The causes of non-uniform heating relate

to interference of electromagnetic waves and variations in dielectric, physical and thermal properties of food components which leads to uneven absorption of energy and heat dissipation.

Some cooking ingredients contain foodborne pathogens. It is recommended that all food products are cooked thoroughly. This involves raising the temperature of microwave heated food to levels where the microorganisms are destroyed, whilst preserving nutrients. Liquid water and ice have different dielectric properties. Frozen food (ice) has low loss and absorbs less microwave energy (Chamchong and Datta, 1999 a, b) [50] compared to thawed food which is more lossy and able to absorb more power. For this reason most microwaves incorporate a defrost functionality.

The microwave energy absorbed by a load is proportional to the dielectric loss factor and the square of the electric field strength. An electromagnetic wave loses part of its energy when travelling through a lossy dielectric medium. This loss of energy is attributed to heat generation where the power is converted to thermal energy within the medium. Conversion of electromagnetic energy into thermal energy is governed by the below equation (Goldblith, 1967) [55].

$$P_v = 2\pi f \epsilon_0 \epsilon' E^2 \quad (3.5)$$

Where

P_v - dissipated power per unit volume (W/m^3),

f - Frequency of electromagnetic wave (Hz),

ϵ' - Relative dielectric loss factor

ϵ_0 - Permittivity of free space - (8.854×10^{-12} F/m),

E - Electric field strength (V/m) in food.

The dielectric loss in a material due to electric conductivity (σ , S/m) is given by:

$$\varepsilon'' = \frac{\sigma}{2\pi\varepsilon_0 f} \quad (3.6)$$

In some instances, evaporative losses from the food surface can be significant, requiring the inclusion of an evaporative loss term in the heat transfer equation. The evaporative loss is considered as minimal when the surface temperature of the food is kept below 70°C

3.7 Solid-State Based Microwave Heating

A Solid-State Source (transistor) can be thought of as a controllable valve where a small signal is used to control much larger energy flow. This was first demonstrated in 1947 at Bell Laboratories in New Jersey. William Shockley whilst working on the concept for more than 10 years was unable to realise a working model. He enlisted the help of Bardeen and Brattain and together they were able to demonstrate a working proto-type “a point contact transistor”. Shockley went on to create a new type of transistor, “a bipolar transistor” which had superior performance compared to the “point contact transistor”. However, these earlier devices lacked power and were not considered suitable for microwave heating applications.

The continuous demand for higher data rates over the last 20 years together with advances in semiconductor device technology has led to the development of high power devices with good efficiency, such that their use in microwave heating applications has become feasible. These devices are capable of generating accurate, frequency-agile, controllable and responsive energy levels, enabling precise and even distribution of energy to heat food homogeneously. This renewed interest in the use of solid-state power for domestic microwave oven and other emerging applications (plasma lighting, car ignition, composite curing and biomedical applications) has led to a growth in research activity, focusing on performance benefits, cost reduction and commercialisation.

There are significant performance benefits of solid-state technology over the

magnetron based systems, as well as challenges relating to successful implementation and reliable operation. Solid-state for domestic heating (Fig. 3.5) offers several advantages. This includes monitoring forward and reflected power, which helps track energy levels into the cavity and load; an ability to change the frequency of operation allowing precise control of excited modes; precise control over power and relative phase (for multi-feed systems) which leads to rapid and uniform heating (through continuous power delivery), repeatability and low voltage operation. Magnetron based systems in contrast are operated in a pulsed (ON/OFF) mode where the different power levels are realised by adjusting the ON/OFF time ratio via pulse width modulation. The resulting temperature overshoots contribute to uneven heating. Whilst device reliability under variable loading conditions remains a concern, warranting further investigative work, design freedom with respect to power scalability allows multiple system combinations which enhance heating uniformity and system efficiency.

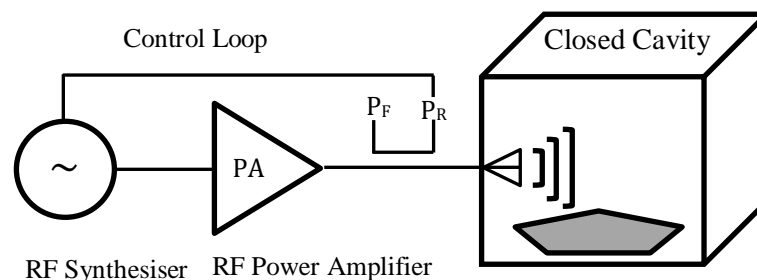


Fig. 3.5 Solid-state powered microwave oven.

3.7.1 Solid State Microwave Oven

The use of solid state technology for microwave heating was first proposed in the late 1960's and early 1970's. The first patent for solid-state microwave oven technology was granted to Bruce R. McAvoy, (1971) [1]. The work was based around the provision of plurality of solid state oscillator's (Fig.3.6) generating multiple frequencies in the microwave region. The number and location of oscillators was arranged such that it provided a uniform heat distribution [1]. This led to more research, and further patents

were granted during this decade to Kern K.Chang, (1972) for his work on a “solid-state microwave heating apparatus” [2], which comprised of a cylindrical cavity with multiple solid-state sources mounted (heat sinked) to the inner wall of the cavity. The power was coupled into the cavity (electric field) via dipole antennas to heat the load.

T. Othani, (1975) developed a hybrid microwave oven, which was a combination heating system (Fig.3.7) consisting of a conventional magnetron as a high power source with an auxiliary solid-state source to attain better heating uniformity [3]. The magnetron was used as the main power source owing to its high power capability and the solid-state oscillators were used as secondary sources. The combination was used to attain continuous heating performance during the magnetron ON-OFF cycles.

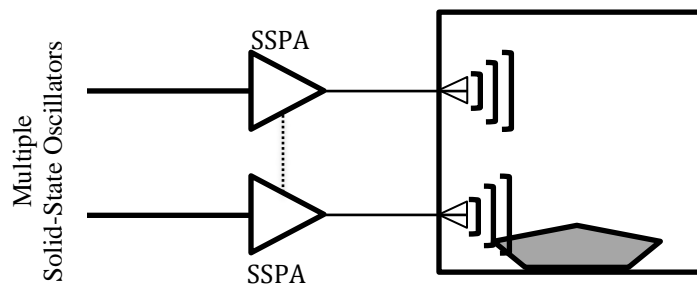


Fig. 3.6 Microwave oven with a plurality of solid-state oscillators.

R.A. Dehn, (1977) proposed a microwave heating apparatus incorporating multiple couplers and solid-state sources [4]. The patented work consisted of multiple solid-state oscillators exciting wire-like resonant couplers mounted on a tubular housing. He used micro-strip circuitry with each oscillator which excited a resonant coupler (Fig.3.8). The coupling structures were longitudinally spaced and angularly staggered, this enabled energy to be coupled to different regions of the cavity structure to maintain an even heat distribution. The absorption of energy in an optimally matched state, where there is no reflected power effectively isolates the couplers, enabling closer spacing and placement of the structures.

S.H. Bickel, (1978) [5], successfully patented a solid-state microwave oven power source (Fig.3.9). This comprised of negative resistance transistors and capacitors coupled to a dc power source for the purposes of maintaining multiple solid state power sources in a phase locked condition and combining the power into a single load [5]. Power from solid-state microwave source (comprising of multiple solid-state oscillators; an equal phase combiner and impedance matching network) is coupled in-phase through multiple coaxial cable antenna structures, selectively positioned adjacent to the cavity wall.

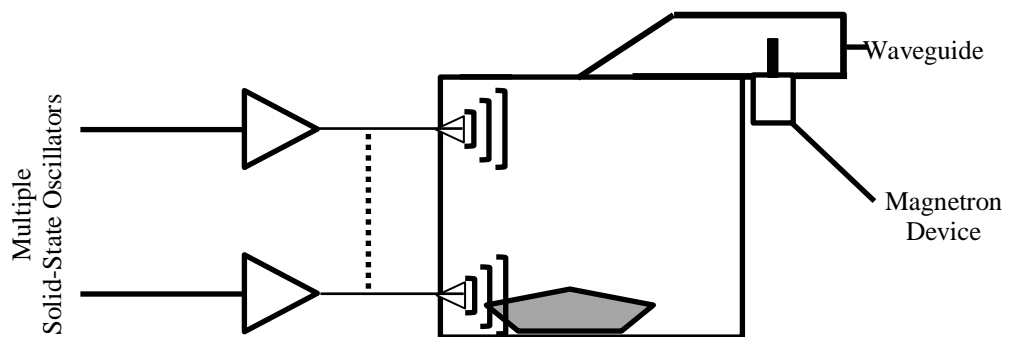


Fig. 3.7 A Combination Microwave Oven.

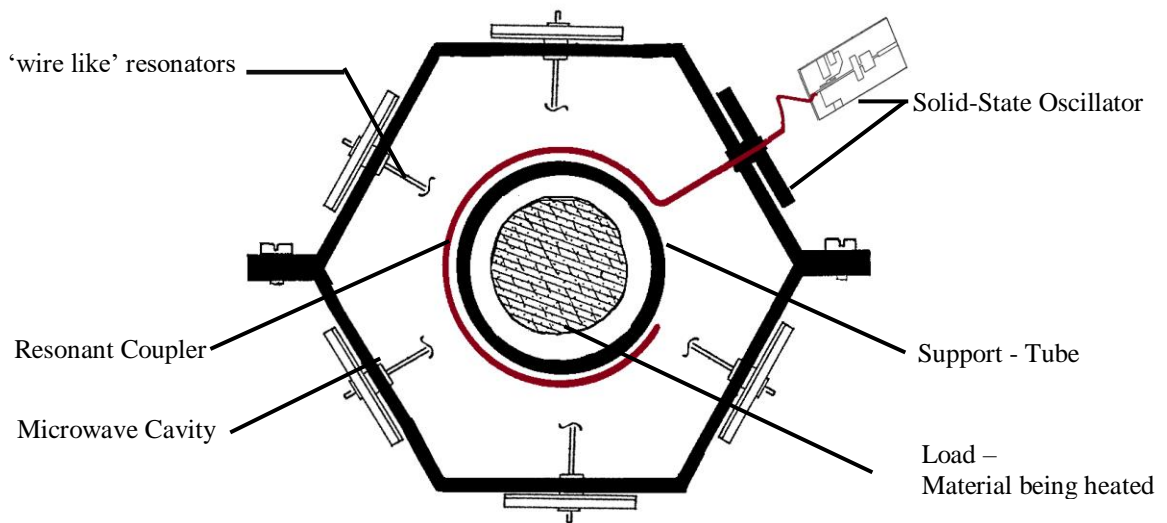


Fig. 3.8 Microwave Oven – multiple couplers & solid state sources

“Bickel” [5] recognised that if the sources were not phased locked, and allowed to drift, then they are likely to absorb each other’s generated power. This reduced the amount of energy reaching the load in the oven, which under extreme reflective states led to the destruction of individual sources. The loss of power was seen as particularly undesirable with solid state power sources, owing to their low efficiency and output power at that time.

The proposed cylindrical resonator had a maximum field strength at the centre which decayed to zero at the side conducting walls. The solid-state oscillators are positioned on the surface (where the magnetic field is maximum) and coupled to the resonant field by magnetic coupling loops. To maintain optimum phase lock conditions the load is centrally located.

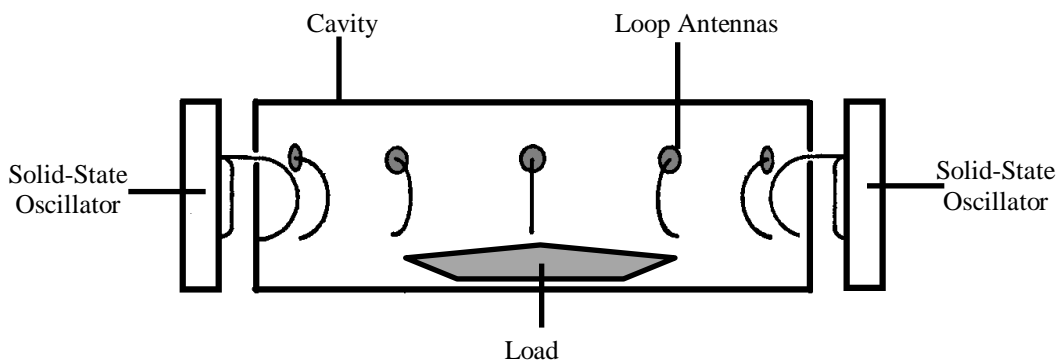


Fig. 3.9 Solid-State Microwave Oven – multiple solid state sources

The possible destruction of solid state sources was also recognised in earlier work by Kern K Chang, (1972) [2]. He proposed the use of a microstrip circulator as a solution. A circulator; whilst protecting the power transistor from high reflected energy states, directs all reflected energy into a resistive load where it is absorbed. The use of circulators and resistive loads causes power loss and system inefficiency, which is undesirable. The power absorbed by the resistive load is dissipated as heat to the surroundings and other parts of the system. This unwanted heat must be removed by air or water cooling to preserve reliability, further increasing DC power consumption and system inefficiency.

3.7.2 Microwave Heating with Control

Alejandro Mackay et al, (1980) [7] identified that whilst power supply and magnetron efficiencies were high (~95% and~65% respectively) the oven efficiency was only in the region of around 45%. They attributed this to an inability to convert available magnetron power to heat, and suggested that this was due in part to losses in the cavity walls and the coupling structure. Another major contributing factor was the impedance mismatch between the magnetron and the loaded cavity. The mismatch condition and circuit efficiency degraded significantly with small loads and varied considerably with the position of the load inside the cavity.

For their work, they were granted two patents; a controlled heating microwave oven (1980) in the United States (Fig.3.10) and a controlled heating microwave oven using different frequencies (1980) in Canada [6-7]. The proposed heating apparatus comprised of a cavity; a frequency agile energy source; a detector to monitor power absorption by the load across the operating bandwidth, and a control mechanism for selecting the operating frequencies based on power absorption levels. Whilst they were able to demonstrate control, high efficiency and improved heating uniformity, the non-adaptive nature of the coupling structure meant their technique was of a limited value for domestic microwave heating (variable load) applications.

Tomotaka Nobue et al, (1983) also identified limitations of magnetron based domestic microwave ovens [8]. The main limitation was the lack of control over power, which could only be varied through an ON-OFF time division mode as a means of heating different loads. In their work they acknowledged that only a proportion of the available power contributed to heating the load inside the cavity, and the exact amount of power absorbed was dependent on the type and size of the load. As with the earlier work by Alejandro Mackay et al, (1980), this was attributed to an impedance mismatch between the magnetron and the cavity, which emphasised the importance of maintaining a satisfactory impedance match between the load and the source.

Tomotaka [8] observed that in a multi-mode rectangular cavity the electromagnetic modes shift in frequency as the load is heated. He also observed that the frequency generating the electromagnetic modes correlated to frequency where the reflected power from the loaded cavity was minimal. By continuously operating at these pre-determined frequency points, he noticed that the efficiency reduced as the load was heated. Whilst it is acknowledged that selection of electromagnetic modes, field patterns or distributions in the cavity play important roles in attaining uniform heating, Tomotaka suggested that under variable loading conditions, a multitude of electric field patterns cannot maintain uniform heating.

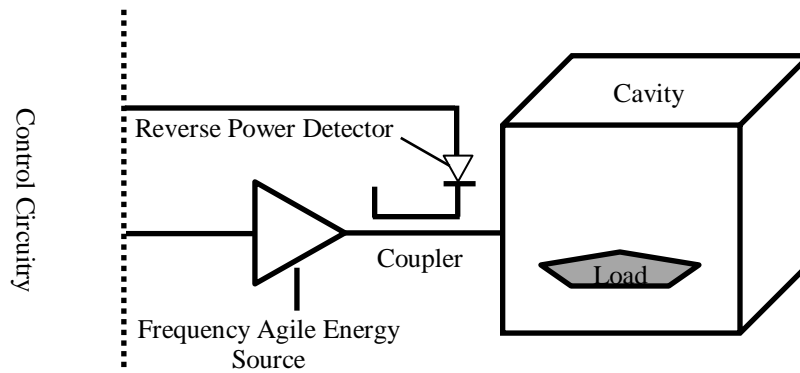


Fig. 3.10 Controlled Heating Microwave Oven

He went on to suggest that even when electromagnetic modes suitable for attaining uniform heating are identified, it is impossible to select these modes in accordance with the amount of reflected power in a multi-mode cavity. His observations were valid, however, no means of identifying and capturing low reflective states over a wider bandwidth were proposed. Whilst the reflected power states can be used to detect the presence of electromagnetic modes, the details of the electric field pattern remained largely unknown. These can now be realised with the aid of 3D EM simulations. Issues relating to SSPA bandwidth utilisation and variable load conditions were not addressed and remained unanswered

Hisashi Okatsuka et al, (1985) proposed a microwave heating apparatus (Fig.3.11), which comprised of a single pre-amplifier module and multiple amplifier modules [9] for amplifying the output of the preamplifier module. In this research, Hisashi's team took the view that besides its notable disadvantages, magnetron based microwave heating was potentially hazardous. The high voltage (several thousand volts) required to energise the magnetron can potentially expose an operator to serious danger of an electrical shock if insufficiently insulated. Furthermore generating such high voltage requires a high voltage transformer (KVA ratings). This was in contrast to solid-state systems which had a low operating voltage (tens of volts). The limited power from a single solid state source is recognised and attributed to weak microwave energy inside the cavity. The need to intensify this energy to sufficiently high levels through the use of multiple sources is acknowledged in this work.

A rise in impedance mismatch due to heating and other effects leads to reflected power states which can potentially damage the solid-state devices. This has been cited as an obstacle to practical implementation of solid-state systems. In order to maintain safe and reliable operation, solid-state devices must be kept sufficiently cool and the need to dissipate heat generated by the amplifiers has been discussed. There is a clear focus on implementation of a time delay function and a staggered “switch on” of solid-state sources with increasing temperature. The use of a circulator and high power load to absorb reflected power and protect the solid-state device against an impedance mismatch is also advocated.

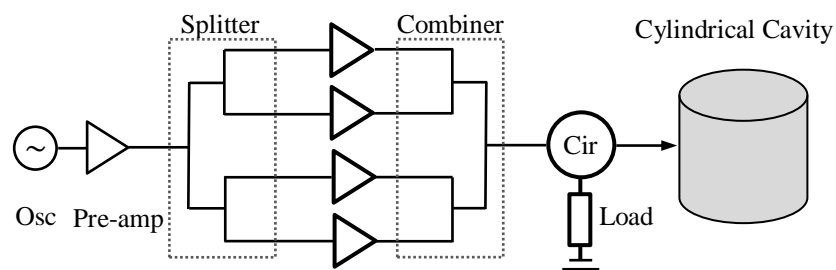


Fig. 3.11 Microwave Heating System comprising of multiple sources

3.7.3 Microwave Heating with Distributed Semiconductor Sources

Peter James Hadinger, (2004) patented a microwave heating apparatus which used distributed semiconductor sources [14]. He claimed that the efficiency of microwave heating can be improved by placing multiple sources throughout or adjacent to a microwave heating environment (Fig. 3.12), such that the energy is distributed throughout the chamber. The distribution of sources is customised to specific size and shape of microwave chamber. This is in contrast to conventional microwave ovens, where the energy emerges from a single location and is reliant on the stirrer and turntable for its distribution within the cavity structure. In his research, it noted that whilst the magnetron source is inexpensive and readily available, it lacks control. A typical microwave oven operation requires turning the magnetron ON and OFF in a pulsing fashion to regulate the amount of energy transmitted over time.

Owing to the limited power capability of a single transistor, other attempts to employ solid-state devices in place of a magnetron included a combiner network to generate high power levels. The generated power was then coupled into the cavity using a waveguide. However this also required the use of stirrers and a turntable for even heat distribution. This led to a multi source approach, where each source is spaced apart such that energy is distributed to all portions of the heating compartment. It is suggested that the amplitude and phase of the sources can be controlled (individually or collectively) to direct microwave energy levels to the desired locations.

It is further suggested that the cavity should be divided into virtual compartments and the power to individual heating regions controlled based on the properties of the load. The power from a SSPA is coupled into specific regions of the cavity via a radiating element (antenna, probe). It is claimed [14] that by varying power and phase of individual or multiple sources with respect to the load position, a more uniform heat distribution is achievable (without the need for stirrers and rotating trays). Under fixed loading conditions, the phasing of microwave sources can be pre-set to create energy maxima to heat specific loads in specific locations. Whilst this concept is valid for fixed loads, it is

of a limited use under variable loading conditions. The research does not state a means through which a good impedance match is realised and maintained. The issues relating to reflected power states, and device reliability under variable loading conditions have been largely ignored.

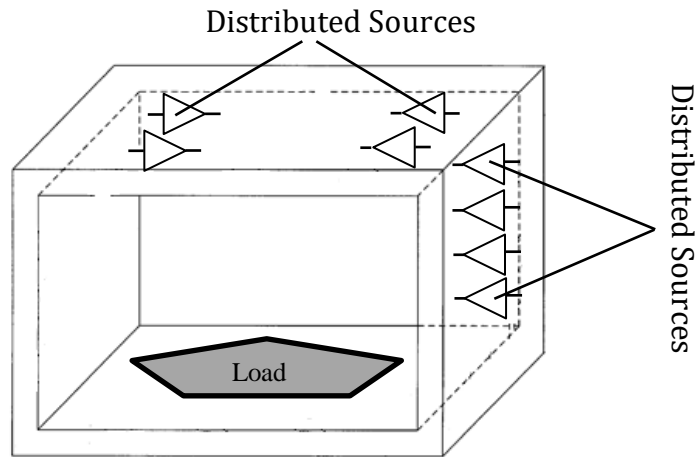


Fig. 3.12 Microwave heating comprising of distributed sources

3.7.4 Microwave Heating with Predefined Modes

Ulf Erik Nordh et al, (2010) proposed the use of predefined modes to select the frequency of operation of two solid-state sources to heat loads in a cavity [15]. The first source is selected to operate (via a control unit) at a known resonance frequency whilst the second source is offset in frequency to compensate for load variations e.g. due to temperature increase. The hot and cold spots which arise due to excitation of the first mode are compensated for by the heating pattern of a second mode. The research was limited to smaller cavities which only had a limited number of excitable modes.

The pursuit of solid-state technology is driven by the desire to attain uniform heating of the load, whilst ensuring maximum available power is absorbed by the, load to achieve a satisfactory degree of efficiency. Ulf Erik-Nordh suggested the use of

predetermined frequency points (regions) for microwave heating applications, where the loads are well defined. The loads are categorised by their types and a uniform heating profile is achieved through selection of an appropriately optimized mode. The energy is coupled into the cavity via a main waveguide or through a plurality of secondary waveguides (coming off the main waveguide).

Tomotaka Nobue et al, (2011) realised that the semiconductor devices had a low thermal durability compared to the magnetron, and were likely to breakdown when exposed to high reflected power and temperatures. To combat this he proposed a compartmentalised heating apparatus (Fig. 3.13), where the reflected power is directed into a second compartment [16], thus keeping heat well away from the solid state source. Tomotaka also suggested that by placing the load in the centre of the cavity, and directing energy into the load from the sides (top and bottom sections) helped improve heating uniformity.

The reflected power due to impedance mismatches in solid-state systems requires careful attention. One proposed solution, includes a heating apparatus where the reflected power is absorbed by a dummy resistance plate, mounted on an outer wall of the heating chamber such that the heat is retained within the enclosure. Other works have suggested detection of reflected power, and selection of the oscillating frequency to retain an impedance match. This process requires a continuous tracking of reflected power states and fast response times, processing speeds and an ability to capture the reflective states over the operating bandwidth. Whilst fast response times may now be realisable, questions around capturing reflective states over wide bandwidths remain unanswered.

Peter James Hadinger, (2004) suggests that solid-state sources can be prevented from destruction (reflected power and high thermal temperatures) by guiding the reflected power from the heating chamber to a high power load. The proposed two chamber concept attempts to overcome this loss of energy, by directing the reflected power from chamber two to chamber one and vice versa in an attempt to make use of the reflected energy,

whilst maintaining isolation between the two generators. This two chamber solution whilst potentially useful in applications where two identical loads are heated simultaneously is not practical or efficient for domestic microwave applications.

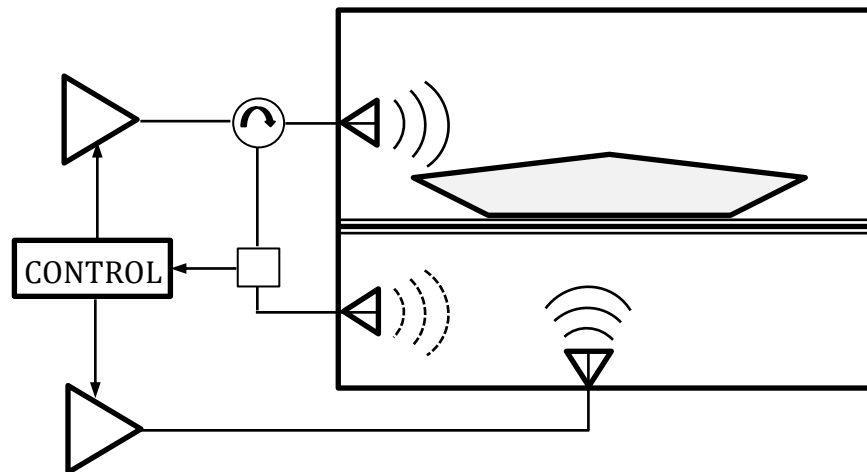


Fig. 3.13 Compartmented Microwave Heating

3.7.5 Microwave Heating with SSPA and Antenna Array(s)

Ranjit Gharpurey & Jacob A. Abraham, (2013) proposed a microwave heating unit comprising of antenna array(s) (Fig. 3.14), which was configured to generate different radiation patterns [17]. The array (comprising of multiple antennas) was used to couple energy from its respective SSPA into the cavity. The heating unit (a cuboidal cavity), had the first antenna array positioned along the first surface of the cavity and a second antenna array positioned along a second surface of the cuboidal cavity, and so on. In a cylindrical cavity, the antenna array was positioned along the cylindrical surface such as to steer the microwave beam within the cavity. Further, the first antenna array was configured to radiate power over a first frequency range, and a second set is configured to radiate power over a second frequency range. The beam pattern and its location was varied by adjusting phase and amplitude of the RF input signal for each antenna in the array. Uniform and rapid heating was achieved through multiple RF signals, each having a different respective frequency and radiating pattern.

Jose Augusto Lima et al, (2015), also proposed a method for implementing beam forming techniques using solid state amplifiers, and an array of antennas for heating materials in a microwave oven [18]. His system comprised of multiple solid state sources, each source had its own transmitting antenna to radiate electromagnetic energy into the oven through its respective phase shifter(s). A feedback loop was used to detect the reflected power and changes in phase were used to control the radiation patterns.

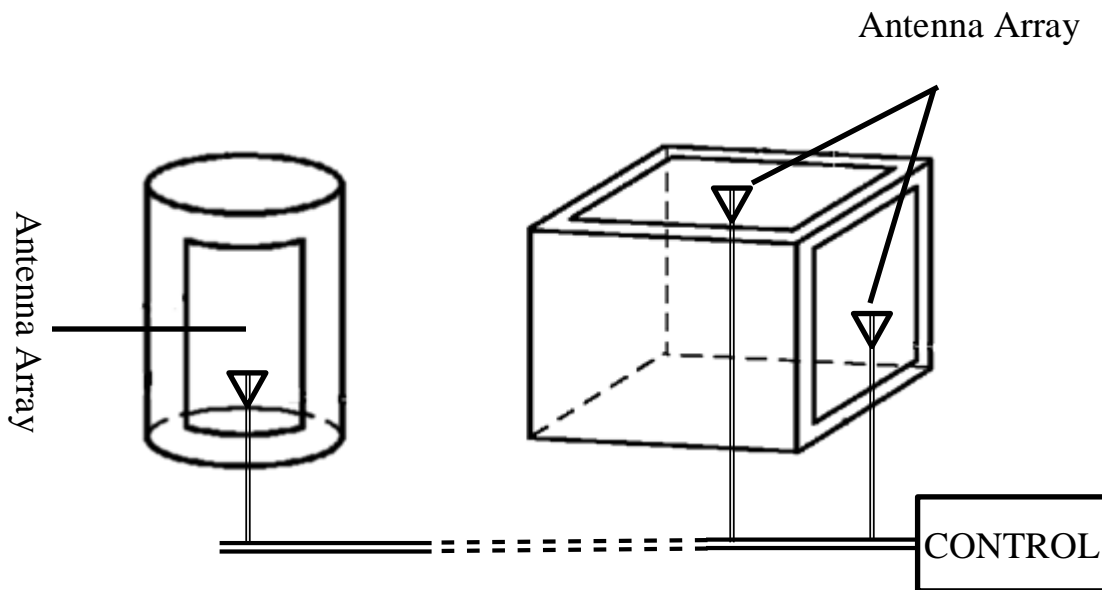


Fig. 3.14 Microwave heating system with antenna arrays

3.7.6 Microwave Heating Versatility.

Olle Niklasson et al, (2016) proposed a compartmentalised (versatile) heating apparatus (Fig.3.15) comprising of a plurality of different sources [19]. The first source was configured to supply energy at the bottom of the food source (for browning) and a second source was configured for volumetric heating in the upper chamber. A grill element located in the ceiling and a control unit for selecting the appropriate cooking cycle based on food category [19] were also included. The first source has an antenna in the lower part of the cavity and the second source has a feeding port in the upper part of the cavity. The microwave source(s) may be a solid state amplifier, a magnetron or a

combination of the two. The advantages of solid-state sources e.g. manipulating the heating pattern through frequency, phase and output power are clearly stated.

Microwave ovens used for volumetric heating lack effectiveness in attaining browning/crisp effect. The grill element in the proposed concept aims to improve browning, without affecting the performance of standard microwave heating obtained through mode excitations. The uniform distribution of multiple solid-state sources is advantageous, in that rotation of the plate is not required. This provides a greater freedom for designing the food container which does not have to be cylindrical.

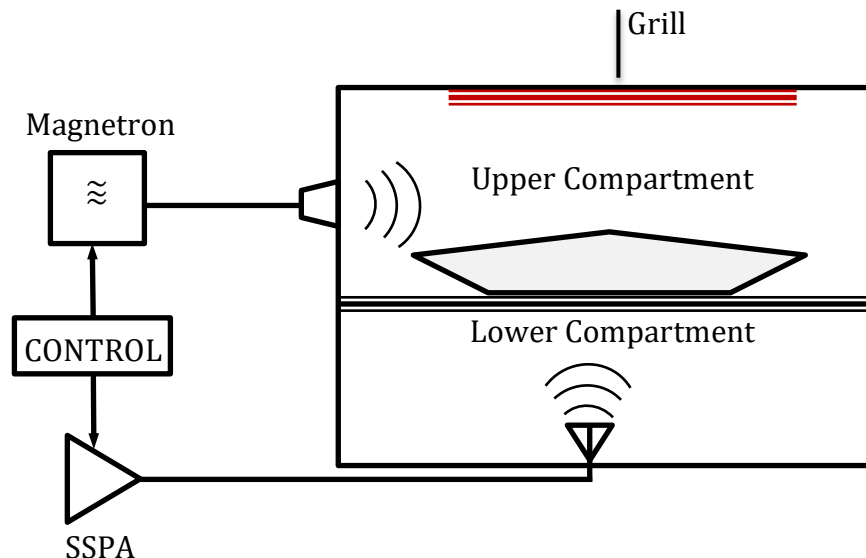


Fig. 3.15 Versatile Microwave Heating

3.7.7 The future of Microwave Heating

The future of microwave heating is destined for a change as appliance manufacturers look to replace the magnetron with more flexible energy sources. Whilst the magnetron is a reliable power generator, its use restricts field pattern mobility (due to its limited bandwidth, 'ON-OFF' functionality and the inability to select frequency, phase or amplitude, which leads to the formation of hot and cold spots in the food (Fig.3.16). The resulting standing waves inside the cavity are the cause of temperature differences.

A stirrer and turntable are typically used to sweep the food through the EM field to minimize this effect.

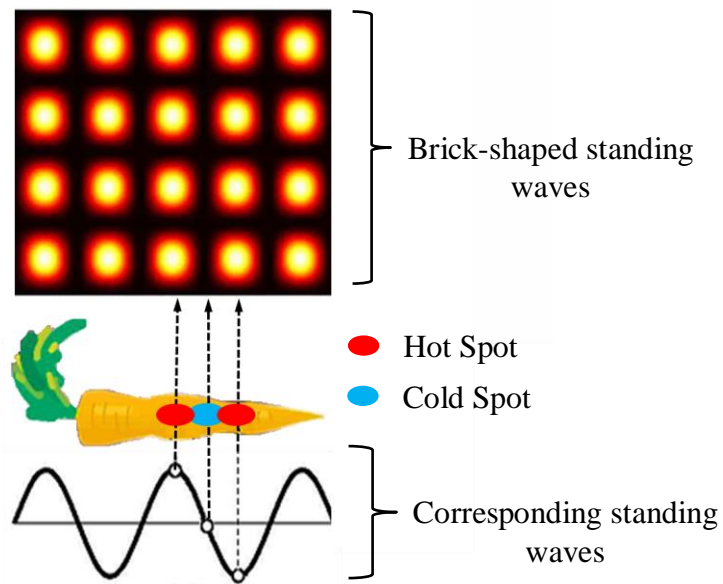


Fig. 3.16 Standing Waves – lead to hot and cold spots

Solid-state microwave heating systems offer control over frequency and phase. This means that nodes and antinodes can be moved around the cavity, which leads to a more uniform heating. The effectiveness can be further increased by using multiple sources which combine to generate the desired heating profile. Amplitude control can also be used to control temperature profiles through a power ramp cycle which leads to controlled temperature profiles and delicate cooking cycles.

Semiconductor device manufacturers (Ampleon, NXP, Macom and Infineon) offer high power RF transistors (Fig.3.17), specifically designed for RF Energy (ISM band) applications. This means that solid-state microwave ovens are no longer confined to laboratory based research. These companies are actively engaged with the RF energy alliance to develop products and standards that support a rapidly evolving commercial and consumer market. The RF Energy Alliance RFEA was founded in September 2014 to standardize, promote and educate audiences in solid-state heating systems.

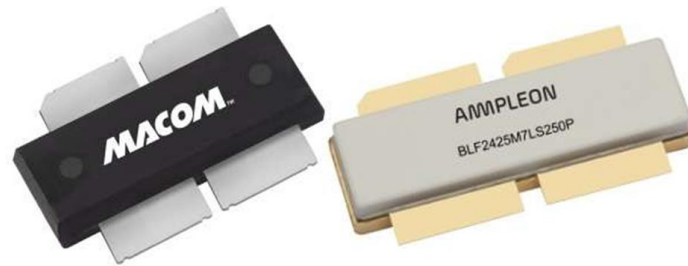


Fig. 3.17 High Power RF transistors specifically designed for RF Energy applications

Joint collaborations between semiconductor device and appliance manufacturers, e.g. AMPLEON and MIDEA has also led to the world's first commercially available solid state microwave oven, a 200 W table top oven. Designed for space constrained kitchens and for portable on-the-go food applications, the oven can be powered either from a mains power source or from a 24V DC battery. Other appliance manufacturers (Goji Food Solutions, Wayv Technology, Whirlpool and Miele) are also actively engaged in the development of solid-state based microwave heating systems and have hinted at forthcoming new products that promise to revolutionise cooking.

3.7.8 The constraints for practical implementation of solid-state technology

Whilst higher power transistors have made the use of solid-state technology more realisable, concerns over device reliability, systems and heating efficiency under variable loading conditions remain. These concerns need to be properly addressed in order for solid state device technology to be a viable alternative to the magnetron. The biggest challenge for microwave heating appliances has been the delivery of power to a variable load inside the cavity. The load impedance varies with size, shape, consistency of the food, its chemical composition, with changes in temperature and placement within the oven. These variations in load lead to unmatched loading conditions and highly-reflective energy states which result in system inefficiency.

Impedance mismatches limit the amount of power that can be delivered to the load whilst increasing the amount of reflected power back to the source. Mitigating this requires the use of circulators and high power dissipative loads. Whilst the circulator protects the transistor by directing all the reflected power to a high power load (where it is dissipated as heat), it also adds path losses (typically 0.25dB), cost and mechanical complexity to the power amplifier module. The high power ‘drop-in’ circulators and loads incur tooling (pockets machined into the heatsink) and assembly cost, which involves securing and soldering of the the two parts. If mounted poorly arcing can occur at the circulator pins which can damage the device and the printed circuit board.

The constraints involved in delivering power under variable loading conditions requires re-positioning or retuning of the coupling (antenna) structure. Whilst easily realisable for fixed loads under laboratory conditions this has proven very challenging for real life applications. A dynamic structure consisting of electromechanical parts is one possibility that has been considered, where the positioning of the coupling structure is adjusted electromechanically with load variations. This also adds cost and complexity to the system, and as yet this concept has not been realized for practical applications.

Therefore a need exists in the field of RF generated microwave heating and medical applications where all of the available power needs be delivered to the cavity under variable loading conditions (without physical or electromechanical realignment of the couplig structure). Due to cost and size constraints, the structure needs to be simple and cost effective. Failure to overcome these obstacles means that the true potential of solid-state technology (homogeneous and efficient heating, power ramping) cannot be fully realised. The added cost of circulator, high-power loads and cooling requirements, at present limit the use of this technology for domestic applications. An ‘isolator-less’ solution where the SSPA is directly integrated to the antenna (coupling structure) will help reduce the module size and cost to levels where it is directly competitive with the magnetron.

3.8 Factors Influencing Microwave Heating

It is widely known that microwave heating leaves hot and cold spots in food sources. This is due to complex interaction of electromagnetic fields with lossy materials inside a resonant cavity structure. Improving heating uniformity has been a longstanding objective of microwave processes. Vadivambal et al. (2010) [58] reviewed various literatures on microwave heating and identified a real need to improve heating uniformity in microwave ovens. Due to limitations of the technology available at the time, his research was mostly centred on the composition and geometry of food sources. In recent times the attention has shifted to understanding the phenomenon of non-uniform heating both experimentally and through computer simulations [59]–[60]. Heating uniformity has been the theme of various research papers, concentrating mostly on shape, size [111] and dielectric properties of food materials [50],[54], placement on the turntable [95] and power cycling [70].

Other techniques used to improve heating uniformity have included combination heating, infrared and hot air [79], [81], variable frequency [89], [63] and mode stirrers [84]. Bows and Kashyap et al. [63], concluded that better heating uniformity can be achieved by sweeping the frequency ($2450 \pm 50\text{MHz}$) compared to mode stirrer operation inside the cavity. With the aid of computer modelling, Geedipalli et al. (2007) [53] reported improvements of up to 40% in heating uniformity. Factors that influence heating uniformity are listed in the following sections.

3.8.1 Dielectric Properties

Dielectric properties provide valuable information about a material and play an important role in determining the likely interaction between an electric field and the material, e.g. a food source [74]. Dielectric materials experience three types of polarisation in the presence of a uniform electric field;

1. Electronic Polarisation. All materials;
2. Ionic Polarisation. Ionic crystalline solids (NaCl).
3. Orientation Polarisation. Materials whose molecules have dipole moments (H₂O), which applies to food sources.

In the presence of an electric field, the water within food substances experience orientation polarisation, which results in microwave energy being absorbed and dissipated as heat from within. The parameters that are used to describe material properties relevant to microwave heating are the dielectric constant, dielectric loss and the loss tangent. The complex relative permittivity ϵ^* consisting of real and imaginary parts (eqn.3.7) determines the dielectric constant and the dielectric loss factor.

$$\epsilon^* = \epsilon' - j\epsilon'' \quad (3.7)$$

Where:

ϵ' = The dielectric constant is a material's ability to store electric energy (for vacuum $\epsilon' = 1$).

ϵ'' = The dielectric loss factor is a material's ability to dissipate electric energy as heat.

During microwave heating, the dielectric loss factor determines a materials ability to absorb electric energy and dissipate it as heat. In low loss materials, the value of dielectric loss factor is considered negligible, Materials with $\epsilon'' < 0.01$ absorb more energy but are unable to dissipate it as heat [105], whereas lossy materials have an ability to convert more of the absorbed electrical energy into heat energy. Materials used in microwave applications are more generally categorised by their dielectric loss tangent ($\tan \delta$), which is an angular ratio of dielectric loss factor and dielectric constant (eqn.3.8).

Electric current flow through a material is referred to as electrical conductivity σ , it is the rate at which a specified material conducts electricity or the rate at which heat

passes through a specified material (eqn.3.9). The electric components of microwaves can be converted into power dissipation per unit volume (for lossy materials) using eqn 3.10 [55]. Electrical conductivity is strongly dependent on the number of electrons in a material, with typical conductivity of tap water being in the order of 0.005 - 0.05(S/m). This variation in conductivity is attributed to the presence of impurities in tap water.

Magnetic permeability is defined as the relative increase or decrease in the resultant magnetic field (within a material) compared to the magnetizing field surrounding the material. The magnetic permeability of most biological materials is same as that of free space ($\mu_0 = 4\pi \times 10^{-7} \text{ N/A}^2$). Owing to their makeup, biological materials do not interact strongly with the magnetic field component of electromagnetic waves.

$$\text{Dielectric loss tangent, } \tan \delta = \frac{\epsilon''}{\epsilon'} \quad (3.8)$$

$$\text{Electrical conductivity, } \sigma = 2\pi f \epsilon_0 \epsilon'' \quad (3.9)$$

Where:

f = The frequency (Hz)

ϵ_0 = The free space permittivity ($8.854 \times 10^{-12} \text{ F/m}$)

ϵ'' = The dielectric loss factor

$$P_v = 2\pi f \epsilon_0 \epsilon'' E^2 \quad (3.10)$$

Where

P_v = The conversion of power per unit volume (W/m^3),

f = The frequency (GHz)

ϵ'' = The relative dielectric loss factor

ϵ_0 = The permittivity of free space ($8.854 \times 10^{-12} \text{ F/m}$)

E = The electric field strength (V/m)

3.8.2 Physical Properties

Microwave heating is a complex process, and its effectiveness is compromised by variations in material properties, including dielectric properties, size, shape, chemical composition as well as placement within the cavity and system design. Heat absorption is also influenced by sensory properties of foods such as texture and consistency [61]-[62]. Food sources contain many ingredients and it is entirely possible that each has a different dielectric property and heating rate.

There have been numerous attempts to improve the inherent nature of non-uniform heating, e.g. 'ready-to-eat meal' container geometries have been optimised to encourage even energy distribution and penetration depth at 2450MHz (Table 2) [127]. Bows and Richardson (1990) [63] state that temperature distribution can be optimised through careful planning and selection of food layout. Meals composed of multiple ingredients are more likely to have an uneven temperature distribution due to differences in dielectric and thermo-physical properties. This impacts the heating rate due to variable EM distribution and absorption conditions [64].

Geometry influences the energy absorption and heating rates. An object with a large surface area will heat more rapidly due to its greater interaction with microwave energy. Whereas a curved shape absorbs more energy at its centre [65] which results in uneven heating at the edges. This is proven by the heat transfer model (based on Lambert's law) which was developed to study the effects of shape geometry on temperature distribution [66]-[67]. Chen et al. (1993) [68] also carried out similar work by studying the effect of load on microwave power absorption in distilled water (ranging from 20-200g) and potato samples of different diameters. The study concluded that power absorption is linked to the size of the load. Other similar studies [69]-[70] have recommended flattening of loads to aid energy penetration, which has led to faster heating rates. As a rule of thumb load thickness should be maintained at less than 2.5 times the microwave penetration depth at the operating frequency.

The penetration depth decreases with increasing frequency eqn.3.11.

$$PD = \frac{\lambda\sqrt{\epsilon_r'}}{2\pi\epsilon_r''} \quad (3.11)$$

Where:

$\epsilon = \epsilon_0 (\epsilon_r' - j \epsilon_r'')$, complex dielectric constant reduces with an increase in temperature.

$$\tan \delta = \epsilon_r'' / \epsilon_r'$$

δ = dielectric loss angle, measured in degrees

λ = wavelength, measured in m, $\lambda = c / f$

f = frequency, measured in Hz

ϵ_0 = absolute dielectric constant = 8.85×10^{-12} As/Vm

$c = 3 \times 10^{10}$ cm/s speed of light

Table 3.1. Penetration depths of microwave energy for various materials at 2450MHz

Material	Measurement Temperature in °C	Penetration depth in cm	As the temperature increases, the molecules have more thermal energy and therefore the magnitude of random thermal motion is greater. This means that the range of deviations from a perfect alignment under the influence of a EM field is also greater. The molecules are less closely aligned and therefore the orientation polarisation of the material (and hence the dielectric constant) is reduced.
water	45	1.4	
water	95	5.7	
ice	-12	1100	
bread	25	2 ... 5	
potato, raw	25	0.9	
mashed potato	25	0.8	
peas, carrots	25	1	
meat	25	0.9 ... 1.2	
hollow glass	25	35	
porcelain	25	56	

3.8.3 Chemical Composition

Food ingredients, salt and water in particular have a significant influence on the microwave power absorption capacity of dielectric materials. Food sources with high moisture content heat faster due to the presence of polarised water molecules. This increases the rate of collisions (as the polarised molecules align themselves in the direction of changing electric field) which leads to a faster heating rate. Similarly, food sources high in salt content have higher ionic concentration, which leads to increased energy absorption [72].

A food source with high water and salt content absorbs most of the energy impinging on its surface leading to a pseudo shielding effect. As a consequence less microwave energy reaches the centre of dense materials, which leads to non-uniform heating. The packaging of food sources with high moisture and salt content should be designed to maintain a thin base to aid the heating process. The effects of chemical composition (carbohydrates, fats, protein and water) on microwave heating have been outlined by George and Burnett (1991) [62], Kress-Rogers and Kent (1987) [71], and Gunasekaran et al. (2002) [72].

3.8.4 Placement inside the cavity

It has been stated in some detail that power absorption is a function of heating rate which is dependent on material properties, and varies for a frozen to non-frozen state (Chamchong and Datta, 1999a) [50]. Power absorption is also a function of load placement within the resonant cavity. Energy distribution inside the cavity is a series of electric field maxima and minima, which can be thought of physically as matched and unmatched regions. Loads placed in ‘matched’ regions will absorb more power, and heat more quickly compared to “unmatched” regions where the match is poor and very little or no power is absorbed. Turntables and mode stirrers have been added to microwave ovens to move the load position between these areas in an attempt to gain uniform heating.

Zhang and Datta (2003) [54] carried out a study, which considered the effect of microwave power absorption in single and multiple foods. They concluded that power absorption varies at different locations for shapes having similar dielectric properties. The relationship is a non-linear function of distance from the centre of the turntable. They also concluded that the relative power absorption in simultaneous heating of two different food sources follows the same relationship when heated individually.

3.9 Summary

Solid-state architectures (through power, relative phase and frequency control) enable microwave heating appliances to have complex heating combinations and resolution control which helps improve cooking consistency, whilst reducing cooking time. A potential use of multiple channels (antenna feeds) can help create a steady input of microwave energy into the cavity, which allows the creation of various cooking profiles by directing energy into defined areas through relative phase control (steering of energy).

A linear energy delivery into the microwave can be obtained through the use of power control, e.g. through pulse width modulation, whilst forward and reverse power measurements and feedback add intelligence to the apparatus. A measure of return loss profile shows optimally matched energy absorption regions (across the frequency band). The feedback loop can be used to ensure energy is directed at the right frequencies and couples efficiently into the load.

An accurate and stable frequency source with precise amplitude and relative phase control, when used with modulator and digital signal processing helps spread energy across the operating bandwidth. The availability of multi-output and phase locking synthesisers facilitates multi-source operation, with each emitting energy at the same frequency to achieve higher power levels within the cavity. Uneven heating (hot and cold spots) can be minimised by changing the relative phase (from one source to another) to alter the energy distribution such that it is continuously changing or intentionally directed.

3.10 References

- [1] B. R. McAvoy, "Solid state microwave oven," US Patent 4097708, Jan 21, 1971.
- [2] K. K. Cheng, "Solid state microwave heating apparatus," US Patent 3691338, Sep 12, 1972.
- [3] T. Ohtani, "Hybrid microwave heating apparatus," US Patent 3867607, Feb 18, 1975.
- [4] R. A. Dehn, "Microwave heating apparatus with improved multiple couplers and solid-state power source," US Patent 4006338, Feb 1, 1977.
- [5] S. H. Bickel, "Solid state microwave oven power source," US Patent 4097708, Jan 27, 1978.
- [6] Alejandro MacKay, "Controlled heating microwave ovens," US Patent 4196332, 1978
- [7] Alejandro MacKay, "Controlled heating microwave ovens using different operating frequencies," Canada Patent 1081796, 1980
- [8] Tomotaka Nobue, "Microwave oven having controllable frequency microwave power source," US Patent 4415789, 1983
- [9] Hisashi Okatsuka, "Microwave heating apparatus with solid-state microwave oscillating device," US Patent 4504718, 1985
- [10] Patrick Jackuault, "Microwave oven, in particular for rapid heating to high temperature," US Patent 5420401, 1995
- [11] Bernard R. Cheo, "Active RF cavity including a plurality of solid-state transistors," US Patent 5497050, 1996
- [12] Derrick J. Page, "Microwave power radiator for heating applications," US Patent 5558800, 1996
- [13] Per O.Risman & Charles R.Buffler, 1997
- [14] Peter Handinger, "Microwave heating using distributed semiconductor sources," US Patent 20040206755, 2004
- [15] Ulf E. Nordh, "Microwave oven switching between predefined modes," US Patent 20100155392, 2010

-
- [16] Tomotaka Nobue, "Microwave heating apparatus," US Patent 20110108548, 2011
- [17] Ranjit Gharpurey, "Microwave oven with antenna array," US Patent 20130175262, 2013
- [18] Jose A. Lima, "Microwave oven using solid-state amplifiers and antenna array," US Patent 20150136760, 2015
- [19] Olle Niklasson, "Versatile microwave heating apparatus," US Patent 9332597, 2016
- [20] R.J. Meredith, *Engineers' Handbook of Industrial Microwave Heating*, IEE, 1998.
- [21] Tiefeng, S. & Kaldi, L. "High-power solid-state oscillator for microwave oven applications" *IEEE/MTT-S Int'l Microwave Symposium* (2012).
- [22] Durnan, G., "Solid-state improvements in microwave cooking", *Int'l Microwave Symp., WFJ Workshop: Power Amplifiers with variable loads*. San Francisco (2016).
- [23] T. Oguro, "Trends in magnetrons for consumer microwave ovens," *J. Microwave Power*, vol. 13, no. 1, pp. 27-36, Mar. 1978.
- [24] V.V. Yakovlev, "Frequency control over the heating patterns in a solid-state dual-source microwave oven," *IEEE MTT-S Int'l Microwave Symp. Dig.* (Phoenix, AZ, May 2015), 978-1-4799-8275-2/15.
- [25] E. Jerby, "Localized microwave-heating (LMH) model and potential applications," *Proc. GCMEA-3, Cartagena, Spain, July 25-29, 2016*.
- [26] E.E.W. Kassner, "Apparatus for the generation of short electromagnetic waves;" U.S. Patent 2094602, Oct. 5, 1937
- [27] E.E.W. Kassner, "Process for altering the energy content of dipolar substances;" U.S. Patent 2089966, Aug. 17, 1937.
- [28] E.E.W. Kassner, "Apparatus for generating and applying ultrashort electromagnetic waves;" U.S. Patent 2109843, Mar. 1, 1938
- [29] W. M. Hahnemann, "Radiating Device," U.S. Patent 2161 292, June'6, 1939.
- [30] M. Rothstein, "Dielectric heating," in *Encyclopaedia of Polymer Science*, vol. 5. New York: Interscience Publishers, 1966.

-
- [31] W. C. White, "Early history of industrial electronics," Proc. IRE, vol. 50, pp. 1129–1135, May 1962.
- [32] W. M. Roberds, "Problems in the design of high-frequency heating equipment: Proc. IRE, vol. 34, pp. 489–500, July 1946.
- [33] E. W. Allen, Jr., and H. Garlan, "Evolution of regulatory standards of interference; Proc. IRE, vol. 50, pp. 1306-1311, May 1962.
- [34] T. M. Shaw and J. A. Galvin, "High-frequency-heating characteristics of vegetable tissues determined from electrical conductivity measurements," Proc. IRE, vol, 37, 'pp. 83–86, Jan. 1949.
- [35] P. W. Morse and H. E. Rivercomb, "UHF heating of frozen foods,' Electronics, VO. 20, pp. 85-89, Oct. 1947.
- [36] P. P. Derby, "Electron discharge devices:' U.S. Patent 2463524, Mar. 8, 1949.
- [37] R. O. Nelson, "A magnetron oscillator for dielectric heating J.Appl. Phys., vol. 18, pp. 356-361>1947.
- [38] W. M. Hall, "Heating Apparatus," U.S. Patent 2618735, 1.952.
- [39] Tappan News, pp. 3-8, Nov. 1955.
- [40] R. V. Decaxeau, "The Amana story," Microwave En. Appl. Newsletter, vol. X, no. 2, pp. 3-4, 1977.
- [41] N. H. Moore, "Microwave energy in the food field," Address at 20th Anniversary Mtg of Research & Development Associates, Tues., April 13, 1966. Published in Mic. En. Appl. Newsletter, vol.1, no. 1, pp. 5-7, Jan.-Feb. 1968.
- [42] Advertisement, "Microwave electric-oven 'Elektronika'," Economic News (MOSCOW), spring 1980.
- [43] R. Wechsler, "Solid-state power control of microwave ovens, "Appliance Engineer, pp. 72-74, Dec. 1976.
- [44] Advertisement," TDK ferrite gaskets for microwave ovens," Applzance Magazine, p. 6, Oct. 1977.
- [45] D. Winstead, '<Microprocessor controls for microwave ovens:' J. Microwave Power, vol. 13, no. 1, pp. 7-12, Mar. 1978.
- [46] Anon., "Japan developing solid-state power for ovens," MSN, p.21, NOV. 1978.

-
- [47] Ghammaz, A., S. Lefevre and N. Teissandier. 2003. Spectral behavior of domestic microwave ovens and its effects on the ISM band. *Annals of Telecommunications* 58(7): 1178-1188.
- [48] Celuch, M., W. Gwarek and M. Soltysiak. 2009. Effective modeling of microwave heating scenarios including susceptors. In *Recent Advances in Microwave Theory and Applications, 2008. MICROWAVE 2008. International Conference on*, 404-405. IEEE.
- [49] Yakovlev, V. V. 2006. Examination of contemporary electromagnetic software capable of modelling problems of microwave heating. *Advances in Microwave and Radio Frequency Processing. Part III*.178-190.
- [50] Chamchong, M. and A. K. Datta. 1999b. Thawing of foods in a microwave oven: II. Effect of load geometry and dielectric properties. *The Journal of Microwave Power and Electromagnetic Energy: A Publication of the International Microwave Power Institute* 34(1): 22-32.44
- [51] Bengtsson, N. E. and T. Ohlsson. 1974. Microwave heating in the food industry. *Proceedings of the IEEE* 62(1): 44-55.
- [52] Basak, T. and K. G. Ayappa. 1997. Analysis of microwave thawing of slabs with effective heat capacity method. *AICHE Journal* 43(7): 1662-1674.
- [53] Geedipalli, S., V. Rakesh and A. Datta. 2007. Modelling the heating uniformity contributed by a rotating turntable in microwave ovens. *Journal of Food Engineering* 82(3): 359-368.
- [54] Zhang, H. and A. K. Datta. 2003. Microwave power absorption in single-and multiple item foods. *Food and Bioproducts Processing* 81(3): 257-265.
- [55] Goldblith, S. A. and D. I. C. Wang. 1967. Effect of microwaves on *Escherichia coli* and *Bacillus subtilis*. *Applied and Environmental Microbiology* 15(6): 1371.
- [56] Tong, C. H. and D. B. Lund. 1993. Microwave heating of baked dough products with simultaneous heat and moisture transfer. *Journal of Food Engineering* 19(4): 319- 339. 101
- [57] Soltysiak, M., U. Erle and M. Celuch. 2008. Load curve estimation for microwave ovens: Experiments and electromagnetic modelling. *Microwaves, Radar and*

- Wireless Communications, 2008. MIKON 2008. 17th International Conference on, 1-4. IEEE.
- [58] Vadivambal, R. and D. S. Jayas. 2010. Non-uniform temperature distribution during microwave heating of food materials—A review. *Food and Bioprocess Technology* 3(2): 161-171.
- [59] Wäppling-Raaholt, B. and P. Moret. 2006. Microwaveable Frozen Foodstuff.
- [60] Knoerzer, K., M. Regierb and H. Schubertb. 2007. A computational model for calculating temperature distributions in microwave food applications. *Innovative Food Science & Emerging Technologies* 9(3): 374-384.
- [61] Zhang, H. and A. K. Datta. 2000. Coupled electromagnetic and thermal modeling of microwave oven heating of foods. *The Journal of microwave power and electromagnetic energy: a publication of the International Microwave Power Institute* 35(2): 71-85.
- [62] George, R. M. and S. Burnett. 1991. General guidelines for microwaveable products. *Food Control* 2(1): 35-44.
- [63] Bows, J. R. and P. S. Richardson. 1990. Effective of component configuration and packaging materials on microwave reheating a frozen three-component meal. *International Journal of Food Science & Technology* 25(5): 538-550.
- [64] Mudgett, R. 1988. Electromagnetic energy and food processing. *The Journal of Microwave Power and Electromagnetic Energy: A Publication of the International Microwave Power Institute* 23(4): 225-230.
- [65] Ohlsson, T. and P. O. Risman. 1978. Temperature distribution of microwave heating spheres and cylinders. *Journal of Microwave Power* 13(4): 303-310. 50
- [66] Ayappa, K. G., H. T. Davis, E. A. Davis and J. Gordon. 1992. Two dimensional finite element analysis of microwave heating. *AICHE Journal* 38(10): 1577-1592.
- [67] Remmen, H. H. J., C. T. Ponne, H. H. Nijhuis, P. V. Bartels and P. J. A. M. Kerkhof. 1996. Microwave heating distributions in slabs, spheres and cylinders with relation to food processing. *Journal of Food Science* 61(6): 1105-1114.

- [68] Chen, D. S. D., R. K. Singh, K. Haghighi and P. E. Nelson. 1993. Finite element analysis of temperature distribution in microwaved cylindrical potato tissue. *Journal of Food Engineering* 18(4): 351-368.
- [69] Giese, J. 1992. Advances in microwave food processing. *Food Technology* 46(9): 118- 123. 46
- [70] Chamchong, M. and A. K. Datta. 1999. Thawing of foods in a microwave oven: I. Effect of power levels and power cycling. *The Journal of Microwave Power and Electromagnetic Energy: a publication of the International Microwave Power Institute* 34(1): 9-21.98
- [71] Kress-Rogers, E. and M. Kent. 1987. Microwave measurement of powder moisture and density. *Journal of Food Engineering* 6(5): 345-376.
- [72] Gunasekaran, N. 2002. Effect of fat content and food type on heat transfer during microwave heating. MS (Thesis). Blacksburg, VA: Virginia Polytechnic Institute and State University.
- [73] Pathak, S. K., F. Liu and J. Tang. 2003. Finite difference time domain (FDTD) characterization of a single mode applicator. *Journal of Microwave Power & Electromagnetic Energy* 38(1): 37-41.
- [74] Buffler, C. R. 1993. Microwave cooking and processing: Engineering fundamentals for the food scientist. New York: Van Nostrand Reinhold.
- [75] Celuch, M. and W. Gwarek. 2000. Advanced features of FDTD modeling for microwave power applications. In 35th Microwave Power Symposium, Montreal, Canada.
- [76] Bows, J. R. 1999. Variable frequency microwave heating of food. *The Journal of Microwave Power and Electromagnetic Energy: A Publication of the International Microwave Power Institute* 34(4): 227-238.
- [77] Chapman, B., M. F. Iskander, R. L. Smith and O. M. Andrade. 1993. Simulation of sintering experiments in single-mode cavities. In *Materials Research Society Symposium Proceedings*, 53-53. Materials Research Society.
- [78] Curet, S., O. Rouaud and L. Boillereaux. 2006. Heat Transfer Models for Microwave Thawing Applications.

- [79] Datta, A. K. and H. Ni. 2002. Infrared and hot-air-assisted microwave heating of foods for control of surface moisture. *Journal of Food Engineering* 51(4): 355-364.
- [80] Bradshaw, S., S. Delpont and Van Wyk.E. 1997. Qualitative measurement of heating uniformity in a multimode microwave cavity. *Journal of Microwave Power and Electromagnetic Energy* 32(2): 87-95.
- [81] Datta, A. K., S. S. R. Geedipalli and M. F. Almeida. 2005. Microwave combination heating. *Food Technology* 59(1): 36-40.45
- [82] Drouzas, A. E., E. Tsami and G. D. Saravacos. 1999. Microwave/vacuum drying of model fruit gels. *Journal of Food Engineering* 39(2): 117-122.
- [83] Ayappa, K. G., H. T. Davis, G. Crapiste, E. A. Davis and J. Gordon. 1991. Microwave heating: an evaluation of power formulations. *Chemical Engineering Science* 46(4): 1005-1016.
- [84] George, J. and R. Bergman. 2006. Selective re-meshing: A new approach to include mode stirring effects in the steady state FDTD simulation of microwave heating cavities. *Microwave and Optical Technology Letters* 48(6): 1179-1182.
- [85] Bhuwan Pandit, R., J. Tang, F. Liu and G. Mikhaylenko. 2007. A computer vision method to locate cold spots in foods in microwave sterilization processes. *Pattern Recognition* 40(12): 3667-3676.
- [86] Huo, Y. and B. Q. Li. 2005. Boundary/finite element modelling of three-dimensional electromagnetic heating during microwave food processing. *Journal of Heat Transfer* 127:1159-1166. International Electro technical Commission (IEC). 1999. Household microwave ovens - methods for measuring performance. IEC publication 60705.
- [87] Jia, X. and P. Jolly. 1992. Simulation of microwave field and power distribution in a cavity by a three-dimensional finite element method. *Journal of Microwave Power and Electromagnetic Energy* 27(1): 11-22. 47
- [88] Dahl, C. A., M. E. Matthews and E. H. Marth. 1981. Survival of *Streptococcus faecium* in beef loaf and potatoes after microwave-heating in a simulated cook/chill foodservice system. *Journal of Food Protection*. 44:128-133.

- [89] Kashyap, S. C. and W. Wyslouzil. 1977. Methods for improving heating uniformity of microwave ovens. *Journal of Microwave Power and Electromagnetic Energy* 12(3): 223-230.
- [90] Knoerzer, K., M. Regier and H. Schubert. 2008. A computational model for calculating temperature distributions in microwave food applications. *Innovative Food Science & Emerging Technologies* 9(3): 374-384.
- [91] Chen, H., J. Tang and F. Liu. 2008. Simulation model for moving food packages in microwave heating processes using conformal FDTD method. *Journal of Food Engineering* 88(3): 294-305.
- [92] Kopyt, P. and M. Celuch-Marcysiak. 2003. FDTD modelling and experimental verification of electromagnetic power dissipated in domestic microwave ovens. *Journal of Telecommunication and Information Technology* 159-65.48
- [93] James, C., M. V. Swain, S. J. James and M. J. Swain. 2002. Development of methodology for assessing the heating performance of domestic microwave ovens. *International Journal of Food Science & Technology* 37(8): 879-892.
- [94] Kopyt, P. and M. Celuch. 2007. Coupled electromagnetic-thermodynamic simulations of microwave heating problems using the FDTD algorithm. *The Journal of Microwave Power and Electromagnetic Energy: A publication of the International Microwave Power Institute* 41(4): 18-29.
- [95] Wappling-Raaholt, B. and T. Ohlsson. 2000. Tools for improving the heating uniformity of foods heated in a microwave oven. *Microwave world* 21(1): 24-28.
- [96] Liu, C. M., Q. Z. Wang and N. Sakai. 2005. Power and temperature distribution during microwave thawing, simulated by using Maxwell's equations and Lambert's law. *International Journal of Food Science & Technology* 40(1): 9-21.
- [97] Ni, H., A. K. Datta and R. Parmeswar. 1999. Moisture loss as related to heating uniformity in microwave processing of solid foods. *Journal of Food Process Engineering* 22(5): 367-382.
- [98] Ehlers, R. A. and R. A. Metaxas. 2007. An investigation on the effect of varying the load, mesh and simulation parameters in microwave heating applications. *The*

- Journal of microwave power and electromagnetic energy: a publication of the International Microwave Power Institute 40(4): 251-259.
- [99] Ryyänen, S. and T. Ohlsson. 1996. Microwave heating uniformity of ready meals as affected by placement, composition, and geometry. *Journal of Food Science* 61(3): 620-624. 51
- [100] Swami, S. 1982. Microwave heating characteristics of simulated high moisture foods. MS Thesis ed. Amherst, MA, USA: University of Massachusetts.
- [101] Ohlsson, T. and N. Bengtsson. 2001. Microwave technology and foods. *Advances in food and nutrition research* 4:365-140.
- [102] Ohlsson, T. and N. E. Bengtsson. 1971. Microwave heating profiles in foods: A comparison between heating experiments and computer simulation. *Microwave energy applications newsletter* ed. SIK publication.
- [103] Ohlsson, T. 1991. More uniformity in heat from microwave ovens. *Food Technology International-Europe*. 55:277-281.
- [104] Pandit, R. B. and S. Prasad. 2003. Finite element analysis of microwave heating of potato-transient temperature profiles. *Journal of Food Engineering* 60(2): 193-202.
- [105] Metaxas, A. C. and R. J. Meredith. 1983. *Industrial Microwave Heating*. IEE Power Engineering Series 4. Peter Peregrinus Ltd., London, UK. MMWR. 2008. Multistate outbreak of salmonella infections associated with frozen pot pies. *Centers for Disease Control and Prevention* 57(47): 1277-178.
- [106] Xiaowei, G., M. Lin and S. Yiqin. 2010. Electromagnetic field optimisation procedure for the microwave oven. *International Journal of Electronics* 97(3): 339-347.
- [107] Swain, M. J., A. Spinassou and M. V. L. Swain. 2008. A test procedure to characterize the heating performance of domestic microwave ovens. *International Journal of Food Science & Technology* 43(1): 15-23.
- [108] Tang, J., F. Hao and M. Lau. 2002. Microwave heating in food processing. *Advances in bioprocessing engineering*. 1-44.

- [109] Tilford, T., E. Baginski, J. Kelder, K. Parrott and K. Pericleous. 2007. Microwave modeling and validation in food thawing applications. *The Journal of Microwave Power and Electromagnetic Energy: A publication of the International Microwave Power Institute* 41(4): 30-45.
- [110] Risman, P. O. and M. Celuch-Marcysiak. 2000. Electromagnetic modeling for microwave heating applications. In 13th International Conference on Microwaves, Radar and Wireless Communications. 2000. MIKON-2000.
- [111] Vilayannur, R. S., V. M. Puri and R. C. Anantheswaran. 1998. Size and shape effect on nonuniformity of temperature and moisture distributions in microwave heated food materials: Part II Experimental Validation. *Journal of Food Process Engineering* 21(3): 235-248.
- [112] Taher, B. J. and M. M. Farid. 2001. Cyclic microwave thawing of frozen meat: experimental and theoretical investigation. *Chemical Engineering and Processing* 40(4): 379-389.
- [113] Curcio, S., M. Aversa, V. Calabrò and G. Iorio. 2008. Simulation of food drying: FEM analysis and experimental validation. *Journal of Food Engineering* 87(4): 541-553.
- [114] Pedreño-Molina, J. L., J. Monzó-Cabrera and J. M. Catalá-Civera. 2007. Sample movement optimization for uniform heating in microwave heating ovens. *International Journal of RF and Microwave Computer-Aided Engineering* 17(2): 142-152.
- [115] Wäppling-Raaholt, B., P. O. Risman and T. Ohlsson. 2006. Microwave heating of ready meals-FDTD simulation tools for improving the heating uniformity. *Advances in microwave and radio frequency processing*. Springer Berlin Heidelberg.
- [116] Van, T. Ohlsson and B. M. Nicolai. 2002. A combined electromagnetic and heat transfer model for heating of foods in microwave combination ovens. *Journal of Microwave Power and Electromagnetic Energy* 37(2): 97-111.

- [117] Watanabe, M., M. Suzuki and S. Ohkawa. 1978. Analysis of power density distribution in microwave ovens. *Journal of Microwave Power and Electromagnetic Energy* 13(2): 173–182.
- [118] Datta, A. K. and R. C. Anantheswaran. 2001. *Handbook of microwave technology for food applications*. CRC.
- [119] Peyre, F., A. Datta and C. Seyler. 1997. Influence of the dielectric property on microwave oven heating patterns: application to food materials. *The Journal of Microwave Power and Electromagnetic Energy: A publication of the International Microwave Power Institute* 32(1): 3-15.
- [120] Chamchong, M. and A. K. Datta. 1999. Thawing of foods in a microwave oven: II. Effect of load geometry and dielectric properties. *The Journal of Microwave Power and Electromagnetic Energy: a publication of the International Microwave Power Institute* 34(1): 22-32.
- [121] Khraisheh, M. A. M., T. J. R. Cooper and T. R. A. Magee. 1997. Microwave and air drying I. Fundamental considerations and assumptions for the simplified thermal calculations of volumetric power absorption. *Journal of Food Engineering*. 33(1-2): 207-219.
- [122] Wäppling-Raaholt, B., N. Scheerlinck, S. Gait, J. R. Banga, A. Alonso, E. Balsacanto and I. VAN. 2002. A combined electromagnetic and heat transfer model for heating of foods in microwave combination ovens. *Journal of Microwave Power and Electromagnetic Energy* 37(2): 97-111.
- [123] Akarapu, R., B. Q. Li, Y. Huo, J. Tang and F. Liu. 2004. Integrated modeling of microwave food processing and comparison with experimental Measurements. *Journal of Microwave Power and Electromagnetic Energy* 39(3/4): 153.
- [124] Campanone, L. A. and N. E. Zaritzky. 2005. Mathematical analysis of microwave heating process. *Journal of Food Engineering* 69(3): 359-368.
- [125] <https://socratic.org/questions/what-is-the-dipole-moment-of-water>
- [126] [https://www.pueschner.com/en/microwave-technology/penetration depths?p=basics/eindringtiefe.php](https://www.pueschner.com/en/microwave-technology/penetration-depths?p=basics/eindringtiefe.php)

CHAPTER 4 – POWER AMPLIFIER DESIGN CONSIDERATIONS

4.1 Power Amplifier Key Parameters

The use of SSPA's for microwave heating applications has been proposed and discussed in previous chapters. The communications and broadcast systems have been largely responsible for an evolution in semiconductor device physics, which has led to the development of very high power amplifiers. These amplifiers are capable of accommodating high peak-to-average power ratio (PAPR), to provide a high efficiency and linearity over a wide dynamic range. Power amplifiers in solid-state heating applications by contrast, are able to operate at or close to their maximum power rating, (saturation region), where efficiency is at its highest.

Besides having a high efficiency, the SSPA's intended for microwave heating applications must be simple and of low cost. The topologies and techniques employed in communications systems are likely to be prohibitively complex and expensive for these applications. A SSPA for microwave heating applications needs an approach, which limits the use of expensive components (e.g. circulator and high-power dissipative loads).

The main performance characteristics of a power amplifier include output power, efficiency, gain and linearity. There is usually a trade-off between each of these characteristics, so an understanding of each of these characteristics is essential in meeting the targeted specifications. Amplifier characteristics along with their commonly used modes of operation are introduced in the following sections.

4.1.1 Output Power

The output power of a SSPA is generally determined from the power capability of a transistor and the available power supply. This is an important parameter in determining performance capability and suitability for the targeted application(s).

4.1.2 Efficiency

The efficiency is a measure of an amplifier's ability to convert dc power into signal or RF power. It is an important parameter in solid-state applications where device reliability (under variable loading conditions) must be preserved, cooling and operating costs kept low. An ideal amplifier delivers power to the load that is equal to the DC power taken from the supply, and thus has an efficiency of 100%. In practical applications, this is not realisable as some of the power is consumed during the amplification process.

4.1.3 Gain

The gain of an amplifier (G) is a ratio of the magnitude of the output signal power in watts (P_o) to the magnitude of the input signal power in watts (P_i). Gain can also be listed in terms of voltage, current, or power depending on the application.

4.1.4 Linearity

Linearity is an amplifiers ability to amplify a signal without distortion. Whilst linearity is essential in communications systems, it is not considered important for solid-state applications, hence it is not discussed in any detail.

4.2 Power Amplifier modes of operation

Amplifiers are categorised into different classes (e.g. A, B, AB, C, and F) according to their modes of operation, circuit configurations, bias and drive conditions. These classes range from entirely linear with low efficiency (class A) to entirely non-linear with high efficiency (class F). This section presents a brief overview of different classes of amplification and discusses their suitability for solid-state heating applications.

4.2.1 Class A

Class A amplifiers have the highest linearity over other amplifier classes with a theoretical efficiency of 50 percent. In order to achieve high linearity and gain, the output stage of a class A amplifier is on at all times, in other words, the device conducts over a full 360 degrees of the output waveform. Due to the low efficiency associated with class A amplification and the thermal problems that result, it is not considered suitable for microwave heating applications.

4.2.2 Class B

Ideal class B amplifiers overcome the heating and inefficiency problems associated with class A amplification by operating at zero quiescent current, such that the dc power consumption is small. The theoretical efficiency (78.5%) is higher than that of the class-A which means that Class B amplification is a potential candidate for microwave heating applications.

4.2.3 Class AB

The class AB amplifier is a compromise between linearity of class A and efficiency of class B. It has a higher efficiency than a class A amplifier, however this comes at expense of a reduction in linearity which means that a signal with an amplitude modulated envelope will get distorted at peak power levels (at or close to saturation region). The transistor is biased close to pinch-off, typically at 10 to 15 percent of I_{dss} . It is ON for more than half a cycle (180° conduction angle) but less than a full cycle (360° conduction angle) of the input signal. The conduction angle, which is a function of the input drive can be set to give a range of efficiencies varying from 50% (Class A) to 78.5% (class B). Class AB has a wide bandwidth and has the potential for upto 3dB higher power gain compared to class B operation.

4.2.4 Class C

The previous classes are considered linear as the output signal's amplitude and phase are linearly related to the input signal's amplitude and phase. In applications (microwave heating) where linearity is not important and efficiency is critical, non-linear amplifier classes such as class C are considered. In class C operation the transistor is biased such that the output current is zero for more than one half of an input sinusoidal signal cycle. This gives a much improved efficiency (100% for an ideal class C) at the expense of heavily distorted output signal. Biasing the transistor below its threshold, means that a larger input drive is required to drive the class C stage, which has lower gain compared to class A, B and AB. Further the power capacity of a class C is small at low conduction angles (Fig. 4.1). Whilst the improved efficiency is greatly advantageous, the extra cost (larger driver) and the reduced power capacity means that a more detailed analysis is required to assess class C suitability for solid-state heating applications.

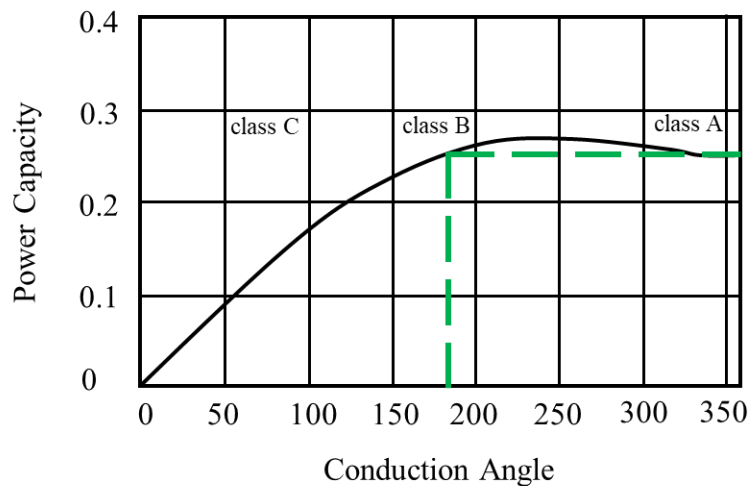


Fig. 4.1 The power capacity comparisons of Class A, Class B and Class C amplifiers [35].

4.2.5 Class D

Class D is a switch mode amplifier with a theoretical efficiency of 100%. This is possible due to the fact that there is no overlap region between the current and voltage waveforms. In practice due to non-zero switching and reactive parasitics, an ideal drain voltage waveform is not realizable, which limits achievable efficiency. A practical class-D amplifier comprises of two or more transistors (as switches) to generate half-sinusoidal current and square voltage waveforms. A series “LC” network at the output acts as a passband filter for the fundamental frequency components, whilst terminating the harmonic content intelligently. Class D overcomes power wastage and thermal dissipation by minimizing the voltage and current overlaps through the switching mechanisms.

4.2.6 Class E

Class E is also a switch-mode amplifier, it comprises of a single transistor, a passive load network and has a theoretical efficiency of 100 percent. In its simplest form, a FET is used as an “ON/OFF” switch with a duty cycle of 50 percent. The switch is closed during the positive cycle, which allows AC current to flow (through the switch) to the ground. During the negative cycle the switch is open and the current flows into the resistive load, which leads to a voltage buildup. The transistor “ON/OFF” operation and the load network shapes the current (I) and voltage (V) waveforms to prevent a simultaneous buildup of high voltage and current (with no overlaps), thus minimizing power dissipation. Whilst the amplifier has a theoretical efficiency of 100 percent, the realizable efficiency is in the region of 80 percent. This is due to power losses in intermodulation and harmonic products. The power capacity of a class E amplifier is better than that of a class C at low conduction angles. It has a low power gain (similar to class C) and exhibits very large voltage swings (upto 3.5 times the supply voltage), which means that the power transistor has to be able to handle much larger voltages. This is likely to lead to reliability problems in solid-state applications where the total voltage at the device plane can be a sum of forward and reflected voltages.

4.2.7 Class F and Inverse Class-F

The class-F amplifier offers high power and efficiency capability with a limited number of controlled harmonics [1]. An ideal class-F amplifier has half-sinusoidal current and a rectangular voltage waveforms, in conjunction with the short circuit for even harmonics and open circuit for odd harmonics. There is no overlapping between the current and voltage waveforms, which results in zero internal power dissipation. Ideally the voltage waveform at the drain (Fig. 4.3) should be a perfect square, the current waveform should be half-sine wave and 180° out of phase with the voltage waveform.[21]-[22]. Class-F amplifier has a theoretical efficiency of 100% (eqn.4.1), assuming there are no power losses in the harmonics, however in practical applications this reduces to around 80% as only the 2nd and 3rd harmonics are controlled. Inverse wave shaping is regarded as inverse class-F; here the output matching network of a Class F⁻¹ has to ensure a short circuit condition at the third harmonic and an open circuit condition at the second harmonic. In inverse class F (F⁻¹) the current and voltage waveforms are interchanged. With the same supply voltage, an inverse class-F amplifier has larger peak voltage value than that of class-F.

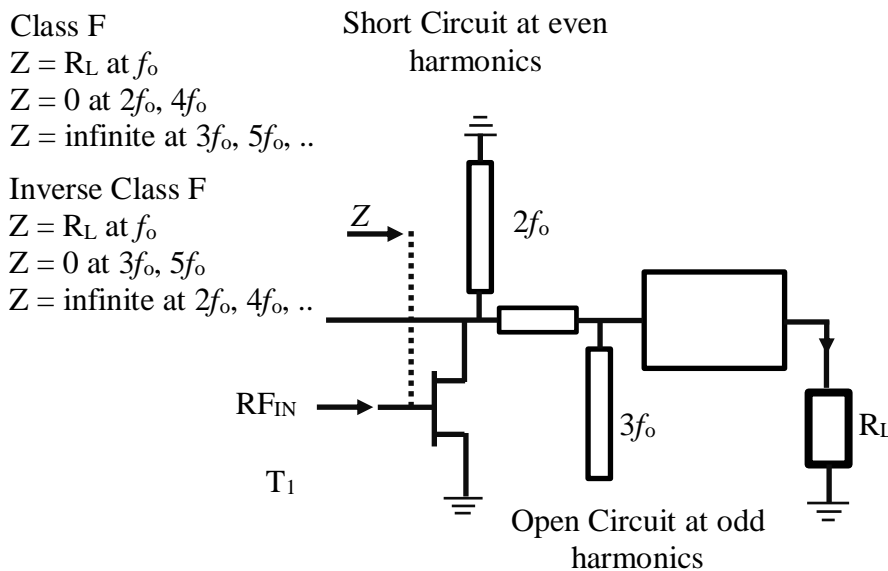


Fig. 4.2 Typical Class F Amplifier

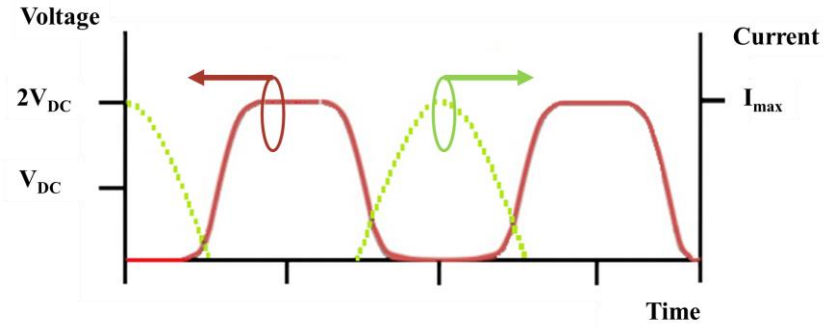


Fig. 4.3: Harmonic Limited Class-F Voltage and Current Waveforms [23]

$$\eta_{\max} = \frac{P_{0-\max}}{P_{dc}} \cdot 100 = \frac{\frac{I_{dq-\max}}{4} \cdot \frac{2}{8} V_{ds}}{\frac{I_{dq-\max}}{\pi} \cdot V_{ds}} \cdot 100 \quad (4.1)$$

Various harmonic termination networks comprising of transmission lines and lumped elements have been reported in literature [2]-[4], their impact is lessened by device parasitics. Further device breakdown was a common problem associated with Class F (F^{-1}) until the emergence of wideband gap (larger voltage swing) devices. These device are not considered for microwave heating applications due to their relatively high cost. A performance vs cost analysis of available device technologies (suitable for solid-state heating applications) can be found in device comparative analysis [37].

4.2.8 Class J

Efficiency, reliability and low cost are essential component of SSPA's in solid-state heating systems. Various high efficiency topologies have been proposed and discussed during the course of this study, among these class F delivers good efficiency by controlling the odd-even harmonics. Class J amplification [14]-[17] involves the characterisation of fundamental impedance and reactive harmonic terminations at the intrinsic device plane. The reactive fundamental and harmonic terminations combine to give a larger fundamental voltage component which leads to the same efficiency as a class B amplifier. The proposed implementation utilises the capacitive load element (C_{DS}) to

manipulate the harmonic impedances. However the need to present a complex load at the fundamental frequency, and the potential phase mismatches can lead to performance degradation. Isolation of the fundamental and harmonic matching networks has been proposed [12]-[13], to target high levels of efficiency and reduced complexity.

In summary, class-J operation requires an appropriate termination of fundamental and 2nd harmonics, to achieve high efficiency than a class AB amplifier. This requires an accurate selection of the input termination such that the output component of the second harmonic (with correct phase) is realised. Loading conditions play an important role in PA efficiency, therefore the ability to reduce power dissipation at harmonics whilst ensuring maximum power transfer at fundamental is key to maintaining high levels of efficiency.

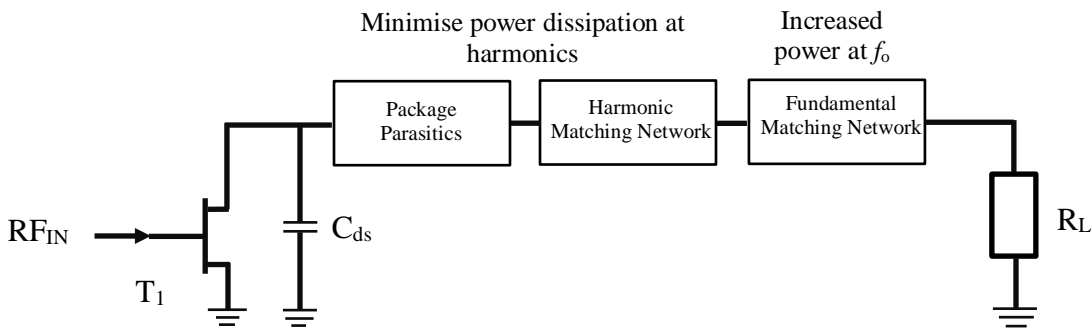


Fig. 4.4: Class-J Amplifier Matching Network

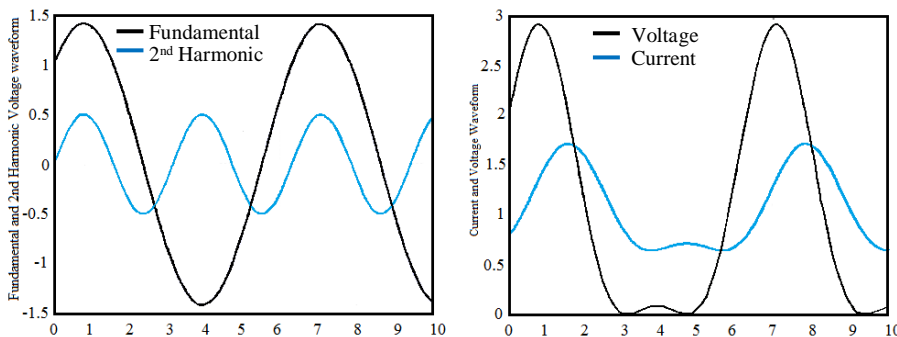


Fig. 4.5: Fundamental and 2nd Harmonic Voltages (left) and Class-J Voltage & Current Waveform [20]

4.3 SSPA Architectures

Besides having a high efficiency, the SSPA architecture for microwave heating applications must be simple and of low cost. The topologies and techniques employed in communications systems and summarised in this section are likely to be prohibitively complex and expensive for these applications. SSPA design for microwave heating, needs an approach, where the use of expensive components (e.g. isolator and high-power dissipative loads) is not necessary. Isolator-less operation is considered important for two reasons; firstly an isolator and high power load add substantial cost to the SSPA, secondly the presence of an isolator restricts access to device level impedances. However, isolatorless operation can potentially expose the RF power transistor to hostile impedance environments which can lead to very high junction temperatures and device breakdown. From a device reliability perspective it is important to ensure that it continues to operate into a matched load. Semiconductor device manufacturers (Ampleon, NXP, Macom and Infineon) offer high power LDMOS RF transistors specifically designed for RF energy (ISM band) applications. The transistors considered and typically used in the PA architectures listed in this section, are designed to withstand a load-mismatch of 10:1 through all phases for short periods of time (10-15mS) under CW operating conditions

4.3.1 Envelope Tracking

One of the approaches that can be used to improve the efficiency of SSPA's is envelope-tracking (ET). It enables high levels of efficiency and is much sought after in applications where efficiency is a key requirement and battery or power supply is limited. In envelope tracking, the supply voltage to the power amplifier is monitored and adjusted dynamically to ensure that the amplifier is operating at peak efficiency for instantaneous output power, at all times, as shown in Figures 4.6 & 4.7.

The implementation of envelope tracking requires monitoring, capturing or generation of signal envelope, fast processing speeds and a means to control the supply

voltage to the amplifier, such that it follows the signal envelope [24]-[27]. A key element of the ET system is its ability to generate the envelope signal, which is derived from baseband signals,eqn.4.2.

$$\text{Envelope} = \sqrt{I^2 + Q^2} \tag{4.2}$$

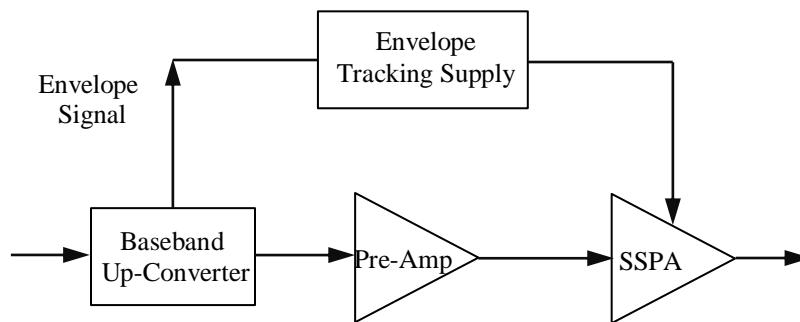


Fig. 4.6: Simplified Envelope tracking amplifier

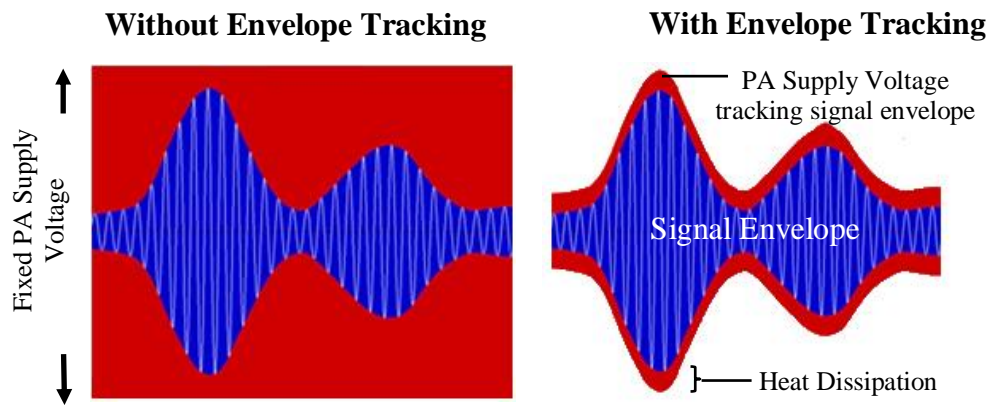


Fig. 4.7: Envelope tracking concept [28]

Envelope tracking supply captures the envelope information, and uses this to supply a voltage to the PA that is a faithful replica of the captured waveform. This minimizes power loss and heat dissipation. The power supply generating the varying voltage to the PA is key to the overall effectiveness of envelope tracking system. It is fundamental that the envelope tracking power supply follows the modulation envelope

(requires modulation frequencies that are two or three times that of the modulation signal bandwidth). The power supply must also be highly efficient with low noise to realize the full benefits of ET.

In order to obtain maximum efficiency, a supply voltage profile that follows the points of maximum efficiency for various output power levels is generated. A look-up table can be generated from this information to ensure that the correct voltage is provided to the amplifier for a given envelope magnitude. This is often referred to as envelope shaping. Finally some form of phase/timing adjustment may also be required to ensure that the envelope of the RF waveform and the voltage supplied to the amplifier synchronise. Poor synchronization between the waveforms can result in increased power dissipation (voltage peaks not occurring at the same time as the RF envelope peaks) and signal distortion where the amplifier is driven deep into compression.

In summary Envelope tracking utilises a PA supply voltage that follows the RF envelope shape enabling the amplifier to be operated at a voltage that gives the optimum efficiency at any instantaneous power level. Envelope tracking has the potential to operate into variable loads, however this requires fast processing, a wideband dynamic power supply and accurate envelope signal extraction for power supply. The concept is deemed unnecessary for solid-state heating systems as the RF carrier is not modulated.

4.3.2 Doherty Amplifier

The basic concept of Doherty amplifier involves improving the efficiency of an amplifier at average and peak power(s) [29]-[30]. Doherty amplifiers are widely used in base station applications where the PA needs to maintain good levels of efficiency at average and peak power's. The difference between the two power levels is referred to as the peak-to-average power ratio (PAR).

In its simplest form a Doherty amplifier (Fig.4.8) comprises of two amplifiers; a main amplifier biased in class-AB mode to provide a flat gain response and high

efficiency at average power levels and a peak amplifier biased in class C mode to meet the requirements at higher power levels. The input signal to each of the amplifiers is split using a power divider network (90° phase difference) and the amplified signals is combined at the output with a simple $\frac{1}{4}$ wave line acting as a power combiner.

At lower power levels (where the input signal is less than the peak amplifier's threshold) only the main amplifier is supplying power to the load. The impedance at the main amplifier's output ensures that it saturates below its maximum peak power capability and operates at its most efficient point (at average power). The peak amplifier remains inactive during this period representing a high impedance (open circuit) at the inverter. When the input power level exceeds the transition point of the peak amplifier, it starts to deliver current to the load, increasing the RF output voltage on the load. As a result of this active load-pull effect, the impedance at the output of the main amplifier reduces and its power contribution rises. The output power of both amplifiers continues to increase with increasing input signal levels until peak power capability is reached.

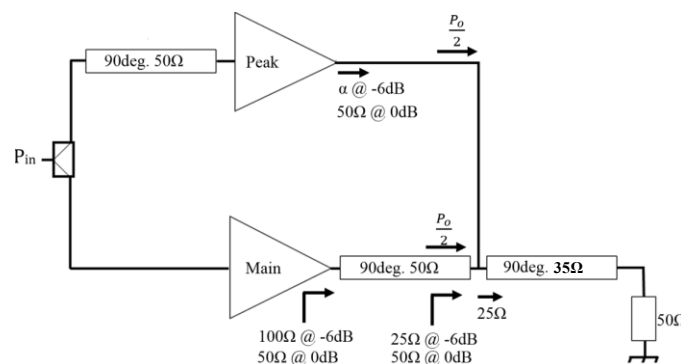


Fig. 4.8: Symmetrical Doherty Amplifier with a 6dB PAR ($\alpha = \frac{1}{2}$)

There are several variations of the Doherty architectures, e.g symmetrical and asymmetrical as shown in Fig. 4.8 & 4.9. The choice of architecture depends on the peak to average power ratio (Fig.4.10). Doherty architecture may be of interest in solid state heating applications, where the appliances may be expected to operate at average power,

except for when higher power level is required to heat larger loads or to increase the speed of heating.

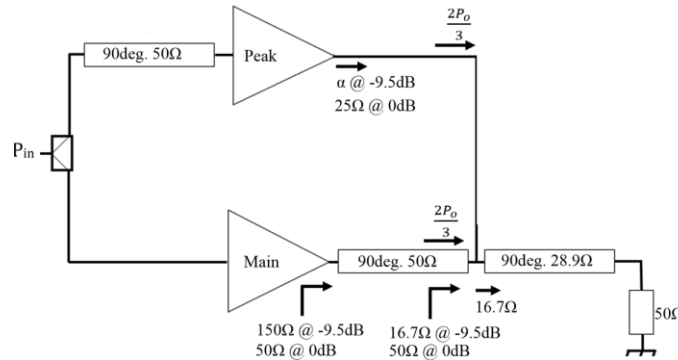


Fig. 4.9: Asymmetrical Doherty Amplifier with a 9.5dB PAR ($\alpha = 1/3$)

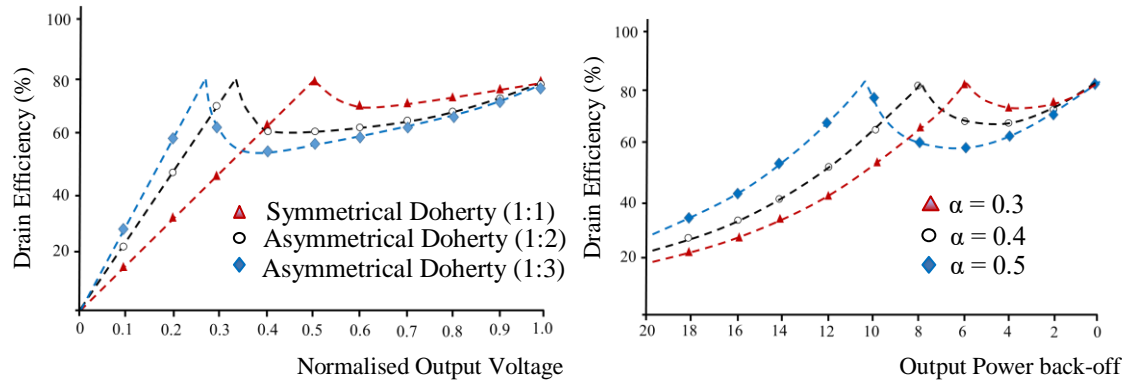


Fig. 4.10: Drain Efficiency vs Normalised load voltage amplitude [36]

4.3.3 Chireix’s Outphasing Amplifier

Outphasing in its simplest form involves separation of an amplitude modulated (AM) signal component into two phase modulated (PM) signals, each with a constant envelope and opposite phase [31]. The two constant envelope phase modulated signals are amplified by two independent and identical PA stages (Fig.4.11). As the envelope signals are now constant the information contained within the envelope is of little value, instead all meaningful information is encompassed in the phase component. The resulting output signals are combined to produce an amplified version of the original AM signal [32]-[33]. The concept is heavily reliant on a signal component separator (SCS) to convert

the input AM signal into two output PM signals of constant envelope. This raises the possibility of high efficiency and linear amplification.

A properly selected load compensation can significantly enhance the efficiency over a considerable range of output power back-off (Fig.4.12). Due to fixed envelope (AM) characteristics, the implementation of Chireix's concept avails linear operation over a wideband limited only by the SCS and bandwidth of power combining networks, thus making the concept highly attractive for broadcast applications. The practical implementations of the concept have been limited due to the cost and complexity.

Solid-state heating and domestic microwave cooking applications in particular operate under variable loading conditions, retaining PA efficiency under these conditions is highly challenging. Various PA architectures and concepts have been listed and their usefulness for microwave heating applications has been discussed. It is conceived that the earlier microwave cooking appliances will adapt the simpler, easy to implement PA topologies (such as class B), offering good levels of efficiency at or close to saturated power levels (assuming the appliances will be operated at saturated power levels for a majority of the time). This restricts the benefits of solid-state technology, as power scaling seriously degrades the systems efficiency at lower powers to levels where it will not be acceptable for a modern appliance. Load modulation topologies have also been discussed and it is anticipated that later generations of appliances will adapt these concepts to maintain high levels of efficiency at all power levels, enabling the creation of a truly unique, scalable and efficient appliance.

The descriptions of amplifiers in the previous sections has assumed ideal devices. In reality power amplifiers suffer from a number of limitations that ultimately reduces their efficiency and output power. In practical high power applications, thermal heat transfer, drain source resistance, maximum channel current and drain-source break down voltage restrict the performance.

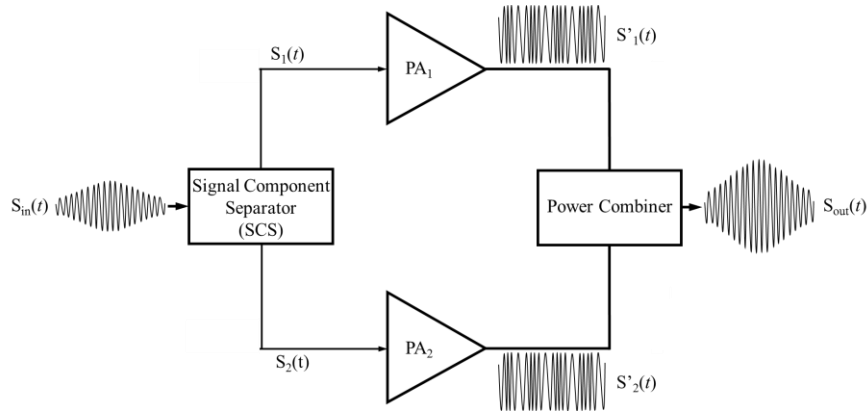


Fig. 4.11: Simplified block diagram of Outphasing system

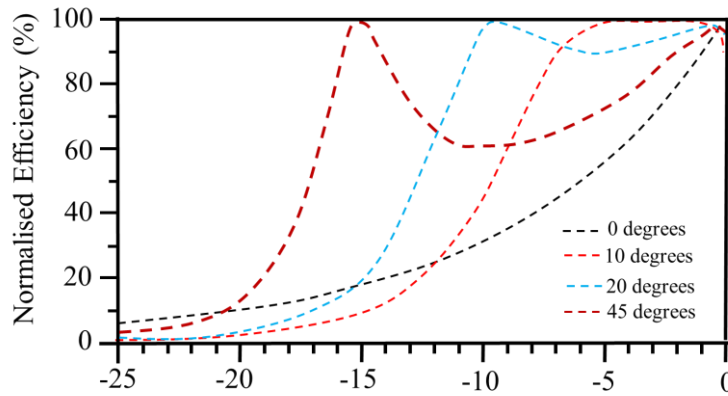


Fig. 4.12: Theoretical efficiency of Chireix's Outphasing system at four different compensation angles[34]

4.4 RF Matching Network Design Considerations

At the heart of any amplifier design is the RF power transistor, which is designed to operate over a single or a range of frequencies. Due to its internal structure and physical properties the impedance at the high power device plane is usually very low ($\sim 2\Omega$). In practical applications there is a requirement to match this low impedance to the system impedance (50Ω). High power transistors designed to meet power requirements of solid-state applications have lower impedances (eqn.4.3), which leads to complex and physically larger matching networks. This is undesirable in solid-state applications, where

space, cost and ruggedness are of a greater importance.

$$R_{\text{die}} = \frac{(V_{\text{ds}} - V_{\text{knee}})^2}{2 \cdot P_{\text{out}}} \quad (4.3)$$

In order to make the devices user friendly and PA designs less sensitive to production tolerances, power transistors are often pre-matched inside the package. However, space inside the package is limited and external-matching networks must be realised in order to match the device to system impedance. For improved yield the networks should be designed over a wide bandwidth, as this will minimise tuning and RF parameter spread during the production process. Whilst this increases the electrical robustness of the design, due care and attention must also be given to other parameters such as the choice of PCB laminate, track widths, connectors and heat sink in order to maintain system reliability.

A typical design process starts with the selection of a power transistor, that is capable of meeting circuit and system level requirements. The power and efficiency capability, along with the input and output impedances is obtained through load-pull measurements. The test conditions, prior knowledge of transistor die periphery and internal matching networks, help determine if the device is suitable for solid-state applications. Optimal impedances for best performance trade-offs (power and efficiency) are selected from the load pull data. The load-pull measurement set-up typically comprises of two tuners; one at the input and the other at the output of the device, both are used to search for optimum impedances.

Upon reaching optimal performance, it is prudent to calculate the Q-factor ($R_{\text{im}}/R_{\text{re}}$) as this gives an indication of the likely challenges during the design process. A high Q suggests that the device is narrowband and not suitable for wideband applications. Such a device is susceptible to high current or voltages nodes which are likely to compromise device reliability under variable loading conditions.

$$Q_{\max} = \frac{f_{\max}}{2.BW} \quad (4.4)$$

Whilst device models are accurate and reliable at lower power levels their use at higher power levels must be validated with measurements. Several different topologies can be used for the input and output matching networks, a low pass network (Fig.4.13) is widely used as it's easier to realise. For solid-state applications a broadband response (W shaped S_{11}) is preferred over a narrowband (V shaped S_{11}) response (Fig.4.14). The latter is sensitive to load, temperature, device-to-device manufacturing process, and component tolerance variations. Wideband performance can also be obtained by designing the input & output networks such that their respective resonances sit outside the operational bandwidth (a 200MHz above and below the operational bandwidth is recommended to stop the resonance entering the operational bandwidth). An input return loss (S_{11}) of better than -10dB over the operational bandwidth, whilst acceptable for most applications, may not be sufficient for solid-state systems where load variations (size and temperature) will increase the mismatch losses.

At high power levels and especially under variable loading conditions, large currents are transported through the transmission lines, attention must therefore be paid to the minimum track width (50Ω line width), as smaller line width may be unable to carry the currents and burn out.

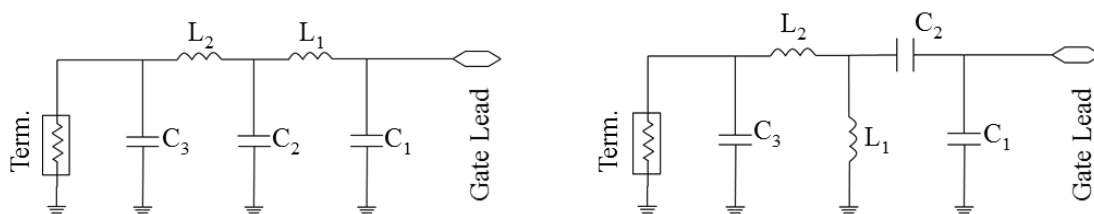


Fig. 4.13: Low pass (left) and band pass (right) matching topologies

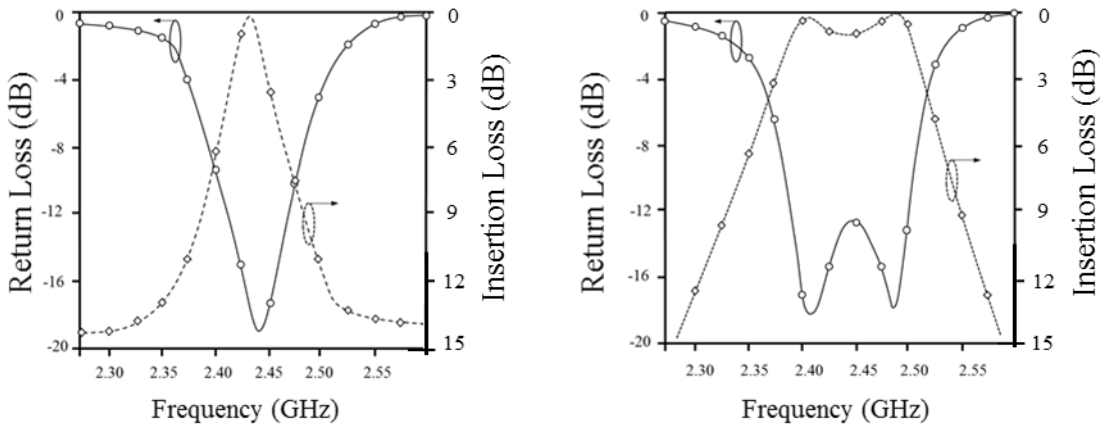


Fig. 4.14: Input return and circuit losses - Narrow Band (V-Shaped) vs Broadband (W-Shaped) response.

A dc bias network comprising of a quarter wavelength needs to be incorporated into the design - it presents an open circuit, an infinite impedance to the matching circuit and is shorted with a shunt capacitor at the other end (without influencing the matching circuit). Due to the high current flow on the drain side the track width is 50Ω line width; a wider line influences the matching circuit and must be incorporated in the matching circuit design flow, whereas a thin line may not be able to carry the high current. A thinner track width can be used on the gate side where there is no current flow.

4.5 PA Design Considerations for Microwave Heating Applications

4.5.1 Overview

A typical SSPA is designed to operate under matched (50Ω) conditions. This ensures a smooth transition of power from the source to the load. However the load environment in microwave heating applications is non-constant. This variable impedance operating environment, ensues a mismatch between the source and the load which gives rise to high reflective states. During these high reflection states, a large proportion of this power is dissipated as heat. The heat causes the transistor junction temperature to rise above its recommended level (maximum junction temperature for safe operation).

RF power transistors are also susceptible to peak drain-source and gate-source voltage breakdown. This typically happens under mismatched conditions, where a combination of the forward and reflected waves can result in high voltage swings at the device plane. A high impedance state results in larger than expected peak voltages, whereas a low impedance results in high values of peak currents. High levels of currents at the output of the device can damage the bond wires and cause degradation in the device's performance, which may not be noticeable at first sight. More bond wires can be added to improve the ruggedness, however physical die dimensions; bond pads and the availability of capacitor values (LC matching network), restrict the number in practical applications. It is common practice to use a circulator at the output of solid-state amplifiers, this protects the amplifier against load variations.

The use of isolator less solid-state amplifiers in the new and emerging RF energy applications means that the amplifier for the most part is operating into a non 50-ohm load environment. Operation into mismatched loads for extended periods of time, can result in performance degradation and the likelihood of device breakdown increases [1]. High power devices such as those intended for solid-state applications are affected the most, due to thermal, peak voltage and current swings at the device plane. Despite the challenging operating conditions SSPA's are expected to operate reliably and without performance degradation. Monitoring, capture and management of these load variations is a key requirement in ensuring safe and reliable operation.

The effect of a non-constant impedance environment on device reliability, and power delivery into the cavity is investigated using a lumped element (RLC) model to represent a cavity. Cavities and waveguides used extensively in microwave heating applications have similarities with RLC circuits, this includes energy storage and exchange between the electric & magnetic fields. When an external source is excited at the same frequency as the resonance frequency (of the RLC circuit or cavity), an EM field is generated. During current flow in the inductor, energy is stored in the magnetic field and when current flows in the capacitor energy is stored in the electric field.

Owing to these similarities, an equivalent circuit lumped element model (Fig.4.15) is used to demonstrate cavity behaviours. This model is used to study single, and two port systems to ascertain forward and reverse power behaviours under variable load and phase conditions. The method has limitations in that single-mode cavities are distributed resonant structures and as such cannot be represented accurately by lumped element equivalent models over a wide range of parameters.

It is also envisaged that there will be many applications where the power from a single source is insufficient – limited by the transistor maximum power rating. In such instances power combining becomes an essential requirement which can be accomplished at the printed circuit board (PCB) level. This takes away some of the flexibility and performance benefits of solid-state heating, e.g. efficiency at lower power levels. The use of a microwave cavity as a power combiner is one alternative, which requires the use of multiple ports and feed structures. The challenges of using multiple ports (feed structures) are also investigated using the cavity equivalent model.

Designing power amplifiers for a fixed load, over a wide bandwidth (where the return loss is greater than greater than 10dB's) can be a difficult task. This is due to variations in impedance with the frequency. The challenge becomes even greater in microwave heating applications where the load is non constant. This effect is studied and presented in some detail using cavity equivalent RLC circuit and ideal coupling structure behaviors.

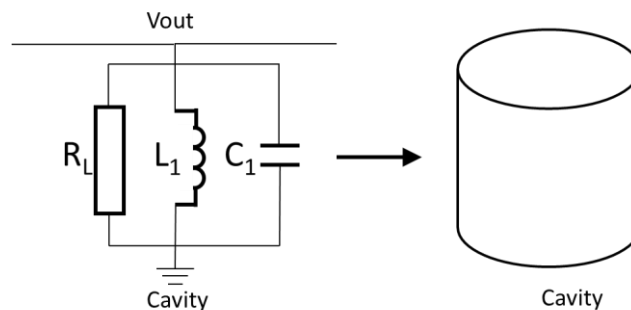


Fig. 4.15. Cavity equivalent lumped element model.

4.5.2 Single Port Cavity Excitation

4.5.2.1 Load variations in a single port cavity

SSPA's used in microwave heating applications will operate into variable loading conditions due to different size, shape and consistency of foods. As the loads vary, the SSPA will experience varying and potentially damaging levels of VSWR. The VSWR depends on the load mismatch. It degrades as the load moves away from an optimally matched condition. A VSWR ratio of $\infty:\pm 1$ occurs when the load is an open or a short circuit and a VSWR ratio of 1:1 occurs where the load and source are perfectly matched. For a given forward travelling voltage wave (V^+), it can be shown (Fig.4.16) that under open or short conditions, the reflected voltage (V^-) waveform is nearly of the same magnitude. Under these operating conditions most of the power is reflected back to the source. Further, due to standing wave behaviour, the SSPA experiences high voltage and current states as the cavity load varies from a high impedance (open circuit) state to a low impedance (short circuit) state. The reflection coefficient Γ (eqn 4.5), often expressed in terms of return loss (eqn 4.6), is also defined by the incident and reflected voltage terms ($\Gamma = V^-/V^+$).

The incident wave is V^+ and the reflected wave is V^- . The V^{\max} condition appears when the transmitted and reflected waves add constructively and V^{\min} condition appears when the transmitted and reflected wave add destructively.

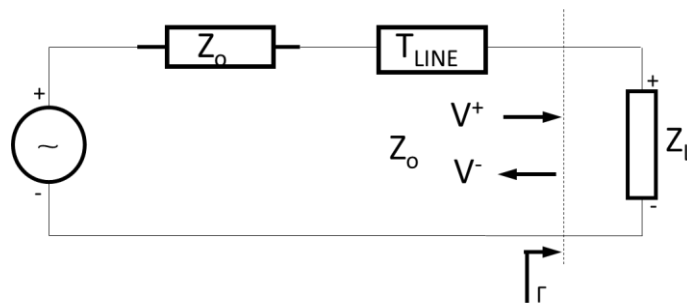


Fig. 4.16. Impedance mismatches between transmission line and the load.

$$\Gamma = \frac{(Z_L - Z_0)}{(Z_L + Z_0)} \quad (4.5)$$

Where: Z_L = load impedance and Z_0 = system characteristic impedance

$$R_L = -20 \log[\text{mag}(\Gamma)] \quad (4.6)$$

$$\text{VSWR} = \frac{|V^{\max}|}{|V^{\min}|} \quad (4.7)$$

Where:

$$V^{\max} = V^+ + V^- \text{ and } V^{\min} = V^+ - V^-$$

$$\text{VSWR} = \left[\frac{1+|\Gamma|}{1-|\Gamma|} \right] \quad (4.8)$$

$$\text{For } Z_L > Z_0, |Z_L - Z_0| = Z_L - Z_0; \text{ VSWR} = \left(\frac{Z_L + Z_0 + Z_L - Z_0}{Z_L + Z_0 - Z_L + Z_0} \right) = \frac{Z_L}{Z_0} \quad (4.9)$$

$$\text{For } Z_L < Z_0, |Z_L - Z_0| = Z_0 - Z_L; \text{ VSWR} = \left(\frac{Z_L + Z_0 + Z_0 - Z_L}{Z_L + Z_0 - Z_0 + Z_L} \right) = \frac{Z_0}{Z_L} \quad (4.10)$$

The lumped element model (Fig.4.15), is used to study the cavity impedance behaviours under variable loading conditions, as the load R_L is varied from 5Ω to 95Ω in 20Ω steps (Fig.4.17). The coupling coefficient is optimized for a 50Ω load, and set to a fixed value of 1. Simulations data (Fig.4.18) shows that for smaller loads the impedance points move to the left of Z_{opt} and for larger loads the impedance points move to the right of Z_{opt} . As the cavity load varies from its optimally matched condition, the return loss deteriorates (Fig.4.18b). This corresponds to high reflected power states, with an increasing VSWR (Fig.4.18c). These changes in load can have a profound effect on device reliability and overall heating efficiency.

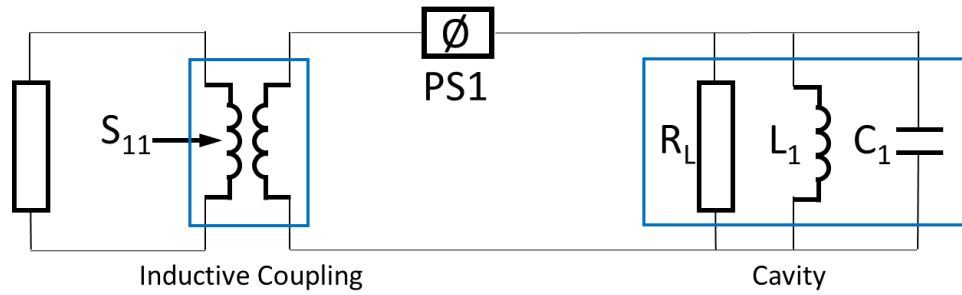


Fig. 4.17. Simulation Test Bench used for characterising cavity loading conditions.

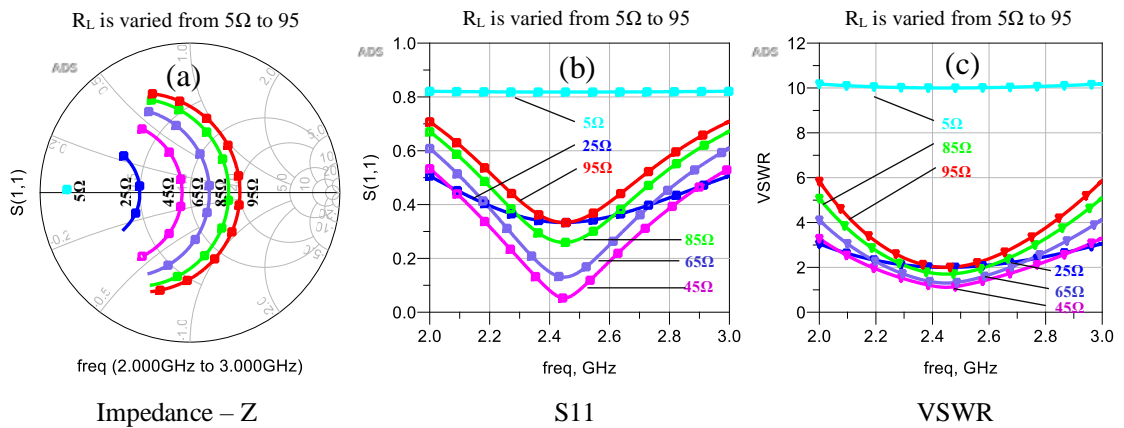


Fig. 4.18. The impedance, Z , return loss $S11$ and VSWR as a functions of load (as it is varied from 5 to 95Ω in 20Ω steps).

As the load varies from its optimum condition to a very high (infinite) impedance, the SSPA (Fig.4.19) operates into an open circuit, and similarly moving towards a very low (zero) impedance state, the amplifier operates into a short circuit. In the first instance the device experiences peak voltages (Fig.4.20b) and in the second instance it experiences peak currents (Fig.4.20a) at its output. Both scenarios are undesirable as less of the power is available to heat the load (Fig.4.20c). Furthermore as the VSWR exceeds its recommended value (VSWR = 10:1 for a typical LDMOS transistor), the device becomes susceptible to breakdown. This is the fundamental challenge and limitation of solid state heating.

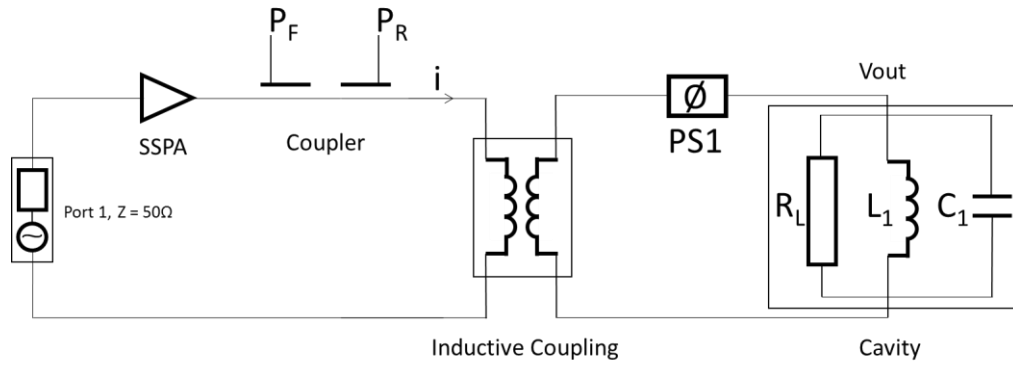


Fig. 4.19. ADS test bench for 1 port analysis.

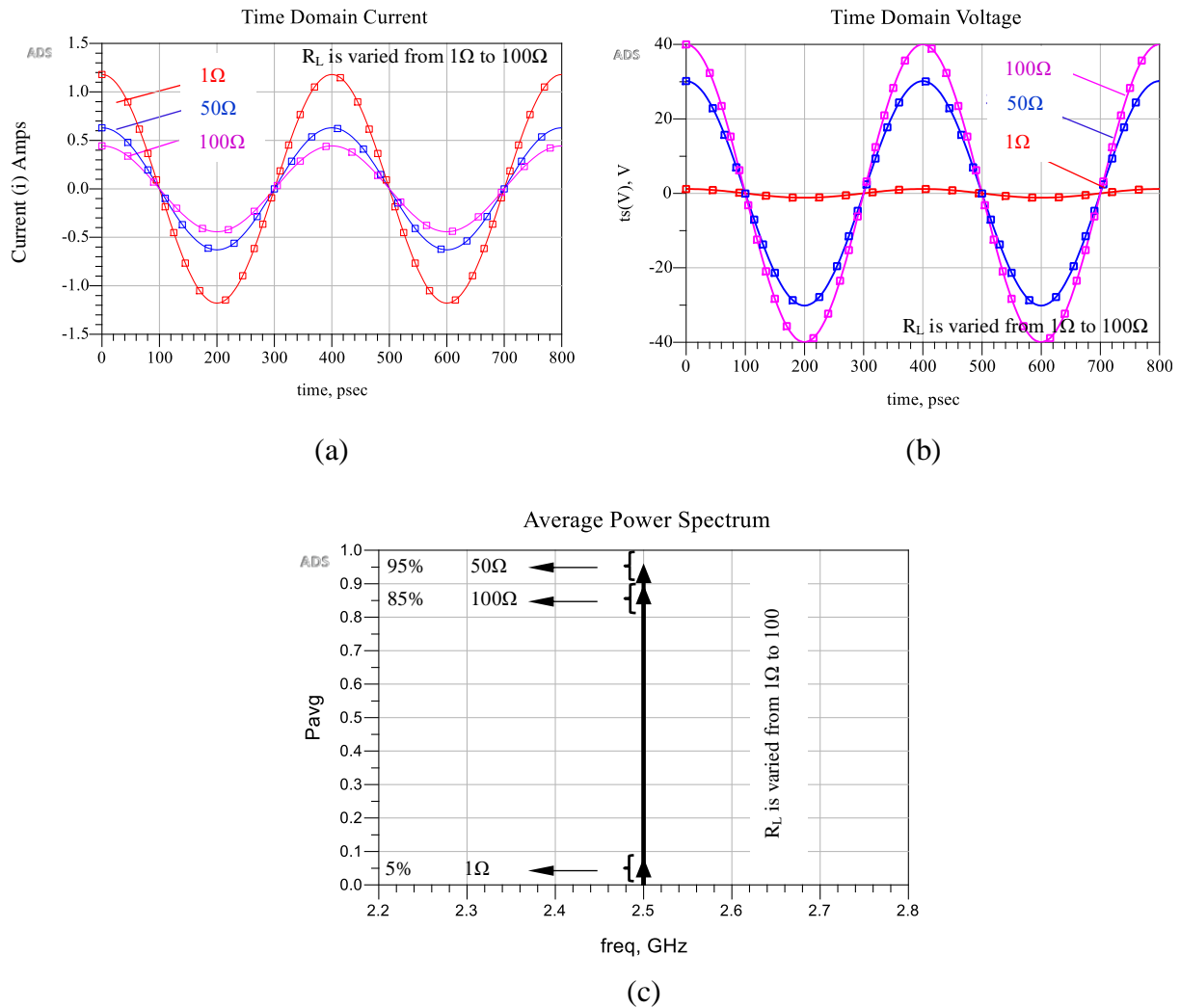


Fig. 4.20 (a) Output Voltage as a function of load mismatch, (b) Output Current as a function of load mismatch (c) Output power as a function of load mismatch. (Phase = 0 deg. Coupling Coefficient $C=1.0$)

Variations in the load can be compensated for by retuning the coupling structure or the matching networks such that $\sqrt{Z_0 \cdot Z_L} = 50\Omega$ (where Z_0 = system impedance and Z_L = cavity impedance). An adaptive matching network would be the preferred choice, however this is difficult to realise in practice. Manual re-tuning of the matching network, in response to changes in the load has been discussed in chapter 5 for cylindrical cavity resonators. This involves re-positioning and rotation of the coupled loop, until a new optimally matched frequency point appears. The SSPA frequency of operation is adjusted to this new value to ensure maximum power transfer and safe operation. This process does not lend itself to consumer applications however.

It has been established that variable loading conditions present a serious challenge to practical implementations of solid-state technology. It is clear that variations in the load result in impedance mismatches at the device plane, which if not corrected, result in system inefficiency and device failure or breakdown.

4.5.2.2 Phase variations in a single port cavity

Aside from the load variations, phase of reflected signals plays an important role in device and system reliability. The voltage and current waveforms and the power spectrum for a 30V LDMOS transistor, operating under two extreme loading (377Ω and 1Ω) and variable phase (PS1, 0° - 360°) conditions is investigated using test circuit shown in (Fig.4.21). The 377Ω load represents a near open circuit condition at the SSPA output. Under certain phase conditions this leads to the formation of peak voltage states ($V^+ + V^-$), which are equal to twice the operating voltage e.g a 30V LDMOS transistor can experience voltage, which approaches 60V as shown in Fig.4.21. Exceeding the maximum rated voltage can result in instant breakdown. These extreme breakdown mechanisms, are reliant on the reflected power vectors to align in phase at the output, which is a remote but real possibility. There is little that can be done in terms of controlling the phase of the reflected signals that appear at the output, other than to try and prevent

excessive reflected power states by ensuring a continuous, acceptable match between the source and the load. Whilst the negative effects of phase in the reflected signal have been highlighted it becomes apparent that control over phase can be used to manipulate the field pattern inside the cavity.

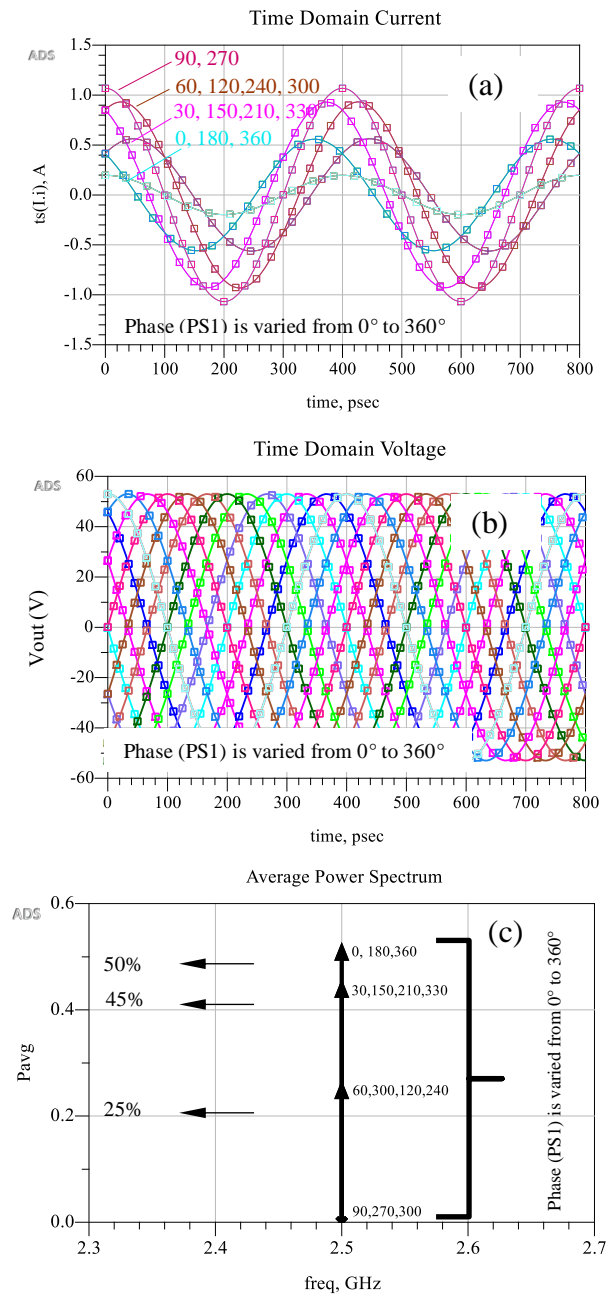


Fig. 4.21. (a,b) Current and Voltage spectrum in time domains as function of phase mismatch (c) average power spectrum as function of phase mismatch, load = 377Ω Coupling Coefficient = 1

Similarly the 1Ω is assumed to represents a small load (a near short circuit) at the output. Under these operating conditions, the voltage reduces and the current increases, which can lead to high levels of heat dissipation and fusing of bondwires within the device and PCB tracks [38].

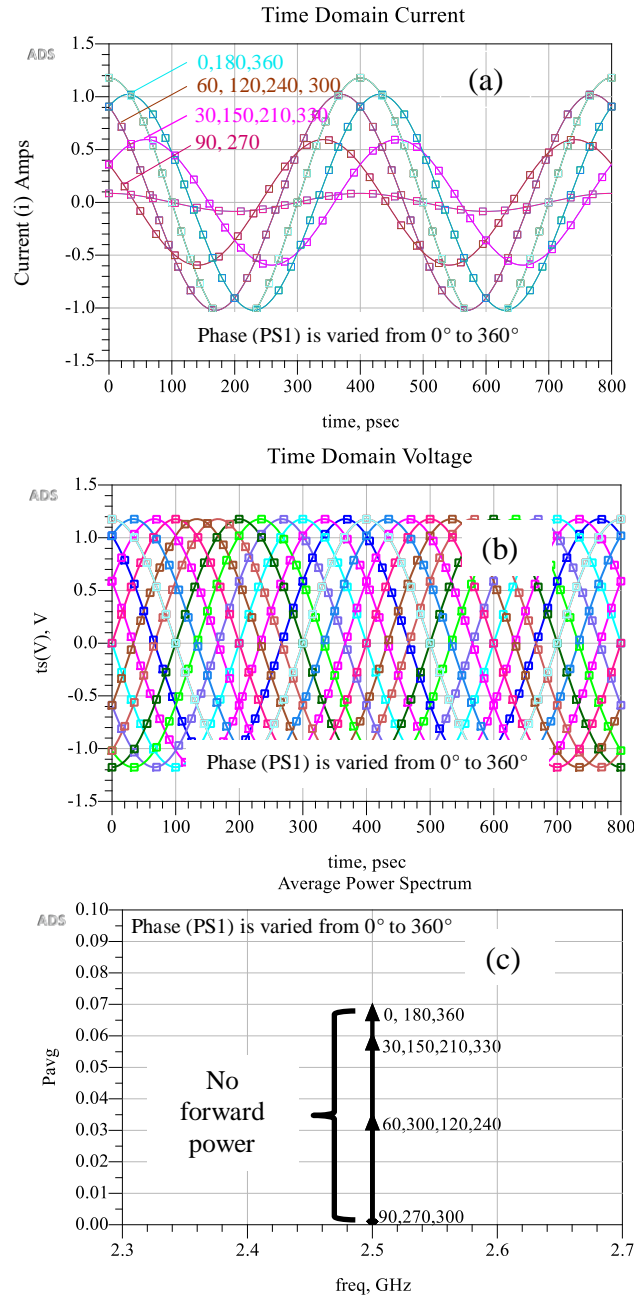


Fig. 4.22. (a,b) Current and Voltage spectrum in time domain as function of phase mismatch (c) average power spectrum as a function of phase mismatch, load = 1Ω Coupling Coefficient 1.0

4.5.2.3 Coupling coefficient in a single port cavity

The coupling structure plays a major role in transferring available power into the resonant cavity, and is a vital component of solid state heating apparatus. The influence of the coupling structure is investigated using test circuit shown in (Fig.4.19). This work considers two different scenarios. In order to understand the influence of the coupling structure in matching source impedance to the cavity load impedance the coupling coefficient is varied when the load is a 50Ω . Whilst during the second part of the simulation, impedance variations due to changes in phase are also taken into account.

With a coupling coefficient of 1, the 50Ω load is optimally matched (critically coupled). However with a change in the coupling coefficient value, the load becomes undercoupled ($C < C_{opt}$) or overcoupled ($C > C_{opt}$) resulting in an impedance mismatch as shown in Fig.4.23a. As the coupling coefficient (C) deviates from its optimum value (C_{opt}), the return loss worsens and the VSWR value increases. A smaller 5Ω load is optimally matched, when the coupling coefficient is 3.15 and a larger 377Ω load is optimally matched when the coupling coefficient is 0.36. This suggests that changes in the load can be compensated, through adjustments of the coupling structure. Further, changes in phase and variations of the coupling coefficient, shift the optimally matched regions in frequency. The optimally matched points shift in frequency with a gradual deterioration of the matched condition as shown in Fig.4.23b. Whilst this is of a limited use in single mode cavities, it has enormous potential in multi-mode cavities where a frequency sweep can be used to excite multiple modes.

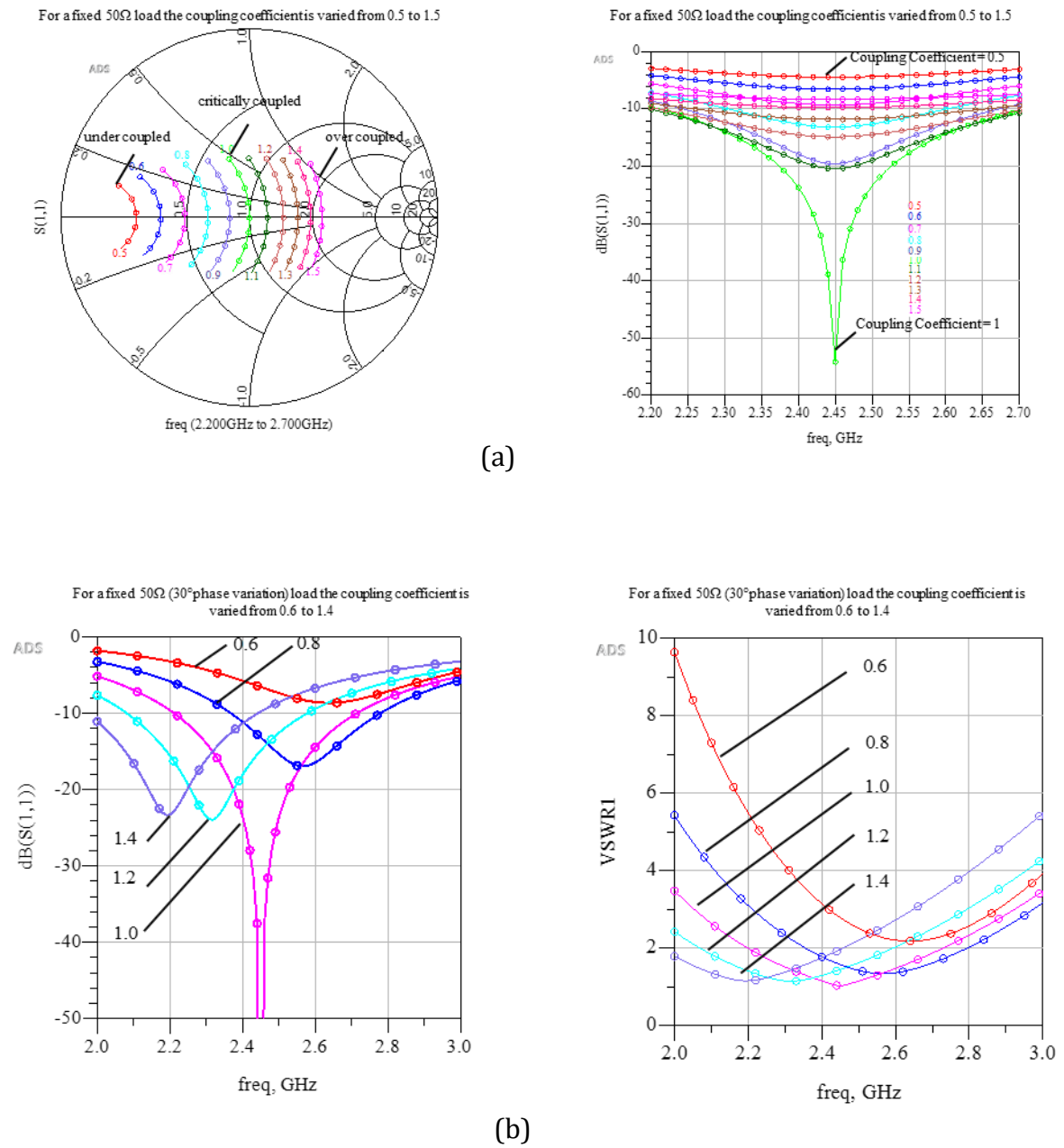


Fig. 4.23. S_{11} as a function of coupling coefficient – (a) 50 Ohm load phase = 0 degrees (b) 50 Ohm load phase = 30 degrees

4.6 Two port cavity excitation

A two-port system, shown in Fig. 4.24, comprises of two separate power amplifiers feeding into a single cavity through two separate coupling structures. The system enables a convenient way of combining power, and in this case, a doubling of the power available from the single semiconductor device. For example, two semiconductor devices each capable of delivering 300W of output power, can be arranged in a microwave oven that can deliver a practical 600W. However, there are a number of significant drawbacks. These include increased reflected power ($2 \cdot P_{out}$ worst case), due to direct coupling between the ports, which results in reflection coefficients that are greater than unity. This can seriously effect device reliability and diminish heating efficiency. However, a closer look suggests that this approach offers some potential benefits. The delivery of power from two separate sources provides additional power control, and the ability to excite modes independently at different frequencies or at the same frequency by varying the phase. For better heating uniformity and targeted power delivery (larger cavities), the power can be coupled at two separate points. The exact power coupling location can be determined from the size of the cavity, location and volume of the load.

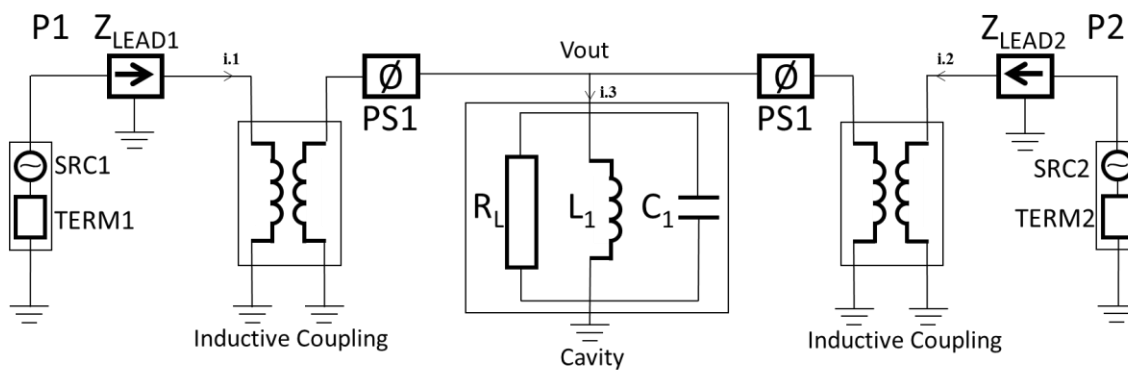


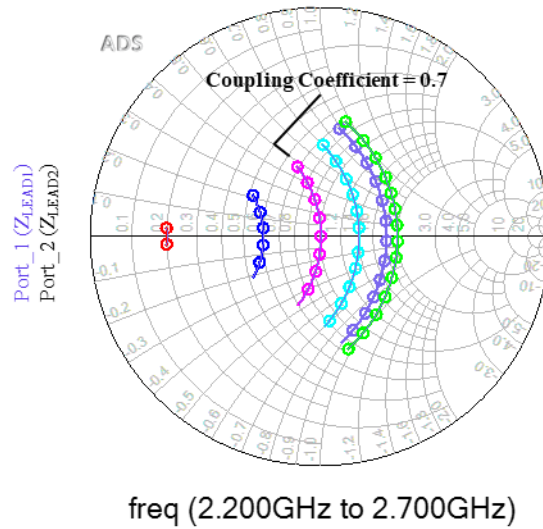
Fig. 4.24. A two-channel system feeding into a single cavity.

4.6.1 Load variations in a two port cavity

This section looks at the potential implications of load variations in a 2 port system. Device reliability in the absence of an isolator at the SSPA output is a key requirement for solid-state heating applications. The introduction of a second source to the cavity equivalent model (Fig. 4.17), influences the impedance seen by the first source through an effect that is generally termed ‘load-pull’. In order to ensure that both sources are matched to the cavity, the coupling coefficient, C is re-optimized to 0.7.

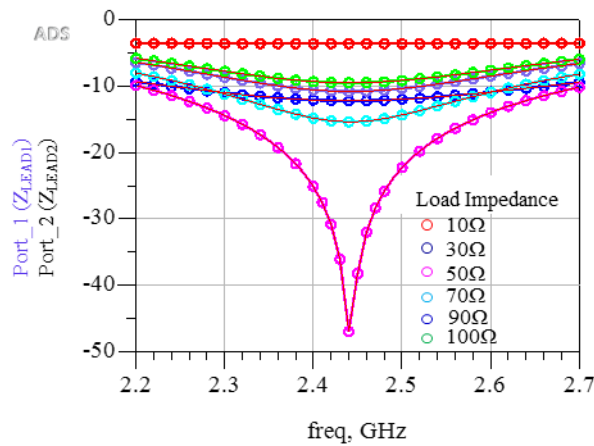
As stated in section 4.6, in a two port system a power level equal to the total transmitted power (P_1, P_2), can appear at port 1 or port 2 (Fig.4.24). This is due to impedance mismatches introduced by the variable load e.g. in an empty cavity or in a cavity with a small load, very little of the available power is absorbed by the load. Under these operating conditions a large portion of the available power is reflected back towards one or both of the ports. Besides the load variations, the level of reflected power is dependent on the phase alignment of the reflected waves at ports 1 and 2, under such operating conditions isolator-less SSPAs experience hostile impedance environments, which takes them beyond their safe operating regions ($S_{11} < -10\text{dB}$). The effect of these changes due to load variations is shown in Fig.4.25. The impedance at Port 1 and Port 2 is measured using Z_{LEAD1} and Z_{LEAD2} elements shown in Fig. 4.24. The Z_{LEAD1} and Z_{LEAD2} notation is used as it can also represent impedances at device plane in instances, where the coupling structure is used to transform device level impedances to the cavity load environment. This type of implementation is explored further in chapter 7.

2 Port System - For a fixed 50Ω load the coupling coefficient is re-optimised to 0.7



(a)

2 Port System - For a fixed 50Ω load the coupling coefficient is re-optimised to 0.7



(b)

Fig. 4.25. S_{11} as a function of impedance mismatch in a 2 port system – constant phase.

$$T=0.7$$

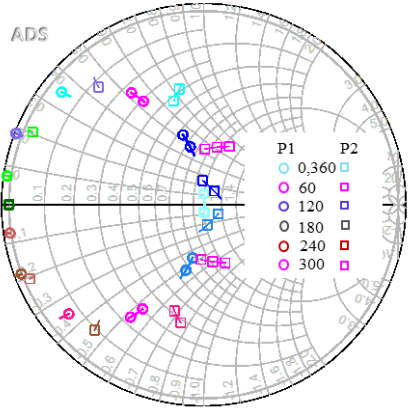
4.6.2 Phase variations in a two-port cavity

Changes in relative phase between the two excitations, rotate the impedance seen by both SSPAs along the constant admittance circles towards the inductive and capacitive parts of the Smith chart respectively. It follows that there is a possibility to control the

phase of the reflected power, to each SSPA by changing the relative phase of the input signal. This technique can be used to constrain the impedance mismatch at both excitation ports, by monitoring the reflected power, and then using fast algorithm speeds (via a control loop) to change the phase of the input signals.

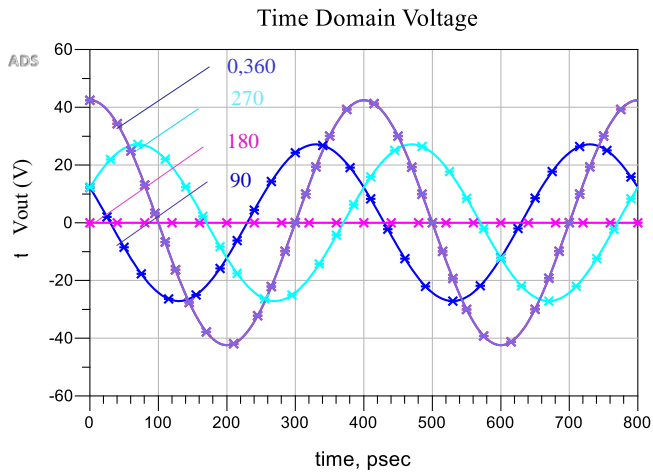
The effect of phase imbalance between the two ports for a 50Ω load (Fig.4.24), is investigated by holding the phase constant at port 1, whilst varying the phase at port 2 from 0-360 degrees. The resulting impedance variations are demonstrated through current and voltage waveforms, which vary in amplitude and with phase as shown in Fig.4.26. The matching conditions at each of the ports are now different, whilst this behavior is troublesome from a device reliability perspective (worsening S_{11} values), it offers the potential to change field pattern behaviours inside the cavity.

Under mismatched conditions, the comparatively higher VSWR values in a two-port system means higher peak voltages and currents values. The effect of load and phase variations for a 1-port network was shown, to have (worst case) a peak voltage that is twice the normal operating value. A two port network under similar operating conditions, has a peak voltage of 80V (Fig.4.27) which is almost three times the normal operating voltage. Similarly the current value rises under small impedance conditions, which suggests that semiconductor devices (in the absence of an isolator at the SSPA output) will experience more hostile mismatch conditions and therefore are more likely to breakdown. By carefully mapping these load variations on a Smith chart together with the device “load pull data” unsafe operating regions can be identified. This information can then be used to design matching networks to ensure that the device is protected against high VSWR conditions.

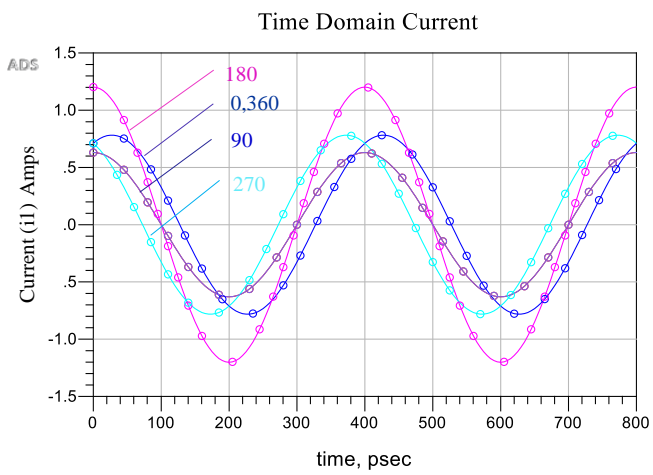


freq (2.400GHz to 2.500GHz)

(a)



(b)



(c)

Fig. 4.26. (a) S_{11} as a function of phase in a 2 port system . $T=0.7$ (b) Peak voltage and (c) current as a function of phase mismatch in a 2 port system; load = 50Ω

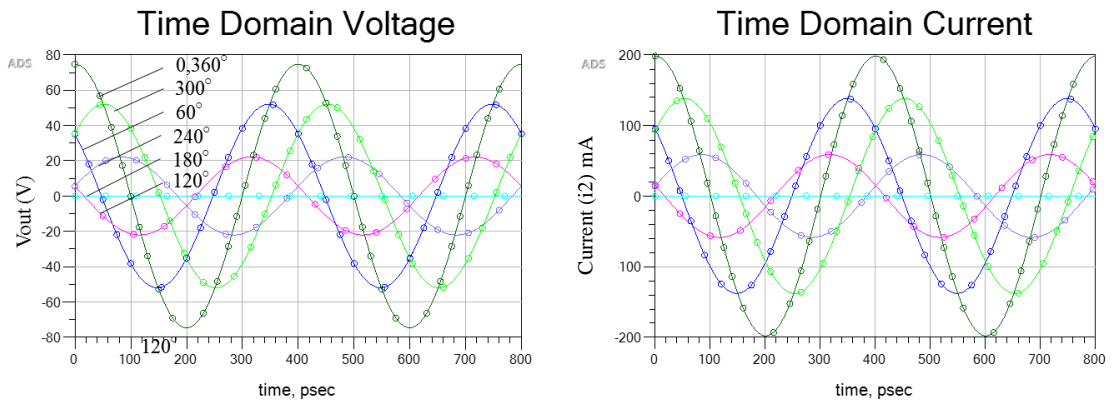


Fig. 4.28 Peak voltage and current as a function of load mismatch in a 2 port system; load = 377Ω.

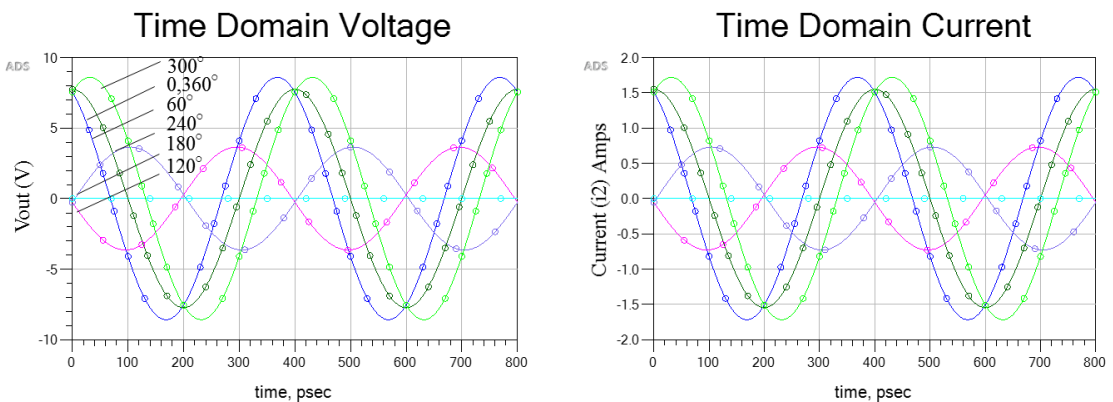


Fig. 4.27. Peak voltage and current as a function of load mismatch in a 2 port system; load = 5Ω.

4.6.3 Coupling coefficient

For a two-port network, the optimum coupling coefficient is 0.7 (Fig.4:28), if the coupling coefficient is maintained at 1.0 (as was the case for a single port), then the port impedance moves to a higher impedance value to the right of the 50Ω point on the Smith chart. For a smaller 5Ω load the coupling coefficient is varied until a critically coupled state is observed at a value of 2.25. The process is repeated with a larger 377Ω load and here a critically coupled state is observed with a coupling coefficient value of 0.25. In a single port application these values had been 3.15 and 0.36 respectively. This suggests that the coupling coefficient value needs to be re-optimised as more ports are introduced into the cavity.

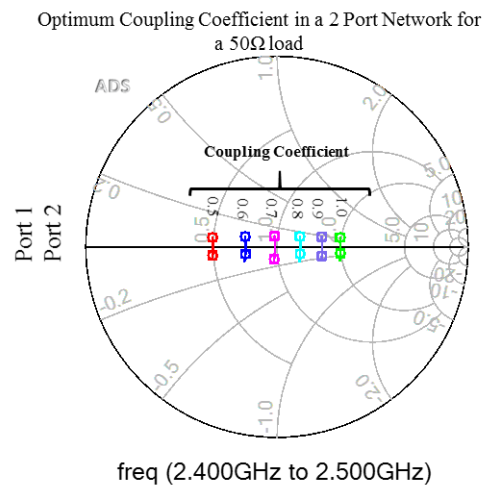


Fig. 4.28. Cavity load impedance as a function of coupling coefficient in a 2 port system; phase = 0, $Z=50\Omega$

4.7 Summary

A brief outline of power amplifier design concepts (modes of operation) has been presented along with a discussion on their suitability for solid-state heating applications. At the heart of any amplifier design is a RF power transistor which is designed to operate over a single or a range of frequencies. Due to its internal structure and physical properties, the impedance at the device plane is usually very low. In practical applications, there is a requirement to match this low impedance to the system impedance (50Ω). High power transistors designed to meet power requirements of solid-state applications have lower impedances which leads to complex and physically larger matching networks. RF matching networks design consideration (narrow band vs broadband) and concerns relating to device reliability have been identified and addressed.

A typical SSPA is designed to operate under matched (50Ω) conditions. This ensures a smooth transition of power from the source to the load. However the load environment in microwave heating applications is not constant. This variable impedance

environment causes a mismatch between the source and the load which gives rise to high reflective states.

In microwave heating apparatus the fundamental component responsible for ensuring a smooth transfer of power from the source to the load is a coupling device. The role of this device is investigated using lumped element RLC circuit to represent a cavity. Cavities are used extensively in microwave heating applications and have similarities with RLC circuits. This includes energy storage and energy exchange between electric & magnetic fields. Owing to these similarities an equivalent circuit lumped element model (Fig.4.18) was used to demonstrate approximate cavity behaviour. This model is used to study single, and two channel systems to ascertain forward and reverse power behaviours under variable load and phase conditions. The method has limitations in that single-mode cavities are distributed resonant structures and as such cannot be represented accurately by lumped element equivalent models over a wide range of parameters.

Through the use of this model it has been demonstrated that impedance variations due to changes in load (size, shape, and constituents) can impact both performance and reliability of a solid state semiconductor device. These findings are broadly in line with expectations. During this part of the study it has been observed that whilst the coupling device is used to transfer power from the SSPA into the cavity, it has another very important role. It can be used to match device level impedances to the cavity load environment.

4.8 References

- [1] W.McGenn, J.Powell, M.Uren, J.Benedikt, P.J. Tasker, “RF Waveform Method for the Determination of the Safe Operating Area of GaN HFET’s for Amplifiers Subjected to High Output VSWR,” Proc European Microwave Integrated Circuits Conference 2010, pp. 282-285.
- [2] https://wikipedia.or/wiki/Microwave_oven
- [3] Network Analyzer basics – Agilent
- [4] An-807 Reflections – Texas Instruments.
- [5] Wilson Tang, Tom Au-Yeung “Measure a Voltage Standing Wave Ratio (VSWR) to QuantifyTrasnmission Line Imperfections.
- [6] 50V RF LDMOS, An ideal RF power technology for ISM, broadcast and commercial aerospace applications
- [7] Jonathan Dodge, P.E. “Power MOSFET Tutorial”, Application Note APT-0403 Rev B, March 2, 2006.
- [8] Application Note 1823 – Microsemi
- [9] Application Note AN1107 – “Understanding RF Data Sheet Parameters” Freescale Semiconductor, Inc.
- [10] XiaoLi Wang, “Simulation of LDMOS High Frequency Power Transistor”.
- [11] Liangjun Jiang, “Hot Carrier Effect on LDMOS Transistors”, Spring 2007.
- [12] Peter Wright, Jonathan Lees, Johannes Benedikt, Paul J. Tasker, and Steve C. Cripps “A Methodology for Realizing High Efficiency Class-J in a Linear and Broadband PA” IEEE TRANSACTIONS ON MICROWAVE THEORY AND TECHNIQUES, VOL. 57, NO. 12, DECEMBER 2009
- [13] Abdullah AlMuhaisen, Peter Wright, J. Lees, P. J. Tasker, Steve C. Cripps and J. Benedikt “Novel Wide Band High-Efficiency Active Harmonic Injection Power Amplifier Concept” Centre for High Frequency Engineering, Cardiff School of Engineering, Cardiff University, Cardiff, UK
- [14] S. C. Cripps, RF Power Amplifiers for Wireless Communications, 2nd Edition, Norwood, MA: Artech House, 2006.

- [15] F. H. Raab, "Class-F power amplifiers with maximally flat waveforms," *IEEE Trans. Microw. Theory Tech.*, vol. 45, no. 11, pp. 2007–2012, Nov. 1997.
- [16] S. Gao, "High-efficiency class-F RF/microwave power amplifiers," *IEEE Microw. Mag.*, vol. 7, no. 1, pp. 40–48, Feb. 2006.
- [17] Y. Y. Woo, Y. Yang, and B. Kim, "Analysis and experiments for high efficiency class-F and inverse class-F power amplifiers," *IEEE Trans. Microw. Theory Tech.*, vol. 54, no. 5, pp. 1969–1974, May 2006.
- [18] Steve C. Cripps, Paul J. Tasker, Alan L. Clarke, Jonathan Lees, and Johannes Benedikt "On the Continuity of High Efficiency Modes in Linear RF Power Amplifiers" *IEEE MICROWAVE AND WIRELESS COMPONENTS LETTERS*, VOL. 19, NO. 10, OCTOBER 2009
- [19] P. Wright, J. Lees, P. J. Tasker, J. Benedikt, and S. C. Cripps, "An efficient broadband Class J mode PA realised using RF waveform engineering," in *IEEE MTT-S Int. Dig.*, Jun. 2009, pp. 653–65
- [20] Jungjoon Kim, Jangheon Kim, Junghwan Moon, Jungwhan Son, Ildu Kim, Seunghoon Jee, and Bumman Kim "Saturated Power Amplifier Optimized for Efficiency Using Self-Generated Harmonic Current and Voltage." *IEEE TRANSACTIONS ON MICROWAVE THEORY AND TECHNIQUES*, VOL. 59, NO. 8, AUGUST 2011
- [21] A. B. Ramon, "Class-F and Inverse Class-F Power Amplifier Loading Networks Design Based upon Transmission Zeros," in *Microwave Symposium Digest*, 2014 *IEEE MTT-S International*, 2014, pp. 1–4.
- [22] F. H. Raab, "Maximum Efficiency and Output of Class-F Power Amplifiers," *IEEE Transactions on Microwave Theory and Techniques*, vol. 49, no. 6, pp. 1162–1166, 2001.
- [23] https://www.researchgate.net/publication/269398857_Automatic_Frequency_Controller_for_Power_Amplifiers_Used_in_Bio-Implanted_Applications_Issues_and_Challenges/figures?lo=1
- [24] Z. A. Mokhti, "Development of A High-efficiency Power Amplifier For Envelope Tracking Applications," Ph.D dissertation, Dept. Eng., Cardiff University, Cardiff

- UK, 2016.
- [25] Z. Yusoff, “The Auxiliary Envelope Tracking RF Power Amplifier System,” Ph.D dissertation, Dept. Eng., Cardiff University, Cardiff, UK, 2012.
- [26] F. Du and H. Yu, “High efficiency test system for envelope tracking Power amplifier,” in China Semiconductor Technology International Conference (CSTIC), 2017.
- [27] F. Auer, S. Schiller, and M. Kamper, “Linearity and Efficiency Improvement using Envelope Tracking Power Amplifier,” *GeMiC*, vol. 1, pp. 88–91, March, 2016.
- [28] <https://www.edn.com/5G/4427022/Use-digital-predistortion-with-envelope-tracking>.
- [29] B. Kim, I. Kim, and J. Moon, “Advanced doherty architecture,” *IEEE Microwave Magazine*, vol. 11, no. 5, pp. 72–86, 2010.
- [30] R. Pengelly, C. Fager, and M. Ozen, “Doherty’s Legacy: A History of the Doherty Power Amplifier from 1936 to the Present Day,” *IEEE Microwave Magazine*, vol. 17, no. 2, pp. 41–58, 2016.
- [31] H. Chireix, “High Power Outphasing Modulation,” *Proceedings of the IRE*, vol. 23, pp. 1370–1392, 1935.
- [32] T. W. Barton and D. J. Perreault, “Theory and Implementation of RF-Input Outphasing Power Amplification,” *IEEE Transactions on Microwave Theory and Techniques*, vol. 63, no. 12, pp. 4273–4283, 2015.
- [33] N. Faraji and T. W. Barton, “An RF-input chireix outphasing power amplifier,” in *Power Amplifiers for Wireless and Radio Applications (PAWR)*, 2016 IEEE Topical Conference on, 2016, pp. 11–14.
- [34] J. Bi, “Chireix’s / LINC Power Amplifier for Base Station Applications Using GaN Devices with Load Compensation,” M.S. thesis, Dept. Elec. Eng., Delft University of Technology, Delft, Netherlands, 2008.
- [35] Ali M Nijnejad “integrated circuits for communications” Berkeley.
- [36] John Gajadharsing “Theory and Design of Doherty Amplifiers”, NXP, Nijmegen, The Netherlands, Sept 2010.

- [37] https://www.infineon.com/dgdl/Infineon-Experience-the-difference-in-power-with-CoolMOS-CoolSiC_CoolGaN-ProductBrief-v06_00-EN.pdf?fileId=5546d462636cc8fb0163fe86543408b0
- [38] Kenneth C Chen, Larry K Warne, Yau T Lin, Robert L Kinzel, Jonathan D Huff, Michael B McLean, Mark W Jenkins and Brian M Rutherford, "Conductor fusing and gapping for bond wires" Progress in Electromagnetics Research M, Vol.31,199-214,2013

CHAPTER 5 - COUPLING ENERGY INTO THE CAVITY**5.0 Power Coupling:**

It has been noted that variations in cavity load cause impedance and optimally matched points to vary in frequency, over a bandwidth significantly wider than the typical magnetron bandwidth of 20 MHz. Remembering that SSPAs can offer significantly wider bandwidth operation than the magnetron, using conventional, narrowband waveguide-based coupling structures designed for magnetron operation will present limitations. Therefore, a new coupling approach that can exploit the available bandwidth is needed. The basic requirements of a coupling structure for solid state heating are; (a) to ensure that the generator is well-matched to the cavity load; (b) to be able to excite ‘as many modes as possible’ inside the cavity to maximize heating control and uniformity. This ensures that the load dependent variations (in reflection coefficient), are not detrimental to cavity efficiency and device reliability

It is important to consider how a wider operational bandwidth can be exploited in a practical arrangement. Intelligent frequency hopping where the input reflection coefficient (S_{11}) is ‘pre-scanned’ over the operating bandwidth, to identify points at which the load is well-matched can be used to control the SSPA frequency and power level. For example, during instances of high reflected powers, one can search for new frequency regions where the load is more optimally matched, or lower the input drive to reduce the output and reflected power. This concept is unsuitable for magnetron based heating, and can only work with a broadband SSPA driven by a precise frequency source, and a broadband coupling structure in place of a waveguide. This approach can be shown to be highly effective in minimizing reflection coefficients, ensuring not only system efficiency, but also device reliability.

These coupling techniques must also promise to simplify system architecture, and reduce cost to the point where the use of multiple SSPA modules can provide a practical

and cost effective solution. Any proposed technique, must have the potential to reduce cost through adapting a design, where costly isolator and the associated power-load termination used in traditional PA design is not required. This will reduce transmission losses, whilst improving efficiency and output power. As an example, consider a 300W SSPA driving into a circulator with a 0.25dB insertion loss. This translates to a 20W loss in power and a 4% drop in efficiency. Further performance benefits can be realized through intelligent frequency hopping and targeted power delivery at selected frequencies.

Various methods are used to couple power into a cavity [16], with a waveguide feed approach being adopted and universally used in magnetron based domestic microwave oven applications. Due to the limitations discussed earlier, a different type of coupling technique is needed for solid-state microwave heating applications. An approach that directly integrates the coupling structure, to the output of the SSPA and into the cavity wall using a standard N-type connector is preferred.

Another key requirement in delivering high degrees of control, in the proposed solid-state heating systems is the ability to measure forward and reflected power over the 2.4-2.5GHz frequency band. This allows dynamic identification of matched frequency points, and regions of low VSWR over which power can be efficiently delivered into the cavity, whilst avoiding unmatched conditions. This is essential, both from a heating efficiency and device reliability perspective.

SSPA efficiency and reliability, whilst heavily dependent on the load at the fundamental frequency, is also influenced by the harmonics. Harmonic content plays a significant role in shaping the voltage and current waveforms at the intrinsic device plane. High efficiency amplifiers, for example, those employing class-F and inverse class-F modes, use harmonic control (short or open circuits at second and third harmonic frequencies) to shape the output voltage waveform. In class-F, a flattening or squaring of

the voltage waveform through harmonic termination minimises overlap between drain current and voltage waveforms, reducing dissipated power whilst maintaining high fundamental power. Through harmonic control and variation in drive, it can be shown that the efficiency of an ideal class-A PA can be improved from 50% to something approaching 100% [23], with the increase dependent on the order of harmonics being controlled. Improvements in both efficiency and output power are accomplished by allowing odd harmonics to develop, to shape the voltage waveform to an approximate square wave in the case of class-F, or allowing even harmonics only to develop such that the voltage waveform resembles a half-sinusoid as in the case of an inverted class-F [28]-[30]. Device parasitics can make practical implementation of harmonic terminations challenging. None the less, depending on the device technology, it is usually possible to control the impedances at a finite number of harmonics. Whereas usually, specific matching networks are designed to synthesise these specific impedance environments, this work looks at the interesting idea of controlling impedance through the design of the coupling structure itself, allowing simplification and potentially, the complete removal of the traditional matching network.

Another key requirement of the coupling technique is that it should simplify PA architecture to the point where multiple, compact SSPA modules can be easily integrated into an oven to provide a practical and cost effective solution. Improvements in match over a wide band and under variable loading conditions will allow isolator-less operation, where the use of solid-state sources becomes a real possibility, due to minimised risk of exposing the device to hostile and potentially destructive loading environments. Coupling power directly into the cavity, without the need for the usual, bulky waveguide feed structures, and indeed the bulky matching networks usually associated with high efficiency PAs, simplifies system architecture, whilst isolator-less operation can help reduce material and assembly costs

5.1 Coupling structures

Coupling structures provide a means of transferring energy into a cavity. The excitation of cavity modes is typically achieved through electric or magnetic coupling. During electric coupling, the electric field of the coupling structure is parallel to the electric field of the cavity, and similarly with magnetic coupling, the magnetic field of the coupling structure is parallel to the magnetic field of the cavity. Cavity modes are usually excited through apertures (holes and slits) in waveguide structures.

5.1.1 Magnetic coupling

For magnetic coupling, the aperture is located between the waveguide and the cavity, such that the magnetic field in the waveguide is parallel to the magnetic field in the cavity. Round holes in the wall(s) separating the waveguide and cavity are readily used for magnetic coupling

5.1.2 Electric coupling

For electric coupling the aperture is located between the waveguide and the cavity wall, such that the electric field in the waveguide is normal to the electric field in the cavity. A narrow slot in the wall(s), separating the waveguide from the cavity is used for electric field coupling.

The use of multiple waveguide structures for domestic solid-state microwave ovens is considered impractical as it will add extra volume and mechanical complexity. Further, as the signal is routed to different parts of the cavity, it will reduce by an amount that is equivalent to the cable and connector insertion losses. As a result a direct means of coupling energy into the cavity, using coaxial line needs to be explored. The coaxial line can also be used to provide either electric or magnetic coupling by means of electric probes or current loops.

5.1.3 Electric probes and Current loops

An electric probe is simply the center conductor of a coaxial line, which is extended inside the cavity, such that its direction is parallel to the direction of the electric field in the cavity. Whereas a current loop is formed by the center conductor of the coaxial line, which has been terminated in a short circuit such that it forms a full or a half loop. The loop produces a magnetic field that is perpendicular to the plane of the probe and in the same direction as the magnetic field in the cavity. The advantages of current loops are that they are compact in size, with a relatively high directivity. However the loops have a very high resonance (Q factor), which means that impedance matching (over a range of loads) can be difficult to realise. This means of coupling has to be researched further and developed using semi-empirical techniques.

5.2 Loop coupling structure

In its simplest form, a single loop is a metallic conductor bent into the shape of a closed curve, such as a circle or a square. One end of the loop is used as the input for the signal whilst the other end is connected to the cavity wall to form a short circuit. These loops can be electrically large (conductor length $\geq 0.11\lambda$) or small (conductor length typically $\leq 0.1\lambda$) [1]. A trade off between small & large loop lengths is presented in literature [47]. The axial current distribution in an electrically small loop is assumed to be uniform, that is, the current has the same value at any point along the conductor. As well as transferring power into the cavity, the loop can also be used to detect reflected power at the ports.

During power transfer (into the cavity), the electromagnetic field of an electrically small loop is the same as that of a magnetic dipole. The loop plane is normal to the polar axis of a spherical coordinate (x,y,z) system. The voltage (V) at the loop terminals and the current (I), that flows around the loop are a function of the loop impedance (eqn.5.1). For electrically small loops, this impedance is a combination of external inductance (L^e),

radiation resistance (R^r) and the internal impedance of the conductor ($Z^i = R^i + j\omega L^i$; where R^i = internal resistance and L^i = internal inductance), which represents the loop ohmic losses.

$$Z = R + j\omega L = R^r + Z^i + j\omega L^e = R^r + R^i + j\omega(L^e + L^i) \tag{5.1}$$

The small loop equivalent circuit (Fig.5.1), typically includes a capacitor (C) connected in parallel with the impedance Z , to account for the distributed capacitance between the loop conductors. The effect of this capacitance is negligible in loops with a uniform current distribution, as there would be no change along the loop conductor. The radiation resistance of a small loop is proportional to the square of the product of the areas and the number of turns (eqn.5.2).

$$R^r = \frac{\zeta}{6\pi} \beta^4 (NA)^2 \tag{5.2}$$

Where

$$\beta = 2\pi/\lambda$$

A = Area of loop

$$\zeta = \sqrt{\mu_0/\epsilon_0} = \text{wave impedance of free space} \sim 377\Omega$$

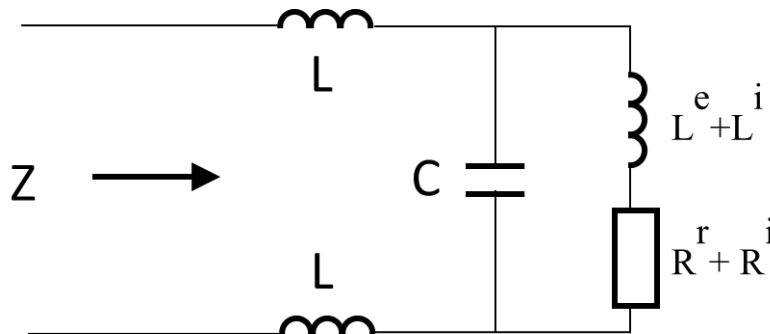


Fig. 5.1. Equivalent circuit for input Z of a small loop

For a single loop, whose turn is not too closely spaced, the internal impedance can be approximated using eqn 5.3, where z^i = internal impedance per unit length of a straight conductor, which has the same cross sectional area as the loop conductor [34]. If the turn is closely spaced, than the proximity effect must be included in determining z^i [3].

$$Z^i = z^i \cdot \text{Total length of the conductor} \quad (5.3)$$

The external loop inductance can be determined from one of the many formulas available for the inductance of coils [35]. For a single-turn circular and square loops this can be calculated using eqn 5.4 and 5.5 respectively, whereas the radiation efficiency can be calculated using eqn 5.6.

$$L^e = \mu_0 b [\ln(8b/a) - 2] \text{ circular loop} \quad (5.4)$$

$$L^e = \frac{2\mu_0 b}{\pi} [\ln(b/a) - 0.774] \text{ square loop} \quad (5.5)$$

Where

b = mean radius of a circular loop or mean side length of a square loop

a = radius of loop conductor

$$\eta = \frac{\text{Average Power Radiated}}{\text{Average Power Supplied}} = \frac{R^r}{R^r + R^i} \quad (5.6)$$

The loop can also be used to detect reverse power at the signal ports. This typically involves a measure of the voltage developed across the open-circuit terminals of the loop. The voltage (V_{oc}) (Fig.5.2), is proportional to the component of the incident magnetic flux density normal to the plane of the loop (B_z^i). The field is assumed to be uniform over the area of the loop. The voltage across an arbitrary load impedance Z_L connected to the terminals of the loop, with input impedance Z is determined from the Thévenin equivalent circuit shown in (Fig. 5-2).

$$V_{oc} = j\omega NAB_z^i \quad (5.7)$$

$$V_L = \frac{V_o Z_L}{Z + Z_L} \quad (5.8)$$

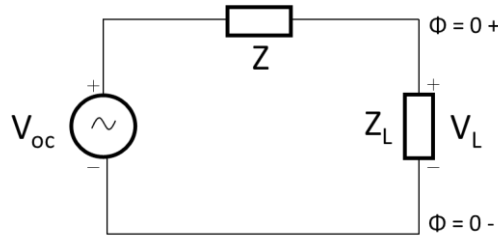


Fig. 5.2 Thevenin equivalent circuit for the receiving loop

5.2.1 Loop coupling structure - matching considerations

For a small loop to operate properly within a cavity structure, it needs to have a resonance at the transmit frequency, and the feedline must be matched to the radiation impedance of the cavity. Both of those conditions must be met in order to get a VSWR equal to unity. A loop exhibits a complex impedance (resistance R and reactance X ; where $Z = R + jX$) at its feed point. The resistance R does not change with frequency, whilst the reactance X is frequency dependent. Furthermore, the complex impedance of the loop changes as the load varies. Due to the complex nature of the impedance, there is reactive (phase) element that needs to be considered during the matching process, as this can cause a complex load to reflect some of the power. When the reactance $X = 0$ the impedance is purely resistive, and the load can absorb 100% of the supplied power. The process of impedance matching thus involves the removal of frequency dependent reactance component from the complex impedance such that $Z = R$. Even if the cavity (load) is resonant such that it presents a pure resistance, it still needs to be matched to the SSPA output impedance before maximum power transfer can be achieved. The feed point impedance R is thus the sum of radiation impedance and the loss resistance. Unless you

have a feed point of 50Ω , the VSWR will not be close to unity, and in such instances, most of the transmit power will be reflected. An impedance transformer between the SSPA and the cavity load impedance can ensure a smooth transfer of power, and this process is referred to as impedance matching.

Whilst most E-field probes have a fairly good bandwidth under matched (50Ω) conditions, they are of a limited use under variable loading conditions (e.g. domestic microwave ovens), where variations in the load necessitate re-sizing of the probe(s), which is difficult to realise outside of the laboratory environment. Whereas with the use of a H-field loop coupling structure, variations in the load can be overcome by reshaping the loop (varying the capacitance), changing the position and orientation of the loop inside cavity, such that impedance matching can be realised for different loads. Although single loop coupling structures exhibit a very narrow bandwidth, and also need retuning with load variations to ensure loop gain is maximised in the frequency band of interest, their radiation pattern is omnidirectional and well suited for cavities exhibiting multiple modes such as a rectangular cavity. The potential to excite multiple modes, means that this type of coupling structure has a greater potential for solid-state heating applications, compared to the E-field antennas, whose radiation pattern is directional and less likely to excite all the modes. This means that more (>1) E-field probes are required for multi-mode excitations.

Matching networks (Fig.5.3) are generally used to improve the power transfer from a generator to a load. At a given frequency (ω_0), the impedance of the loop can be transformed to the resistance R_0 by using various networks [36]. A capacitor C (eqn.5.9) is typically used to bring the loop close to resonance at ω_0 , or the spacing s and length of the lines l can be adjusted to make the impedance R_0 . However, the match obtained with these simple networks generally has a very narrow bandwidth. Whilst the capacitor C can be used to tune the resonant frequency, the impedance match can be tricky. One way of coupling the transmit power to the cavity is through an un-tuned coupling loop which acts as a RF transformer, with air as its dielectric. A loop of wire (typically a coax cable) is

secured to the feed line, and placed near the loop element. The ‘feed’ impedance can be adjusted by making the coupling ‘tight’ or ‘loose’, which is a measure of how close the parallel coupling loop is to the element. An advantage of this technique is that by changing the shape of the coupling loop, a wide range of impedance matches can be achieved across many different frequency points. The matching is fairly constant across these frequency points, unlike that achievable when using a tuning capacitor, which needs adjusting every few KHz. The typical means of adjusting the coupling are shown through illustrations (Fig.5.4) and are listed below:

- (a) Modifying the shape of the coupling loop
- (b) Modifying the angular orientation between the main loop and the coupling loop
- (c) Modifying loop distance inside the cavity

$$C = \frac{1}{\omega_0(\omega_0 L - R\sqrt{R_0/R - 1})} \approx \frac{1}{\omega_0(\omega_0 L - \sqrt{RR_0})} \quad (5.9)$$

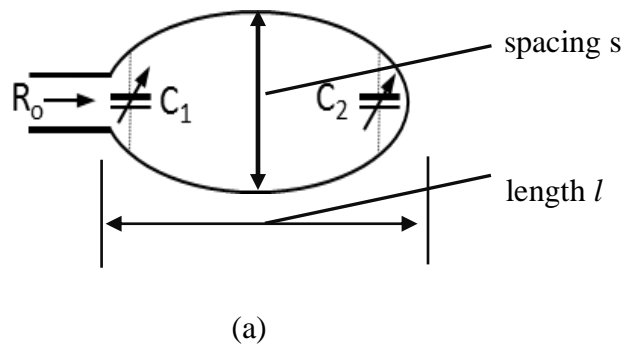


Fig. 5.3 Typical matching networks used with coupling loops. Match to a resistance R_0

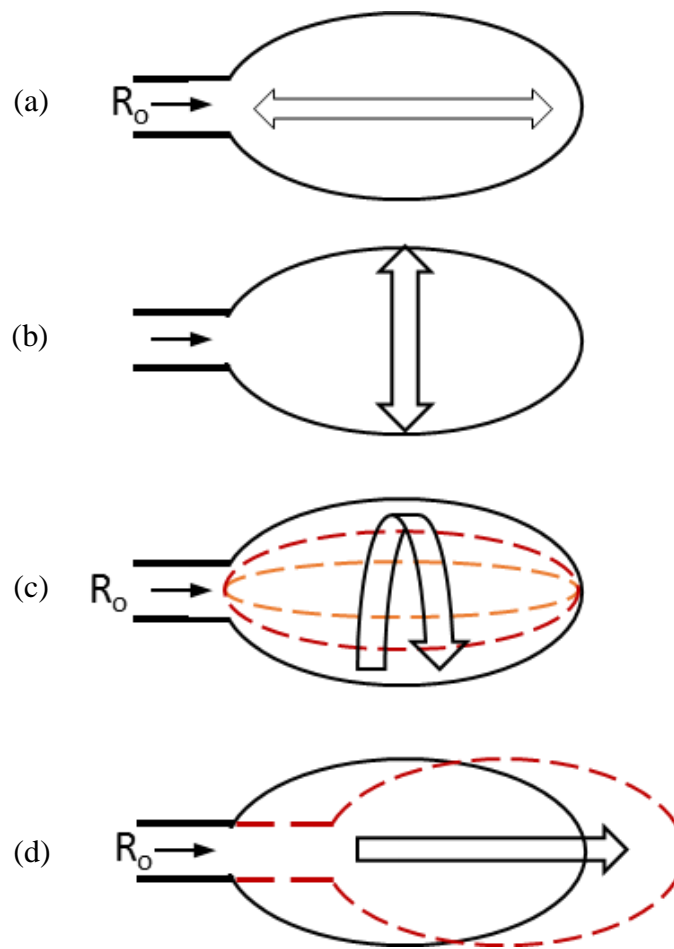


Fig. 5.4 Means of adjusting coupling in loop. (a,b) Modifying the shape of the loop (c) modifying angular orientation of the loop (d) modifying loop distance inside the cavity

5.3 Single loop coupling structure

5.3.1 Single loop lumped element model:

Magnetically coupled resonant loops can be analysed either by a coupled mode theory [41-42], or by using an equivalent circuit model. It has been shown that an equivalent circuit model is simpler, and reasonably accurate for the analysis of resonant magnetically coupled loops. Numerous works, based on equivalent circuit models, have been reported [41-45]. The single loop coupling structure described in section 5.2 and its simpler variant, a lumped-element model are used to predict the loops responsiveness to

load variations. Each parameter in the lumped element model, is expressed as a function of loop geometry and the separation between the loops. This means that the loop geometry can be systematically changed, and the power transfer efficiency of the coupled loop (under variable loading conditions) can be predicted. The power transfer efficiency is characterized for various loop geometry parameters to realise an optimum structure. The simulated results (section 4.5) clearly show that there is a trade off between power delivery efficiency and critical coupling which depends on loop size, frequency of operation and the load impedances.

The magnetically coupled resonant loop (Fig.5.5a), can be represented by an ideal circuit model (Fig.5.5b, where its only possible to change the coupling coefficient), and its equivalent lumped element model shown in Fig. 5.5.c. The lumped element model components L , R and C (the self-inductance, parasitic resistance and the resonance capacitance of the loop) are dependent on the geometry of the loop. The cavity equivalent model shown earlier in Fig. 4.15, is used to characterise the loop coupling structure (ideal circuit model vs lumped element model), under fixed and variable loading conditions. From the simulated data shown in Fig.5.6 (polar complex and magnitude log-lin format at fundamental and second harmonic frequencies), we can see that the ideal circuit model (Fig.5.5b) and its lumped element equivalent's performance is the same at both the fundamental and second harmonic frequencies. This equivalent lumped element model (owing to its greater flexibility), is used to simulate and develop the magnetically coupled loops for variable loading conditions.

From the simulation data shown earlier (Fig. 4.18), it was established that a single loop coupling structure is narrowband, and averse to load variations. Here again we note through simulated data shown in Fig. 5.7 (obtained using lumped element equivalent model), that as the cavity load impedance (R_L) is reduced from its optimally matched condition (50Ω to 10Ω), the impedance trace moves to the left of the 50Ω point and towards a short circuit (*low Z*). Similarly, as the load impedance (R_L) is increased (50Ω - 100Ω) the impedance trace moves to the right of 50Ω point, and towards an open circuit.

The use of a single loop coupling structure, means that these changes in load will result in an impedance mismatch as shown in table 5.1; here the loop was optimized for a fixed 50Ω load ($C=1$). The second harmonic component (shown in both polar complex form and magnitude log-lin format, Fig 5.6.a, c), is also shown to drift with load variations. In most applications, the load (R_L) is fixed and the input impedance (Z_{in}) is a function of loop geometry (L, C and R). However, under variable loading conditions a part of the RF signal is reflected back at the input of the resonant loop, due to a mismatch between the Z_{in} and the source resistance R_s . The power delivery efficiency into the cavity is degraded by the mismatch, by an amount that is proportional to $1-|\Gamma_{in}|^2$.

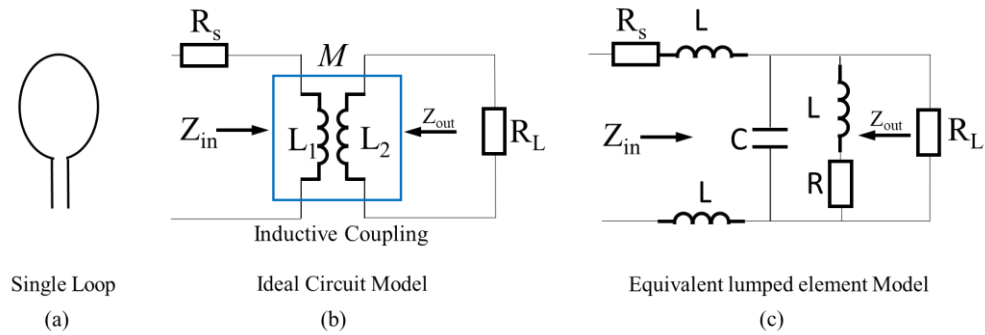


Fig. 5.5.a,b,c. General depiction of magnetically coupled resonant loop (a); its ideal circuit model (b) and its lumped element equivalent model (c)

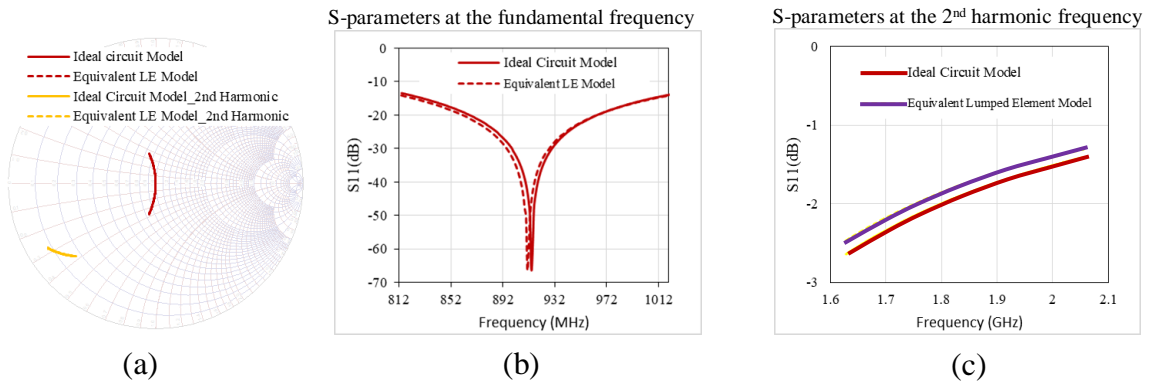


Fig. 5.6 Simulated (using lumped element equivalent model Fig.5.5b,c) impedance at the fundamental (900MHz-930MHz) and 2nd harmonic (1.8-1.86 GHz) freq's under fixed load (R_L) conditions is shown in both polar complex (a) and magnitude log-lin format (b, c).

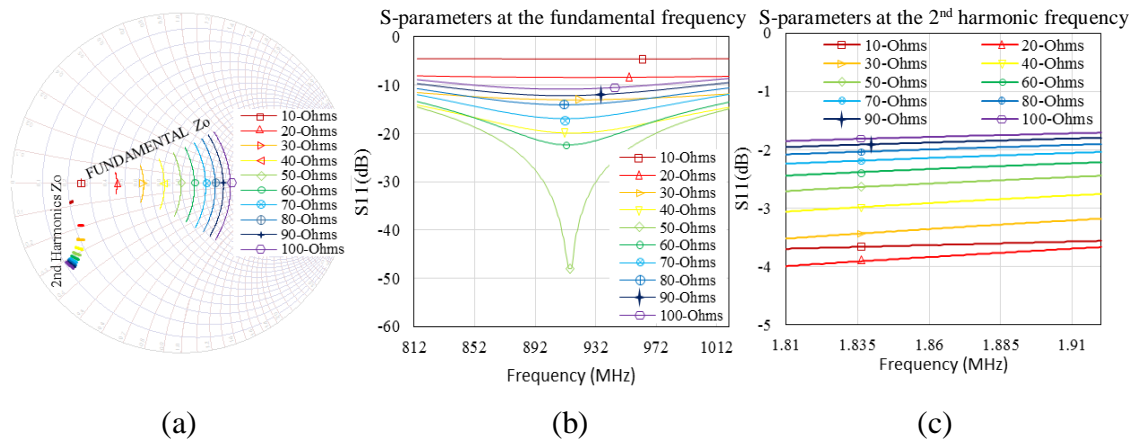


Fig. 5.7 Simulated (using lumped element equivalent model Fig.5.5c) impedance at the fundamental (900MHz-930MHz) and 2nd harmonic (1.8-1.86 GHz) freq's under variable load (R_L) conditions is shown in both polar complex (a) and magnitude log-lin format (b, c).

Table 5.1 – S_{11} as a function of variable load – Static Single loop

Load	Coupling Coefficient (β)	Frequency		
		886MHz	916MHz	936MHz
		S11(dB)		
10 Ω	1	-4.56	-4.56	-4.56
20 Ω	1	-8.35	-8.40	-8.38
30 Ω	1	-12.04	-12.18	-11.93
40 Ω	1	-19.09	-19.91	-21.11
50 Ω	1	-27.06	-47.95	-28.63
60 Ω	1	-21.11	-22.38	-21.22
70 Ω	1	-16.53	-16.89	-16.53
80 Ω	1	-13.76	-14.02	-13.72
90 Ω	1	-12.21	-10.81	-11.90
100 Ω	1	-10.75	-10.78	-10.63

5.3.2 Single loop lumped element model with harmonic tuning - cylindrical cavity

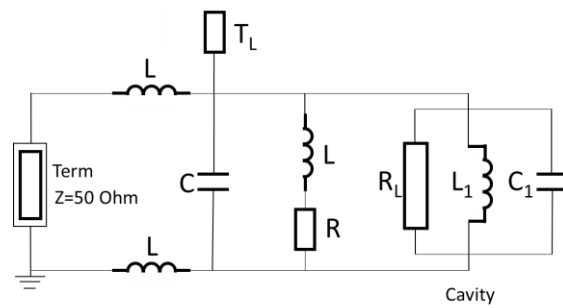
With increasing demands and expectations placed upon solid-state to deliver high power and efficiency, new approaches to power amplifier and efficient means of coupling power into the cavity need exploring. One technique for improving efficiency, which allows for smaller, light weight SSPA's with reduced cooling requirements and enhanced reliability is to tune the output harmonics. High efficiency operation typically occurs when the harmonics of the output voltage have the right magnitude and phase to form a square

wave. This can be realized by placing short circuits at the even and an open circuit at the odd harmonics. A short at the 2nd harmonic suppresses the second harmonic component and an open circuit 3rd harmonic component makes the output voltage waveform closer to a square wave.

The practical realisation of harmonic tuning is made difficult by packaged RF and microwave power transistors, presenting additional reactances (from the package), which limit the impedance range that can be presented to the intrinsic device e.g the capacitance of a standard LDMOS package is of the order of 5-6pF, which corresponds to a jX_c (4GHz) of $-j7\Omega$ reactance at the 2nd harmonic of a 2-GHz signal, effectively shortening the harmonic. Since high efficiency classes of operation depend on specific harmonic terminations at the device intrinsic plane, this implies that the package prevents high-efficiency operation with LDMOS transistors. GaN HEMT or SiC MESFET device technologies, on the other hand exhibit a square law behavior which makes them more susceptible to generating second and higher order harmonics. These higher order products require careful attention, and must be carefully managed (terminated) and exploited to minimize the power losses. The gains in performance by harmonic tuning have been well documented [8].

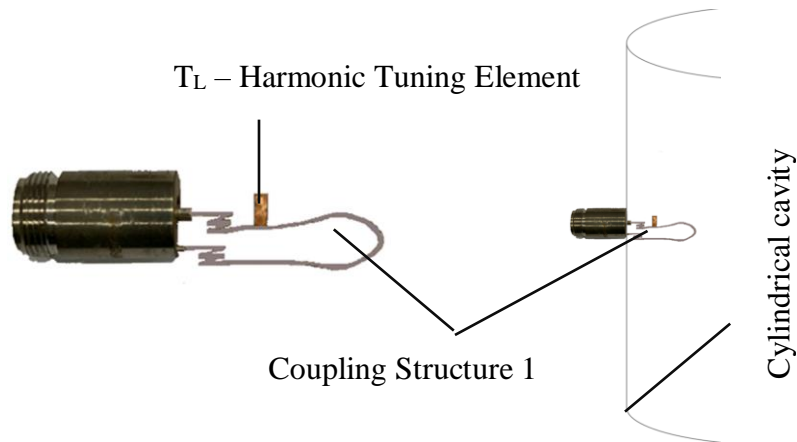
Whilst the concept of harmonic termination is well documented and often employed to improve SSPA performance when operating in a well-defined 50 Ω load environment, the implications of operating into a non-50 Ω load needs further attention and investigation. The potential to control second harmonic load impedances using the loop coupling structure is explored and presented in this section. The importance of, and control over second harmonic termination, and what it means for SSPA efficiency and reliability have been discussed in detail [9]. An alternative novel coupling structure (coupling structure 1, Fig.5.8), employs an open transmission line (T_L) to control the second harmonic impedance as shown in Fig.5.9. From the simulation data, we note that for a fixed load (R_L) the 2nd harmonic impedance has been transformed towards a short

circuit. The use of T_L to control 2nd harmonic impedance under variable loading conditions, is also investigated by varying the load impedance (R_L) from 10 Ω -to-100 Ω . Simulated data (Fig.5.10), shows that the 2nd harmonic impedance has been successfully transformed towards a short circuit, and is to the same area of the Smith chart. Using this magnetically coupled resonant loop approach, the SSPA can be directly integrated with the loop, which serves as a frequency and load dependent radiator. Coupling structure characteristics thus become a part of the PA design process.



(a)

Single Loop equivalent lumped element model



(b)

Physical realisation

(c)

Cylindrical cavity with loop attached

Fig. 5.8 Single Loop equivalent lumped element model with a harmonic tuning element (a) and its physical realisation (b) cylindrical cavity with the loop attached

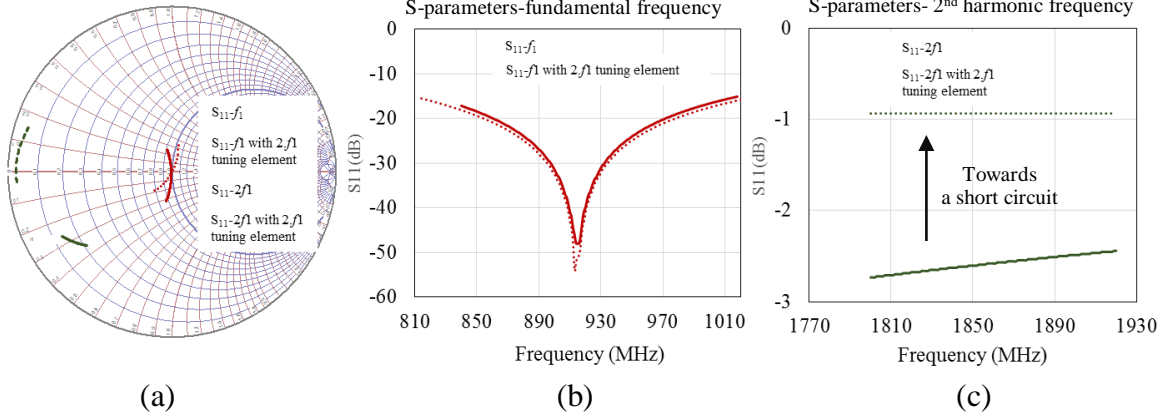


Fig. 5.9 Simulated (using lumped element equivalent model Fig.5.8) impedance at the fundamental (900MHz-930MHz) and 2nd harmonic (1.8-1.86 GHz) freq's under fixed 50Ω load (R_L) conditions is shown in both polar complex (a) and magnitude log-lin format (b, c).

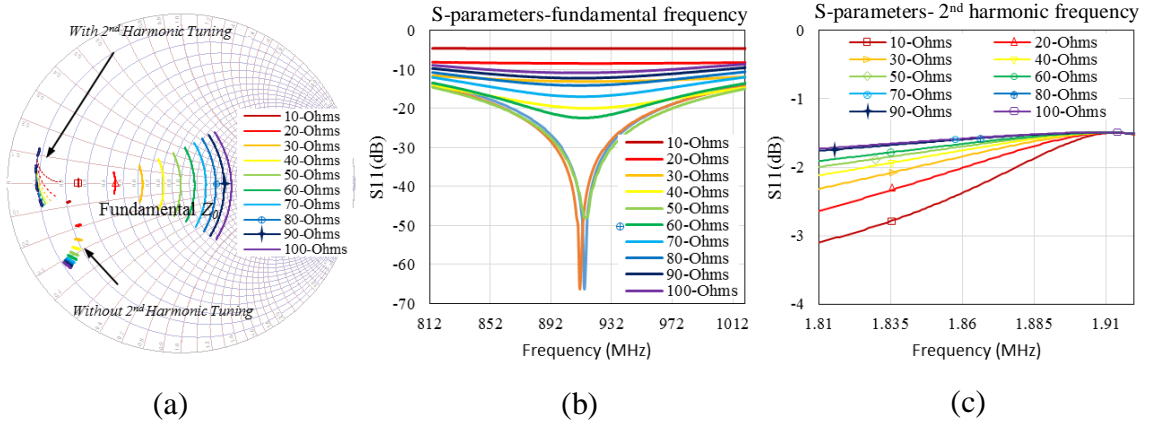


Fig. 5.10 Simulated (using lumped element equivalent model Fig.5.8) impedance at the fundamental (900MHz-930MHz) and 2nd harmonic (1.8-1.86 GHz) freq's under variable loading (R_L) conditions is shown in both polar complex (a) and magnitude log-lin format (b, c).

5.3.3 Single loop coupling structure construction and integration into a cylindrical Cavity.

The coupling loop is developed using a semi-empirical technique, drawing on prior knowledge of loop antenna structures, cavity impedance behaviours, experience of

matching network design and simulation software. The strategy adapted involved using Keysight ADS circuit simulator, to develop cavity equivalent model, whilst a 3D simulator (Comsol-multiphysics) was used to characterise the cavity impedance and field distribution behaviour.

In its simplest form, the magnetic coupling loop was formed by extending the coaxial cable (via a modified N-type collar and connector) into the cavity resonator, and then bent to form a loop with one of its ends grounded to the connector ground and hence the cavity wall. The center of the loop is located midway between the top and the bottom walls of the single mode cylindrical cavity, as shown in Fig. 5.11. The size of the loop is relatively small compared to the wavelength, therefore the voltage at all parts of the loop is assumed to be zero, whilst the current is large, and the input impedance is nearly equivalent to that of a short circuit. The current is responsible for producing a magnetic field tangential to the walls of the cavity. The energy couples to the magnetic field, defined by a resonance mode that is tangential to the wall and perpendicular to the plane of the loop.

Whilst the size of the dipole moment is proportional to the loop area, the orientation of the loop is also important. In a TM_{01} mode cavity (coupled with an external circuit), the cavity resonator and the coupling loop form a parallel resonant circuit. The coupling coefficient (β), is a function of the system characteristic impedance and the cavity load impedance (R_L). From equations 5.10-5.11, it is noted that the coupling coefficient determines the reflection coefficient at the SSPA output, the resonance bandwidth and the power dissipated into the cavity. The coupling coefficient, therefore plays an important role in solid state heating apparatus. It is possible to adjust the value of β by changing the loop geometry. For a 50Ω load, $\beta = 1$ and the load is said to be critically coupled (no reflected power), the cases where $\beta < 1$ and $\beta > 1$ are referred to as under and over coupled, which results in reflected power signals. This coupling through the air achieves the desired impedance transformation. The principles of coupled loop-to-cavity resonators and loop size calculations are described in detail in literature [38-40].

$$\beta = \frac{P_{\text{dis}}}{P_{\text{cav}}} = \frac{R_L}{n^2 Z} \quad (5.10)$$

Where:

P_{dis} = Power dissipated into the load

P_{cav} = Power delivered into the cavity

$$\rho_{\text{cav}}|_{f=f_{\text{res}}} = \frac{\beta-1}{\beta+1} \quad (5.11)$$

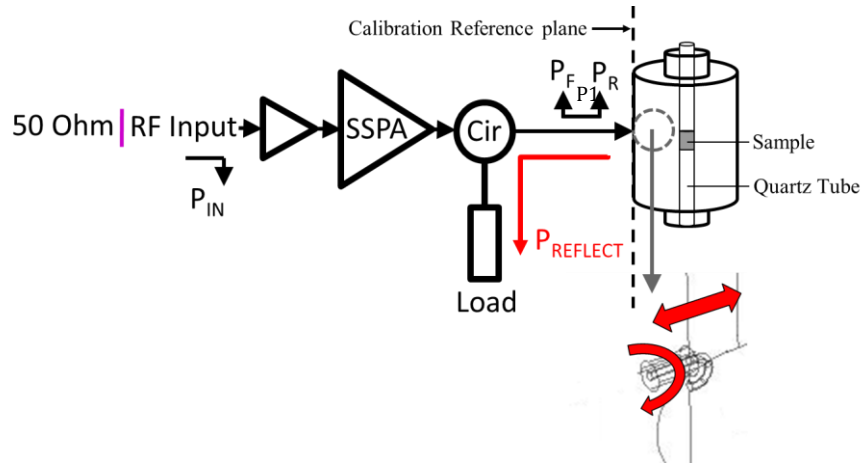


Fig. 5.11 Measurement set-up used for characterising a coupling loop within a cylindrical cavity resonator.

5.4 Single loop coupling structure characterisation using a cylindrical cavity.

Although, for typical domestic heating applications, a multi-mode rectangular cavity is used, for the purposes of this study, a single mode-cylindrical cavity, designed to operate with a single, dominant TM_{01} mode at 900-960MHz frequency band is used to simplify the analysis. This type of cavity provides a predictable environment, where the electric and magnetic field distribution are relatively easy to determine and visualize. Coupling into the cavity is achieved by constructing a physical replica of the loop model (coupling structure 1) shown in Fig.5.8b. The matched condition is realized by using semi-empirical techniques discussed in section 5.2.1.

From the measurement data (Fig.5.12), it is observed that the load (0.085l of water) is critically coupled at 913MHz. Away from this optimal frequency point, the match deteriorates and the level of reflected power begins to increase rapidly. This is shown by the measured reflection coefficient (S_{11}), the forward and reflected power, and VSWR data. The reflected power measurements follow the s-parameter response. The simple loop coupling has a limited bandwidth (~ 9 MHz) over which an acceptable level of match ($S_{11} < -10$ dB) exists. The VSWR measurement data shows a value of just above 1 at the critically coupled frequency (913MHz), indicating an efficient transfer of available power into the cavity to heat the load. At this frequency of operation, the device operates safely, however, away from this frequency the value of VSWR rises (with increasing reflection coefficient), leading to a drop in power delivered to the load. These high reflective states can damage the transistors within an SSPA, hence a circulator and high power dissipative load are typically used at the SSPA output as a protection against hostile loading conditions.

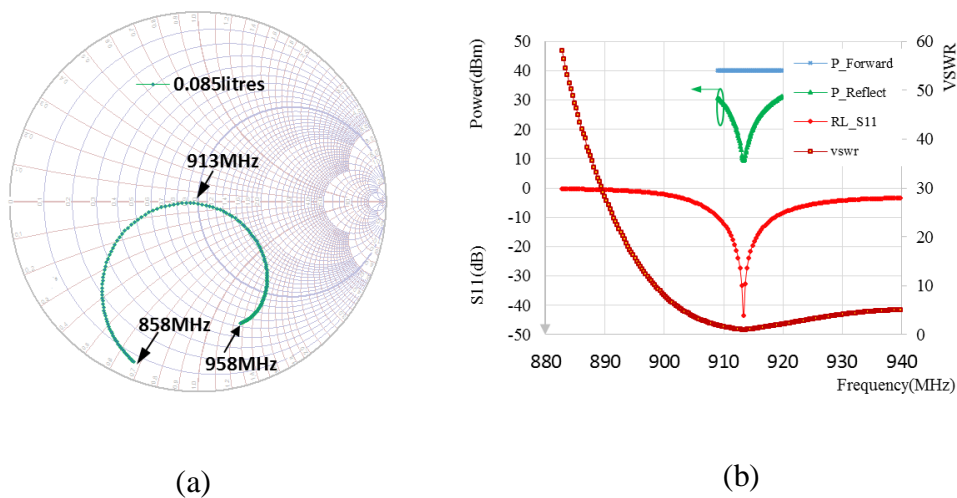


Fig. 5.12 Measured impedance data is shown in polar complex form (a) and magnitude log-lin format along with the forward/reflected powers and the VSWR (b) at the Fundamental frequency (900MHz-960MHz) for a fixed load (0.085l of water) using a single loop coupling structure shown in Fig.5.8.

5.4.1 Limitations of a single loop under variable loading conditions

Impedance variations due to changes in load (0.05l-to-0.12l of water) are investigated and presented. A rise in the volume of water increases the impedance, moving it to the right of the 50Ω point on the Smith chart, whereas a decrease in volume moves the impedance to the left (Fig.5.13). The impedance is reactive in nature and lies in the bottom half of the Smith chart e.g. the load is capacitive.

Reflection coefficient measurements (Fig.5.13b) also show that variations in water volume change the frequency at which the load is optimally matched, with a rise in the volume reducing the frequency. This advocates the need for an intelligent methodology (algorithm) to search for frequency points where the load is optimally matched, thus ensuring high levels of power delivery efficiency under varying loading conditions. The inability to locate and track these frequency points means that there will be an impedance mismatch at the SSPA output, exposing it to high VSWR conditions with potentially severe implications on both cavity efficiency and device reliability. This is clearly undesirable and of great concern for device and heating apparatus manufacturers.

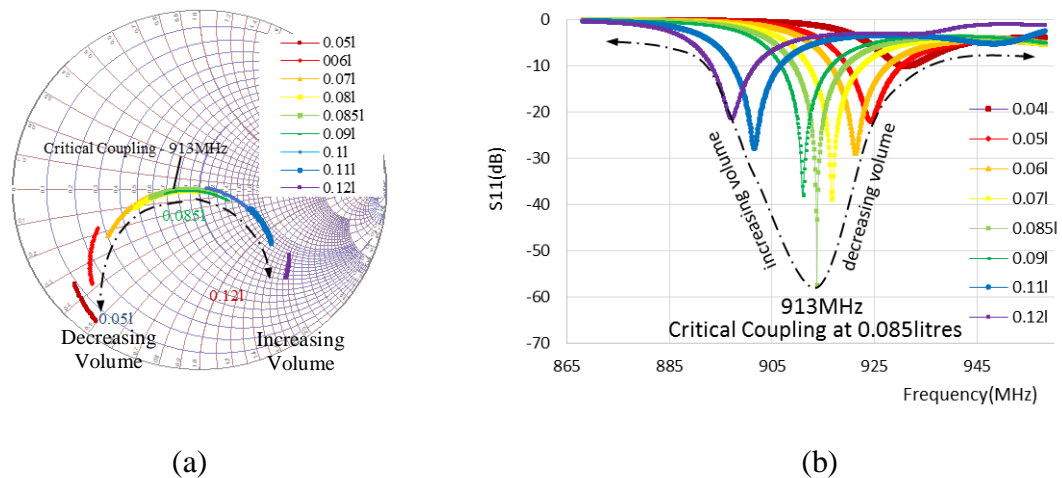
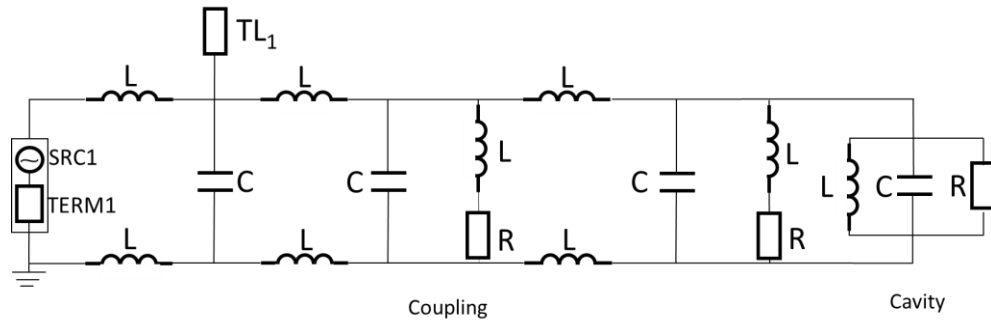


Fig. 5.13 Measured impedance data is shown in polar complex form (a) and magnitude log-lin format (b) at the Fundamental frequency (900MHz-960MHz) under variable loading conditions (0.04l-to-0.12l of water) using a single loop coupling structure shown in Fig.5.8.

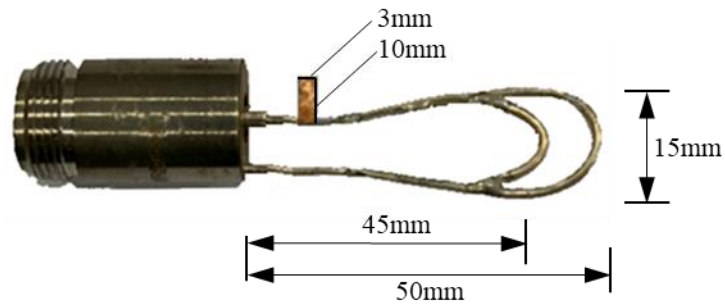
5.5 The optimised coupling structure with a wider bandwidth and tolerance to load variations

It is clear that the coupling structure, is a key element in transferring SSPA generated power into a load, within the single-mode resonant cavity (under single and variable loading conditions). It is also clear however, that the single loop coupling structure, whilst useful under known single load operating conditions has major limitations in accommodating variable loading conditions. An alternative two loop approach (coupling structure 2, Fig.5.14) is presented, which involves modifying the single loop coupling structure for extended bandwidth operation, without the need for mechanical adjustment. The impedance traces in Fig.5.15a, show comparisons between the single loop and the proposed wideband coupling approach for a fixed load (0.085l of water). The impedance trace with the proposed two loop approach encircles the 50Ω point, and the s-parameter data (Fig.5.15b), shows a return loss of better than -15 dB over a 70MHz operational bandwidth. The VSWR data (Fig.5.15c), shows that with this approach, the SSPA will continue to operate efficiently and safely into a matched load over a wider bandwidth, without the need for physical adjustment of the loop. This is in contrast to the high-Q single loop structure's limited operational bandwidth. The proposed technique is, as a result, more tolerant to load and temperature variations, which becomes important when considering the idea of isolator-less power amplifier designs for low-cost microwave heating applications.

Further, with the proposed approach, a return loss of -15dB at the optimal frequency suggests that 97% of the available power will be delivered to the cavity. This is compared to a return loss of -42dB and a delivery efficiency 100% when using the single loop. This loss in cavity efficiency (3%) is relatively small and worth sacrificing for the gains made in operating bandwidth. With this proposed approach the delivery efficiency remains high (over 90%), and relatively constant over the operating bandwidth, whereas with a single loop coupling structure it drops very sharply to less than 50% over a 10MHz bandwidth.



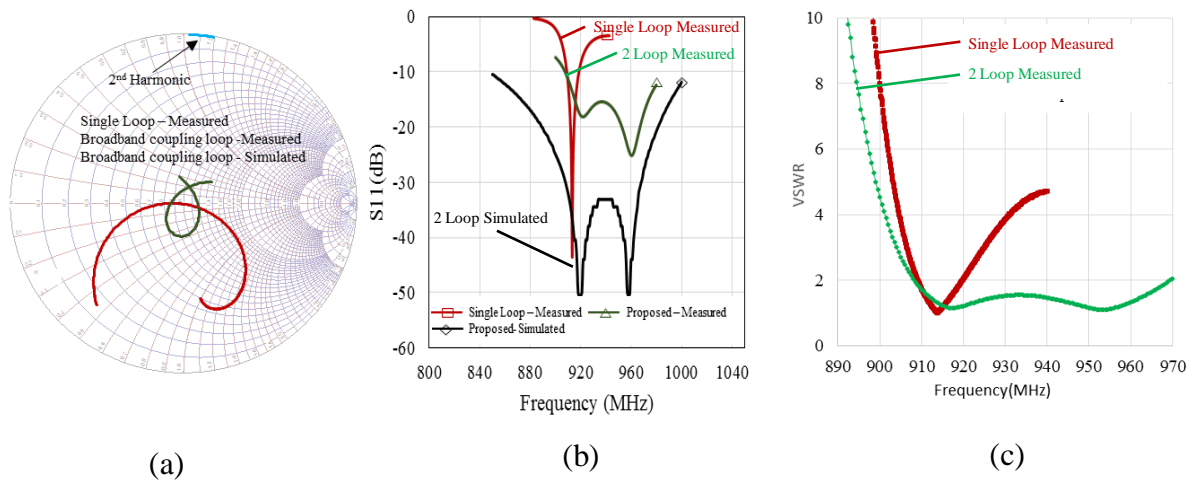
(a)



Coupling Structure 2

(b)

Fig. 5.14 Equivalent lumped element of the 2-loop broadband coupling structure with harmonic tuning (a) and its physical realisation.



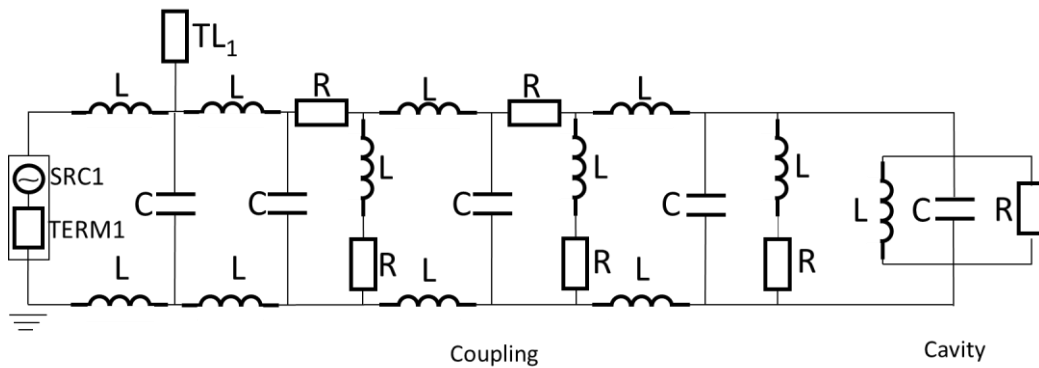
(a)

(b)

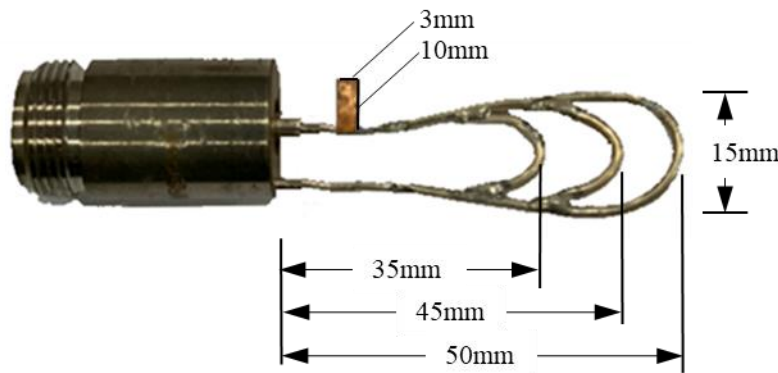
(c)

Fig. 5.15 Measured impedance data is shown in polar complex form (a) and magnitude log-lin format (b) at the Fundamental frequency (900MHz-960MHz) for a fixed load (0.085l of water) using a single and two loop coupling structures shown in Fig.5.8 and Fig.5.14.

The two-loop coupling structure is developed further by incorporating a third loop (coupling structure 3) as shown in Fig.5.16. With the equivalent lumped element model of a three loop coupling structure it is shown, through simulations (Fig.5.17), that a larger range of load impedances can be successfully matched to 50Ω , and the operational bandwidth extended significantly. The improvements in impedance match at both the fundamental and second harmonic frequencies are explored further in chapter 6. Whilst the benefits may not appear significant for a single mode cavity, this concept has a huge potential in multi-mode cavity operation, where many modes are scattered over a larger bandwidth.



(a)



Coupling Structure 3

(b)

Fig. 5.16 Equivalent lumped element model of a 3 loop broadband coupling structure (with harmonic tuning) optimized for variable loading conditions

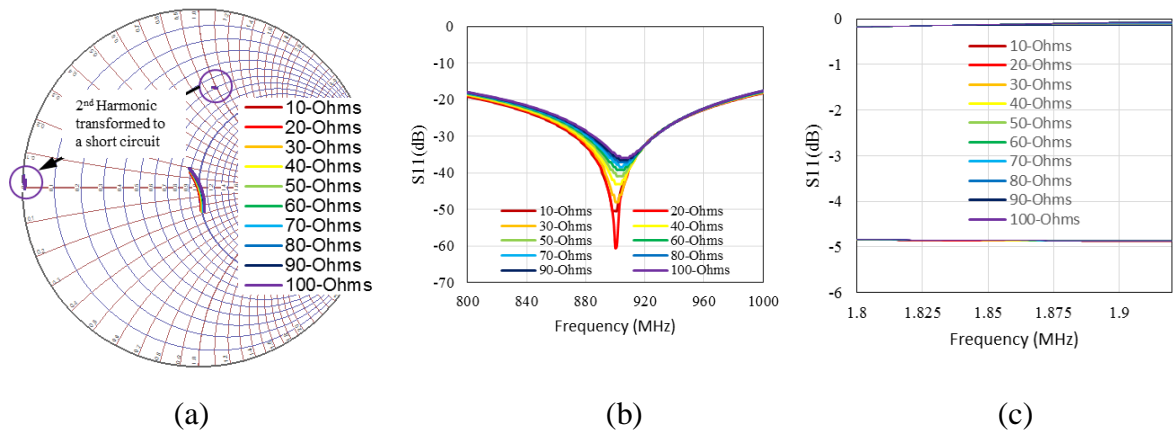


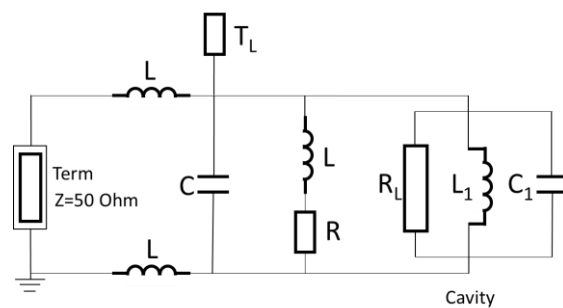
Fig. 5.17 Simulated impedance data is shown in polar complex form (a) and magnitude log-lin format (b) at the Fundamental (900MHz-960MHz) and 2nd harmonic frequencies for a range load impedances (RL , 10 Ω -to-100 Ω) using a three loop coupling structures lumped element equivalent model shown in Fig.5.16.

5.6 Single loop coupling structure characterisation for using a rectangular cavity

Large, over-moded rectangular resonant cavities used in commercial and domestic microwave heating applications, possess complex impedance behaviours with tightly packed resonant modes, within a relatively narrow frequency range. This behavior is well suited to excitation using magnetrons, where an exact control of the frequency is not possible. However, typical variations in load can cause a spreading these resonances, such that required excitation frequencies can lay outside of the magnetron operating bandwidth (2450MHz \pm 10MHz) [33]. This phenomena will clearly affect the heating efficiency, as more of the available power is reflected back to the source.

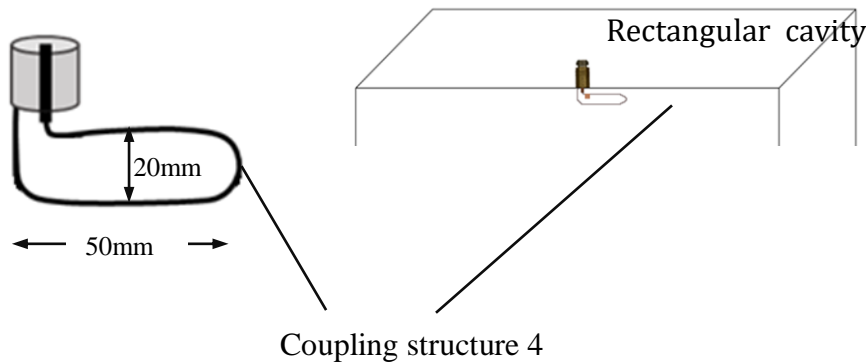
To characterize large rectangular cavity impedance behaviour, at the fundamental (2400-2500MHz) and second harmonic (4800-5000MHz) frequencies, coupling structure 4 (a single loop coupling structure, Fig.5.18), was used to measure reflection coefficient under variable loading conditions. With a single loop coupling structure, it was only

possible to obtain a good impedance match at single frequency point(s), or over a very narrow bandwidth. Whilst it is possible to deliver power efficiently into the cavity at these specific frequencies; through detection of matched states, and then selection of SSPA operating frequency to deliver power at the optimally matched points, practical implementation can be very challenging. The power delivered into the cavity over the unmatched regions drops very significantly, such that overall efficiency is poor and there is a serious chance of damaging the SSPA.



(a)

Single Loop equivalent lumped element model



(b)

Physical realisation

(c)

Rectangular cavity with loop attached

Fig. 5.18 Single Loop equivalent lumped element model with a harmonic tuning element (a) and its physical realisation (b) rectangular cavity with the loop attached

5.6.1 Limitations of single loop coupling structure in a rectangular cavity

Typical microwave oven usage involves heating loads, which are equivalent to 0.325l of water or less [46]. However in order to understand the true effect of load variations, the cavity load was varied from 0.1l-to-1.0l in 0.1l steps. The measured reflection coefficient data was recorded, in both polar complex and magnitude log-linear formats as shown in Fig.5.19. As discussed previously in section 5.4.2, by intelligently selecting the SSPA frequency of operation, the power delivery efficiency can be greatly improved here too.

Furthermore, as the volume of water is increased from 0.1l to 0.5l the matched and unmatched regions appear in clusters (matched regions in the lower and upper end of the frequency band and unmatched regions in the middle of the frequency band), and the range of points over which the power can be delivered safely and efficiently has increased. A further rise in the volume of water results in scattering of the optimally matched impedance points, which now sit in the centre of the frequency band.

The concept of intelligent frequency hopping proposed in chapter 1, and discussed in section 5.4.2 of this thesis (where the SSPA frequency of operation is chosen to coincide with optimally matched frequency point's), is given credence by the measurement data shown in Fig.5.19. The use of intelligent frequency hopping means that the SSPA is always operating into a well matched load. Injecting power into the cavity at targeted frequencies that provide less than 10dB insertion loss, means that at least 90 percent of the available power is delivered into a 45cm cavity. The use of a single loop coupling structure under variable loading conditions would necessitate a very fast, real time detection and adaptation of the SSPA operating frequency.

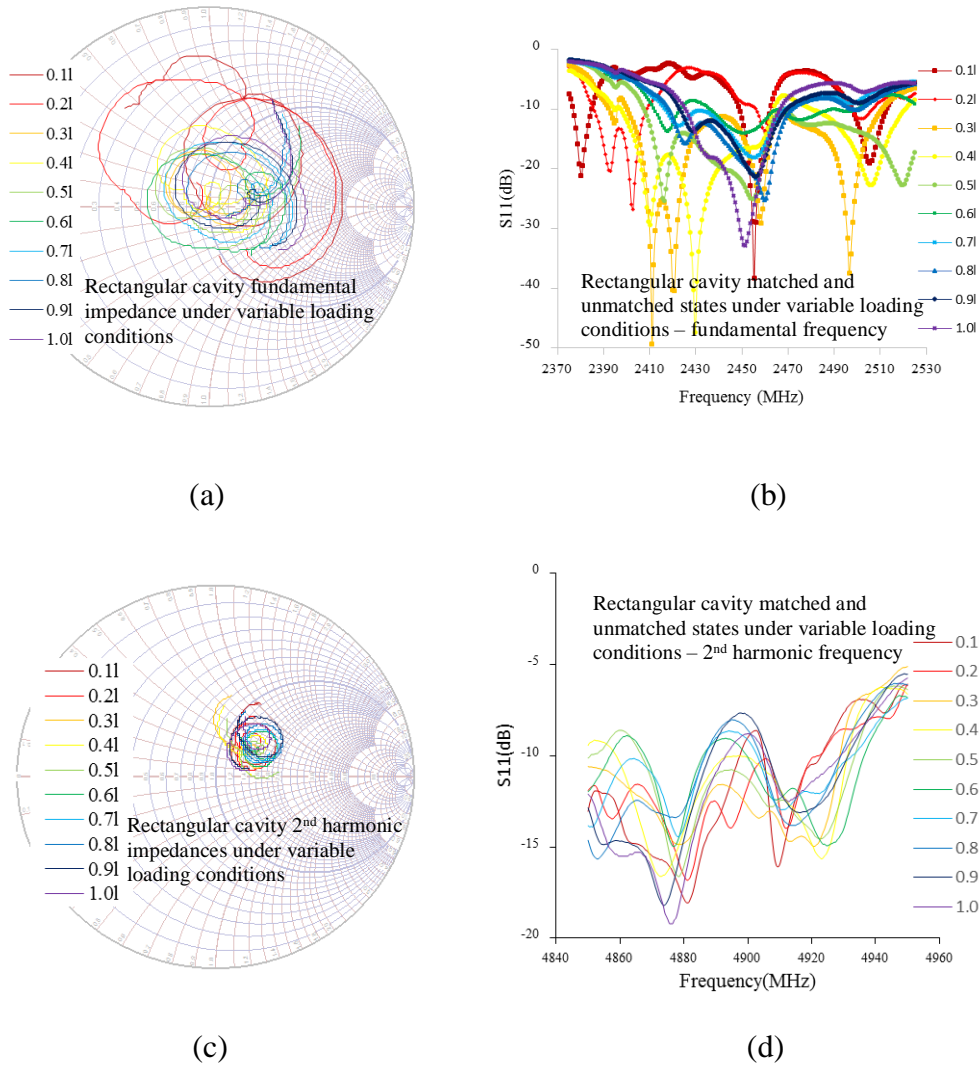
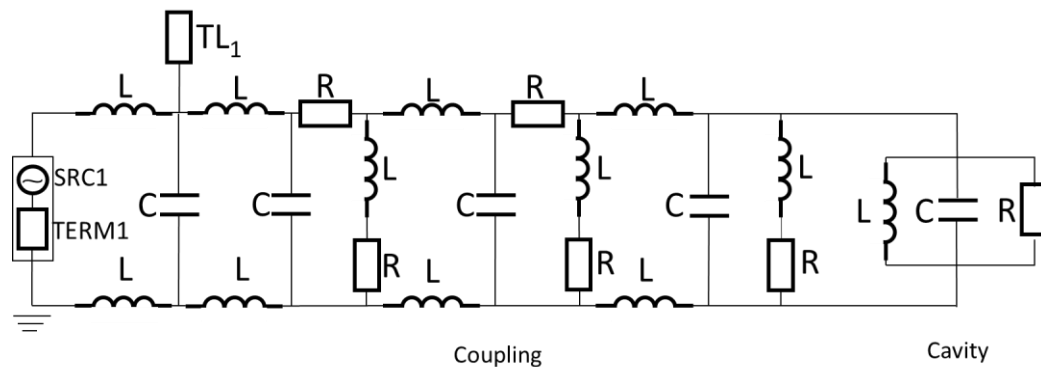


Fig. 5.19 Measured impedance data is shown in polar complex form (a,c) and magnitude log-lin format (b,d) at the fundamental (2400MHz-2500MHz) and 2nd harmonic frequencies (4800-5000MHz) under variable loading conditions (0.11-to-1.01 of water) using a single loop coupling structure shown in Fig.5.8.

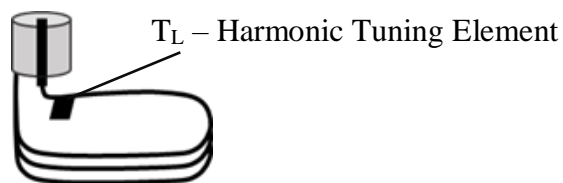
5.6.2 Load variations in a rectangular cavity

Whilst solid-state technology offers several performance benefits, practical implementation owing to variable loading conditions have posed several challenges. In order to overcome these limitations coupling structure 5, a novel wideband, harmonically tuned coupling structure (Fig.5.20), is used for transferring power from solid-state generators directly into a multi-mode resonant cavity. The coupling structures adaptability

to cavity impedance variations is characterized (through measurements) by varying the load, volumes of water from 0.1l-to-1.0l in 0.1l steps. The reflection coefficient (S_{11}) parameters, and optimally matched frequency points are recorded for each of the loading conditions. The variations in impedance due to changes in load are captured and shown in Fig.5.21a/b. Measurement data shows a much broader response (bandwidth>100MHz), compared to the single and two loop coupling structures. It can be seen that the structure enables broadband operation, and is shown to match a range of impedances presented at the fundamental frequency. This ensures that almost all of the available power is delivered into the cavity. The reflection coefficient remains below -13dB for all the loads, across the full ISM operating bandwidth of 100MHz. This is equivalent to 95 percent of the available power being delivered to the cavity at all times. This is a significant step towards isolator-less, solid-state heating applications under variable loading conditions. The close grouping of second harmonic impedances, helps in effective termination of these products as shown in figure 5.21.c/d. The termination of second order harmonics is helpful, in realizing system efficiency and preserving SSPA reliability.



(a): Lumped element model



Coupling Structure 5

(b): Physical depiction of the lumped element model

Fig. 5.20 Equivalent lumped element model of a 3 loop broadband coupling structure (with harmonic tuning) optimized for variable loading conditions.

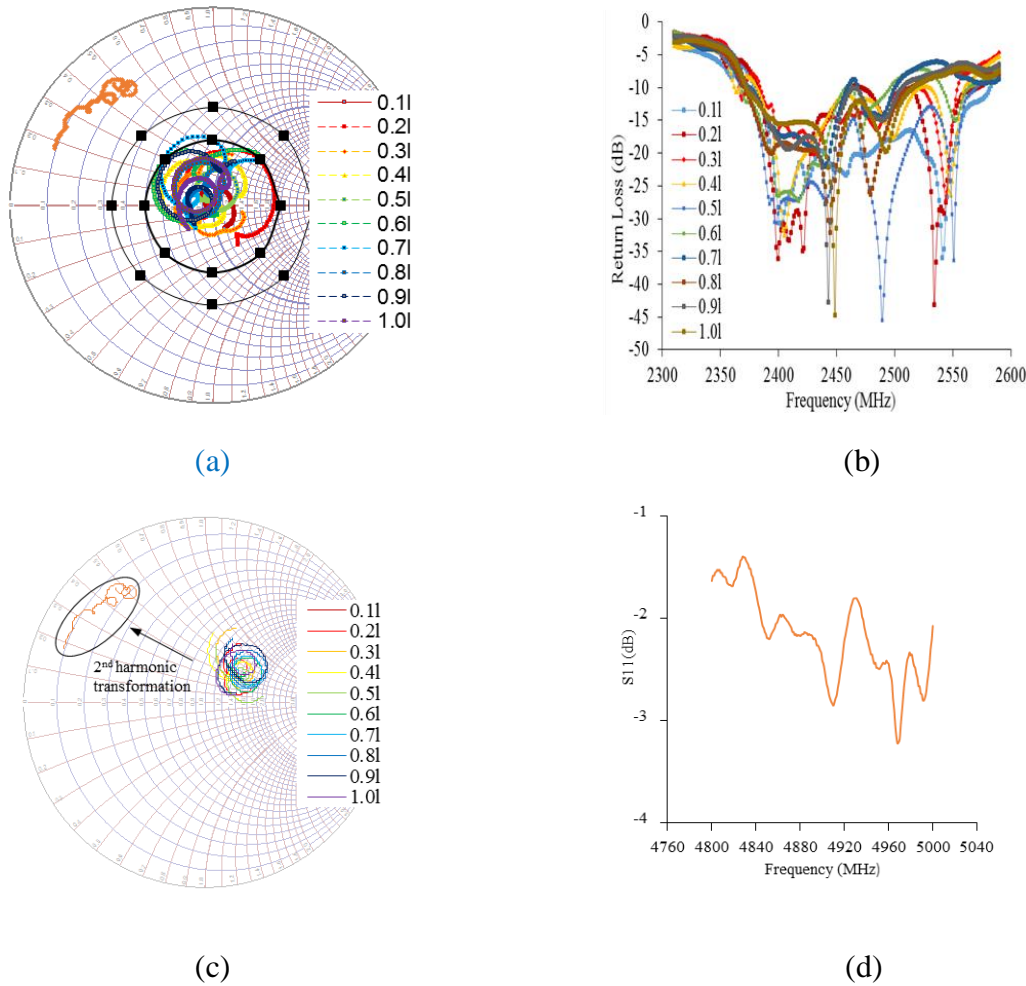


Fig. 5.21 Measured impedance data is shown in polar complex form (a,c) and magnitude log-lin format (b,d) at the fundamental (2400MHz-2500MHz) and 2nd harmonic frequencies (4800-5000MHz) under variable loading conditions (0.1l-to-1.0l of water) using a three loop coupling structure shown in Fig.5.8.

For emerging solid-state microwave cooking and heating applications, where cost and performance is paramount, this compact approach also promises to simplify system architecture by; removing the need for bulky waveguide feeds, the requirement for external power combining networks and in doing so, reducing cost without increasing cavity external volume. Improving broadband match at the fundamental frequency, and the inclusion of harmonic tuning both help improve overall system efficiency.

5.6.3 Single loop lumped element model with harmonic tuning-rectangular cavity

Ensuring high SSPA efficiency, and device ruggedness is a key requirement in solid-state heating systems. In order to maximise efficiency, the active devices within the SSPA are usually driven into compression, which leads to nonlinear behavior and the generation of harmonics. Although linearity isn't important in a heating system, efficiency and power, which are heavily influenced by the load impedances at the fundamental and harmonic frequencies, certainly are. This behavior is best appreciated by observing the voltage and current waveforms at the intrinsic plane of an active device [20]. The use of impedances to control the shape and size of these waveforms, through a powerful technique known as waveform engineering [30], [33-34] can maximise efficiency, output power and importantly, improve reliability of the devices within the SSPA by avoiding voltage breakdown and other hazardous conditions. Importantly, besides improving power delivery efficiency into the cavity (through optimally matched conditions), the SSPA efficiency can also be optimised by controlling the harmonic load impedances. Presenting a short-circuit at the second harmonic can help shape the voltage and current waveforms for maximum SSPA efficiency, whilst limiting the excursion of the voltage waveform at the device output, thus protecting it from voltage breakdown problems. The lumped element model approach was again used, to identify the necessary shunt inductive elements to achieve a reflective second harmonic impedance without impacting the fundamental – a requirement for high-efficiency PA operation. This was achieved in reality by adding a small shunt stub to the coupling structure, as shown in Fig.5.20b.

As discussed in section 5.3.2, harmonically tuned SSPAs produce zero overlapping of voltage and current waveforms which leads to a theoretical efficiency of upto 100%. This is based on accurate harmonic manipulation at the device's (transistor) generator plane and the high efficiency of SSPA's in solid state applications means, less DC power consumption, higher stability and reduced cost. However in practical applications the efficiency is rarely close to 100%, this is due to non-ideality of transistor and other components and package parasitics. Thus, special matching network are needed to minimise the intrinsic voltage/current overlaps. Whilst different kinds of harmonic

control circuits have been reported [31], here we use a transmission line (TL_1) with coupling structure 3 (Fig.5.16), to demonstrate the manipulation of 2nd harmonics.

From the measurement data shown in Fig.5.19, we note that the 2nd harmonic impedance is located near the centre of the Smith chart. Before attempting to optimize the impedance match at second harmonic frequencies, it is necessary to understand how this impedance varies with different loading conditions. This is done by changing the volume of water from 0.1l-to-1.0l in 0.1l steps. It is noticeable (Fig.5.19b), that whilst the impedance over the band (2.4-2.5 GHz) of operation fluctuates with multiple peaks and nulls for different volumes of water, the impedance at second harmonic (Fig.5.19d), remains fairly constant with its position concentrated to one area of the Smith chart. This meant that a single stub could be used to transform the 2nd harmonic impedances.

The s-parameter data of the fully optimised coupling structure, measured at room temperature for a 0.325l load (Fig.5.21), shows that the impedance at the 2nd harmonics has been successfully transformed, from a centrally located region to the outer edges of the Smith chart. The harmonic content has been easily rotated towards a short circuit at the intrinsic device plane, providing the possibility for high efficiency PA operation

5.7 The optimised coupling structure - rectangular cavity

The problems related to the the use of a single loop coupling structure (narrow band, intolerance to load variations), in multi-port and multi-mode rectangular cavities, can also be overcome by developing wider bandwidth coupling structures (coupling structure 6, Fig.5.23c). This can allow a more harmonious co-existence of multiple SSPA's under challenging operating conditions. Simulation data with a four loop coupling structure, and a transmission line stub TL_1 , shows that for a range of cavity loads (R_L , is varied from 10-100 Ω), the impedance trace encircles the 50 Ω point (Fig.5.22), with a significant increase in the operating bandwidth. Whereas the insertion loss measurements for a 0.325l water load show an operating bandwidth of

over 200MHz, where the $S_{11} < -15\text{dB}$. These insertion loss measurements can be split into four regions, with a prominent resonance at centre, where the $S_{11} < -30\text{dB}$'s. This behaviour can be exploited, in a four port system for example, where each of the SSPA's operates over a certain portion of the operating bandwidth. Under such operating conditions, it is assumed that as long as each of the SSPA's continues to operate into a matched load, it will stay isolated from the other three SSPA's and therefore will not be subjected to restrictive vswr conditions.

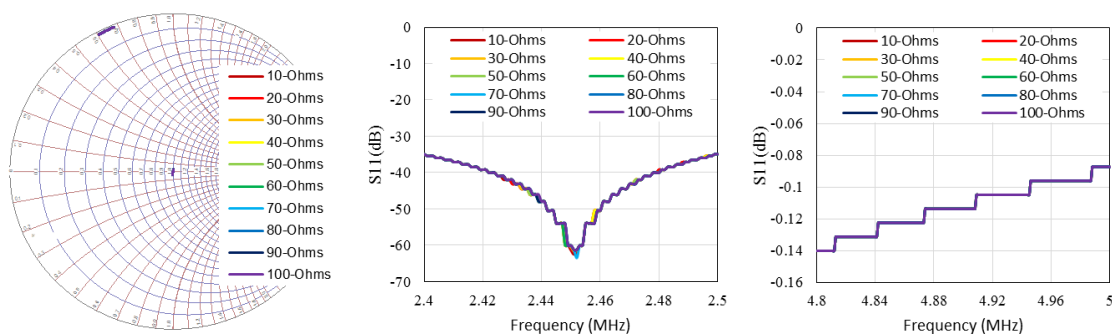


Fig.5.22 Simulated load impedance using a 3 loop coupling structure shown in polar complex and log-lin format at the fundamental) 2.4-.5) and 2nd harmonic frequencies (4.8-5.0GHz) as the load (R_L) is varied from 10Ω-to-100Ω.

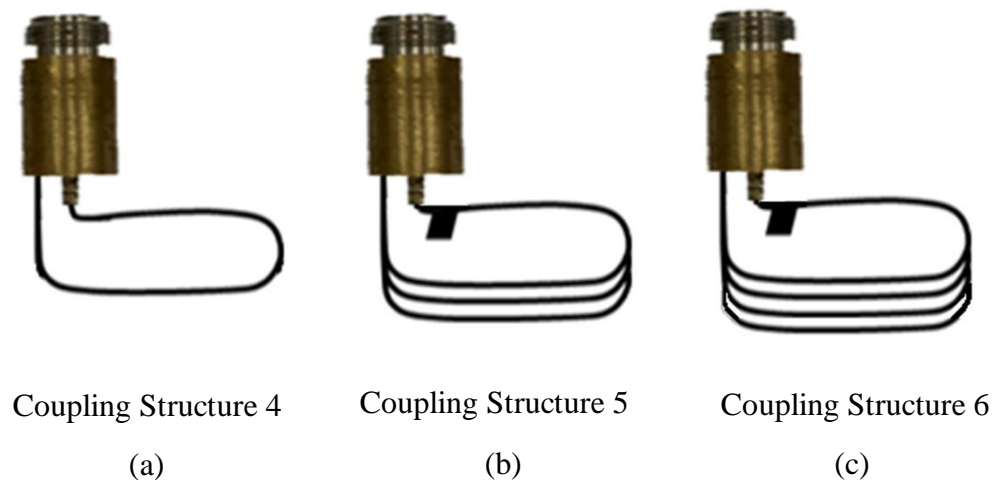


Fig.5.23 Rectangular cavity loop development for extended bandwidth

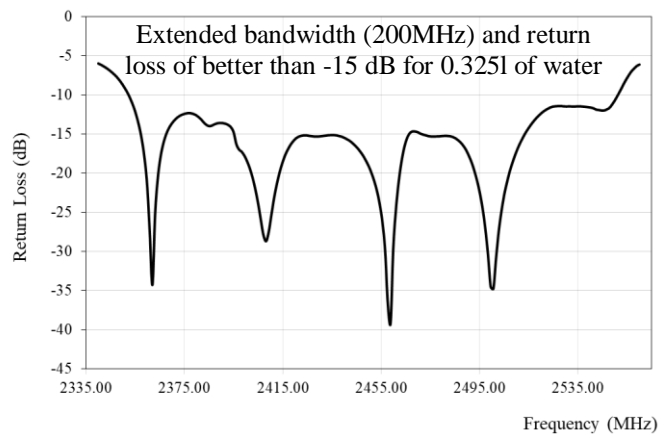


Fig. 5.24 Measured S_{11} using a four loop coupling structure for 0.325l of water, load showing 4 resonances (optimally matched frequency points) which combine to give a broader (200MHz) bandwidth with a return loss of better than -15dB

So far, it has been shown how careful design of the coupling structure, can achieve a well matched 50 Ohm load, and good control over the second harmonic impedance. One of the aims of this work, however is to simplify and minaturise SSPA matching networks to allow a direct integration of the power amplifier and coupling structure. Most current semiconductor power devices, even with the higher supply voltages (50V) that are becoming more common, possess optimum output impedances that are typically less than 5Ω . So, it is very important to note that the coupling structures proposed in this work, have the potential to accommodate this impedance transformation, and match the loaded cavity impedance to a value that is much lower than 50Ω . This is demonstrated here through modified lumped element model simulations, which show how the broadband (100 MHz) impedance locus has been transformed from 50Ω (suitable for the 50 matched PAs used for these experement) to sub 5Ω , suitable for direct attachment to a power device, as shown in Fig.5.25 to Fig.5.26.

The potential benefits of such a structure are shown in Fig.5.25. Fig. 5.25a shows a SSPA matched to 50Ω (via the PA Matching Network), with a circulator and high power load at its output as protection against high VSWR conditions, which may arise due to mismatches introduced by a changing impedance environment. The cavity matching network, then transforms the cavity impedance to 50Ω to ensure a smooth transfer of

power. Whereas Fig. 5.25b, shows a much simpler approach where the source is matched to an intermediate impedance, which is then transformed to the cavity load environment. The latter approach opens up the possibility of simpler device-to-cavity matching networks, thus eliminating the need for multiple impedance transformations.

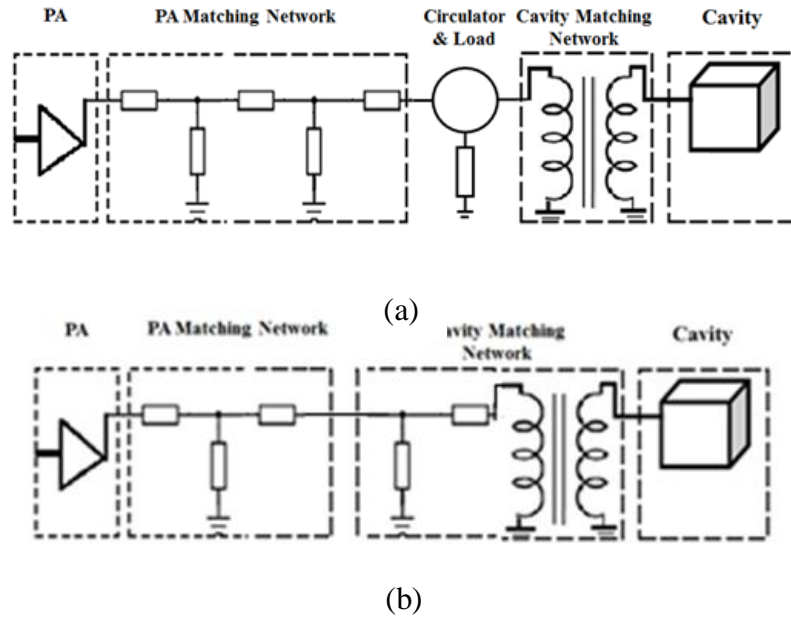


Fig.5.25. Block diagram (a) Solid state system (Conventional Approach)
(b) Solid – state system (Proposed Approach)

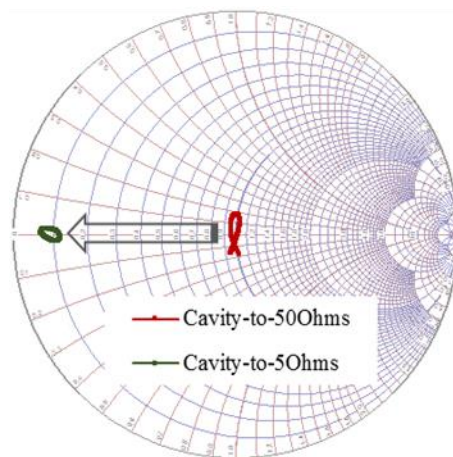


Fig. 5.26 Transforming Cavity load impedance (a): to 50Ω (b): to 5Ω using loop coupling structure lumped element model.

5.8 Summary

In this chapter, a novel approach for designing high efficiency, broadband coupling structures (for delivering RF generated power into a cavity) has been presented. These structures are compact and can easily be integrated into solid-state microwave ovens used for heating and cooking applications. Single mode cylindrical and multi-mode rectangular cavities have been adapted and are used as test vehicles to demonstrate the performance through simulations and small signal measurements. The load and frequency dependent variations in the fundamental and resonant harmonic impedance environments inside the cavity have been captured and characterized to formulate a wideband coupling structure. This structure transforms the cavity impedance to 50Ω at the SSPA output. Control over second harmonics is also demonstrated by successfully transforming the second harmonic impedance to a short circuit. This is of a great benefit as it serves to improve SSPA efficiency by reducing the overlap between voltage and current waveforms.

The broadband nature of the coupling structure lends its user an intelligent frequency hopping technique where power is delivered into the cavity at optimally matched frequency points or regions. This approach results in a highly efficient power delivery into the cavity under variable loading conditions, thereby reducing the need to tune the coupling structure to accommodate for load variations.

Measurement results clearly show the transformation of cavity load impedance to 50Ω load environment without the introduction of complicated and physically large matching networks. It has been further demonstrated that besides being broadband the coupling structure is tolerant to variable loading conditions (0.1l-to-1.0l of water). The return loss over for this range of loads remains below -13dBs across the operating bandwidth. The proposed coupling structure has the potential to match the cavity load impedances directly to the device impedances which are typically much lower than 50Ω .

This approach has the potential to simplify the matching networks and improve system performance by reducing path losses. The concept is a significant development for microwave heating and in particular isolator-less microwave heating applications where the transistor may be subjected to high VSWR conditions.

The limitations of lumped element models in visualising complex electromagnetic environments (comprising of multiple E/H field patterns) are recognized, hence a decision was made to develop physical structures and validate their performance in a real life practical application. In this design approach, a collar and N-type connector are fitted to the outer wall of a commercial rectangular cavity. The novel broad band coupling structure is fitted to the N-type connector and extended (~2cm) into the cavity such that the cavity internal volume (for load placement) is not compromised.

5.9 References

- [1]. Azeem Imtiaz, Jon Hartley, Heungi Choi and Dr Jonathan Lees “A High – Power High Efficiency Integrated Solid-State Microwave Heating Structure for Portable Diagnostic Healthcare Applications.”
- [2]. Haala J 2000 Analyse von Mikrowellenheizprozessen mittels selbstkonsistenter finiter Integrationsverfahren Dissertation Universitat Karlsruhe
- [3]. Tiefeng Shi, Kaldi Li “ High Power Solid-state Oscillator for Microwave Oven Applications”.
- [4]. Gaurav Tewari “Microwave and Radio-Frequency Heating”
- [5]. Buffler,C. 1986. “Electromagnetic radiation and microwave power” Proceeding of the workshop on microwave applications in the food and beverage industry, Ontario Hydro, Toronto.
- [6]. Marek E,Bialkowski “ Analysis of an N-port Consisting of a Radial Cavity and E-plane Coupled Rectangular Waveguides”.
- [7]. P.Korpas, A Wieckowski, M.Krysicki and M.Celuch “Application Study of New Solid-State High-Power Microwave Sources for Efficiency Improvement of Commercial Domestic Ovens” Warsaw University of Technology, Warsaw, Poland.
- [8]. Maury Microwave Corporation, “Device Characterization with Harmonic Source and Load Pull,” [Online application notes], (200 Dec 7), Available at: <http://www.maurymw.com/support/pdfs/5C-044.pdf>
- [9]. G.R.Simpson and M.Vasser, “Importance of 2nd Harmonic Tuning for Power Amplifier Design,”48th ARFTG Conference Digest, vol.30, Dec.1996,pp.1-6
- [10]. Krishamoorthy Pitchai, Sohan L Birla, David Jones “Assessment of Heating Rate and Non-uniform Heating in Domestic Microwave Oven”, Journal of Microwave Power and Electromagnetic Energy, 46(4), 2012, pp 229-240.
- [11]. Juming Tang, PHD. Professor of Food Engineering “Microwave (and RF) Heating in Food Processing Applications”. Department of Biological Systems Engineering Washington State University, Pullman WA.

- [12]. Juming Tang, PHD. Professor of Food Engineering “Microwave (and RF) Heating in Food Processing Applications”. Department of Biological Systems Engineering Washington State University, Pullman WA.
- [13]. Krishamoorthy Pitchai, Sohan L Birla, David Jones “Heating Performance Assessment of Domestic Microwave Ovens” (2010). Conference Presentations and White Papers; Biological Systems Engineering paper 55.<http://digitalcommons.unl.edu/biosysengpres.55>
- [14]. Klaus Werner, “RF Energy Systems: Realizing New Applications”. RF Energy Alliance, Beaverton, Ore.
- [15]. Michael Vollmer “Physics of the microwave oven”.
www.iop.org/journals/phised
T.Santos, L.C.Costa, M.Valente, J.Monteiro, J.Sousa “3D Electromagnetic Field Simulation in Microwave Ovens; a Tool to Control Thermal Runaway”, Excerpt from the Proceedings of the COMSOL Conference 2010 Paris.
- [16]. Y.Abed, A Davin-Regli, et al, “Efficient discrimination of Mycobacterium tuberculosis strains by 16S-23S spacer region-based random amplified polymorphic DNA analysis”*journal of Microbiology and Biotechnology*, 1995,11, 238.
- [17]. Bratislav Milovanovic, Nebojsa Doncov, Jugoslav Jokovic “Microwave Heating Cavities: Modelling and Analysis November 2004.”
- [18]. Vensa Radisic, “Novel Architecture for High-Efficiency mplifiers for Wireless Applications”*IEEE Trans.MTT*, vol.46,no.11,Nov 1998.
- [19]. J.Lin,T.Itoh,“Active integrated antennas,”*IEEE Trans.MTT.*,vol.42, pp.2186-2194,Dec.1994.
- [20]. Turcotte, Donald L.; Schubert, Gerald (2002). *Geodynamics*,2nd ed. Cambridge. ISBN .978-0-521-66624-4.
- [21]. M.Demmler,P.J.tasker,and M.Scheleceweg“A vector corrected high power on wafer measurement system with frequency range for higher harmonics up to 40GHz” in *proc. 24th EuMC.*,1994, pp.1367-3172.
- [22]. David M.Pozar,*Microwave Engineering*,3rd ed,Jhon Willey& Sons, Inc.

- [23]. G.L.Matthaei, "Tables of Chebyshev Impedance-Transformation Networks of low-pass filter form," *proc.IEEE*, vol.52, no.8, pp.939-963, Aug 1964.
- [24]. J.A.G.Malherbe, *Microwave Transmission Line Filters*, Artech House, Dedham, Mass., 1979.
- [25]. Hyoung Suk Kim "Electromagnetic Waves in Cavity design" Kyung National University, Korea.
- [26]. Dr S Cruz-Pol "Rectangular Waveguides" INEL6216 University of Puerto Rico Mayaguez.
- [27]. J.B.Hasted, Liquid water: Dielectric properties, in *Water A comprehensive treatise*, Vol 1, Ed. F. Franks (Plenum Press, New York, 1972) pp. 255-309.
- [28]. R.Buchner, J.Barthel and J.Stauber, The dielectric relaxation of water between 0° C and 35° C, *Chem. Phys. Lett.* 306 (1999) 57-63.
- [29]. http://www1.lsbu.ac.uk/water/microwave_water.html
- [30]. Y. F. Wu, P. M. Chavarkar, M. Moore, P. Parikh, B. P.Keller, and U. K. Mishra, "A 50-W AlGa_N/Ga_N HEMT amplifier", *IEDM Int. Tech. Dig.*, pp. 375-376, 2000.
- [31]. L.Shen, S.Heikman, B.Moran, R.Coffie, N.Q.Zhang, D Buttari, I.P. Smorchkova, S.Keller, S.P.Den Baars, and U. K.Mishra, "AlGa_N/Al_N/Ga_N high-power microwave HEMT", *IEEE Electronic Device Lett.*, vol. 22, No. 10, pp.457-459, 2001.
- [32]. D. M. Snider, "A theoretical analysis and experimental confirmation of the optimally loaded and overdriven RF power amplifier", *IEEE Trans. Electron Devices*, vol. ED-14, No. 12, pp. 851-857, 1967
- [33]. Yoon Kang, Ali Nassiri, "WAVEGUIDE HARMONIC DAMPER FOR KLYSTRON AMPLIFIER".Argonne National Laboratory, Argonne, Illinois 60439 USA
- [34]. R.G.Medhurst, "H.F.Resistance and Self-Capacitance of Single-Layer Solenoids," *Wireless Eng.*, vol. 24 (March 1947): 80.
- [35]. Formulas and graphs for the internal impedance per unit length of round conductors are in S. Ramo, J. R. Whinnery, and T. Van Duzer, *Fields and*

- Waves in Communication Electronics (New York: John Wiley & Sons, Inc., 1965): 286–297.
- [36]. G.S.Smith, “Radiation Efficiency of Electrically Small Multiturn Loop Antennas,” *IEEE Trans. Antennas Propagat.*, vol. AP-20 (Sep 1972): 656.
- [37]. F. W. Grover, *Inductance Calculations: Working Formulas and Tables* (New York: D. Van Nostrand Company, Inc., 1946).
- [38]. K. H. Patterson, “Down-to-Earth Army Antenna,” *Electronics* (August 1967): 111; and R. W. P. King, “The Shunt-Driven Circular Loop Antenna,” *IEEE Trans. Antennas Propagat.*, vol. AP-19 (September 1971): 692.
- [39]. G. Zhou and G. S. Smith, “An Accurate Theoretical Model for the Thin-Wire Circular Half-Loop Antenna,” *IEEE Trans. Antennas Propagat.*, vol. AP-39 (August 1991): 1167.
- [40]. https://www.nonstopsystems.com/radio/frank_radio_antenna_magloop.htm
- [41]. J.Huh, W.Lee, S.Choi, G.H.Cho, C.T.Rim, “Explicit static circuit model of coupled magnetic resonance system”, 8th International Conference on Power Electronics – ECCE Asia, 2011
- [42]. A.Robichaud, M.Boureault, D.Deslandes, “Theoretical Analysis of Resonant Wireless Power Transmission Link Composed of Electrically Small Loops”, *PIER*, vol.143, pp485-501, 2013
- [43]. C.J.Chen, T.H.Chu, C.L.Lin, Z.C.Jou, “A study of loosely coupled loops for wireless power transfer”, *IEEE Transactions on Circuits and Systems II: Express Briefs*, vol.57, no.7, pp.536-540, 2010.
- [44]. S.H.Lee, R.D.Lorenz, “A design methodology for multi-kW, large air-gap, MHz frequency, wireless power transfer system”, *Energy Conversion Congress and Exposition (ECCE)*, 2011.
- [45]. T.Imura, H.Okabe, T.Uchida, Y.Hori, “Study on open and short end helical antennas with capacitor in series of wireless power using magnetic resonant coupling”, 35th Annual Conference of IEEE Industrial Electronics, 2009
- [46]. <https://www.heecs.eu/>
- [47]. <https://sidstation.loudet.org/antenna-theory-en.xhtml>

CHAPTER 6—MEASUREMENT AND CHARACTERISATION OF SOLID STATE HEATING USING A CYLINDRICAL CAVITY

6.1 Overview

SSPA's typically operate into a constant 50Ω load environment, ensuring a smooth transition of power from generator to the load, and use a circulator and high power load at the output, to protect the transistor against impedance mismatches and fault conditions. However, the natural impedance environment presented by a resonant cavity is not only a function of the cavity dimensions, but also of the load e.g. changes in volume, temperature and material dielectric properties result in different load impedances being presented at the SSPA output. Load impedance variations from the optimal (50Ω) match, results in performance degradation and potential damage to the device.

A circulator and high power load (typically used to protect the device against high VSWR conditions), are expensive with a significant contribution to the overall cost of the SSPA. There is also a RF loss associated with these components, which reduces the available power delivered to the load within the cavity. For these reasons, it is important to consider a 'circulator-less' design, and the hostile loading environment within which the transistor must operate. The cost and the operating environment are two dominant factors, which limit the use of solid-state technology for commercial heating applications. The effects of cavity load variations on SSPA reliability, and heating efficiency are investigated and the means of maintaining a satisfactory impedance match for isolator less SSPA applications is explored and presented.

6.1.0 Single mode cylindrical cavity

For domestic microwave heating applications, a multi-mode rectangular cavity is typically used. However, for the purposes of this study, a single mode (TM_{01}) cylindrical cavity designed to operate over the 900-960 MHz frequency band is used to simplify the

analysis. This type of cavity provides a predictable load environment where the electric and magnetic field distribution are easily determined and visualized as shown in Appendix E.

The single port measurement setup (chapter 5, Fig.5.11), comprising of a RF power amplifier generating 10W-CW power, (with a circulator and high power load to protect the SSPA against high VSWR conditions), is used to characterise cavity impedance behaviour under variable loading conditions. During single port measurements the forward and reverse power measurements at port 1 (monitored using high directivity dual directional coupler and Keysight RPM2 – U2042XA USB peak & average power sensors), are used to assess the matched state; port 2 is idle, and there is no forward power at this port. The change in load temperature is also monitored through apertures in the top and side of the cavity using a pyrometer (Micro – Epsilon CT-SF22-C1) .

The cavity impedance behavior is characterised using 3D simulation software (Comsol Multi-physics, Appendix E), and through measurements under variable loading conditions (volumes of water ranging from 0.04l-to-0.12l). The water is held within a cylindrical quartz tube, which is placed at the center of the cavity, where the H field is uniform and at its strongest. Coupling structure 1, a single loop coupling structure is used to couple energy into the circulating magnetic (H) field within the cavity. Critical coupling is realized by changing the position and orientation of the loop inside the cavity. The variations in impedance, due to changes in volume and temperature of the load are captured, to gain a better understanding of the environment under which the SSPA must operate.

6.1.1 Characterisation of cylindrical cavity operating environment under variable loading conditions.

From the measurement data (Fig.5.12, chapter 5), also summarised here in table 6.1, it is recognised that the load (0.085l of water) is critically coupled at 913MHz. Away from this frequency point, the match deteriorates and the level of reflected power begins

to increase rapidly. This is demonstrated by the reflection coefficient (S_{11}) measurement data for a fixed load (Fig.5.12). The simple loop coupling structure has a limited bandwidth (9MHz), with an acceptable level of match ($S_{11} < -10\text{dB}$). The VSWR measurement data (Fig.5.15), has a value of 1 at the critically coupled frequency (913MHz), indicating a smooth transfer of power into the cavity. At this frequency of operation, the device operates safely. However away from this point the value of VSWR rises (with an increasing reflection coefficient), which leads to a drop in power delivered to the cavity. In the absence of a circulator, and high power load the ensuing high reflected power states can damage the SSPA.

The forward/reflected power and power delivery efficiency with a single loop coupling structure (table 6.1), show that at the optimally matched frequency point (913 MHz), a 10W (CW) forward power results in a reflected power of 0.01W. This increases to 0.1W over the 912-915MHz, and 1W at the band edges 909-918MHz. The corresponds to power delivery efficiencies of 99.99, 99 and 90 percent respectively. Outside of this bandwidth, the level of reflected power becomes unacceptable and less of the generated power is available to heat the load. Under these operating conditions device reliability (in the absence of a circulator) will be compromised.

Table.6.1 Single loop coupling measurements

Frequency	P_{FORWARD}	P_{REFLECT}	Power Delivery Efficiency (%)
913MHZ	10	0.01	99.99
912-915MHz	10	0.10	99.00
909, 918MHz	10	1.00	90.00

The variations in impedance due to changes in load (volume of water, 0.04l-to-0.12l), are investigated and displayed in polar complex format on a Smith chart (Fig.5.13, chapter 5). The results showed that an increase in the volume of water moved the impedance to the right of 50Ω (*high Z*), and a decrease in the volume moved the impedance towards the left (*low Z*). These changes in volume affect both the real and

imaginary components of the impedance.

Reflection coefficient measurements (Fig.5.13, chapter 5), also show that changes in the volume of water not only deteriorate the matched state, but also shift it in frequency e.g. an increase in the volume of water moved the frequency at which load is optimally matched to a lower value, whilst a decrease in the volume of water moved the frequency at which the load is optimally matched to a higher value. Whilst this information can be used to develop an intelligent methodology (algorithm) to search for frequency points, where the load is critically coupled, the inability to locate and change the frequency of operation (with load variations) means that the SSPA is operating into a load which will expose it to high VSWR conditions (Fig.6.1). This is undesirable and has severe implications on cavity efficiency and device reliability.

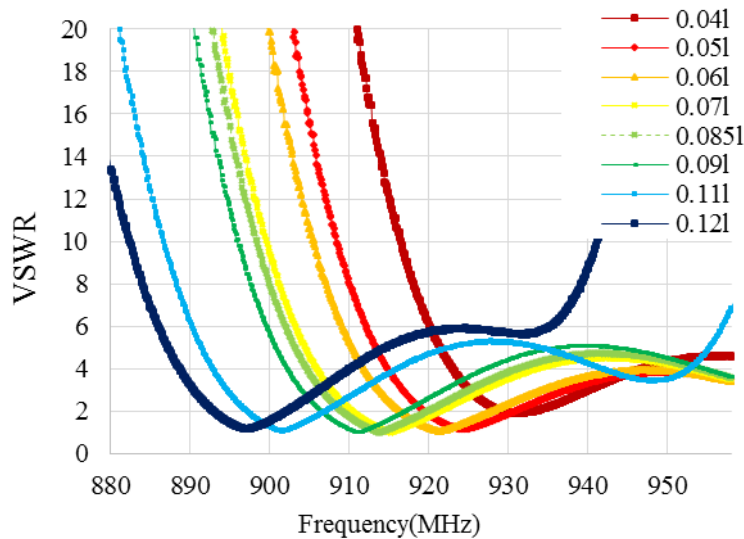


Fig. 6.1:- VSWR measurements 0.04-0.12l of water load.

6.1.2 Characterisation of cylindrical cavity operating environment due to a changes in load temperature.

The dielectric properties of materials vary with temperature [7]. This affects the level of interaction between the material and the electromagnetic energy. In the case of non-ionizing radiation, the electric permittivity (ϵ), describes the interaction of the electromagnetic waves with the material. Permittivity of a material is its ability to absorb, transmit and reflect electromagnetic energy. It is a complex quantity, comprising of dielectric constant (ϵ'), and dielectric loss factor (ϵ''). The real component ϵ' is related to the capacitance of the substance and its ability to store energy, whilst the imaginary component is related to the absorption mechanisms of energy dissipation [14].

Impedance and reflection coefficient measurements show that the load is also sensitive to temperature variations. A rise in temperature increases ion mobility due to dissociation of molecules leading to increased conductivity. At higher temperatures water absorbs and stores less of the available energy. This suggests that both dielectric constant (ϵ'), and dielectric loss factor (ϵ'') reduce with increasing temperature. The resulting impedance variations with temperature show that an increase in temperature (22°C-to-52°C), has resulted in a deterioration of the matched state (Fig.6.2). Further the optimally matched state has moved to a new value located higher in frequency (from 913MHz to 920MHz) as shown Fig. 6.3, whilst the VSWR has deteriorated from 1 (at 913MHz) to 5 (at 920MHz) as shown in Fig. 6.4. This insight can be used to develop heating profiles, where the frequency of operation is adapted to accommodate impedance variations with increasing temperatures.

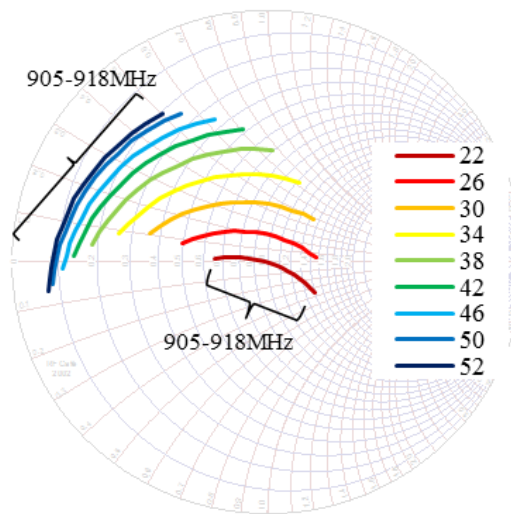


Fig. 6.2:- Impedance variations due to changes in temperature (0.085l of water load).

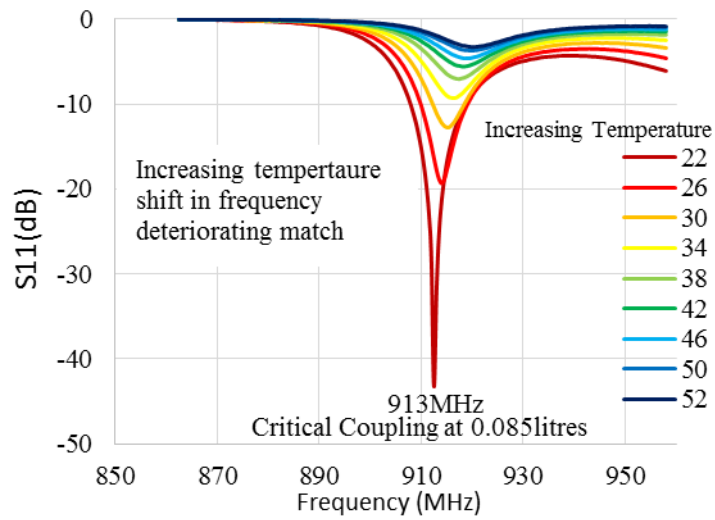


Fig. 6.3:- Reflection coefficient measurements with temperature variations (°C) 0.085 l of water load.

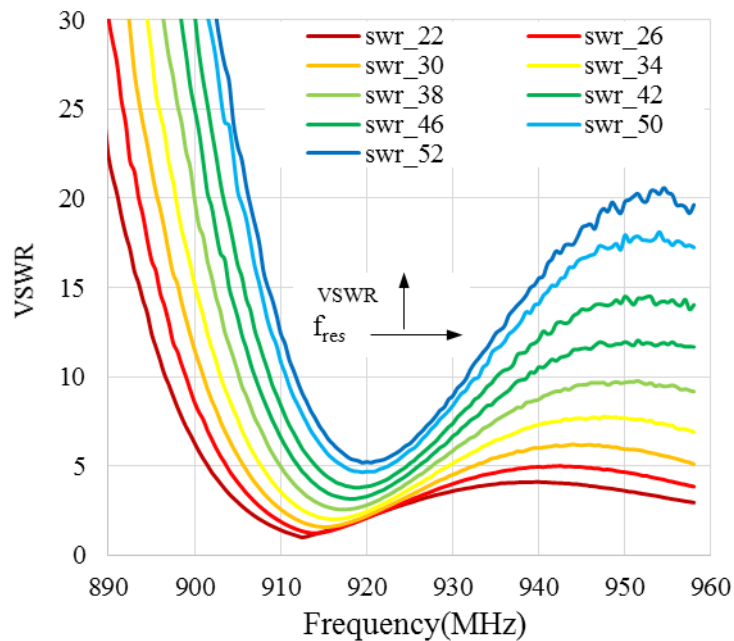


Fig. 6.4:- VSWR measurements with temperature variations for a fixed 0.085l of water load.

6.1.3 Limitations of using a single loop coupling structure

When using a single, static coupling loop, the operational bandwidth is limited (9MHz). Changes in load and even relatively small (30°C) rises in load temperature can cause significant mismatch and high-reflective states to exist, where the VSWR over a 30°C temperature range, has deteriorated from 1:1 at 22°C (913 MHz) to 5:1 at 52°C (920 MHz). A 30°C temperature rise requires a realignment of the coupling structure (through electromechanical or other means), to locate the new operating frequency beyond the 9MHz bandwidth, which can be problematic. Ensuring safe and reliable SSPA operation thus requires cavity impedance characterisation under variable loading conditions and with temperature variation.

6.1.4 Optimising the loop coupling structure for variable loading conditions.

It has been identified, that the transfer of SSPA power into a load within the single-mode resonant cavity (under variable loading conditions), requires some form of adaptive coupling. With this in view, an alternative approach was presented in chapter 5, which involved modifying coupling structure 1, the single loop launch for extended bandwidth operation, without the need for mechanical adjustment. The reflection coefficient and the impedance traces (Fig.5.15), show comparisons between coupling structure 1 (single loop) and coupling structure 3, which has a much wider bandwidth. The impedance trace measured using coupling structure 3, encircled the 50Ω point which resulted in a return loss of better than -15 dB over a 70MHz operational bandwidth. The subsequent VSWR data (Fig.5.15c), showed that with this approach, an isolator less SSPA can potentially continue to operate into a matched load over its operational bandwidth, without physical adjustment of the loop coupling structure. This is in contrast to the high-Q, single loop structure's limited operational bandwidth. The proposed technique is tolerant to load and temperature variations, which is important when considering low-cost microwave heating applications.

With this proposed concept the power delivery efficiency remains high (a return loss of -15dB is equivalent to a power delivery efficiency of 97 percent), over a 70MHz operating bandwidth (Fig.6.6). Whereas with a single loop coupling structure, the delivery efficiency was high at a single frequency point before tapering off to below 50% over a very narrow (10MHz) bandwidth (Fig.6.5). This has been demonstrated for three different loads (0.04l, 0.08l and 0.12l of water), with a static single and three loop coupling structures. Whilst the benefits of greater operational bandwidth may not appear significant for a cylindrical cavity due to single mode excitation, the concept has a huge potential for multi-mode cavity operation, where many modes are scattered over a larger bandwidth. The approach can be adapted to achieve good heating efficiencies for a range of loads.

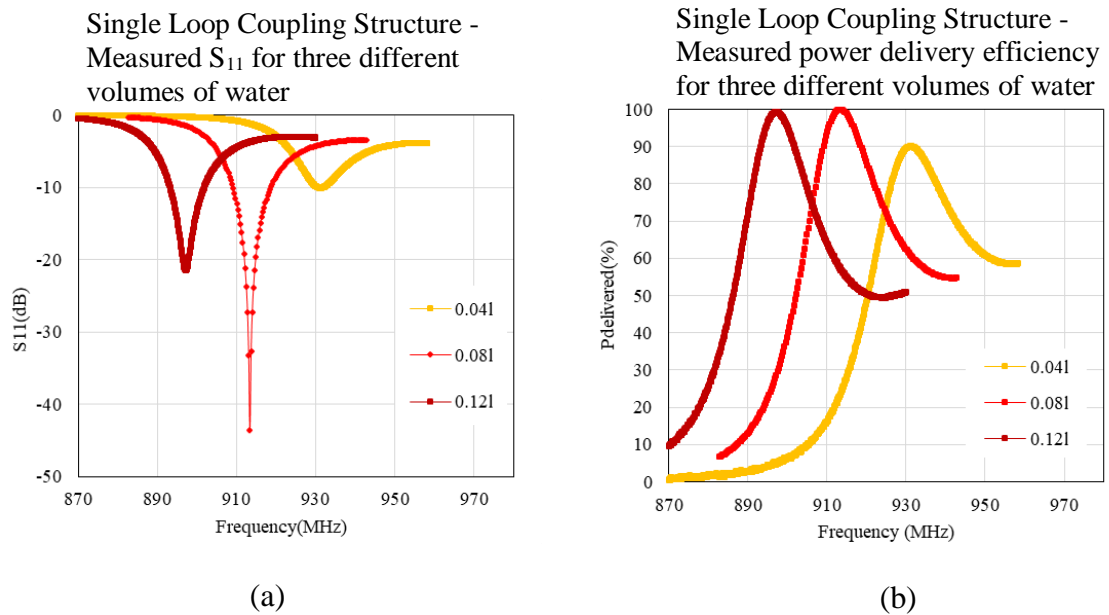


Fig. 6.5 (a) S_{11} and (b) delivery efficiency using a single loop for three different loads(0.04l, 0.08l and 0.12l of water load).

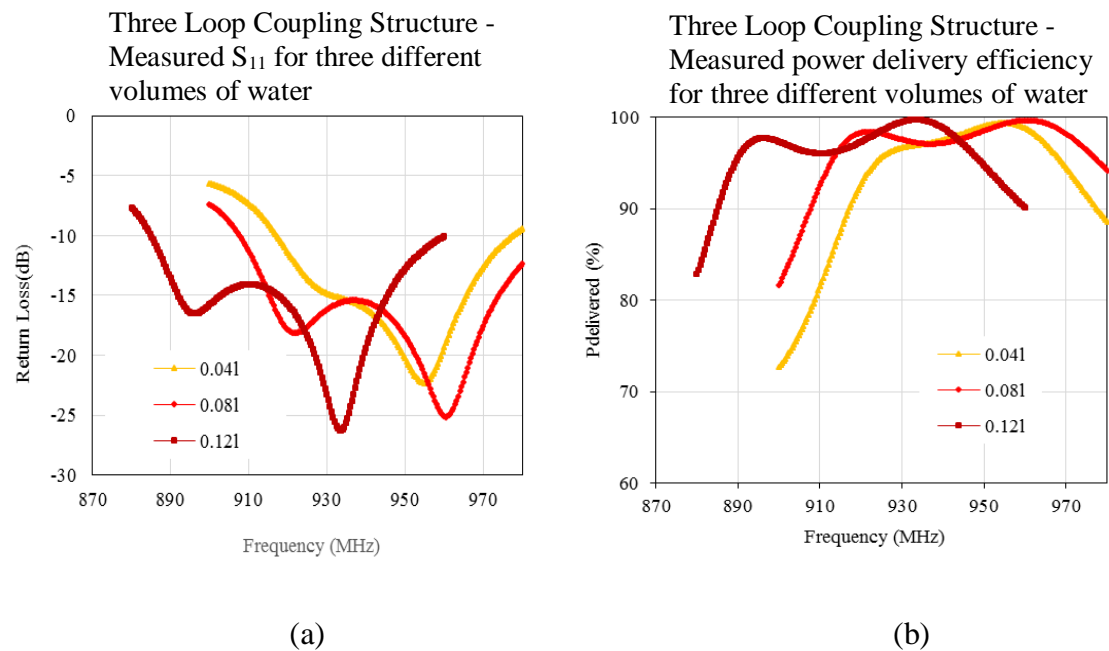


Fig. 6.6 (a) S_{11} and (b) delivery efficiency using three loop coupling structure for three different loads (0.04l, 0.08l and 0.12l of water load).

In the single mode cavity used, impedance variations (due to temperature rise) can also be accommodated by setting the initial optimally matched frequency point at the higher end of the operational bandwidth (909MHz). As the temperature of the load increases, the matched state shifts to a higher frequency which is within the operational bandwidth of coupling structure 3. This ensures that the SSPA continues to operate into a matched load, thereby maintaining high delivery efficiencies without physical re-alignment of the coupling structure. The measurement data (Fig.6.7), shows that an increase in temperature (22°-to-52°C) moves the matched states higher in frequency. When using coupling structure 3, the matched state whilst moving higher in frequency still sits within the SSPA operating bandwidth, which means that the power delivery efficiency can be maintained by changing the SSPA operating frequency. Whereas, with coupling structure 1 (a single loop coupling structure), the matched state (S_{11}) has declined significantly more and a change in SSPA operating frequency alone is not sufficient to retain the power delivery efficiency

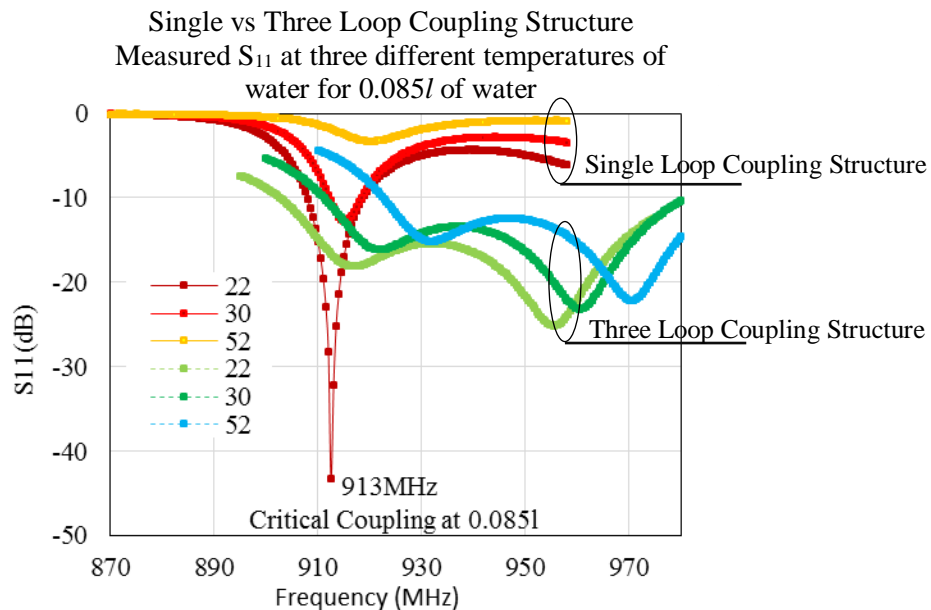


Fig. 6.7: S_{11} (single mode vs proposed) with temperature (22°C, 30°C and 52°C) - 0.085l of water load

6.2 Two port system overview

The power available from a single SSPA ‘module’ is generally limited by the maximum power rating of the transistors used. This means that in most microwave heating applications, the power from a single module will be insufficient. In such instances, power combining becomes a key requirement, and at high power levels (> 250 Watts, CW), the task becomes difficult to accomplish in a cost effective way at the printed circuit board level. The use of the microwave cavity itself for direct power combining offers a possible solution, but it requires the use of multiple ports and feed structures.

The cavity’s operational impedance environment is a function of loading conditions, where each of the power amplifier modules will experience potentially high or even very high voltage standing wave ratio’s (VSWR), and must operate reliably and without performance degradation. Monitoring, capturing, managing and manipulating the impedance environment at each of the excitation ports is a key requirement in ensuring safe, reliable and efficient operation.

For solid-state solutions to be viable in mass-market applications, there is a need to reduce the SSPA module cost to the point, where the technology is competitive in comparison to magnetron-based systems. Removing the need for the traditional circulator and a high power load will help achieve this goal. Whilst this has been addressed for a single port cavity, high VSWR and device reliability remain a concern for two port systems. The impact on SSPA reliability in a 2-port systems is considered and presented.

6.2.1 Two port cylindrical cavity

A two port cylindrical cavity (TM₀₁ mode), is fabricated such that the two coupled ports (port-1 and port-2) are located opposite each other. Each port is fitted with a collar which has been designed to accept a modified N-type barrel connector, and a loop coupling structure. The loop coupling structure is used to characterise two port cavity

impedance behaviour. The cavity is loaded through a cylindrical quartz tube (containing 0.04l of water), which is placed at the center of the cavity where the E/H field is strongest.

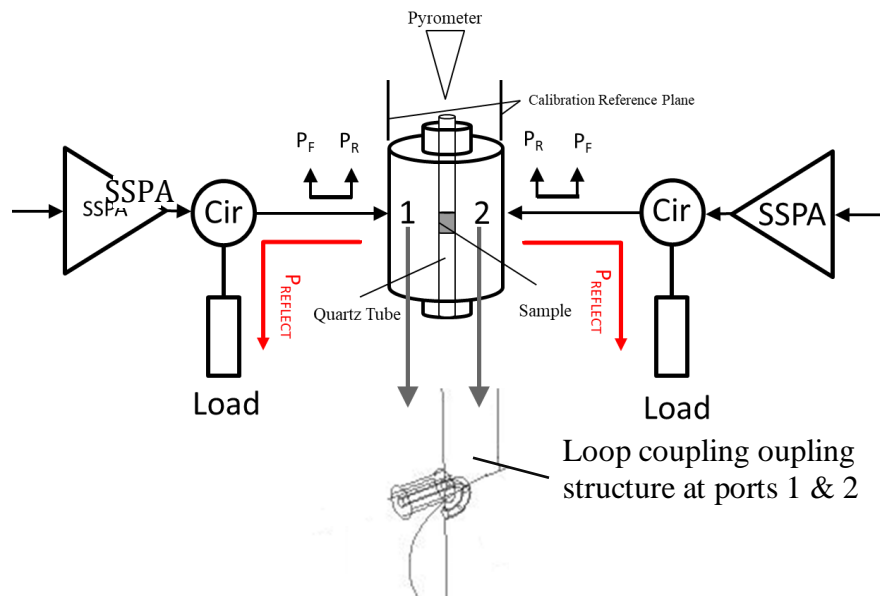
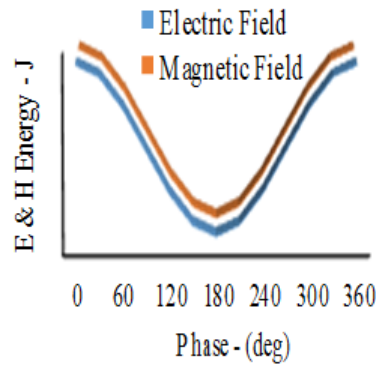


Fig 6.8 Measurement set-up used for monitoring the forward, reflected power and temperature rises inside a 2 port cylindrical cavity.

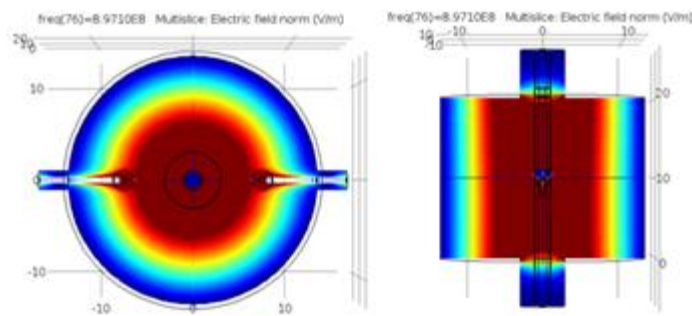
6.2.2 Single loop coupling structure limitations in a 2 port network

With the load placed at the centre of the cavity, the coupling loop at each of the ports is tuned (orientation relative to the circulating H-field), to ensure that the SSPA's are operating into a matched (50Ω) load. Once the two ports are identically matched, RF power from two separate SSPA's is injected into the cavity simultaneously. The forward and reflected power at each of the ports was measured using dedicated directional couplers under different loading conditions. The power delivery into the cavity was controlled in terms of the phase and amplitude of the input signal, and also by ensuring that both signal paths are of equal length. The measurement setup (Fig.6.8) included a two port cylindrical cavity, two SSPA's and dual directional couplers to monitor the forward and reflected power at each of the ports. The forward and reverse power measurements in particular capture the level of mismatch at each of the ports. The rise in temperature is measured

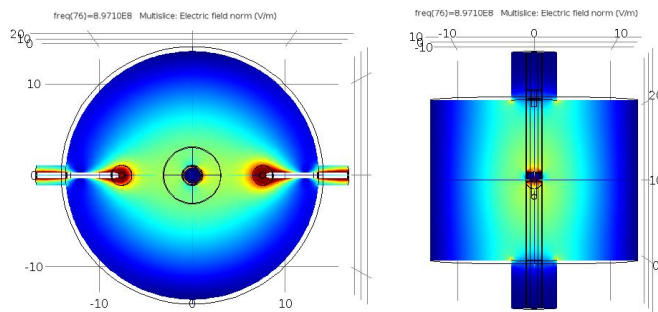
using a pyrometer from the top as shown in Fig.6.8. These basic measurement techniques are used to characterise cavity impedance behavior and the possible impact this has on SSPA performance and reliability.



(a)



(b)



(c)

Fig. 6.9: Two port cylindrical cavity (a) E & H Field strength as a function of phase (b) Top and side views of field strength with phase at 0 degrees (c) Top and side views of field strength with phase at 180 degrees.

The introduction of a second, active, phase coherent source at port 2 is seen to influence the impedance seen by the first source at port 1. The importance of having a coherent phase is highlighted through strong (0 degrees phase offset) and weak field strengths (180 degrees phase offset), shown in Fig. 6.9. In order to ensure that both sources are matched to the cavity load, each of the coupling structures needed to be physically adjusted, to account for the presence of the other. Whilst under optimum loading conditions, power from both SSPA's is absorbed by the load resulting in little or no reflected power, simple cavity equivalent model simulations (chapter 4) have shown that under certain, ideal and worst case loading and phase alignment conditions, a power level equal to the total (port 1 + port 2) can appear at port 1 or port 2. These hostile operating conditions are avoided through detection and selection of frequency points where the load is optimally matched.

6.2.3 Measurements using single loop coupling structure in a two port cylindrical cavity

With a single loop, single port coupling structure the ratio of forward to reflected power was small over a narrow range of frequencies as demonstrated by the measurement data in chapter 5 (Fig.5.15), which is also summarised in table 6.1. However the presence of a second port has moved this optimally matched frequency point from 913MHz to 944 MHz, and away from this frequency the match deteriorates (Fig.6.10/11). The level of reflected power is low at 944MHz, at this frequency both the SSPA's are optimally matched to the load as evidenced by a reflected power of 0.1W when the forward power is 5W. This means that 98 percent of the SSPA power is delivered into to the cavity. At these selected frequency points the potential for device breakdown within the SSPA is negligible. It is also shown (Fig.6.12) that in the presence of low power levels at port 1, the reflected power at port 2 remains unchanged. This implies that under certain operating conditions where the power from a single SSPA is sufficient to heat the load, the second SSPA can be switched off or left to stand in idle mode to maximise heating efficiency.

Table 6.2 –Theoretical values and relationship between Return Loss, VSWR, Transmission loss, P-Transmit and P-Reflect in tabular form

Return Loss (dB)	VSWR	Transmission Loss (dB)	P _{del} (%)	P _{ref} (%)
-	1.00	0.00	100.00	0.00
-19.00	1.25	0.05	98.80	2.20
-9.50	2.00	0.51	88.90	11.10
-6.00	3.00	1.25	75.00	25.00
-2.90	6.00	3.10	49.00	51.00

From the reflected power and VSWR data (summarized in table 6.2), it can be seen that the VSWR (Fig.6.10 to 6.11) varies from 1.4:1 at the optimally matched frequency points to 6:1 at the band edges where 50 percent of the generated power is reflected back. The results show that when both SSPA's are delivering an output power level of 37dBm under optimally matched loading conditions, the degree of reflected power, at both the ports is similar (22dBm). However as the power at port 2 is scaled down from 37dBm to 30dBm, the reflected power at this port also begins to reduce (Fig.6.12). There is also a small reduction in the reflected power at port 1. This indicates that the total amount of reflected power at port 1, is largely due to the matching condition at this port with a small contribution from the signal at port 2. This demonstrates the need for careful positioning of the coupling structures into the cavity, so that the SSPA's are optimally matched to the load. However, full SSPA bandwidth (70MHz) cannot be fully utilized, as deviations from the optimally matched frequency points results in a mismatch. This leaves the SSPA vulnerable to high VSWR conditions and potential breakdown.

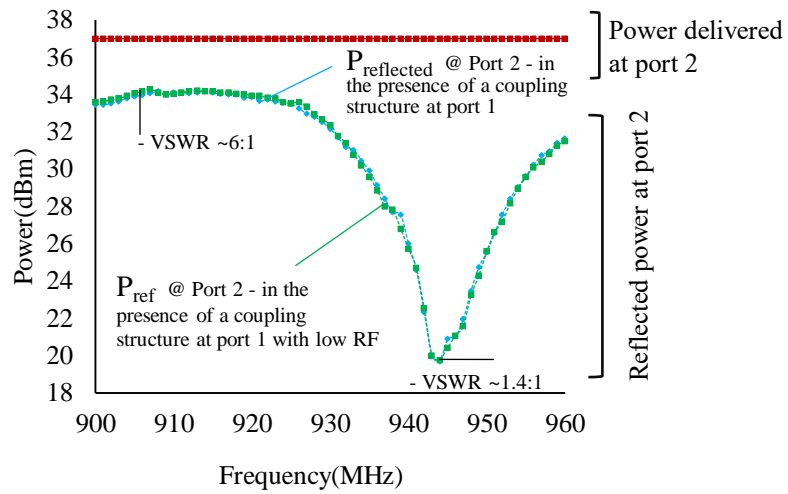


Fig. 6.10 Shows incident power measurements at port 2 - (i) in the presence of a coupling structure at port 1 (ii) In the presence of coupling structure at port 1 with low RF power.

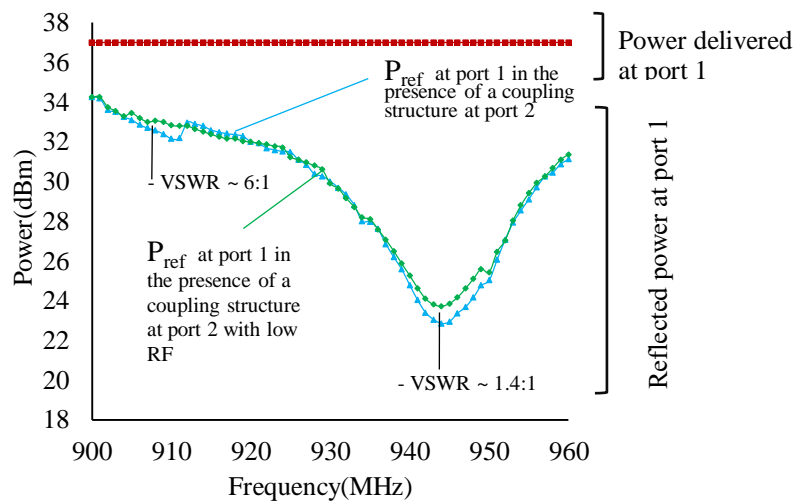


Fig 6.11 Shows P_{inc} measurements at port 1 - (i) in the presence of a coupling structure at port 2 (ii) In the presence of coupling structure at port 2 with low RF power.

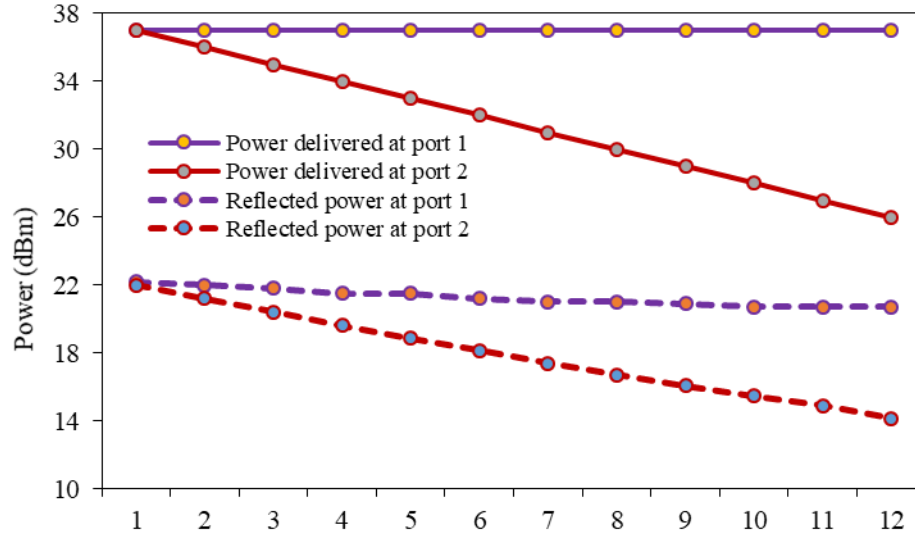


Fig 6.12 Shows P_{del} and P_{ref} measurements at port 1 & port 2 where the forward power at port 1 is set to 37dBm and the forward power at port 2 is varied between 37 and 26 dBm in 1 dB steps.

6.2.4 Measurements using optimized loop coupling structure

As stated in chapter 5, power delivery into a cavity resonator achieved via a simple loop structure, restricts efficient power delivery to a single frequency or over a very small range of frequencies (Fig.5.15). In order to utilize full operational bandwidth of the SSPA, the coupling structures needs to be able to deliver power at any of the frequency points over the SSPA operating bandwidth. The results (Fig.5.15 and Appendix E), also show that by carefully manipulating the loop coupling structure, introduced in chapter 5 it is possible to constrain the impedance match to a VSWR of 2.3:1 over the SSPA operating bandwidth. Coupling structure 3, “the novel three loop coupling structure” is used to capture and transform cavity load impedance to 50Ω . This ensures that the SSPA is always operating into a matched load, just as it did in a single port system. Measurement data (Fig. 6.13), shows the increase in temperature (single port vs two port) for a 0.0851 water load at two different power levels. The measured data shows higher temperature values for a two port network, this is less obvious at lower power levels but the difference is significantly greater at higher power levels. This inequality is explained by the

simulated H-field patterns, which show the energy be concentrated at the centre of the cavity (Fig.6.9) in a two port system, and more dispersive in a single port system (Appendix E). Besides improving heating efficiency, this methodology eliminates unmatched states which can lead to reflected travelling waves and the associated voltage and current maxima.

With a single loop, the optimally matched conditions can start to drift with load variations, just as they did with a single port. This required a physical realignment of the loop coupling structure and a change in SSPA operating frequency.. With the proposed three loop coupling structure, impedance match is maintained (across the full SSPA operating bandwidth), at both ports ($S_{11} < -10\text{dB}$'s) as shown in (Fig.5.15). This ensures that a change in the SSPA's operating frequency does not result in operating conditions, where the transmitted power is reflected. The advantages of a broadband coupling loop, where the SSPA continues to operate into a matched load, and most importantly is not subjected to high VSWR conditions can not be overstated

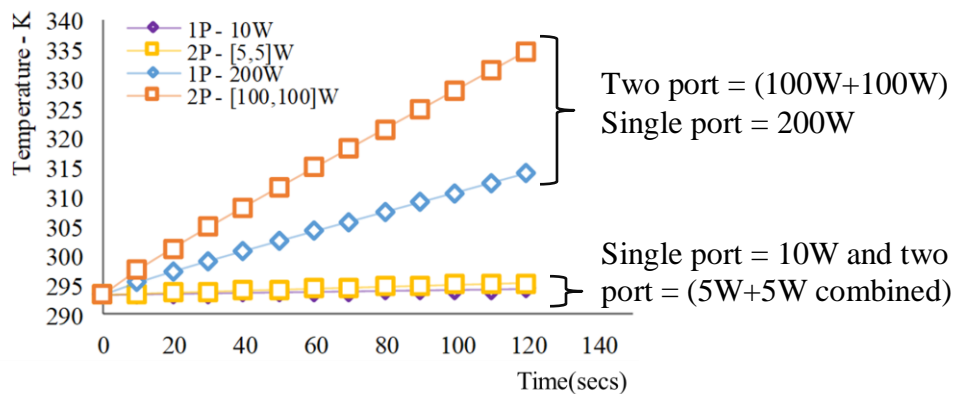


Fig 6.13 Measured temperature rise in 0.085l water load using single and two port cavity delivering equal amounts of power into the cavity at an optimally matched frequency point (944MHz).

6.3 Summary

The challenge of using single and multiple SSPAs for microwave heating applications where the loading conditions are non-constant have been identified. This process involved the use of a 2 port cylindrical cavity. The cylindrical cavity's impedance behaviour has been measured and characterised under variable loading conditions (different volumes of water) and over temperature. It is demonstrated that such variations in load present different impedances at the SSPA output which lead to high reflective states, typically requiring a re-alignment (re-positioning) of the single loop coupling structure.

An alternative three loop coupling structure is used to demonstrate that changes in both single and two port cavity impedance (due to load variations) can be contained to a VSWR of 2.32:1 over a wider (70MHz) bandwidth. This means that the SSPA operating bandwidth can be taken advantage of to ensure very high (>97%) power delivery efficiencies. This was found for the reflect coefficient measurements of better than -15dB across the operational bandwidth. Using this technique and methodology, it has been possible to use the cavity as a power combiner, where power from two separate SSPA's is used to heat 0.085l water load, which was placed in a quartz tube and positioned at the centre of the cavity. Measurements showed an improved temperature profile for a two port cavity where power is delivered into the cavity from two separate ports located opposite each other.

The ability to constrain a range of load impedances to within a vswr of 2:1 ensures that the SSPA reliability is not compromised, and advances the possibility of reducing cost by removing the circulator and high power load. The measurement results for the two-port system (with the proposed broadband coupling structure) show that it is possible to sweep the SSPA operating frequency (902–970 MHz) to locate the optimally matched condition ($S_{11} > 20\text{dB}$) at each of the ports. This ensures power delivery efficiency (into the cavity) of greater than 98 percent.

6.4 References

- [1] Haala J 2000 Analyse von Mikrowellenheizprozessen mittels selbstkonsistenter finiter Integrationsverfahren Dissertation Universitat Karlsruhe
- [2] V.Rakesh, A.K. Datta, M.H.G AMIN and L.D. Hall, "Heating Uniformity and Rates in a Domestic Microwave Combination Oven" Journal of Food Process Engineering, Volume 32, Issue 3, 8 Sept 2009.
- [3] M.E.C.Oliveira, A.S.Franca "Microwave heating of food stuffs" Journal of Food Engineering 53 (2002) 347-359
- [4] H.W. Yang, S.Gunasekaran, "Comparison of temperature distribution in model food cylinders based on Maxwell's equations and Lambert's law during pulsed microwave heating" Journal of Food Engineering 64 (2004) 445- 453
- [5] P.Korpas, A.Wieckowski, M.Krysicki and M.Celuch "Application Study of New Solid-State High-Power Microwave Sources for Efficiency Improvements of Commercial Domestic Ovens," IMPI'S 47 Microwave Power Symposium, Providence, RI, USA, June 2013.
- [6] <https://www.electronics-notes.com/waveguide-impedance-characteristic-matching-iris.php>
- [7]. Ryyna`nen, S. (1995). The electromagnetic properties of food materials: A review of the basic principles. Journal of Food Engineering, 26, 409–429.
- [8] G.Formicone,, F.Boueri, J.Burger, W.Cheng, Y.Kim and J.Titizian, "Analysis of Bias Effects on SWR Ruggedness in RF LDMOS for Aionics Applications," in Microwave Integrated Circuit Conference, 2008.EuMIC 2008.European,2008,pp28-31.
- [9] Kenneth J Russell, "Microwave Power Combining Techniques" IEEE Transactions on Microwave Theory and Techniques", Vol. MTT-27, No.5, May 1979.
- [10] Michal Soltysiak, Malgorzata Celuch, Ulrich Erle "Measured and simulated frequency spectra of the household microwave oven" Microwave Symposium Digest (MTT), 2011 IEEE MTT-S International

- [11] Birla, Sohan; Pitachi, Krishnamoorthy; Subbiah, Jeyamkondan; and Jones, David D., "Effect of Magnetron Frequency on Heating Pattern in Domestic Oven" (2010). Conference Presentations and White Papers: Biological Systems Engineering. Paper 54.
- [12] Nicola, "Energy Thoughts and Surprises", "Do microwave ovens save energy?"
- [13] Tom Murphy "Burning Desire for Efficiency"
- [14] Shyam N. Jha "Nondestructive Evaluation of Food Quality: Theory and Practice"

CHAPTER 7-MEASUREMENT AND CHARACTERISATION OF SOLID STATE HEATING USING A LARGE RECTANGULAR CAVITY

7.1 Overview

Multi-mode (rectangular) cavities, driven by high-power solid-state power amplifiers, are emerging as a serious alternative to the traditional magnetron-based systems in microwave heating applications; examples include polymer curing, large scale component curing for aerospace and automotive, as well as domestic and industrial microwave cooking. As a consequence there is a significant interest and research activity targeted at microwave cooking [2-5]. As already mentioned in chapter 1, this is due to potential revenue from large-volume sales, the need for energy efficiency to meet future regulatory requirements [1], performance benefits such as adjustable power to control the heating rate and finally the ability to change frequency, and relative phase for selective mode excitation and field pattern control. Whilst single mode cylindrical cavities (discussed in chapter 6), provide a predictable load environment, where the electric and magnetic field distribution are easily determined and visualized (Appendix E), the large rectangular cavities have a more complex impedance behaviour (field pattern comprising of multiple modes), which changes with load (size and ingredients) and temperature (Appendix C & D). In order to heat the loads evenly in these cavities, it is important to both identify (the frequency of these resonant modes), and then excite these modes through careful selection of SSPA operating frequency. A coupling structure (discussed and developed in chapter 5), identified as a key element in solid state heating apparatus is used to demonstrate the potential benefits of solid state heating.

The system presented in this chapter comprises a domestic microwave oven cavity resonator closely integrated with a solid-state power amplifier, via a novel broad band coupling structure (discussed previously in chapter 5). Experimental work considers the adaptability of the structure, e.g whether an acceptable impedance match ($S_{11} < -10\text{dB}$) can be obtained and retained under very challenging operating conditions, where the

natural impedance environment of the cavity varies with changes in load (represented by different volumes of water), load placement and with temperature to successfully heat the load evenly.

7.1.1 Load variation in large rectangular cavities:

Whilst the narrowing power-gap between the magnetron and solid-state devices is making solid-state microwave heating more feasible, delivering maximum power under variable loading conditions presents challenges for both magnetron and SSPA based approaches alike. The domestic microwave oven's load environment is non-constant, dependent on food-type, food-size, viscosity, placement and temperature, all directly affecting the load impedance. One way of accommodating load variation, improving heat distribution and enhancing heating efficiency is to explore the possibility of exciting different resonant modes over a wider bandwidth, than those typically accessible with magnetron based technology [8].

The presence of different resonance modes, summarised in Fig. 7.1 and 7.2 and presented in detail in appendices C and D, shows a COMSOL Multiphysics simulation (using the MUMPS solver) [11] revealing the impedance of a typically sized (0.45m x 0.337m x 0.245m) domestic microwave oven, when empty and loaded with 1.0l of water. The spatial distribution of these modes is illustrated through plotted eigenvalues and electric field patterns. Although numerous resonant modes can be seen to exist across a much wider bandwidth of 100MHz, these mode frequencies are inaccessible using traditional magnetron based technology, due to the magnetrons limited operating bandwidth. The inability to access and excite these modes ultimately leads to reduced efficiency and irregular, non-uniform heating, which are both critically important issues that need addressing.

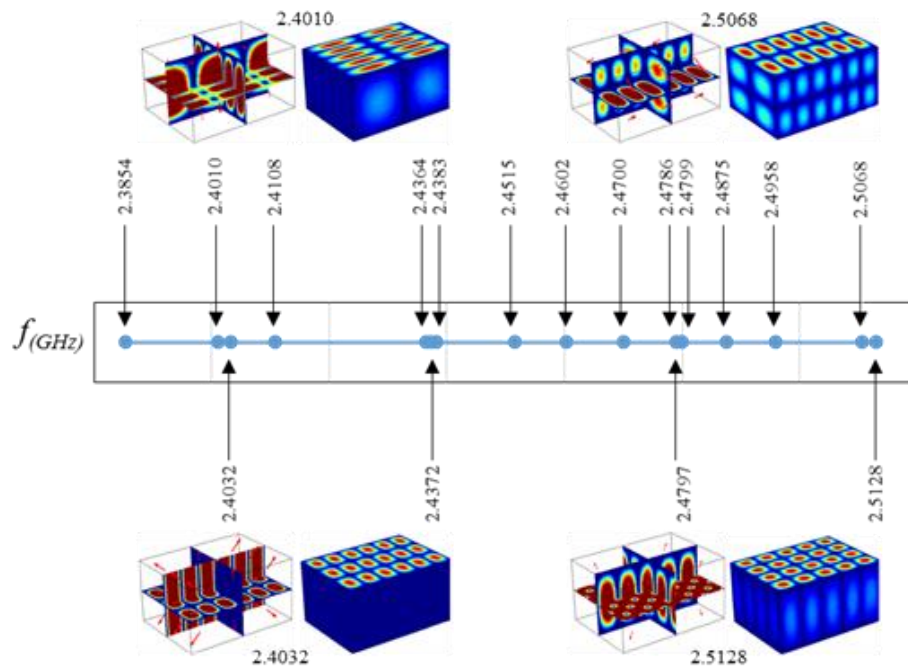


Fig. 7.1 Resonant modes that exist within an empty rectangular microwave oven cavity (size = 36litre), with associated mode distributions (Eigenvalues) for some of these.

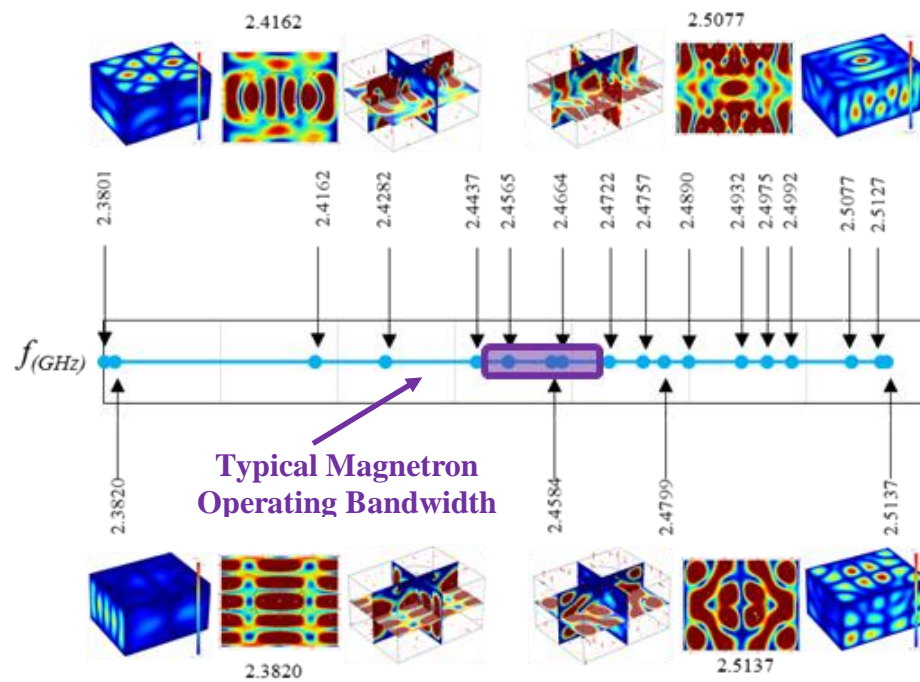


Fig. 7.2 Mode Distribution (Eigenvalues) inside a loaded (1 l of water) Microwave Oven (size = 36litre)

7.1.2 Verification of the coupling structure

The performance of the prototype coupling structure was characterized over the entire 2.4-2.5GHz ISM band, both in Chapter 5 using small-signal techniques, and here using the measurement setup shown in Fig. 7.3. The measurement setup comprises of a Keysight E5071C vector network analyzer, an Agilent EXG Vector Signal Generator, a 50W SSPA, a domestic microwave oven cavity loaded with 0.325l of water and two Keysight RPM2 U2042XA USB peak and average power sensors.

The coupling structure and cavity impedance behavior was characterized in two phases. During the first phase, described earlier in chapter 5, the reflection coefficient (S_{11}) of a loaded cavity was measured under small signal conditions (using a vector network analyser), to identify the resonance modes. The position and orientation of coupling structure 4, was adjusted from within the cavity (using steps listed in section 5.2.1), until a return loss of better than 10dB was realised over the operational bandwidth of 100MHz. Once the desired performance had been achieved, the coupling structure was locked in position using a small grub screw.

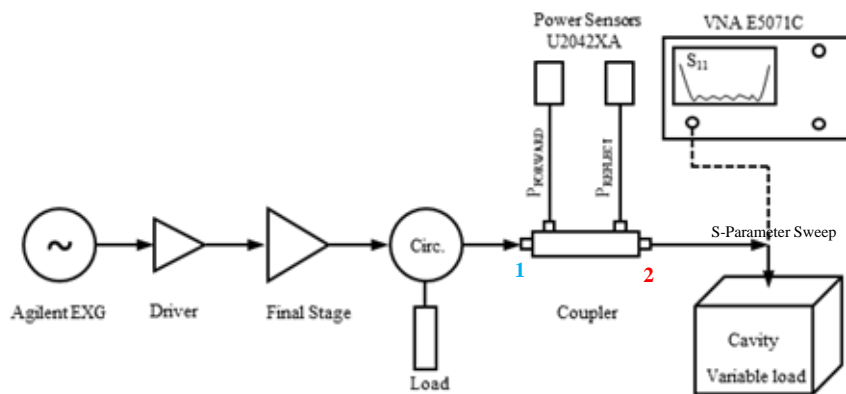


Fig. 7.3. Concept Evaluation – measurement setup

Whereas, during the second phase the coupler structure performance, and its contribution to effective uniform heating is verified under real (large signal) operating conditions. Here, a vector signal generator was used to drive the SSPA, generating fixed powers of 10W, 20W, 40W and 50W at separate frequencies across the full (2400-2500MHz) ISM band. The SSPA output power was coupled into the cavity via the prototype coupling structure shown in Fig. 5.22b. The forward and reflected power was monitored at reference planes 1 & 2, shown in Fig. 7.3. Initial measurement results at low power (Fig.7.4), show that more than than 90 % of the available power was delivered into the loaded cavity over most of the band. When using a forward power of 50 Watts, the percentage of power delivered and available for heating was above 90% for a 35 MHz portion of the operating bandwidth (2400-2435MHz), this dropped slightly to below 90% between 2435-2455MHz and 2480-2560MHz, and to 80 percent between 2465-2480MHz, mostly due to changes in load temperature effecting the impedance. This effect was also visible with lower power levels, albeit to a smaller degree. There appears to be regions, where the source-to-load match degrades with increasing temperature, however, it is worth pointing out that there are other areas of the spectrum where the load is more optimally matched. This raises the interesting idea of exploiting the precise frequency control possible with solid-state generators, to target frequency points and bands to optimise heating efficiency.

As introduced in Chapter 3, the established and industry standard way of calculating the efficiency of domestic microwave ovens (IEC 60705, 1999), typically involves heating 1000g \pm 5g (1 litre) of water, inside a cylindrical glass container (external diameter 190mm, height 90mm), from 10°C \pm 1°C to 20°C \pm 2°C. Using this approach, the time taken to cause this temperature increase can be measured, and the power required (P_{out}) can be calculated using (eqn. 7.1). If the oven input power is known, the cavity efficiency can be calculated using (eqn. 7.5). In the following experiment, cavity efficiency is calculated by considering four different available heating powers; 10, 20, 40 and 50W, delivered into the cavity at point 2 in Fig.7.3. For each available power level

(P_{avail}), the time taken to raise the water temperature by 10, 30 and 40 degrees was measured along with the ambient temperature, and these values recorded in table 7.1. Then, using eqn. (7.1), the actual power absorbed by the water was calculated. Comparing the power available to the cavity and the power absorbed by the water allows the cavity efficiency to be calculated using eqn (7.5). The measured *Time to heat* and *cavity efficiency* values, shown in Table 7.1, and are compared with the theoretical values. The theoretical values assume a similar 90% cavity efficiency.

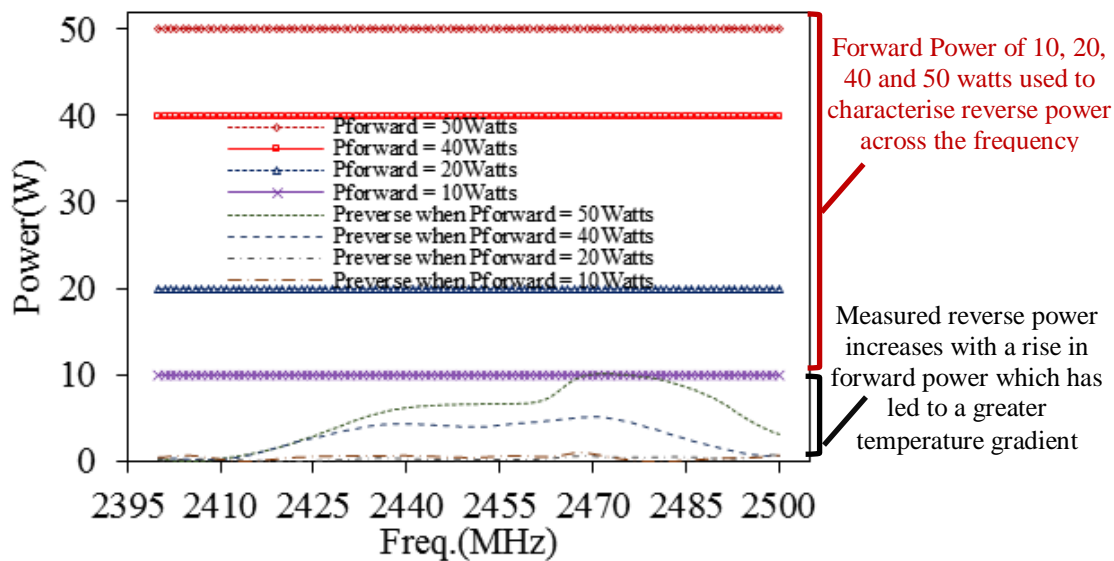


Fig. 7.4 Forward and reflected power measurements across the 2400 – 2500 MHz frequency band, 0.325l water load.

Table 7.1 – Time to heat a 0.325litre load – measured values using a frequency sweep (2400_2500MHz) with 1MHz steps

Output power (W)	20	40	50
Mass - Container (g)	127	127	127
Water (g)	325	325	325
Temp - Ambient (°C)	17	17	18
- Initial (°C)	22	22	20
- Final (°C)	32	50	60
Time(sec) to heat the load - T_H - measured	1000	1150	1270
Time(sec) to heat the load - T_H - calculated	905	1056	1200
Cavity eff. - Measured	84.40	83.66	85.49
Cavity eff.- Calculated	90	90	90

The measured *Time to heat*, required to reach the theoretical temperatures values was longer (~100secs), which resulted in a slight drop in measured cavity efficiency values (85%). The longer *Time to heat*, and the drop in measured *cavity efficiency*, is explained by forward power levels dropping to below 90% over some regions of the operating bandwidth. The measured solid-state *cavity efficiency* is significantly greater than the magnetron based cavity efficiency (50%) [21-22].

$$P_{\text{absorbed(W)}} = \frac{(4.18 \cdot \text{Water}_{(g)}) \cdot (T_F - T_I) + (0.55 \cdot \text{Container}_{(g)}) \cdot (T_F - T_A)}{\text{Measured time}_{(s)}} \quad (7.1)$$

Where;

T_F = Final Temperature

T_I = Initial Temperature

T_A = Ambient Temperature

$\text{Water}_{(g)}$ = Mass of water in grams

$\text{Container}_{(g)}$ = Mass of Container in grams

4.18 = Specific heat of water (1 calorie/gram °C = 4.186 joule/gram °C)

0.55 = Specific heat capacity of container

$$\text{Time to heat} = \frac{(T_F - T_I) \cdot \text{Vol. of Water}}{P_{\text{avail(W)}}} \quad (7.2)$$

$$\text{Oven Efficiency} = \frac{P_{\text{absorbed(W)}}}{\text{DC Input Power(W)}} \quad (7.3)$$

$$\text{DC Input Power (W)} = \frac{P_{dc(W)}}{\text{DC-DC Converter efficiency (90\%)}} \quad (7.4)$$

$$\text{Cavity efficiency} = \frac{P_{\text{absorbed(W)}}}{P_{\text{avail(W)}}} \quad (7.5)$$

$$\text{Cavity efficiency (Mag)} = \frac{\text{Oven efficiency}}{(\text{Inverter efficiency}) \cdot (\text{magnetron efficiency})} \quad (7.6)$$

Where :

Inverter efficiency = 92.5%

Magnetron efficiency = 71%

$$\text{Oven efficiency (Mag)} = \frac{\text{Output Power}}{\text{Input Power}} \quad (7.7)$$

$$\text{Input power (W)(Mag)} = \left(230 * \left[8.44 * \frac{\text{PWM}(\%)}{80} \right] \right) \quad (7.8)$$

In this experiment, a conventional microwave oven is modified for direct coupling into the rectangular cavity, to ascertain impedance behaviours at the fundamental and second harmonic frequencies. The coupling structure is mounted in the cavity ceiling (Fig. 5.18), close to where the SSPA is positioned and bent into an L shape, so that it doesn't protrude deep into the cavity. This necessitated a change in the shape and size of the loops developed earlier for the cylindrical cavity. The reflection coefficient (S_{11}) of a cavity loaded with 0.325 litre of water, is measured at the fundamental (2400-2500MHz) and second harmonic frequencies (4800-5000MHz). using the arrangement shown in Fig.7.3 and the coupling structure shown in Fig. 5.23c. Measured results demonstrate that it is possible to achieve return loss of better than 15dB ($S_{11} < -15\text{dB}$) over the entire ISM band (2400-2500MHz). This is shown both on a Smith chart and in log-lin form in Fig. 7.15, where a change in the impedance environment (as the water is heated between 25° and 65°), shows the optimally matched points (around 2480MHz) shifts in frequency, a degradation in match over the center frequencies and a small improvement over other regions of the band for frequencies between 2480-2500MHz. The behaviour of the 2nd harmonic component is also shown, and its relevance to SSPA efficiency and reliability has already been discussed in previous chapters. Here, the magnitude of the second harmonic reflection coefficient is relatively small and non-reflective, so potential efficiency improvements will be limited for this coupling structure.

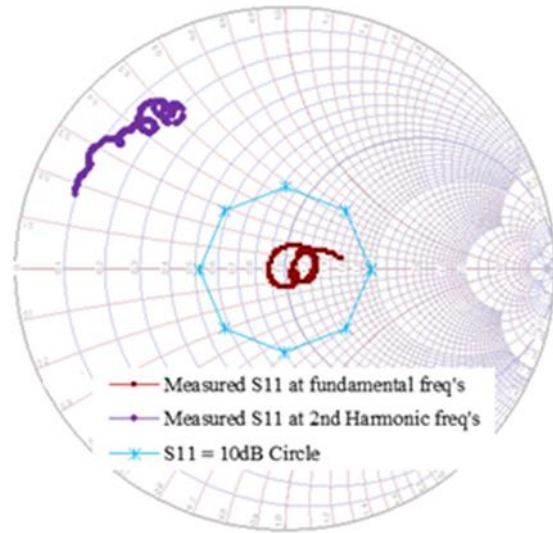
Power absorption within a typical oven cavity, is very sensitive to load placement due to the spatial variation in the electric field. Various studies have demonstrated [32],

and attempted to quantify this variation in magnetron-based ovens for different shaped loads with similar dielectric properties, at different locations. Also, in complex heating apparatus such as a multi-mode rectangular cavity, the impedances (at the N-type launch) can vary significantly for specific modes / frequencies, which again can result in variable heating within the cavity. To address these issues, turntables and mode stirrers are typically added to commercial ovens, to homogenise the electric field to heating uniformity. Heating variation in a solid-state microwave oven (due to load placement), was investigated by placing the load at different specified locations. The changes in impedance response (at the N-type launch connector), are measured (over the full 100 MHz ISM bandwidth) by applying specific levels of microwave power at frequencies over which the load is optimally matched, and then recording the temperature increase over specific time intervals.

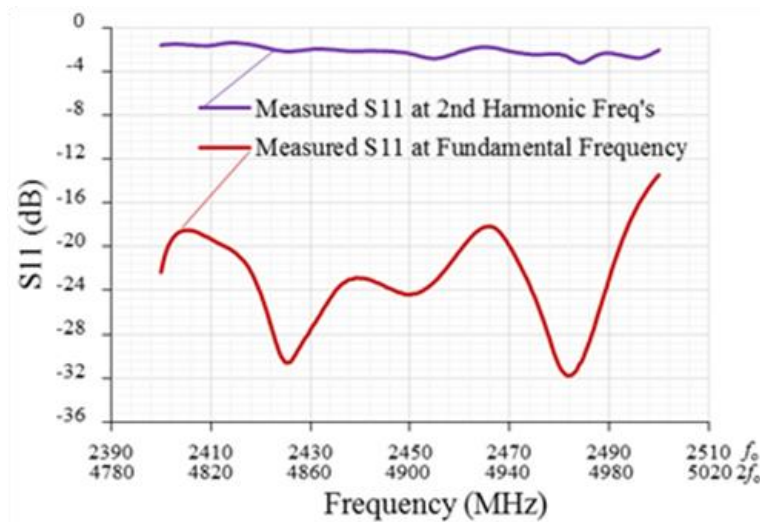
There are other potential benefits linked to the wideband potential of solid-state heating that need to be explored. For small loads for example, applying power at a single frequency to excite specific mode(s) could be useful for targeting efficient heating in specific locations. Alternatively, using swept-frequency excitation, to excite multiple modes may provide more effective and uniform heating to larger loads occupying larger volumes.

Having demonstrated the potential performance benefits of wideband coupling in the chapter 5 (coupling structure shown in Fig.5.23b), the initial coupling structure was optimised (thru small adjustment of the inductive loop shapes, distance between the loops and inclusion of a second harmonic tuning element) to present a 50Ω load (for a range of loads) at the fundamental, and a short circuit at the 2nd harmonic frequencies as shown in Fig. 5.23c (three loop coupling structure). The fundamental impedance trace shown in Fig. 7.5a, remains close to and circles the 50Ω point on the Smith chart and remains well within the -10 dB circle. In fact, the measured return loss value remain very low ($S_{11} < -18\text{dB}$) over the 100MHz operating bandwidth (Fig.7.5b), which means that by using this structure, it is possible to deliver more than 96% of the available power into the cavity.

The comparative forward and reflected power measurements for initial (Fig.7.4) and optimised (Fig.7.6) show that for the optimised structure, for a forward power of 50W, only 3W maximum is reflected back to the source over a 5MHz region between 2472-2477MHz. Reflected power over remainder of the band is negligible (<1.5W).



(a)



(b)

Fig.7.5 S₁₁ at the fundamental (2.4-2.5GHz) and second harmonic (4.8-5.0GHz) for a 0.325l water load using coupling structure shown in Fig.5.23c, shown in (a) both polar complex (b) magnitude log-lin format.

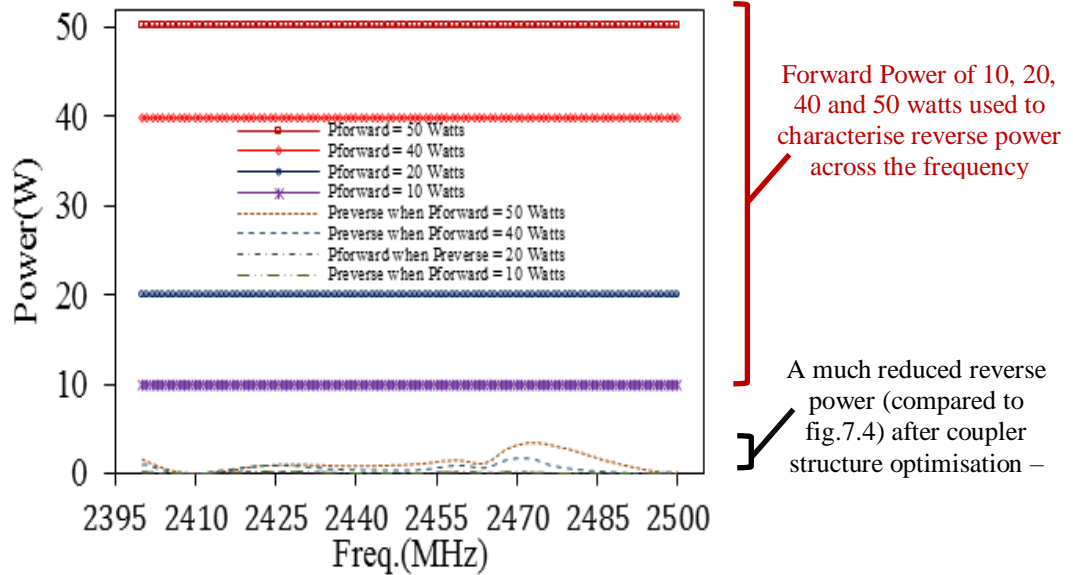


Fig. 7.6 Forward and reflected power measurements across the 2.4–2.5 GHz frequency band for a 0.325l water load, measured using the optimised coupling structure shown in Fig.7.3

Table 7.2 - Solid State heating temperature measurements comparison

Output power (W)	20	40	50
Mass - Container(g)	127	127	127
Water(g)	325	325	325
Temp - Ambient (°C)	17	17	18
- Initial (°C)	22	22	20
- Final (°C)	32	50	60
Time(sec) to heat the load - T_H - measured	925	1045	1100
Cavity efficiency	91.28	92.06	93.65

The measured *time-to-heat* value, for example for the 50W availability case has reduced from 1270 to 1100 seconds. This enhancement in performance is also reflected in the cavity efficiency (93%), which shows an improvement of 8% from previously recorded values shown in Table 7.1.

Whilst the data shown in Fig.7.6 and table 7.2 demonstrates the broadband nature of the coupling structure, the potential to identify and select (either manually or through a bespoke intelligent frequency hopping technique), optimally matched frequency points or regions is extremely interesting, when trying to realise an efficient microwave heating system. As well as maximising delivery efficiency, operation into a continuously matched load ensures that reflected power will be minimised, reliability maximised and isolator-less operation becomes a real possibility.

7.1.3 Single-point vs swept frequency heating

It has been demonstrated that when using a wideband coupling structure and SSPA combination, it is possible to identify and inject power at single, optimally matched frequency points i.e. at 2425MHz and 2482MHz in Fig.7.5, where $S_{11} < -30\text{dB}$. However, since the reflection coefficient is relatively low ($S_{11} < -18\text{dB}$) over the entire 2400-2500MHz frequency band, it is also acceptable to operate the SSPA at any frequency over the operating bandwidth without compromising device reliability. The power delivery efficiency for these ‘other’ frequencies will be slightly lower (~2%) compared to single frequency point operation. This has been demonstrated through a comparison between single frequency and continuous swept frequency heating measurements of a 0.325 l water load. From the measurement data shown in Fig.7.7, it can be seen that single frequency point operation pertaining to an extremely good match ($S_{11} < -32\text{dB}$), achieves slightly higher temperatures, compared to multiple frequency point operation, where the match is variable (18-32dB).

Injecting power at selected frequency points (where the load is optimally matched), ensures evenness of heating as greater than ninety-nine percent of the available power is delivered to the cavity. Whereas, during a frequency sweep, power is injected into the cavity at 1MHz intervals over the 100MHz bandwidth. The match (18-32dB), and power delivery efficiency (96-99%), over this range varies resulting in a slightly lower temperature increase. Swept frequency operation is beneficial for loads occupying large

volumes or areas, where excitation of multiple modes can deliver energy to different parts of the cavity resulting in a more uniform heat distribution. Whereas, a single frequency operation may be more beneficial for smaller loads, where energy delivery into the cavity needs to be concentrated over a smaller region.

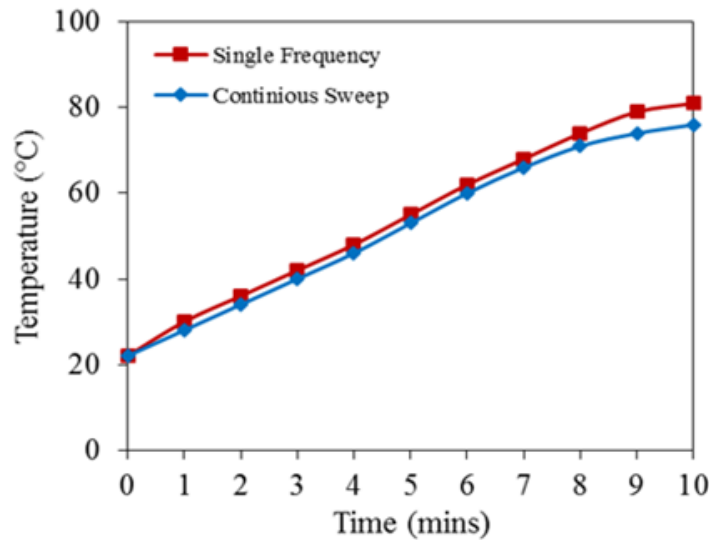


Fig. 7.7 Single frequency vs continuous frequency sweep temperature measurements for a 0.325l water load, with a 150W SSPA.

7.1.4 Microwave Oven Efficiency Comparisons

Domestic microwave ovens are regarded as one of the most efficient household appliances, with typical cavity efficiencies of 50-60% [7],[12]. This value of efficiency is traditionally calculated, by measuring temperature rise in 1l of water over time from 10°C \pm 1°C to 20°C \pm 2°C and was determined to be 53.76% for a 800W rated microwave oven. 1l of water is lossy and absorbs a large portion of the available energy, whilst typical domestic microwave oven usage often involves heating much smaller loads, equivalent to a 0.325l cup of liquid [27]. Furthermore, due to load mismatch issues, it is well established that smaller loads absorb less of the available power, resulting in higher reflected powers and reduced cavity efficiency [22-24].

Comparative measurements are performed using a 160W SSPA (with 60% efficiency), and a commercial-off-the-shelf, 800W rated, magnetron microwave oven. By heating different volumes of water, it can be shown (Fig.7.8), that oven efficiency for the solid-state system can be maintained at a more constant level. This is made possible by changing the operating frequency of SSPA, for each of the loads to achieve an optimum match. The measurement data (Fig.7.9), shows the $P_{delivered}$ efficiency for different volumes of water ranging from 0.2l-1.0l, where an increase in the volume of water has moved the optimally matched point to a higher frequency

Operation at optimally matched frequency points (regions), corresponding to different volumes of water ensures that maximum available energy is delivered into the cavity, to heat the load regardless of the volume. Further, as the $P_{delivered}$ and *cavity efficiency* can be kept high, solid-state oven efficiency is largely governed by the SSPA and PSU efficiencies. A magnetron based (800W) oven, has a reasonably flat efficiency response for large volumes of water (vol >0.6l). However, as the volume of water is reduced (vol <0.6l) the oven efficiency begins to drop significantly. This is due to the increasing mismatch (with smaller loads), and the inability to adopt to changes in the loading conditions.

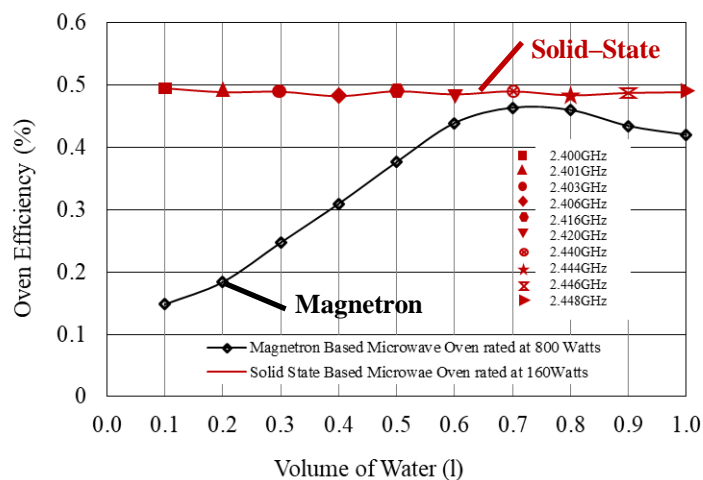


Fig. 7.8 Microwave Oven Efficiency comparison between a Solid-State (160W) microwave oven and a Magnetron based (800W) microwave oven.

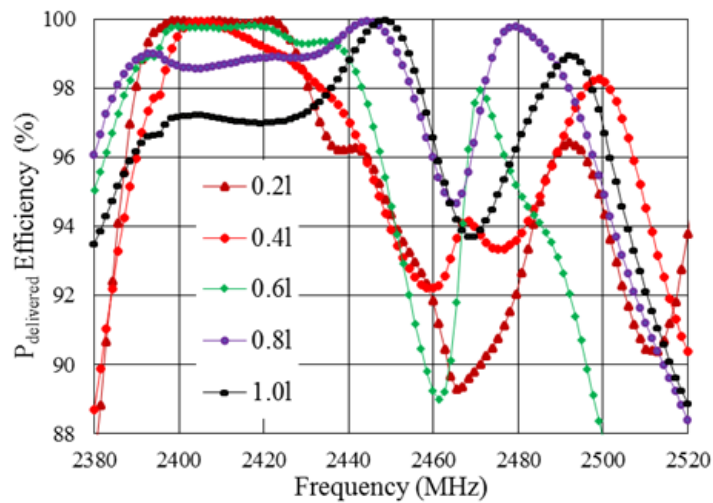


Fig. 7.9 $P_{delivered}$ Efficiency comparison for different volumes of water over the operating frequency band for a Solid-State System

7.1.5 Cavity heating uniformity relative to load placement

Several causes of non-uniform heating in traditional microwave ovens have been discussed in the introductory section. One major cause relates to the placement of the load within the microwave oven, which is investigated and presented in this section. Attempts to overcome this effect in magnetron based microwave ovens includes the use of a mode stirrer or a turntable, that function by modifying the boundary conditions or field patterns inside the cavity, such that the load is more likely to be exposed to an electric field. In this experiment the *Time to heat* parameter is kept constant, as we are only interested in the relative temperature difference between locations and not the overall temperature rise.

A location map, representative of the turntable region shown in Fig.7.10a, was used to study the effects of heating relative to the load position. Heating capacity of a magnetron based microwave oven is measured using a 0.1l cup of water placed at different locations. A 800W rated magnetron based oven (includes turntable), was used to heat the water placed at location 1 for 60 seconds, initial and final temperatures were recorded. The measurement was repeated using separate cups of water (with the same initial temperature) placed at different locations (1-3₁₂). The relative temperature

differences from the center location (where the recorded temperature was at its highest) are shown in Fig.7.10b. As the load is moved to locations “2₁-2₆”, a drop in temperature ranging from 6.1-11.66°C is measured. A further, more consistent drop of ~ 22°C is measured in the outer ring, locations “3₁-3₁₁”.

The measurements were then repeated using a solid-state microwave oven comprising a 160W SSPA, and optimised coupling structure shown in Fig. 5.23c. No turntable or mode stirrer was used. Use of turntable and mode stirrers is not considered for solid state heating applications as it adds extra cost and complexity with little benefits, instead selective mode excitation ensures that load is heated evenly. Here, the SSPA frequency of operation was selected based on a broadband pre-measurement of reflection coefficient (S_{11}), to identify the frequency that yields the best match, as shown in Fig. 7.11a. The measurements presented in Fig. 7.12, show maximum and minimum reflection coefficients of -13dB (at 2414 MHz) and -44dB (at 2483 MHz), at location 3₅ and location 2₅ respectively. The worst case corresponds to 94.9% power transferred and only 5.1% power reflected.

The return loss values (Fig.7.12), correlate well with the temperature measurements (Fig.7.11b), which demonstrates that irrespective of the load position greater than 94% of the power is available to heat the load. A more uniform heating pattern is demonstrated with a solid-state approach, where the largest delta in temperature (“0.23°C”), occurred at worst matched frequency points 2431MHz, 2414MHz. Whilst a manual detection of optimally matched points was necessary in this case to select the correct SSPA frequency of operation, a relatively simple pre-scan measurement and intelligent frequency hopping technique could provide a workable solution for real time practical implementations.

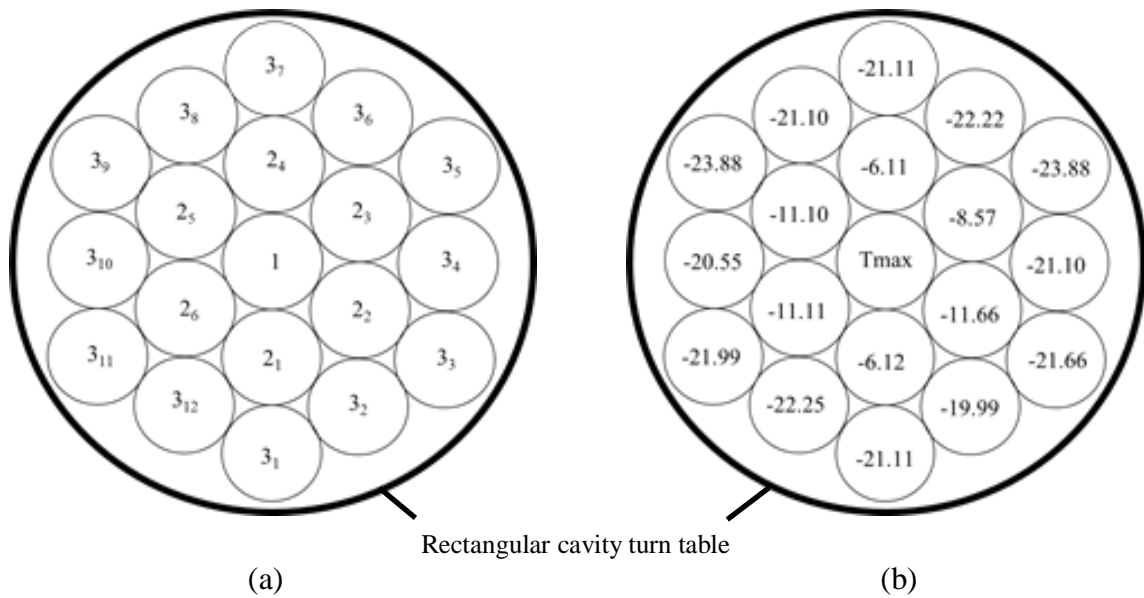


Fig. 7.10 Load placement locations within the oven (b) Magnetron based microwave oven, Δ ($^{\circ}\text{C}$) temperature variations from central location, 0.1l water load, heating time = 60 seconds

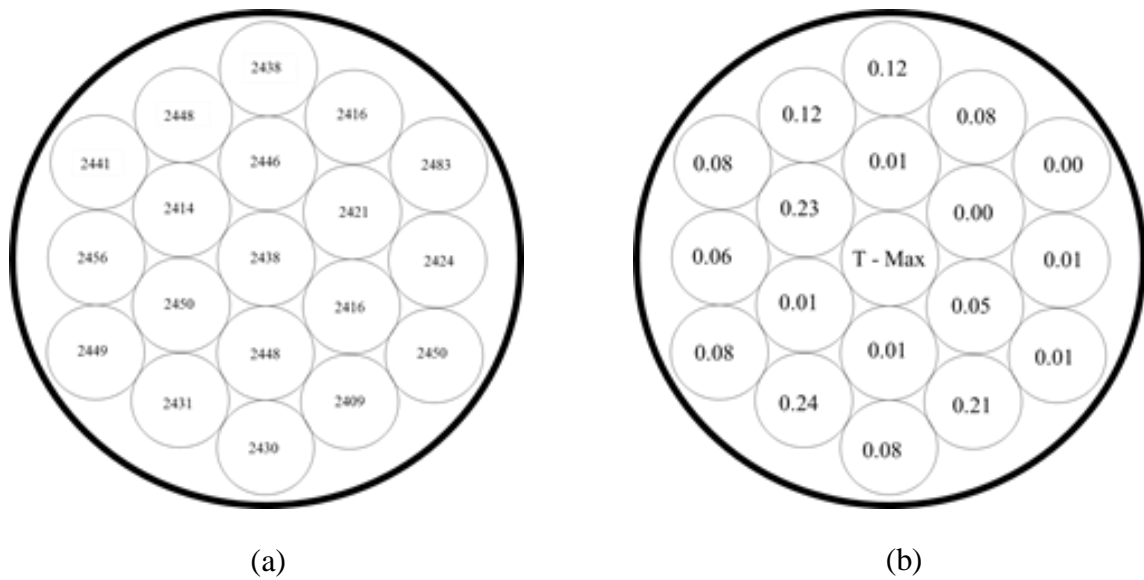


Fig. 7.11 SSPA based microwave oven. Optimally matched frequency points are shown (MHz) for different placement locations 0.1l water load (b) SSPA based microwave oven, Δ temperature ($^{\circ}\text{C}$) variations from central location, 0.1l of water heating time = 60 seconds

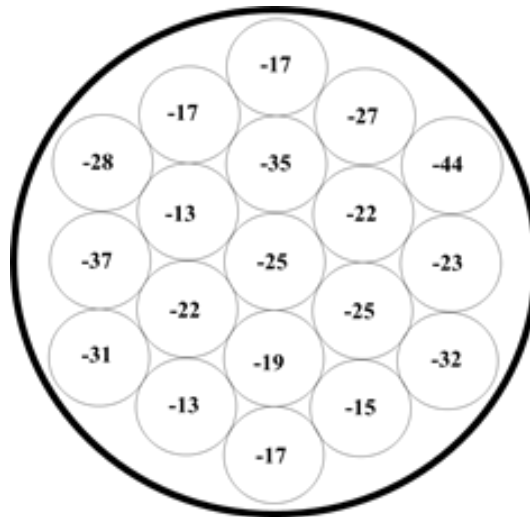


Fig. 7.12 SSPA based microwave oven, S_{11} (dB) at optimally matched frequency points, 0.1l of water

7.1.6 Cavity heating uniformity – surface temperature

Heating uniformity can also be characterized by monitoring surface heating patterns. This was done by heating 0.325l of water for 60 second and recording surface temperature variations. In order to mitigate heating variations due to penetration depth in water, the load was placed in a 17cm diameter cylindrical container, which resulted in a water depth of less than 1.4cm. Heating time variations due to container types are mitigated by using the same “microwave recommended” container for magnetron and solid-state heating. Temperature profile of the exposed surface was captured using a 64 pixels infra-red camera with a measurement accuracy of $\pm 2.5^{\circ}\text{C}$. Water has an emissivity coefficient of 0.95-0.963 which is close to the ideal value of 1 and therefore the accuracy of measurements is not influenced. The emissivity coefficient ϵ is typically used as an indicator for the radiation of heat from a ‘grey body’ compared to the radiation of heat from an ideal ‘black body’ with an emissivity coefficient of one.

The variations in surface temperature for a 800W magnetron based microwave oven showed a 14°C variation in temperature (Fig.7.13). There is a hot spot with a peak

temperature of 62-64°C, followed by several layers or regions where the recorded temperatures are less. The temperature difference increases away from the hot spot. These variations in surface temperatures have also been demonstrated using an even spreading of “grated cheese” on a plate [26]. Corresponding data obtained with a solid-state microwave oven using a 200W SSPA, and operating under frequency sweep conditions (1MHz intervals with a fixed output power), showed a relatively small temperature variation (Fig.7.14). There is a much larger *hot region*, followed by another region which covers most of the surface area. The temperature difference between the two regions is of the order of 4°C or less.

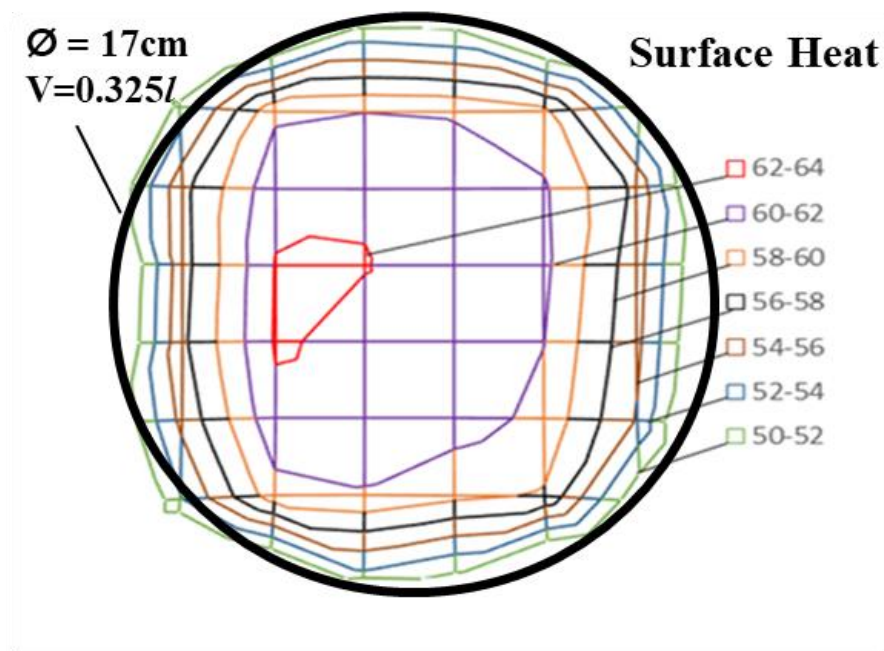


Fig..7.13 Surface temperature measurements using a 800W magnetron based microwave oven, 0.325l water load in a container of diameter 17cm, heating time = 60 seconds

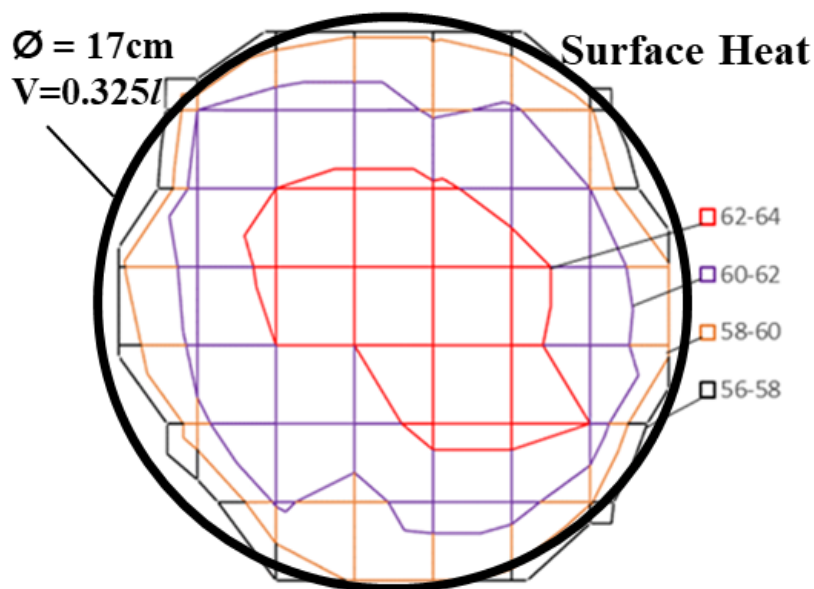


Fig..7.14 Surface temperature measurements using a 200W solid-state microwave oven, 0.325l water load in a container of diameter 17cm, heating time = 240 seconds

7.1.7 The impact of temperature variation

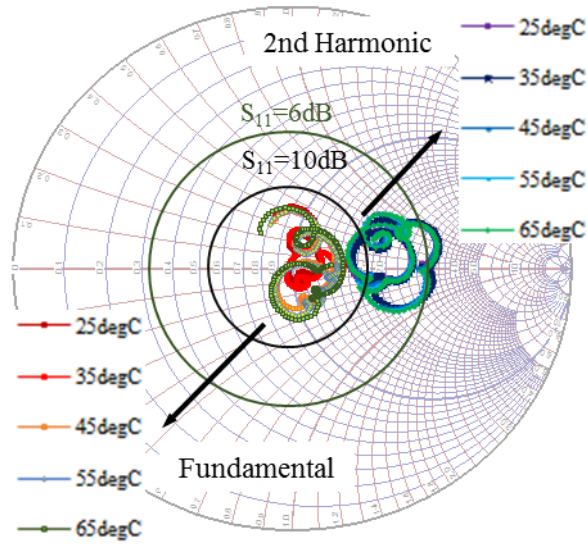
As discussed in chapter 2, microwaves are composed of a magnetic field and an electric field, orientated perpendicularly to one another. The electric field plays the primary role in heating, by promoting the rotation of polar molecules, resulting in heat generation by molecular friction. Molecular friction is the effect of absorption of microwave energy, rotation and vibration of the molecules. Instead of existing as internal vibrational energy the resultant energy is transferred to vibrational energy of molecules against their surroundings. Thus instead of re-emitting electromagnetic waves the absorbing substance dissipates energy as heat.

Further, microwave energy is transferred as heat, and is largely determined by the parameters of the product being heated. The dielectric constant, dielectric loss and

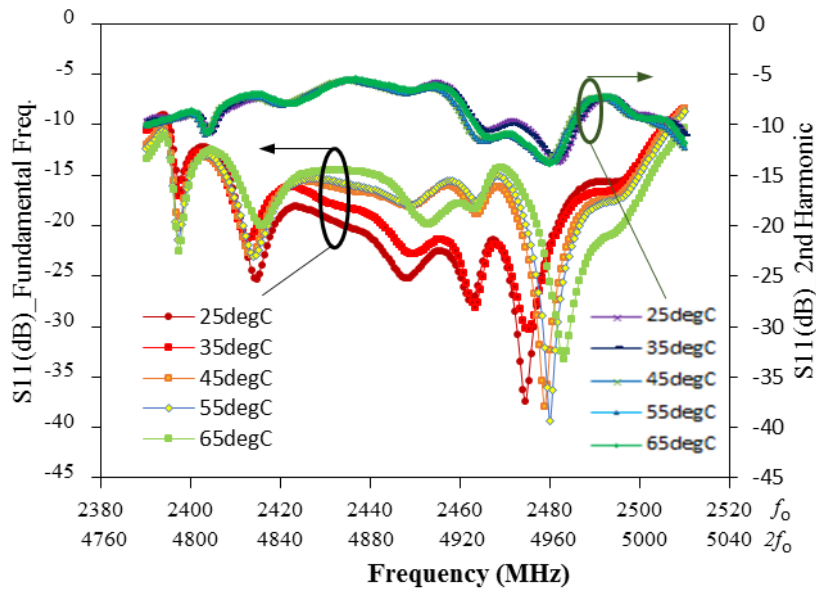
tangential loss parameters are of importance. The dielectric constant, a real component of heating, describes a materials capacity to store electrical energy, whereas the dielectric loss is an imaginary component which reflects a materials ability to dissipate electrical energy as heat. The dielectric constant and loss factor determine the quantity of energy that will be reflected, transmitted or absorbed by the material. Whereas, the loss tangent refers to a materials capacity to be penetrated by an electrical field and subsequently dissipate electrical energy as heat.

Within food substances the principle influences on dielectric behavior are the free ionic salt, moisture and solid contents. As temperature increases evaporation will serve to decrease the moisture level in a food. In turn this will influence the dielectric loss, dielectric constant and the loss tangent. A change in temperature leads to a partial dissociation of salts within a food which effectively lowers the dielectric loss. This change in the material properties caused by an increasing temperature gives rise to changing impedances.

The change in the amount of energy absorbed by the load is characterized, by measuring the reflection coefficient (S_{11}) parameters over a 25°C-65°C temperature range for a 0.325l water load. At 25°C, the worst case reflection coefficient of -14dB is at an operating frequency of 2405MHz. This means that 96% of the available power will be delivered to the load. The reflection coefficient over the rest of the operating frequency is of the order of -20dB, or better suggesting a delivery efficiency approaching 100%. However, an increase in temperature sees a gradual worsening of the impedance match over some regions, and an improvement in other regions of the operating bandwidth. The overall return loss stays below -14dB, which ensures that power delivery efficiency is not compromised by the changing impedance behavior caused by increasing temperatures. The concept of intelligent frequency hopping is just as valid in this instance, and it can be used to ensure that almost all of the available power delivered into the cavity is used to heat the load.



(a)



(b)

Fig. 7.15 S_{11} at the Fundamental (2.4GHz-2.5GHz) and 2nd Harmonic (4.8 GHz-5.0 GHz) freq's measured using coupling structure shown in Fig.7.3b, shown in both polar complex (a) and magnitude log-lin format (b).

7.2 Summary

In this chapter the concept of and key elements used in microwave heating systems have been introduced. The magnetron is a high power, robust device and can tolerate reflections introduced by variable loading conditions at the expense of a shorter lifecycle; it has a limited bandwidth emitting microwaves at $2.45\text{GHz} \pm 10\text{ MHz}$. The modes for a loaded microwave oven are shown to be scattered over a wider bandwidth than the magnetron operating bandwidth. The technology lacks intelligence and there is no direct means of identifying frequency regions or points over which the load is matched. Direct excitation of modes outside of this bandwidth is un-realizable leading to imprecise and uncontrolled heating.

Further from a device reliability and heating perspective, SSPA's must operate into a matched load ($S_{11} < -10\text{dB}$). The solid-state microwave oven presented $S_{11} < -18\text{dB}$ over the entire ISM band frequency sweep operation (to excite multiple modes) is shown not to compromise heating efficiency and device reliability. This has been demonstrated through single point vs swept frequency measurements for a 0.325l water load. During single frequency operation greater than ninety-nine percent of available power was delivered to the cavity. Under frequency sweep operating conditions (1MHz step size) this dropped to between 96-99% due to variations in the matching conditions. In both instances the SSPA continues to operate into a match load.

Non-uniform heating in magnetron based microwave oven is also attributed to travelling wave behavior and lack of control over mode selection (excitation) inside the cavity. This was demonstrated by placing the load at different locations inside the cavity. Measurements have shown that a change in the load position results in the optimally matched points to drift in frequency from their original state to a new state. These changes whilst unrecognizable in magnetron based systems have been clearly identified, prompting a change in SSPA frequency to ensure maximum power transfer into the cavity. Heating uniformity was also characterized by monitoring surface heating pattern.

Temperature profile of the exposed surface (0.325l water load) over 60 seconds' shows a uniform heating pattern with the solid-state system ($\pm 0.2^{\circ}\text{C}$). Similar measurements with a magnetron based system show a greater, 13°C temperature variation.

The broadband nature of the cavity coupling structure lends its use to an intelligent frequency hopping technique where power is delivered into the cavity at optimally matched frequency points or regions. This approach results in a highly efficient power delivery into the cavity under variable loading conditions. This approach significantly reduces the need for deploying different coupling structures to accommodate variations in loads. Compact size and simple construction makes this structure suitable for cooking and heating applications.

Measurement results clearly show the transformation of cavity load impedance to 50Ω load environment without the introduction of complicated and physically large matching networks. It has been further demonstrated that besides being broadband the coupling structure is tolerant to variable loading conditions (0.1-to-1.0l of water where the return loss (s_{11}) is below -14dBs across the operating bandwidth. The structure has the potential to match cavity load impedance points directly to the device optimal impedance identified during the device design cycle using load and source pull techniques. Selecting a set of cavity reflection coefficients from within the cavity load impedance environment can start the fundamental and harmonic load transformation process. The identified cavity reflection coefficients for first and second harmonics can potentially be transformed to transistor's optimal points. This simplifies the matching networks, improves system performance by reducing path losses and makes implementation in multi-mode systems a reality. The concept is a significant development for microwave heating and in particular isolator-less microwave heating applications where the transistor may be subjected to high VSWR conditions.

7.3 References

- [1] <http://www.heecs.eu/>
- [2] Klaus Werner “Advancing Next Generation Microwave Heating Applications AMPERE Newsletter Issue 89 July 7, 2016
- [3] <https://www.digikey.com/en/product-highlight/i/infineon/microwave-oven-block>
- [4] <https://www.electronicweekly.com/news/design/the-future-of-microwave-cooking-is-solid-state-2016-01/>
- [5] <https://www.newscientist.com/article/2089181-next-gen-microwave-ovens-are-small-enough-to-sling-on-your-back/>
- [6] C.Atuonwu & S.A.Tassou (2018): Energy issues in microwave food processing: A review of developments and the enabling potentials of solid-state power delivery, *Critical Reviews in Food Science and Nutrition*, DOI:10.1080/10408398.2017.1408564
- [7] HEECS. 2010. High efficiency electronic cooking systems. Accessed 12/09/2017 from [http://www.eniac.eu/web/downloads/projectprofiles/call3_heecs.p df](http://www.eniac.eu/web/downloads/projectprofiles/call3_heecs.pdf)
- [8] Frequency Distribution in Domestic Microwave Ovens and Its Influence on Heating Pattern Donglei Luan, Yifen Wang, Juming Tang, and Deepali Jain
- [9] Haala J 2000 Analyse von Mikrowellenheizprozessen mittels selbstkonsistenter finiter Integrationsverfahren Dissertation Universitat Karlsruhe
- [10] https://www.muegge.de/fileadmin/user_upload/muegge.de/PDF_Datasheets/Magnetron/Muegge_Flyer_Magnetron_2M244-M23J1_Rev01.pdf
- [11] <http://mumps.enseiht.fr/index.php?page=doc>
- [12] Michal Soltysiak, Malgorzata Celuch, Ulrich Erle “Measured and simulated frequency spectra of the household microwave oven” *Microwave Symposium Digest (MTT), 2011 IEEE MTT-S International*
- [13] Birla, Sohan; Pitachi, Krishnamoorthy; Subbiah, Jeyamkondan; and Jones, David D., “Effect of Magnetron Frequency on Heating Pattern in Domestic Oven” (2010). *Conference Presentations and White Papers: Biological Systems Engineering*. Paper 54.

-
- [14] <https://www.electronics-notes.com/waveguide-impedance-characteristic-matching-iris.php>
- [15] <https://www.radio-electronics.com/info/antennas/waveguide/waveguide-impedance-matching-iris-post.php>
- [16] E.Haebel 1996 CERN, Geneva, Switzerland - Couplers for Cavities
- [17] Haala J 2000 Analyse von Mikrowellenheizprozessen mittels selbstkonsistenter finiter Integrationsverfahren Dissertation Universitat Karlsruhe
- [18] Nicola, “Energy Thoughts and Surprises”, “Do microwave ovens save energy?”
- [19] Tom Murphy “Burning Desire for Efficiency” Steve C Cripps “RF Power Amplifiers for Wireless Communications”, Second Edition (Microwave Technology Library) Hardcover – 31 May 2006
- [21] P. Korpas , A. Wieckowski, M.Krysicki , and M. Celuch “Application Study of New Solid-State High-Power Microwave Sources for Efficiency Improvement of Commercial Domestic Ovens”, Warsaw University of Technology, Warsaw, Poland 2QWED Sp.z o.o., Warsaw, Poland
- [22] Patil NG, Rebrov EV, Eränen K, Benaskar F1, MeuldijkJ, Mikkola JP, Hessel V, Hulshof LA, Murzin DY, Schouten JC. “Effect of the load size on the efficiency of microwave heating under stop flow and continuous flow conditions”. Journal of Microwave Power Electromagnetic Energy. 2012;46(2):83-92.
- [23] Narendra G. Patil, Evgeny V. Rebrov, Kari Eränen, Faysal Benaskar, Jan Meuldijk, Jyri-Pekka Mikkola, Volker Hessel, Lumbertus A. Hulshof, Dmitry Yu. Murzin, Jaap C. Schouten “Effect of the Load Size on the Efficiency of Microwave Heating Under Stop Flow and Continuous Flow Conditions”
- [24] JIŘINA HOUŠOVÁ and KAREL HOKE “Microwave Heating – the Influence of Oven and Load Parameters on the Power Absorbed in the Heated Load”, Czech J. Food Sci. Vol. 20, No. 3: 117–124, 2002

-
- [25] Kausar Chaudhry and Dr J Lees “Two Port Cylindrical Cavity Enables Efficient Power Delivery-Through Power Combining & Scaling in a Solid State System” *ARMMS 2018*
- [26] Hai-HongWangDa-WenSun “Assessment of cheese browning affected by baking conditions using computer vision” *Journal of Food Engineering* Volume 56, Issue 4, March 2003, Pages 339-345
- [27] HEECS. 2011. High efficiency electronic cooking systems. Review of existing standards:gaps and constraints. Accessed 11/10/2017 from <http://www.heecs.eu/wordpress/wp-content/uploads/2012/03/HEECS-D2.2-M6.pdf>
- [28] D. M. Snider, “A theoretical analysis and experimental confirmation of the optimally loaded and over-driven RF power amplifier,” *IEEE Trans. Electron Devices*, vol. ED-14, pp. 851–857, June 1967.
- [29] M. Maeda, H. Takehara, M. Nakamura, Y. Ota, and O. Ishikawa, “A high power and high efficiency amplifier with controlled second-harmonic source impedance,” in *IEEE MTT-S Dig.*, Orlando, FL, Apr. 1995, pp. 579–582.
- [30] W. McAlpin, “High efficiency power amplification with optimally loaded harmonic waveshaping,” in *Proc. RF Tech. Expo’86*, Anaheim, CA, Jan. 30–Feb. 1, 1986, pp. 119–126
- [31] Vadivambal, R., and D. S. Jayas 2010. Non-uniform temperature distribution during microwave heating of foods a review. *Food and Bioprocess Technology* 3:161–171.
- [32] H.Zhang, A.K.Datta “Microwave Power Absorption in Single–and Multiple–Item Food”, *Food and Bioproducts Processing*, Volume 81, Issue 3, September 2003, Pages 257-265
- [33] Aamir Sheikh “High Power Waveform Engineering”, PhD Thesis, Cardiff University, UK, June 2010.
- [34] S. Cripps, *Advanced Techniques in RF Power Amplifier Design*, 1st Edn, Norwood, MA: Artech House, 2002

CHAPTER 8 CONCLUSIONS AND FUTURE WORK

8.1 Conclusion

Solid-state microwave heating is an area of growing interest for semiconductor device manufactures, microwave heating appliance manufacturers and consumers alike. The application includes the use of RF power to heat loads (i.e. food sources) in resonant cavities. The traditional way of generating power for these applications has been through the use of a magnetron, which is coupled into the cavity via a waveguide. Waveguide coupling is non-ideal in terms of accommodating load variations inside the cavity, moreover it is impractical for multiple port solid state heating applications where power from a single source is limited.

Recent advances and developments in semiconductor device technologies have made the use of RF generated power more practical for low power (1kW) applications. For these applications power transistors have the capability (through power combining) to generate power levels that are comparable to the magnetron source. However, there are justifiable concerns about matched SSPA reliability and system efficiency when operating into an unmatched load, as both are known to degrade under non 50Ω loading conditions. These concerns have been addressed and likely solutions which make solid state device technology a viable alternative to the magnetron have been researched and presented. The presented work has put forward viable solutions which place solid state technology alongside the current magnetron based systems.

The challenge for these new and emerging applications has been to make maximum use of the single mode cylindrical and multi-mode rectangular cavities where the impedance is non constant. For example, delivering power to an unmatched load, (a load which changes with state, i.e frozen or thawed, size of the food source and the ingredients it contains), inside a domestic microwave oven is representative of typical operating environment.

An alternative form of coupling (loop coupling), which can be designed to be more responsive to load variations has been considered and presented. A single loop (narrow band) coupling structure was found to be only successful in matching to a fixed load and at a single frequency point. This makes it highly inefficient and unusable in applications where the loads vary significantly. Furthermore, its narrow band characteristics means that a rectangular cavity's full potential (excitation of multiple modes) is unrealisable. Besides load variations, changes in temperature also lead to unmatched loading conditions, high reflected powers and system inefficiency. In order to get back to a matched state a change in SSPA operating frequency is necessary, which is not practical with a magnetron based system.

Narrow band coupling has many drawbacks and limits the amount of power that can be delivered to the load over the SSPA operating bandwidth. This increases the reflected power back to the generator. The constraints involved in delivering power over a narrow frequency band and for a fixed load means that any significant change in load requires physical re-positioning or retuning of the coupling structure. Re-positioning or re-tuning of the coupling structure in a domestic microwave heating application (e.g every time a different load or food source is placed inside the microwave oven) is impractical. A dynamic structure consisting of electromechanical parts is one possibility that has been considered, where the positioning of the structure is adjusted electro-mechanically with load variations. However this will add cost and complexity to the system and as yet this concept has not been realised for practical applications.

The need for a broadband coupling structure in the field of RF-generated microwave heating was identified so that the SSPA and cavity can be brought together to realise full potential of the heating apparatus. Consequently a novel broadband coupling structure (to be used with cylindrical and rectangular resonant cavities) with harmonic tuning capability was developed to optimise the efficiency of power delivery into the load. This eliminated the need for manual or electro-mechanical adjustment of the coupling structure (with load variations) which had been a pre-requisite of a single loop coupling.

Due to cost constraints it was necessary to make the structure simple and cost effective. The novel structure presented in this thesis is of a simple mechanical construction and can couple power directly into a cavity.

The most hostile operating conditions from a semiconductor device's reliability point of view exist when there is a small (or no load) load inside the cavity, under these operating conditions, all the transmitted power is reflected back to the SSPA output connector. In the absence of an isolator or circulator, which are expensive and bulky components so the motivation to eliminate them is clear, this excessive reflected power could lead to high peak voltages and currents at the device plane and thermal dissipation within the device channels leading to a soft or catastrophic breakdown.

Besides maintaining an acceptable level of match for low (0.1*l*) to high (1.0*l*) loads (volumes of the water), the proposed novel broadband coupling structure can be used to detect a 'load' and 'no load' state by measuring S_{11} parameters and or reflected power across the full system operating bandwidth. This gives an indication of the match at individual frequency points (across the frequency band). An intelligent frequency hopping technique (enabled by the novel broadband coupling structure) can then be used to deliver power at selected frequency points where the load is optimally matched. Through the use of this methodology, the no-load condition can be easily detected and the system instructed to deliver no power into the cavity. This prevents the SSPA from operating into hostile loading conditions and thereby prevent any damage to the power transistor. Whereas under "load" conditions the power will be delivered only at frequency points or regions where the reflection coefficient (S_{11}) is less than -10dB. This will help maintain very high levels of cavity efficiency, heating uniformity and device reliability, as demonstrated in chapter 7.

Whilst the use of intelligent frequency hopping is advocated to inject energy only at well matched matched states, its has also been demonstrated that with the use of the

proposed novel coupling structure the match is sufficiently good ($S_{11} < -12\text{dB}$) across a range of loads (0.1l-1.0l of water) over the ISM band (2400-2500 MHz). This suggests that through the use of intelligent frequency hopping, multiple frequency points (over the operating bandwidth) can be selected such that the SSPA will continue to deliver high levels of generated power (over 95%) into the cavity to heat the load. This makes the commercial realisation of an isolator less solid state heating apparatus a real possibility. The work discussed in this thesis has provided a significant step forward for the realisation of new broadband coupling structures which have the potential to be directly integrated to the SSPA's used in the microwave heating apparatus. Various design methodologies supported by experimental results (with a SSPA) have been discussed.

8.2 Future Works

Whilst most of the work discussed in this thesis has provided a significant step for the practical realisation of solid state microwave heating apparatus, this section outlines the future work necessary in moving forward the work undertaken in this research. Stepping through this thesis it can be noted that this research has focused on optimising power delivery into the cavity and thereby improving the system and heating efficiency of a microwave oven under different loading conditions.

The research work has shown that the coupling structure has been successfully implemented with both single mode (cylindrical) and multi-mode (rectangular) cavities under variable loading conditions. However, its implementation in multi-port applications has not been fully explored. Whilst the advantages of using separate SSPA's to realise very high power levels and heating uniformity for larger loads seem obvious for a fixed load, practical implementations under variable loading conditions can be complex and need to be explored further. Any microwave heating apparatus must satisfy the requirements of high power, efficiency and low cost for the specified operating band whilst meeting the appropriate reliability and size requirements. Device reliability poses a serious challenge in multi-port applications. This means that the SSPAs must continuously operate into a matched load and any reflected signal must be significantly lower than the fundamental carrier at

that port(s). Unfortunately, operation over a wide range of frequencies and under unmatched loading conditions has the potential to significantly increase the amount of reflected power such as to damage the SSPA. Whilst the concept of intelligent frequency hopping would overcome these obstacles, its implementation in a practical application needs further research, time and effort. Along with the proposed coupling structure, this is likely to involve the use of sufficiently fast control system algorithms.

Furthermore, it is common that the SSPA high efficiency state is obtained using highly efficient but non-linear modes, where efficiency at lower power degrades. In instances where low power is required, the back-off mode of operation will inevitably degrade SSPA and overall system efficiency. Whilst modern RF power amplifier architectures are designed to maintain reasonable levels of efficiency at back-off power levels their implementation in the early solid-state heating apparatus is thought to be complex and very expensive. Future SSPA design will need to address the efficiency performance under variable loading conditions and across different output power levels.

There are other inherent benefits linked to the wideband potential of solid-state heating that need to be explored. For small loads for example, applying a single frequency to excite specific single modes could be useful for targeting efficient heating in specific locations. Alternatively, using swept-frequency excitation to excite multiple modes may provide more effective and uniform heating to larger loads occupying larger volumes.

Appendix A - Rectangular Waveguide

The intrinsic impedance of a rectangular waveguide (TE & TM modes), phase velocity, group velocity and the guided wavelength can be calculated using the expressions below:

$$\eta_{TE} = \frac{120\pi}{\sqrt{1 - \left(\frac{fc}{f}\right)^2}} = \frac{120\pi}{\cos\theta} \quad (\text{A-1})$$

$$\eta_{TM} = 120\pi \sqrt{1 - \left(\frac{fc}{f}\right)^2} = 120\pi \cos\theta \quad (\text{A-2})$$

Phase velocity and group velocity

$$vp = \frac{c}{\sqrt{1 - \left(\frac{fc}{f}\right)^2}} = \frac{c}{\sqrt{1 - \left(\frac{\lambda_0}{\lambda_c}\right)^2}} \quad (\text{A-3})$$

$$vg = c \sqrt{1 - \left(\frac{fc}{f}\right)^2} = c \sqrt{1 - \left(\frac{\lambda_0}{\lambda_c}\right)^2} \quad (\text{A-4})$$

$$vpvg = c^2 \quad (\text{A-5})$$

Guided Wavelength

$$\lambda_g = \frac{\lambda_0}{\sqrt{1 - \left(\frac{\lambda_0}{\lambda_c}\right)^2}} \quad (\text{A-6})$$

Appendix B - Rectangular Cavity

Quality factor of a TM_{mnp} mode

$$Q_{mnp} = \frac{Z_w abd k_{xy}^2 k_{mnp}}{4R_s [b(a+d)k_x^2 + a(b+d)k_y^2]} \quad (B1.1)$$

Where:

$$k_x = m \frac{\pi}{a} \quad k_y = n \frac{\pi}{b} \quad k_z = p \frac{\pi}{ad} \quad k_{xy} = \sqrt{k_x^2 + k_y^2} \quad (B1.2)$$

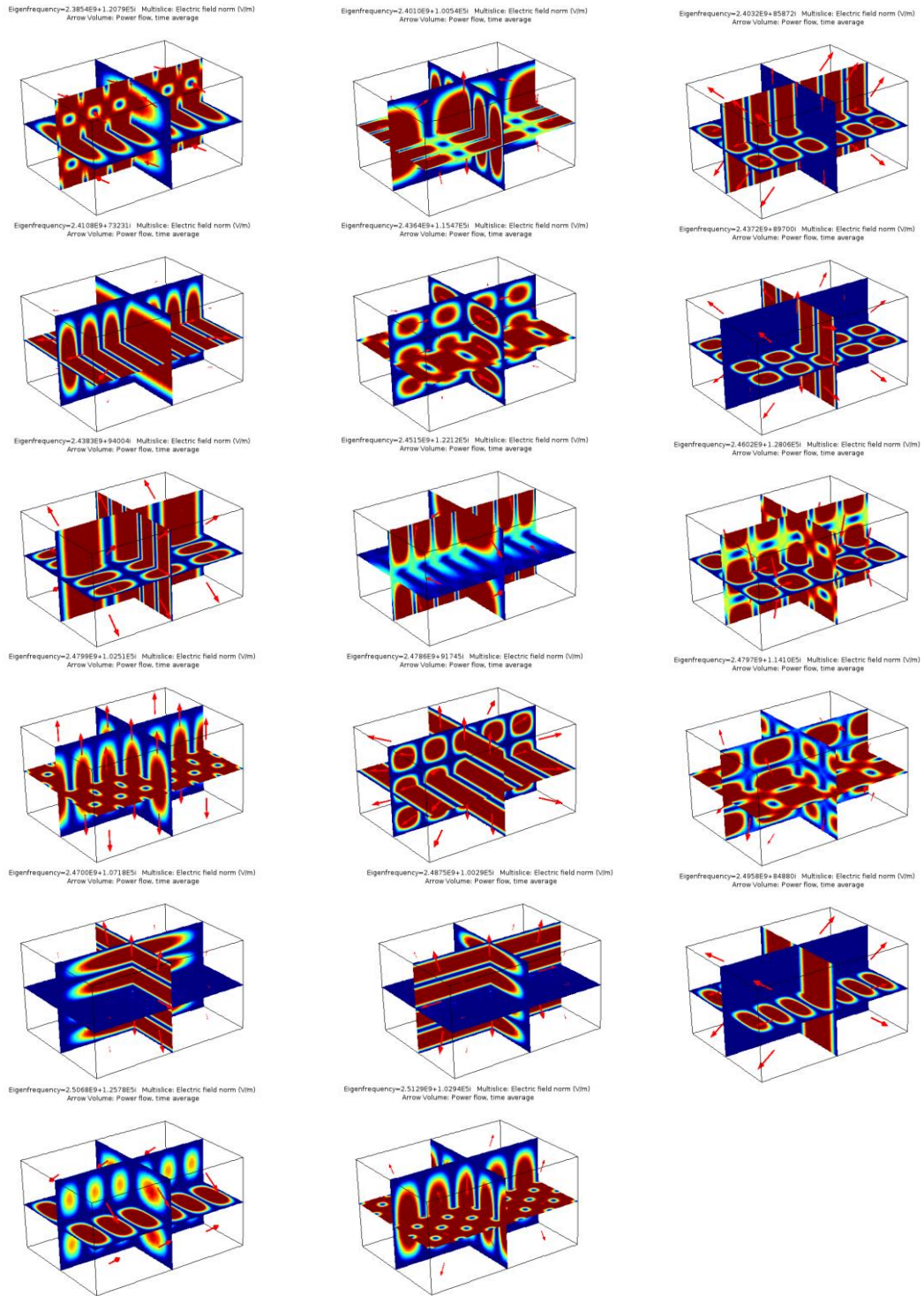
$$k_{mnp} = \sqrt{k_x^2 + k_y^2 + k_z^2} \quad (B1.3)$$

a,b and d are cavity dimensions

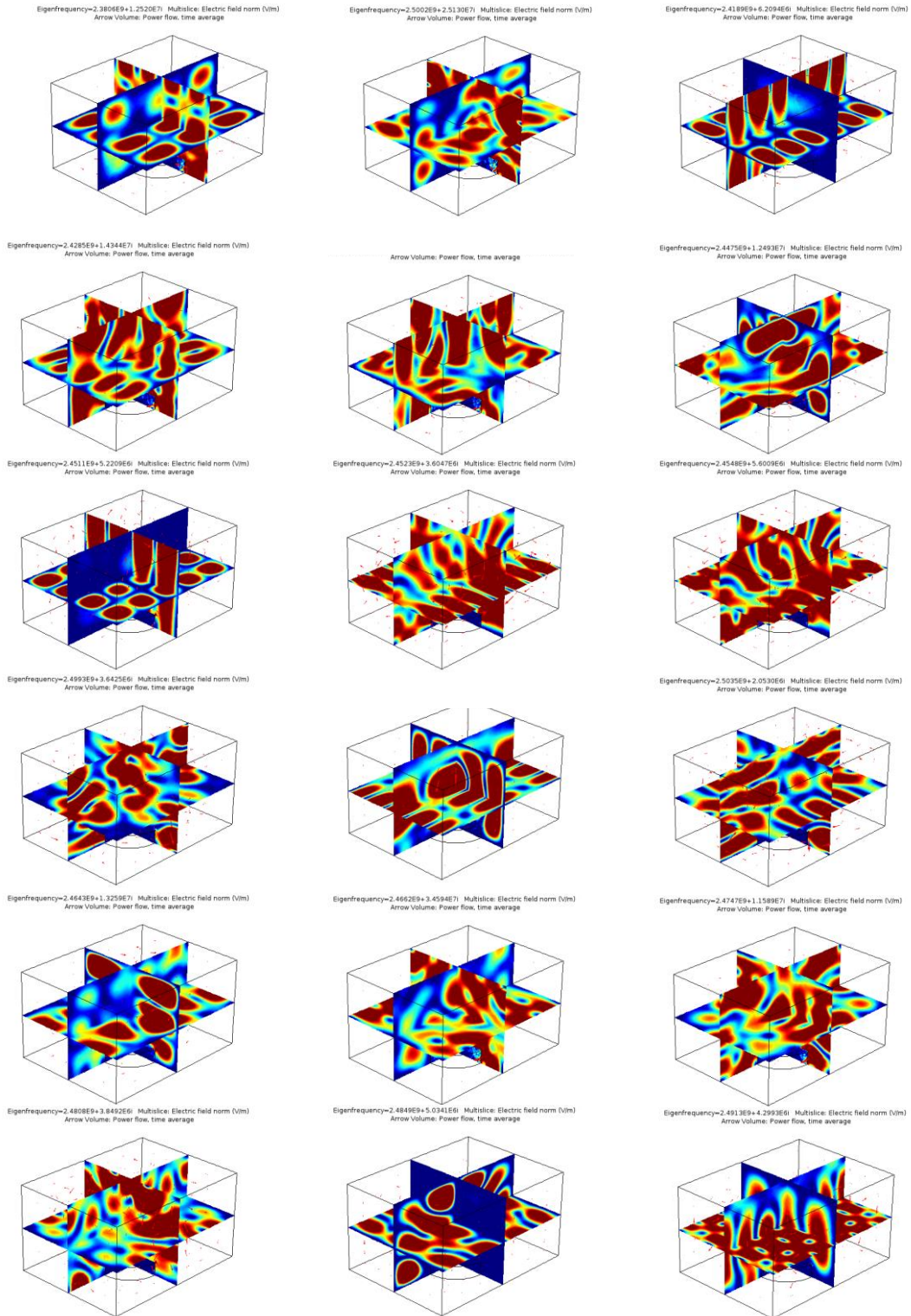
The impedance of the Z_w plane wave and the surface resistance of the walls of the cavity R_s are given below:

$$Z_w = \sqrt{\frac{\mu_0}{\epsilon_0}} \quad \text{and} \quad R_s = \frac{1}{\sigma \delta} \quad \text{and} \quad \delta = \sqrt{\frac{2}{\omega \mu_0 \epsilon_0 \sigma}} \quad (B1.4)$$

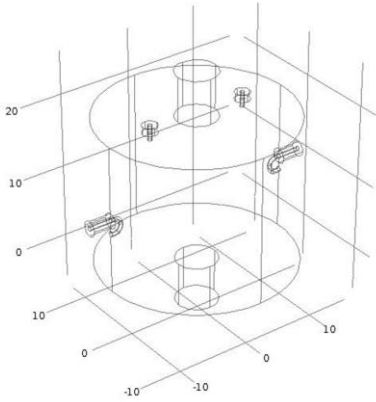
Appendix C - Eigen Values – Unloaded Rectangular Cavity



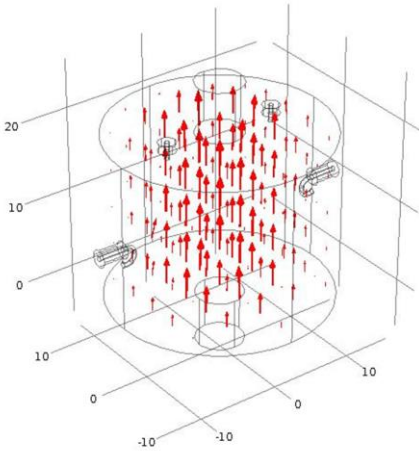
Appendix D - Eigen Values – Unloaded Rectangular Cavity



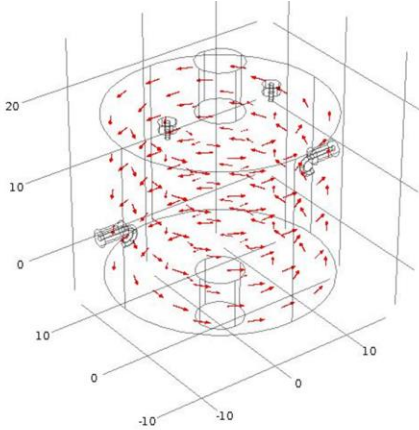
Appendix E – Single Mode Cylindrical Cavity



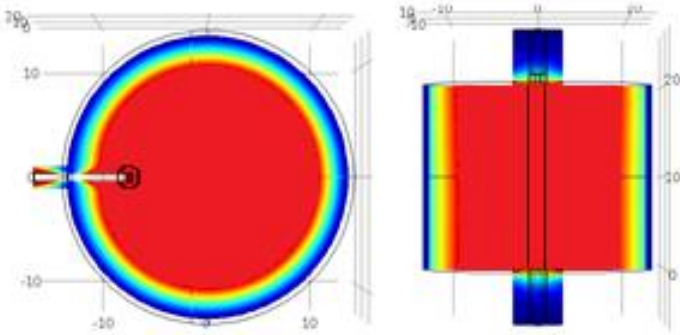
(a) Empty Cavity



(b) – E-Field

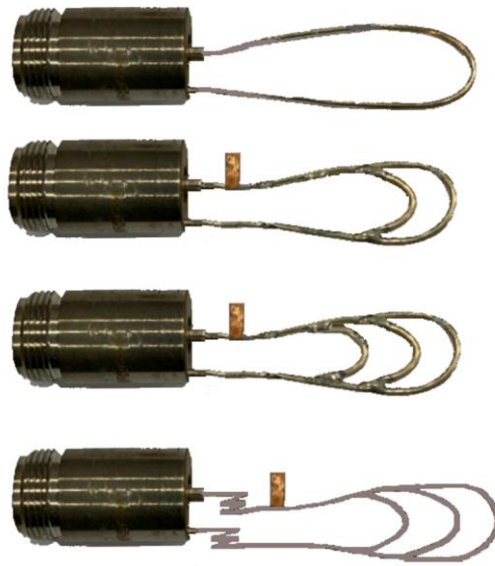


(c) Circulating H-Field

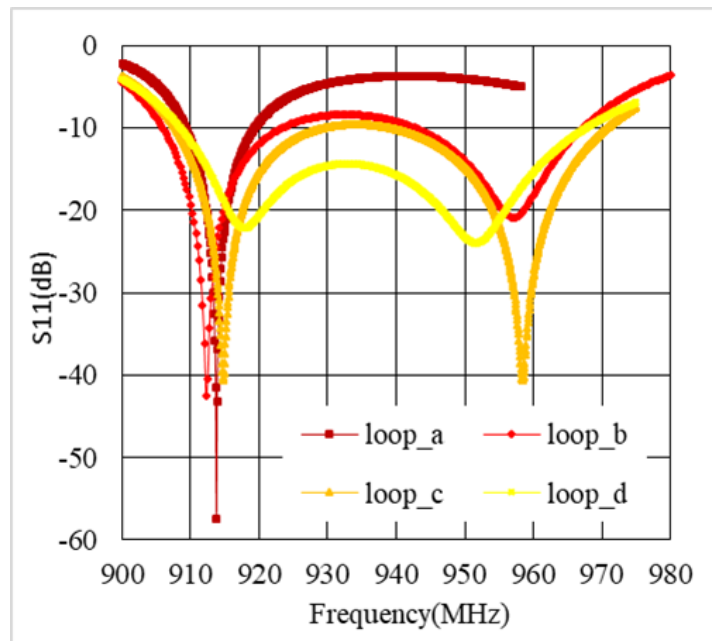


(d) Top and side views show the field distribution inside the cavity

Cylindrical Cavity Single to three loop evolution

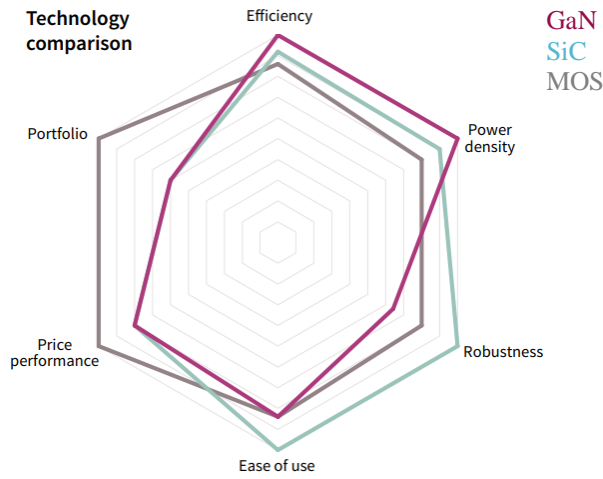


Cylindrical cavity loop development



Cylindrical cavity loop optimisation

RF Transistor Device Technology Comparisons Infineon Technologies AG.



	MOS	SiC	GaN
Efficiency	★★★★☆	★★★★★	★★★★★
Frequency	★★★★☆	★★★★★	★★★★★
Power density	★★★★☆	★★★★★	★★★★★
Efficiency at maximum power density	★★★★☆	★★★★★	★★★★★
Robustness	★★★★☆	★★★★★	★★★★☆
High temperature operations	★★★★☆	★★★★★	★★★★☆
Fit for bidirectional topologies	★★★★☆	★★★★★	★★★★★
Ease-of-use	★★★★☆	★★★★★	★★★★☆
Price performance	★★★★★	★★★★☆	★★★★☆
Portfolio granularity	★★★★★	★★★★☆	★★★★☆

